

Alma Mater Studiorum – Università di Bologna

DOTTORATO DI RICERCA IN

Scienze Chimiche

Ciclo XXV

Settore Concorsuale di afferenza: 03/B1

Settore Scientifico disciplinare: CHIM/03

N-Heterocyclic carbene complexes of rhodium:
structures, dynamics and catalysis

Presentata da: Dr. Gavino Solinas

Coordinatore Dottorato

Relatore

Prof.ssa Adriana Bigi

Prof.ssa Maria Cristina Cassani

Co-Relatore

Dott.ssa Rita Mazzoni

Esame finale anno 2013

Contents

1	Introduction.....	9
1.1	Carbenes – general introduction.....	9
1.1.1	Triplet vs. singlet carbenes.....	10
1.1.2	Electronic effects.....	11
1.1.3	Reactivity	14
1.1.4	N-Heterocyclic Singlet Carbenes	16
1.1.5	Synthesis	16
1.1.6	Imidazolium precursors.....	19
1.1.7	Synthesis of imidazolium salts.....	20
1.1.8	NMR and X-Ray diffraction of N-heterocyclic carbenes and imidazolium salts .	22
1.1.9	Electronic structure of N-Heterocyclic carbenes	23
1.1.10	Reactivity	25
1.1.11	Carbene dimerization	25
1.1.12	Carbene-Lewis acid and carbene-Lewis base adducts	26
1.2	Ionic Liquids as “Green Solvents”	27
1.3	The role of the counterion	29
1.3.1	The hexafluorophosphate problem	30
1.4	N-heterocyclic carbenes–transition metal adducts.....	31
1.4.1	Synthesis	32
1.4.2	Electronic properties	33
1.4.3	Comparison between phosphines and NHCs as ligands	34
1.5	N-Heterocyclic carbene silver(I) complexes.....	35
1.5.1	Synthesis	35
1.5.2	Structures.....	36
1.5.3	NMR.....	37
1.6	Rhodium(I)-NHC complexes	38
1.7	Iron(II)-NHCs complexes	40
1.7.1	Electrochemical measurements.....	41
1.7.2	Nature of bonding of NHCs to iron.....	41
1.7.3	Synthesis	42
1.8	Catalytic properties of transition metal-NHCs complexes.....	43
1.8.1	Heck-type reactions.....	43

1.8.2	Hydrogenation of olefins.....	44
1.8.3	Hydroformylation of olefins.	45
1.8.4	Hydrosilylation reactions	45
1.8.5	Addition of phenylboronic acid to benzaldehyde.....	47
2	Synthesis and Characterization of Imidazolium Salts Incorporating the NHBoc functionalization.....	49
2.1	Introduction	49
2.2	Results and discussion.....	50
2.2.1	Synthesis	50
2.3	Deprotonation of the imidazolium salts	53
2.4	Experimental Section	54
2.4.1	Synthesis of triphenylchloromethane (Trityl Chloride)	55
2.4.2	Synthesis of sodium salt of imidazolium ¹	55
2.4.3	Synthesis of 2-Bromoethylamine-t-butylcarbamate ¹	56
2.4.4	Synthesis of (2-Imidazol-1-yl-ethyl) t-butylcarbamate ¹	56
2.4.5	Synthesis of 1-(2-t-Butoxycarbonylamino-ethyl)-3-methyl-3H-imidazolium iodide (1a) ¹ 56	
2.4.6	Synthesis of 1-(2-BocNH-ethyl)-3-benzyl-imidazolium bromide 1b ⁴	57
2.4.7	Synthesis of 1-(2-BocNH-ethyl)-3-trityl-imidazolium chloride, 1c ⁴	57
2.4.8	Reaction of 1a with KOBut.....	58
3	Counterion exchange	58
3.1	Introduction	58
3.2	Results and Discussion.....	59
3.2.1	Synthesis of 1-(2-t-Butoxycarbonylamino-ethyl)-3-methyl-3H-imidazolium hexafluorophosphate ([2][PF ₆]):.....	59
	Synthesis of 1-(2-t-Butoxycarbonylamino-ethyl)-3-methyl-3H-imidazolium perchlorate ([2][ClO ₄])	62
	Synthesis of 1-(2-t-Butoxycarbonylamino-ethyl)-3-methyl-3H-imidazolium bis(trifluoromethylsulfonyl)imide ([2][NTf ₂])	62
3.3	Experimental Section	67
3.3.1	Synthesis of 1-(2-t-Butoxycarbonylamino-ethyl)-3-methyl-3H-imidazolium hexafluorophosphate ([2][PF ₆])	68
3.3.2	Synthesis of 1-(2-t-Butoxycarbonylamino-ethyl)-3-methyl-3H-imidazolium perchlorate ([2][ClO ₄])	69
3.3.3	Synthesis of 1-(2-t-Butoxycarbonylamino-ethyl)-3-methyl-3H-imidazolium bis(trifluoromethylsulfonyl)imide ([2][NTf ₂])	69

3.3.4	Synthesis of 1-(2- <i>t</i> -Butoxycarbonylamino-ethyl)-3-methyl-3 <i>H</i> -imidazolium nitrate ([2][NO ₃])	69
4	Synthesis and Characterization of Imidazolium Salts incorporating a Benzyl Group	71
4.1	Introduction	71
4.2	Results and discussion.....	71
4.2.1	Synthesis	71
4.2.2	Deprotonation of imidazolium salts	75
4.3	Experimental Part.....	76
4.3.1	Synthesis of 1-benzyl-3-methyl-imidazolium bromide (1d).....	76
4.3.2	Synthesis of 1,3-dibenzyl-imidazolium bromide (1e).....	77
4.3.3	Synthesis of 1-benzyl-3-diphenylmethylimidazolium chloride (1f)	77
4.3.4	Synthesis of 1-benzyl-3-trityl-imidazolium chloride (1g)	77
4.3.5	Synthesis of 1-benzyl-3-tertbutylimidazolium bromide (1h).....	78
4.3.6	Synthesis of 1-tert-butylimidazole (Debus-Radziszewski reaction)	78
4.3.7	Synthesis of 1-benzyl-3-tert-butylimidazolium bromide (1h)	78
4.3.8	Synthesis of 1,3-dibenzyl-imidazolium triflate (1j)	79
4.3.9	Reaction of 1e with KO ^t Bu (1'e)	79
5	Synthesis and Characterization of Silver(I) Complexes <i>with N</i> -Heterocyclic Carbene Bearing the NHBoc Functionalization.....	81
5.1	Introduction	81
5.2	Results and Discussion.....	81
5.3	Experimental section.....	91
5.3.1	Synthesis of 1-(2-NHBoc-ethyl)-3-methyl-imidazolin-2-ylidene silver bromide (3a) 92	
5.3.2	Synthesis of 1-(2-NHBoc-ethyl)-3-benzyl-imidazolin-2-ylidene silver bromide (3b) 92	
5.3.3	Synthesis of 1-(2-NHBoc-ethyl)-3-trityl-imidazolin-2-ylidene silver bromide (3c)93	
6	Synthesis and Characterization of Silver(I) Complexes with N-Heterocyclic Carbene Bearing a Benzyl Group	94
6.1	Introduction	94
6.2	Results and discussion.....	94
6.3	Experimental section.....	98
6.3.1	Synthesis of 1-benzyl-3-methyl-imidazolin-2-ylidene silver bromide (3d).....	99
6.3.2	Synthesis of 1,3-dibenzyl-imidazolin-2-ylidene silver bromide (3e)	99
6.3.3	Synthesis of 1-benzyl-3-trityl-imidazolin-2-ylidene silver bromide (3g).....	100

6.3.4	Synthesis of 1-benzyl-3-tert-butyl-imidazolin-2-ylidene silver bromide (3h)....	100
7	Synthesis and Characterization of NHCs Rhodium Complexes with the NHBoc	
	Functionalization.....	103
7.1	Introduction.....	103
7.2	Results and Discussion.....	103
7.2.1	Synthesis of Rhodium(I) complexes and solution NMR studies.	103
7.3	Stereodynamics	106
7.3.1	Crystal Structure determination for 4a, 5a, 4c	111
7.4	Conclusion.....	116
7.5	Experimental Section	116
7.5.1	Synthesis of [RhCl(NBD){1-(2-NHBoc-ethyl)-3-methyl-imidazolin-2-ylidene}]. (4a)	117
7.5.2	Synthesis of [RhCl(NBD){1-(2-NHBoc-ethyl)-3-benzyl-imidazolin-2-ylidene}]. (4b)	118
7.5.3	Synthesis of [RhCl(NBD){1-(2-NHBoc-ethyl)-3-trityl-imidazolin-2-ylidene}]. (4c).....	119
7.5.4	Synthesis of [RhI(NBD){1-(2-NHBoc-ethyl)-3-methyl-imidazolin-2-ylidene}], (5a) by method B.....	119
7.5.5	Synthesis of 5a by ion exchange.	120
7.6	DFT Calculations	120
8	Synthesis and Characterization of NHCs Rhodium complexes with a Benzyl Group	
	Functionalization.....	121
8.1	Introduction.....	121
8.2	Results and discussion.....	121
8.2.1	Synthesis of Rhodium(I) Complexes and Solution NMR Studies.....	121
8.3	Stereodynamics	127
8.4	Kinetics	130
8.5	Crystal Structure Determination for 4d and 4e.	135
8.5.1	RhCl(NBD)(1- <i>n</i> Butyl,3-Methyl-Imidazolin-2-ylidene)	138
8.6	Conclusion.....	139
8.7	EXPERIMENTAL SECTION	139
8.7.1	Synthesis of [RhCl(NBD){1-benzyl-3-methyl-imidazolin-2-ylidene}] (4d).....	140
8.7.2	Synthesis of [RhCl(NBD){1,3-dibenzyl-imidazolin-2-ylidene}] (4e).....	141

8.7.3	Synthesis of [RhCl(NBD){1-benzyl-3-trityl-imidazolin-2-ylidene}] (4g)	141
8.7.4	Synthesis of [RhCl(NBD){1-benzyl-3-tert-butyl-imidazolin-2-ylidene}] (4h) ..	142
8.7.5	Synthesis of [RhCl(NBD){1-benzyl-3- <i>n</i> -butyl-imidazolin-2-ylidene}] (4i)	142
9	Catalysis.....	145
9.1	Introduction	145
9.2	Results and discussion.....	146
9.2.1	Hydrosilylation at 25°C with a catalyst loading of 1%	146
9.2.2	Hydrosilylation at 25°C with catalyst loading of 0,1%	157
9.2.3	Hydrosilylation at 60°C with catalyst loading of 0,1%	159
9.2.4	Addition of arylaldehydes to phenylboronic acid	161
9.3	Conclusions	163
9.4	Experimental Part.....	163
9.4.1	General procedure for the Hydrosilylation of 1-Alkynes with HSiMe ₂ Ph.....	164
9.4.2	Hydrosilylation products: ¹ H-NMR characterizations.	164
1.4.2	General procedure for the addition of arylaldehydes with phenylboronic acid.....	169
	Addition of arylaldehydes to phenylboronic acid products: ¹ H-NMR characterizations.	170
9.5	Appendix	173
9.5.1	Tables	173
9.5.2	Graphics	179
9.6	NMR Spectra and integrations	192
10	Iron-NHC Complexes	204
10.1	Introduction	204
10.2	Synthesis of Iron(II) Complexes	204
10.3	Experimental Section	208
10.3.1	Synthesis of [FeCp(CO) ₂ {1-benzyl-3-methyl-imidazolin-2-ylidene}][I] (7d) ..	208
10.3.2	Synthesis of [FeCp(CO) ₂ {1,3-dibenzyl-imidazolin-2-ylidene}][I] (7e)	208
11	Study of Norharman and its potential in catalysis	211
11.1	Introduction	211
11.2	Results and discussion.....	214
11.3	Conclusions	216
11.4	Experimental Section	216
11.4.1	Synthesis of 1,2,3,4-Tetrahydro-β-carboline-3-carboxylic acid. ⁵	217

11.4.2 Synthesis of β -carboline ⁵	217
11.4.3 Alkylation of β -carboline. ⁵	218
11.4.4 Deprotonation of the Norharman salt (8). ⁵	218
11.4.5 Preparation of the catalyst.	219
11.4.6 General procedure for the coupling reactions:	220

Summary

In the first chapter a general introduction on carbenes, *N*-heterocyclic carbenes (NHC) and their organometallic derivatives is reported together with highlights on recent developments in catalysis.

Chapters 2, 3, 4 describe the synthesis and characterization of two types of imidazolium salts: the first one having general formula [BocNHCH₂CH₂ImR]X (Boc = *t*Bu-carbamate; Im = imidazole) incorporates the NHBoc functionalization on the side chain; the second, with general formula ([BnImR']₂X, has always a benzyl group on one of the nitrogen atoms.

In chapters 5,6 the synthesis and characterization of a series of silver(I)-NHC complexes derived from the imidazolium salts described in chapters 2 and 4 is presented.

In chapters 7,8 the silver(I)-NHC complexes are used as transmetallating agents for the preparation of new rhodium(I)-NHC complexes with general formula [RhX(NBD)(NHC)] (NBD = norbornadiene). These complexes revealed a restricted rotation barriers about the metal-carbene bond that was studied by VT NMR and DFT calculations.

In chapter 9 the catalytic activity of the new rhodium complexes was investigated in the hydrosilylation of terminal alkynes with HSiMe₂Ph and in the addition of phenylboronic acid to benzaldehyde.

In chapter 10, preliminary results regarding the use of some of the prepared imidazolium salts as precursors for the synthesis of new iron(II)-NHC complexes are presented.

In the final chapter 11 the work developed during a six-months stay at the University of York (UK) under the supervision of Dr. R. E. Douthwaite on Norharman systems as σ -donor ligands in the palladium-catalyzed Suzuki-Miyaura cross-coupling of aryl bromides is presented and discussed.

1 Introduction

1.1 Carbenes – general introduction

Carbenes are uncharged compounds featuring a dicoordinate carbon atom with two valence shell electrons which do not participate in any bonding interactions. The carbon atom contains six electrons, which occupy $1s$, $2s$ and partially $2p$ orbitals. Depending on the degree of the hybridization of these orbitals, carbenes adopt different geometries: either nonlinear (bent), emerging from the sp^2 hybridization or linear in case of the sp hybridization (Figure 1.1-1).¹

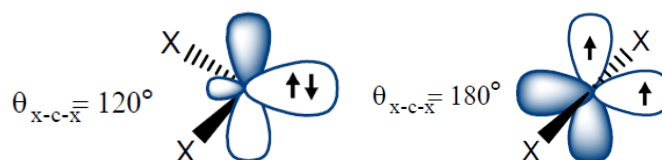


Figure 1.1-1 sp^2 and sp -hybridized orbitals of a carbon atom.

sp -type hybridization leads to mixing of $2s$ and $2p_z$ orbitals, whereas the two nonbonding $2p_x$ and $2p_y$ stay degenerate. The degeneracy is broken when a carbon atom adopts the sp^2 hybridization which involves the additional contribution of the p_x orbital. The latter one becomes energetically stabilized since obtaining some s character and conventionally, after Bertrand², is called σ , whereas the unchanged p_y is called p_π . Figure 1.1-2 presents the break of the degeneracy of the p orbitals after adopting the sp^2 hybridization.

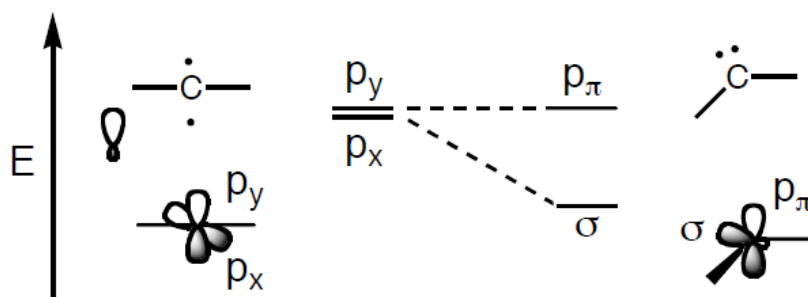


Figure 1.1-2 Break of the degeneracy of carbon's p orbitals when adopting the sp^2 hybridization.

1.1.1 Triplet vs. singlet carbenes

The two lone electrons of a carbene can be assigned to the two empty p orbitals of carbon atom in different ways. Four different electronic configurations are then possible for the sp^2 -hybridized carbon atom (Figure 1.1-3). According to the rule for determination of multiplicity of electronic states: $2S+1$, where S corresponds to the total spin, triplet and singlet carbenes can be specified. Triplet state results from two singly occupied nonbonding p orbitals by two electrons with parallel spins, whereas an excited singlet state is attributed to two singly occupied nonbonding p orbitals by two electrons with opposite spins. Finally, there are two alternative configurations for a ground singlet state: one with the lone electron pair placed in the σ orbital leaving the p_π orbital vacant and the second one with an opposite configuration (p_π filled and σ vacant). Due to the electrostatic interactions between the two electrons, triplet state is usually lower in energy than the singlet states.

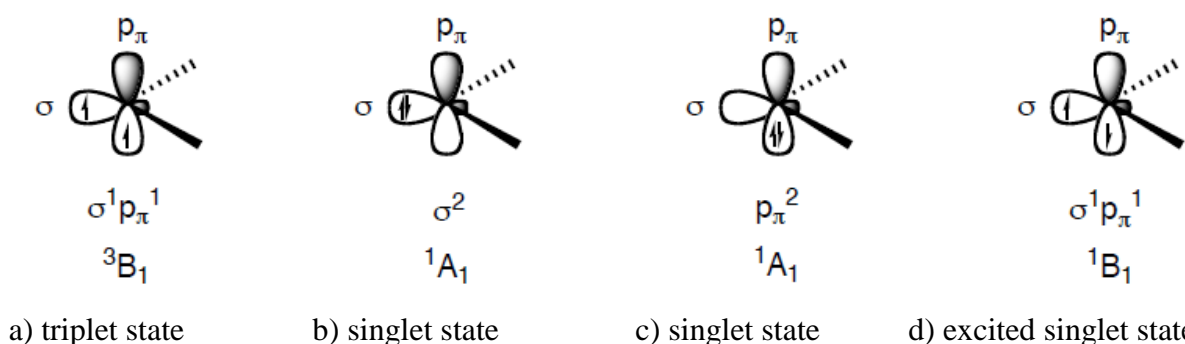


Figure 1.1-3 sp^2 hybrid structure of carbon atom with different assignment of the two nonbonding electrons.

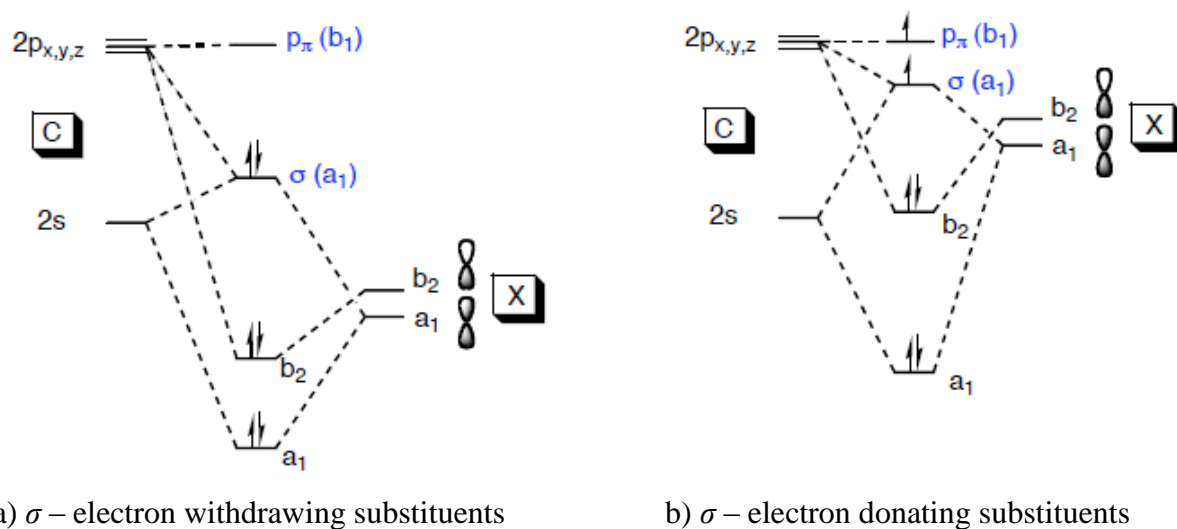
The carbene ground-state multiplicity is related to the relative energy of the σ and p_π orbitals. When the separation between these two levels is large, it is hardly likely for an electron to occupy the upper level, thus singlet state is favored. As a contrary, when these two levels become close to each other on the energy scale, one of the nonbonding electrons can easily ‘jump’ to the higher p_π level. Gleiter and Hoffman³ determined the limit of energy difference to be at least 2 eV to make the ground state of a carbene to be a singlet. Due to the fact that the nature of a substituent on carbon atom can tune the energy of the singlet–triplet splitting, the ground state spin multiplicity and subsequently the reactivity of a particular carbene depends both on electronic and steric effects supplied by the substituent groups.

1.1.2 Electronic effects

Electronic effects can be either inductive or mesomeric.

a) Inductive effects

Inductive influence of the substituents is related to their electronegativity. Electronegative atoms or groups are σ -electron withdrawing substituents, hence they inductively stabilize the σ nonbonding orbital by increasing its s character, leading to lowering its energy in the energy diagram. As a result, since p_π is unchanged, the gap is increased, favoring the singlet ground state. In case of σ -electron donating substituents (electropositive), the $\sigma - p_\pi$ is small and therefore the triplet ground state is favored. Figure 1.1-4 shows the influence of electronegativity of a carbon substituents on the energy gap between p_π and σ orbitals.



a) σ -electron withdrawing substituents

b) σ -electron donating substituents

Figure 1.1-4 Perturbation orbital diagrams showing the influence of the inductive effects.

Table 1.1-1 shows different substituents grouped accordingly to their electronic properties.

Table 1.1-1 Different types of substituents of a carbene center.

σ -withdrawing	σ -donating	π -withdrawing (Z)	π -donating (X)
-F	-Li	-COR	-F
-O		-CN	-Cl
-Cl		-CF ₃	-Br
-N		-BR ₂	-I
-Br		-SiR ₃	-NR ₂
		-PR ₃ ⁺ , ...	-PR ₂
			-OR
			-SR
			-SR ₃ , ...

b) Mesomeric effects

Mesomeric effects refer to the ability of carbene substituents to donate or withdraw electrons via π -type overlapping with the orbitals of a carbon; depending on the type of the substituents, three groups of singlet carbenes with different characteristics can be thus specified, after Bertrand terminology, the highly bent (X,X)-carbenes and linear or quasi-linear (Z,Z)- and (X,Z)-carbenes², where Z refers to π -withdrawing substituents and X to π -donating ones. (Figure 1.1-5).

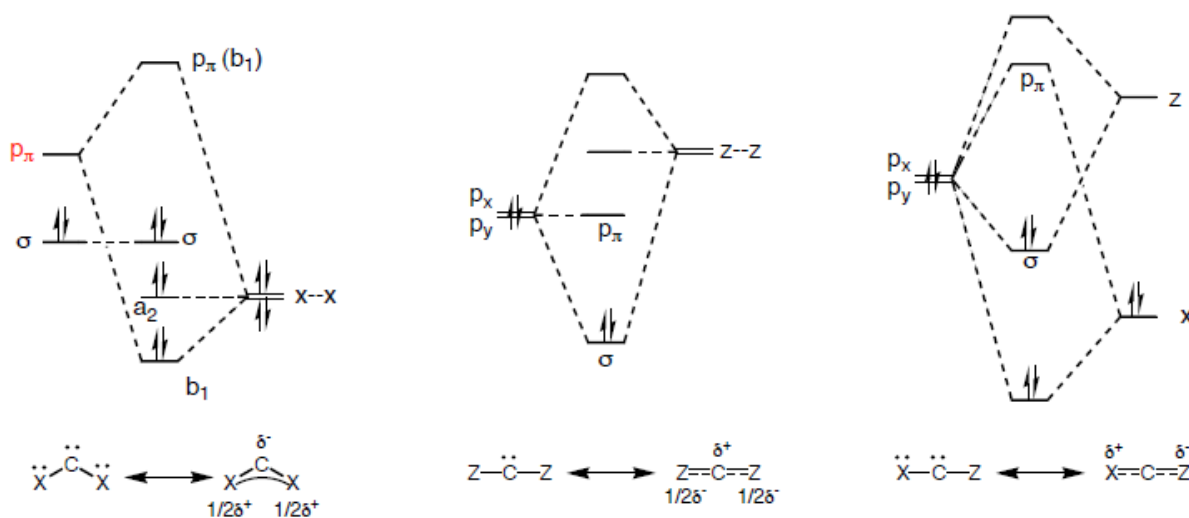


Figure 1.1-5 Perturbation orbital diagrams showing the influence of the mesomeric effects.

(X,X)-carbenes are built from two π -donor groups being at the same time σ -attractors (electronegative) attached to a carbon atom. This way of substitution is called: push, push mesomeric-pull, pull inductive pattern. An interaction between the substituent lone pairs with the vacant carbon p_π orbital leads to a significant increase of the energy of the latter which means a break of the degeneracy between p_π and σ , which in turn support the bent geometry of the carbenes. The most representative examples of these carbenes are diaminocarbenes together with the group of NHC (N-heterocyclic carbenes). The stability of these species relies on a preservation of the electroneutrality of the carbene center. Lone electron pair on a carbon is stabilized by inductive effect of electronegative nitrogen atoms, which on the other hand donate electrons to the nonbonding orbitals of the carbene center (Figure 1.1-6), imposing some multiple bond character; accordingly, the formal structure of carbenes can be written as a superposition of two zwitterionic structures, shown in Figure 1.1-7.

The π donation induces the nucleophilicity of the carbenes.

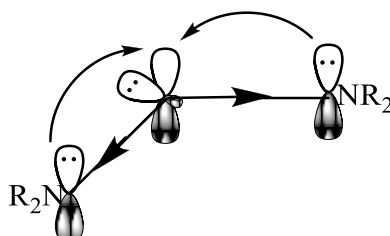


Figure 1.1-6 Electronic effects of the substituents for diaminocarbenes.

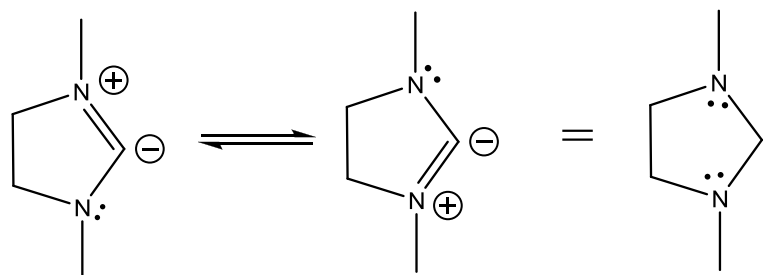


Figure 1.1-7 Resonance structures of NHCs.

(Z,Z)-carbenes possess two substituents both of them being π -attractors σ -donors, which means an electron deficiency in one of the nonbonding p orbitals, compensated by the σ -donation of the electropositive substituents. Diborylcarbenes are examples of this group. Due to the withdrawal effect, the carbenes will act as electrophilic agents.

(X,Z)-carbenes possess two different substituents (π -donor and π -acceptor) which exert an opposite influence. Each of them interact with different p carbon orbitals (p_y and p_x , respectively). The destabilization of p_y and stabilization of p_x breaks the degeneracy, favoring the singlet ground state, even though the geometry is linear due to the sp hybridization. Examples of the push, pull mesomeric substituted carbenes are phosphinophosphoniocarbenes. The last two groups of carbenes will not be discussed in details in the following thesis.

Finally, steric effects are related to the bulkiness of carbon substituents. Bulky substituents kinetically stabilize all types of carbenes. Due to steric interactions, two big substituents will stabilize linear geometry of carbenes, thereby the degeneracy of carbon orbitals and in turn the triplet ground state.

1.1.3 Reactivity

The ground-state spin multiplicity of carbenes is directly related to their reactivity. A carbene in its singlet ground state, possessing a lone electron pair and a vacant p orbital shows an ambiphilic properties and is usually compared to that of carbenium ions (CR_3^+); on the other hand, a carbene in its triplet state with two singly occupied p orbitals is often compared to the diradicals $:\text{CR}_2$. These differences in electronic properties have a direct impact on the mechanisms, which these species react through.

The illustrative example of the difference in the reactivity of singlet and triplet carbenes is an addition to alkenes (discussed in details in section 1.8). Carbenes with a triplet ground state participate in stepwise radical additions, which go through an intermediate with two unpaired

electrons (stereoselective reaction), whereas singlet carbene can react in a single step (stereospecific reaction), Figure 1.1-8.

a)



b)

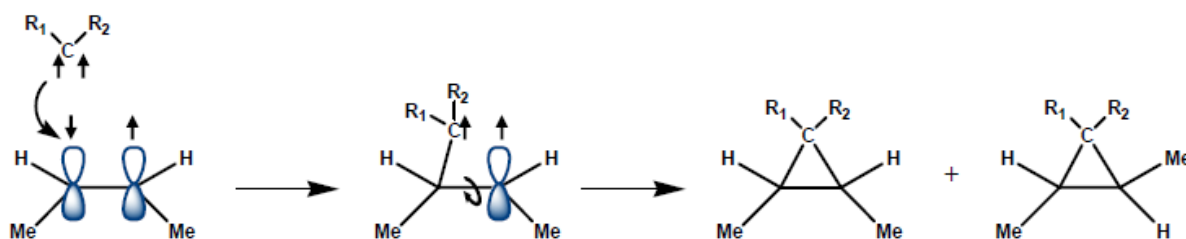


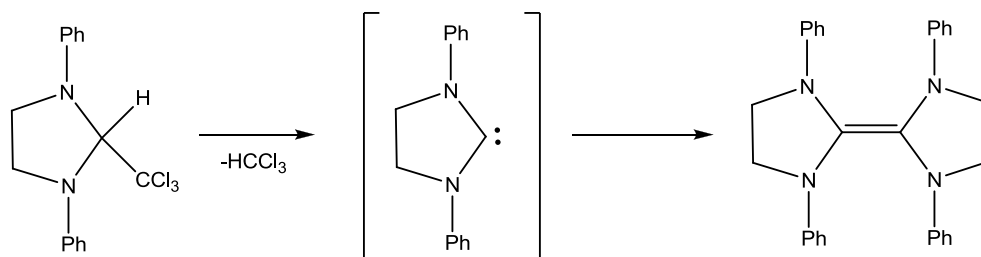
Figure 1.1-8 Addition reaction of a carbene to but-2-ene. The reaction is direct for a singlet carbene (a) and multistep for a triplet carbene (b).

1.1.4 N-Heterocyclic Singlet Carbenes

N-heterocyclic carbenes belong to a wider group of diaminocarbenes; they form complexes with any type of main group and transition metal elements of the periodic table; they are characterized by a great diversity of structural motifs and thus offer a wide range of possibilities for fine-tuning the steric pressure on both the carbene and the coordinated metal, modulating the catalytic properties.

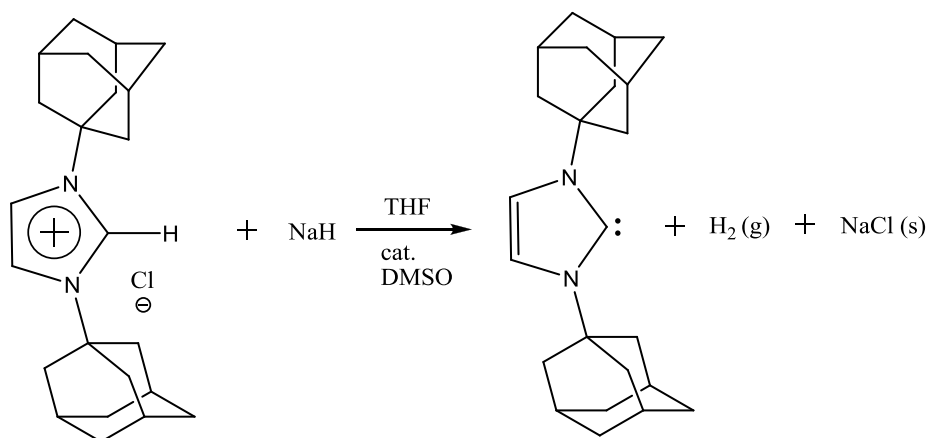
1.1.5 Synthesis

The first efforts to isolate a carbene were put in the early 1960s by Wanzlick, shortly after the discovery of the first metal-carbene complexes (See section 1.4). *N*-heterocyclic organic salts were considered already at that time to be the most prominent precursors for stable carbenes, since some presumptions were employed with regard to an enhanced stability of carbenes possessing amino substituents. The proposed method relied on an extrusion of chloroform from the imidazolidene adduct by a thermal α -elimination as depicted in Scheme 1.1-1, but the reaction led directly to the dimeric electron rich olefin instead of the desired monomeric carbene.⁴



Scheme 1.1-1 Reaction carried out by Wanzlick in order to isolate a first stable carbene.

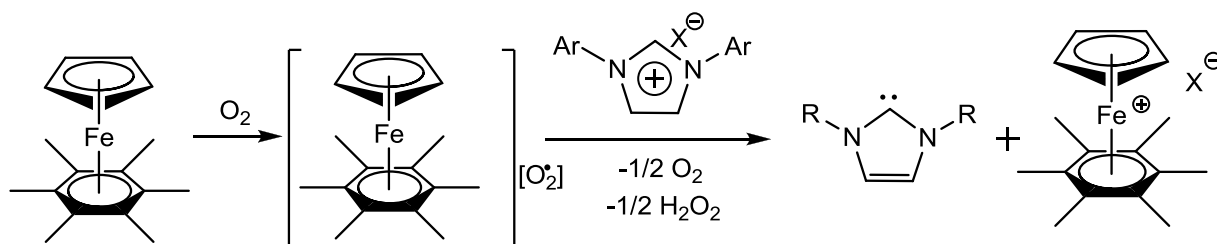
Subsequent work of Wanzlick brought an idea that imidazolium salts with enough bulky substituents on nitrogen atoms could be deprotonated by a base, for example potassium *tert*-butoxide. The idea was realized by Arduengo, when in 1991 he obtained 1,3-diadamantyl-2,3-dihydro-1*H*-imidazol-2-ylidene as a crystalline and thermally stable compound, by deprotonation of the 1,3-di-adamantylimidazolium chloride with sodium or potassium hydride in the presence of catalytic amounts of either *t*BuOK or the dimethyl sulfoxide anion⁵ (Scheme 1.1-2).



Scheme 1.1-2 Arduengo's synthesis of the first stable *N*-heterocyclic carbene.

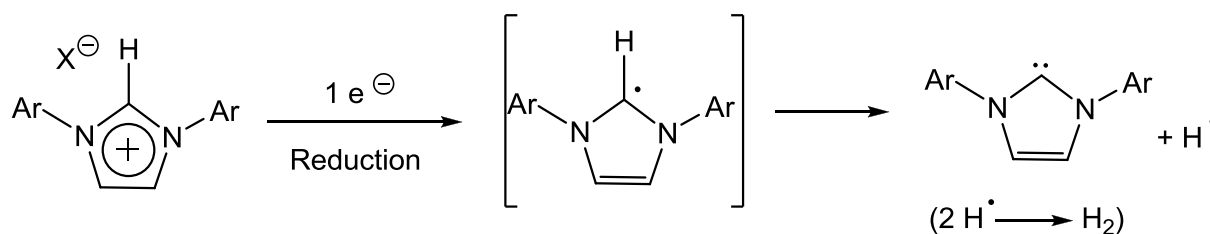
Starting from the first preparation method, few routes to stable singlet *N*-heterocyclic carbenes can be listed.

1. Deprotonation of imidazolium salts with a base (NaH, KH) in the presence of *t*BuO⁻ (or dimethyl anion CH₃S(O)CH₂⁻) either in liquid ammonia or in non-protic solvents such as THF or ethers. The deprotonation requires anhydrous conditions and the use of strong bases, with pK_a values above 14. Apart from KH and NaH, the following bases were also successfully employed for the deprotonation: *tert*-butoxide (*t*BuOK), lithium aluminum hydride (LAH), *n*-butyllithium (*n*-BuLi), potassium hexamethyldisilazide (KHMDS) and 1,8-diazabicyclo[5.4.0]undec-7-ene (DBU). Moreover, Nolan⁶ refers to the protocol proposed by Astruc et al. to deprotonate a series of imidazolium salts, using a radical anion superoxide as a base. The radical was formed in situ by reduction of ambient dioxygen with a 19-electron sandwich complex of Fe^I (Scheme 1.1-3).



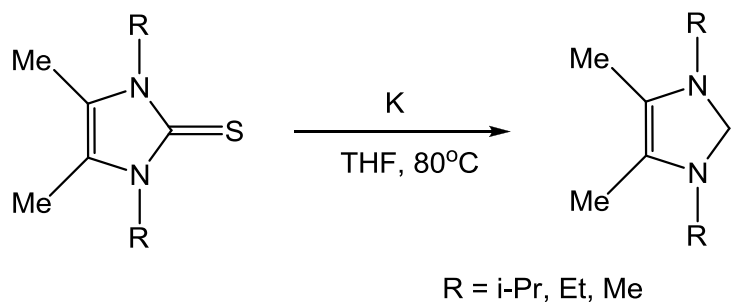
Scheme 1.1-3 Deprotonation of imidazolium salts, using a radical anion superoxide as a base.

2. Electrochemical or chemical reduction of imidazolium salts. A negative potential as low as -2.28 V and an excess of potassium in boiling THF is required to obtain the desired carbenes via the chemical reduction. The mechanism of a reduction process involves a formation of a radical imidazole intermediate, followed by a further loss of a hydrogen radical (Scheme 1.1-4).



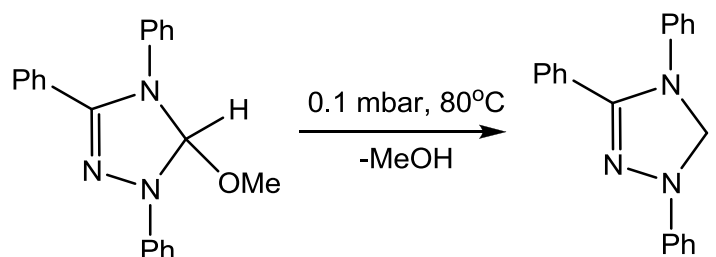
Scheme 1.1-4 Reduction of imidazolium salts.

3. Reduction of imidazole-2(3H)-thiones with potassium in boiling THF (Scheme 1.1-5).



Scheme 1.1-5 Reduction of imidazole-2(3H)-thiones.

4. Thermal elimination ($80^\circ C$) of methanol in vacuo from 5-methoxy-1,3,4-triphenyl-4,5-dihydro-1H-1,2,4-triazole affords 1,2,4-triazol-5-ylidene (Scheme 1.1-6).



Scheme 1.1-6 Thermal elimination.

1.1.6 Imidazolium precursors

As already mentioned, the most versatile method to obtain stable carbenes but also to synthesize complexes of NHCs with metals consists of using the corresponding imidazolium salts.

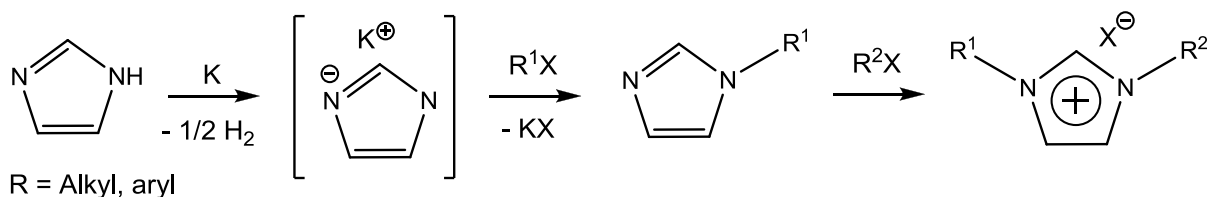
Generally, imidazolium salts are room-temperature non-aqueous ionic liquids (“NAIL”), commonly used as solvents in organic syntheses, which thanks to their unique physical-chemical and recently also widely studied biochemical properties hold applications in variety of scientific fields, such as: organometallic synthesis and catalysis, as electrolytes in electrochemistry, in fuel and solar cells, as a stationary phase for chromatography, as matrices for mass spectrometry, supports for the immobilization of enzymes, as liquid crystals, templates for the synthesis of nanomaterials,⁷ etc.

The first reported room temperature ionic liquids were 1-n-butyl-3-methylimidazolium tetrafluoroborate (BMI.BF₄), hexafluorophosphate (BMI.PF₆) and their analogues. The subsequently synthesized imidazolium salts contained alkyl groups on both N-sides of the imidazole fragment and particularly these types of the salts have been widely studied. These species are liquids in a broad range of temperatures (down to -80°C) and are characterized to have high thermal and chemical stability, large electrochemical window (up to 7 V), high density, relatively low viscosity, and very small vapor pressure. The listed characteristics of the imidazolium salts render them an excellent media for various transformations in solution. Since the ionic liquid effect on catalytic performance of organometallic species has been discovered by Calò,⁸ it is presumed that the beneficial activity can result from the facile conversion of the ILs into NHC-metal complexes;⁹ moreover, their use as immobilizing agents for transition metal catalyst precursors, is justified by an ease of product separation and catalyst recycling.¹⁰ Recently, the diverse array of applications of the ionic liquids based on the imidazolium moiety is expanded by functionalisation of the cation or anion of these species¹¹.

1.1.7 Synthesis of imidazolium salts

Synthesis of imidazolium salts can be roughly divided into two methods:

1. Alkylation of an existing imidazoles with appropriate electrophiles (Scheme 1.1-7).

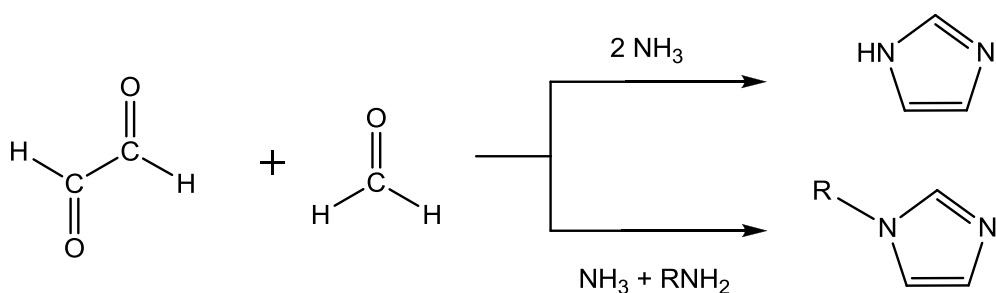


Scheme 1.1-7 Reaction between imidazole and potassium to generate an imidazolide anion and subsequent stepwise alkylation.

2. Ring formation.

“There are no really general ways of synthesizing imidazoles and it is invariably necessary to consider a number of divergent methods whenever a synthesis is contemplated.”¹²

In the literature indeed there are few synthetic procedures reported to afford heterocycles based on imidazole structure. However, the most commonly cited are derived from a general procedure, proposed by Debus in 1858 and developed by Radziszewski up to 1882.¹³ This reaction relies on a condensation of an α -dicarbonyl compound, an aldehyde and two equivalents of ammonia to afford the imidazole (or an 1 equivalent of ammonia together with an 1 equivalent of an amine, to obtain the 1-substituted imidazoles), Scheme 1.1-8. A variety of α -dicarbonyl compounds including glyoxal (a), pyruvaldehyde (b), porphyrin-2,3-diones (c) and benzyl (d) have been already used to successfully afford the corresponding imidazole derivatives.



Scheme 1.1-8 General scheme of Debus-Radziszewski reaction.

The general mechanism of this reaction has not been established, but the most likely route would be initiated by a successive nucleophilic attack of the two molecules of ammonia (alternatively ammonia and an amine) lone pairs towards the carbonyl carbon atom of the α -dicarbonyl compound, coupled with an elimination of water molecules to afford the corresponding Schiff base (α -diimine). The subsequent condensation with an aldehyde leads to a formation of the

desired imidazole derivative. Figure 1.1-9 shows the proposed mechanism to obtain a substituted imidazole ring at position 2 and a side reaction leading to formation of oxazole.

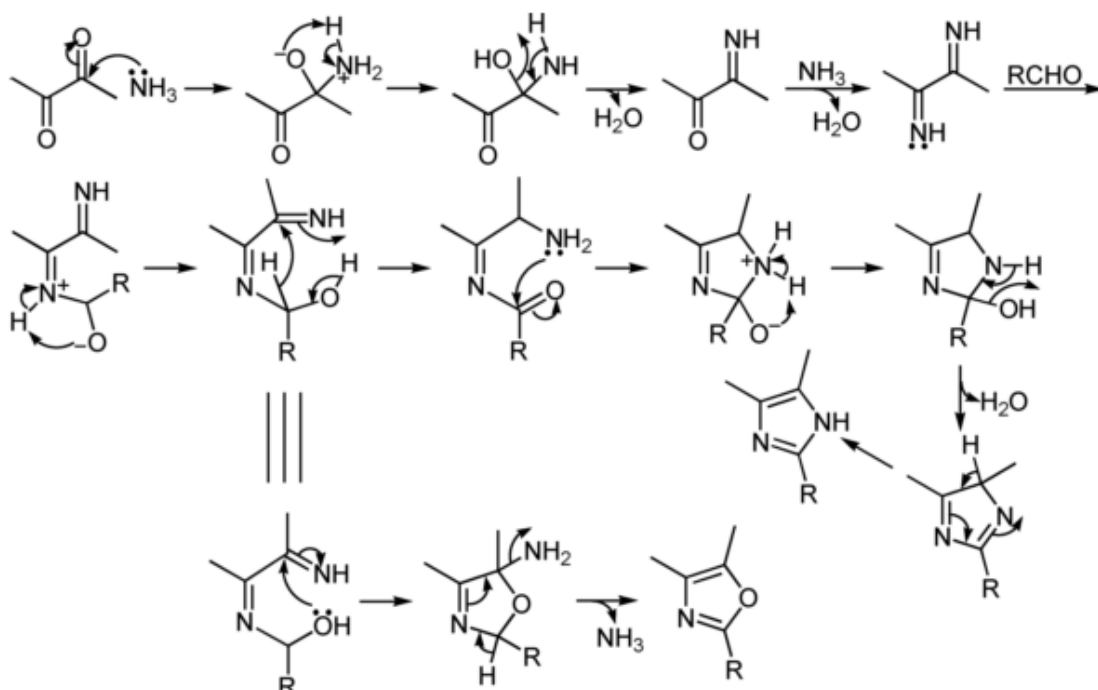
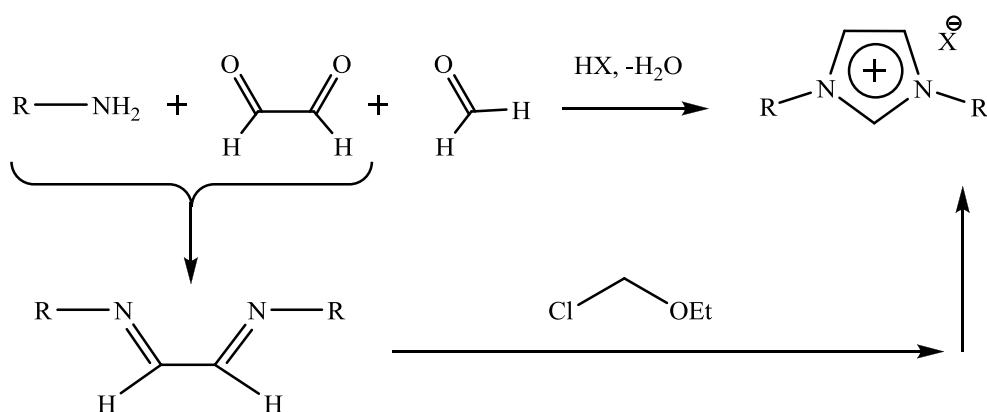


Figure 1.1-9 Proposed mechanism of Debus-Radziszewski reaction of synthesis of an imidazole derivative.

Specifically, the ring formation leading to the imidazolium salts can be realized in four ways, illustrated by the following schemes:

a) symmetric synthesis



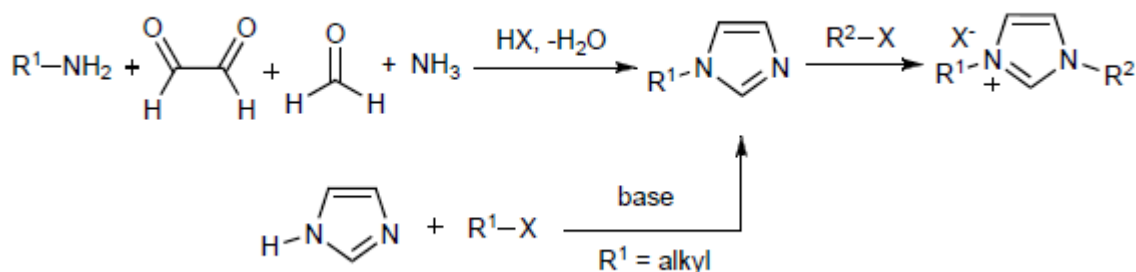
Scheme 1.1-9 Symmetric synthesis of an imidazolium salt.

The above reaction (Scheme 1.1-9) proceeds under acidic conditions through a coupling between the amine and the glyoxal to afford the corresponding Schiff base. Condensation with formaldehyde leads to the imidazolium salt.¹⁴ This one-pot reaction has been successively applied

for a formation of a symmetric N,N'-substituted imidazolium salts with various, bulky aryl- and alkyl- groups. An even more versatile modification of this method, proposed by Glorius et al.¹⁵ relies on the use of silver triflate with chloromethyl pivalate to generate in situ an alkylating reagent, which in a second step leads to an efficient cyclisation of different types of diimines. The described procedure consists of distinct steps with the previous isolation of the Schiff base.

b) unsymmetrical synthesis

An asymmetric mono N-substituted imidazoles, which can be subsequently N-alkylated, are synthesized by one-pot reaction between glyoxal, ammonia (or ammonium chloride), formaldehyde (or paraformaldehyde), and only one equivalent of primary amine (Scheme 1.1-10).



Scheme 1.1-10 Asymmetric synthesis of an imidazolium salt.

1.1.8 NMR and X-Ray diffraction of N-heterocyclic carbenes and imidazolium salts

The carbon atom placed between the two nitrogen atoms (or other X-type substituents like sulfur S) of the imidazolium cationic salts, resonates at the chemical shift in the range: 135 – 180 ppm. The signal deriving from the carbon atom of the corresponding stable carbenes is much more deshielded – chemical shift in the range 205 – 220 ppm for the unsaturated heterocyclic carbenes, and 235 – 245 ppm for the saturated equivalents and a very low field resonances: 235 – 300 ppm appear for acyclic aminocarbenes.

The bond angle NCN in a singlet cyclic carbenes is found to lay in the range 100 - 110°. Expectedly, the angle is bigger in structures of acyclic carbenes (around 120°) due to steric effects. The observed N-C_{carbene} bond lengths are between 1.32 and 1.37 Å, whereas the respective N-C bond in their organic ionic precursors is only a little shorter (1.28 – 1.33 Å). This increase in bond length could be attributed to a decrease in π -delocalization or $p\pi$ - $p\pi$ interaction in the carbene relative to the carbenium ion, however, the change in a hybridization at the carbene center between carbenium ion and carbene is an important factor which must be taken into account while

considering the change in the bond distances¹⁶. It is said that in the case of a free carbene, the in-plane lone pair of electrons at the carbene center is stabilized by more s-orbital character. As a consequence, the N-C σ -bonds take on more *p*-character at the carbene center; this leads to the observed increase in the N-C distances upon deprotonation of the imidazolium salts.¹⁶ To sum up, the discussed structural changes (decrease in C-N distances and increase in the N-C-N angle) appear to be typical for protonation of all singlet carbenes.

1.1.9 Electronic structure of N-Heterocyclic carbenes

Two theories contribute to the establishment of the electronic structure and stability of NHCs.

1. The statement of Dixon and Arduengo¹⁶ that stability of five-membered ring carbenes (Figure 1.1-10a) comes from the inductive effect of nitrogen atoms bonded to the carbene center. The theory is based on the results obtained from neutron and X-ray diffraction studies and fortified by a perfectly matching results from DFT calculations. Figure 1.1-10b shows a contour line diagrams of the electron density, which indicates high electron density in the plane of the molecule (blue cloud) and electron deficiency below and above the molecular plane (yellow cloud). Moreover, contour plots 70 pm above the molecular plane show the presence of the electron density localized only on nitrogen atoms and C=C double bond (Figure 1.1-10c).

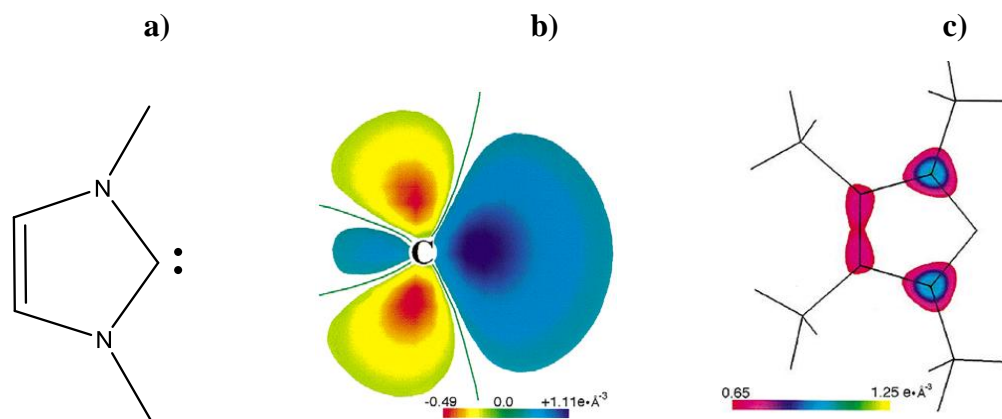


Figure 1.1-10 Valence electron density determined for 1,3,4,5-tetramethylimidazol-2-ylidene.

2. Theory confirming the presence of cyclic electron delocalization introduced independently by Apeloig and Frenking, derived from structural, thermodynamic and magnetic data and ionization potentials. Although this aromatic character is less pronounced than in the imidazolium salt precursors (as it has been confirmed by X-ray diffraction data, See section 1.2.3), it provides an additional stabilization of ca. 20 kcal/mol (Figure 1.1-11).¹

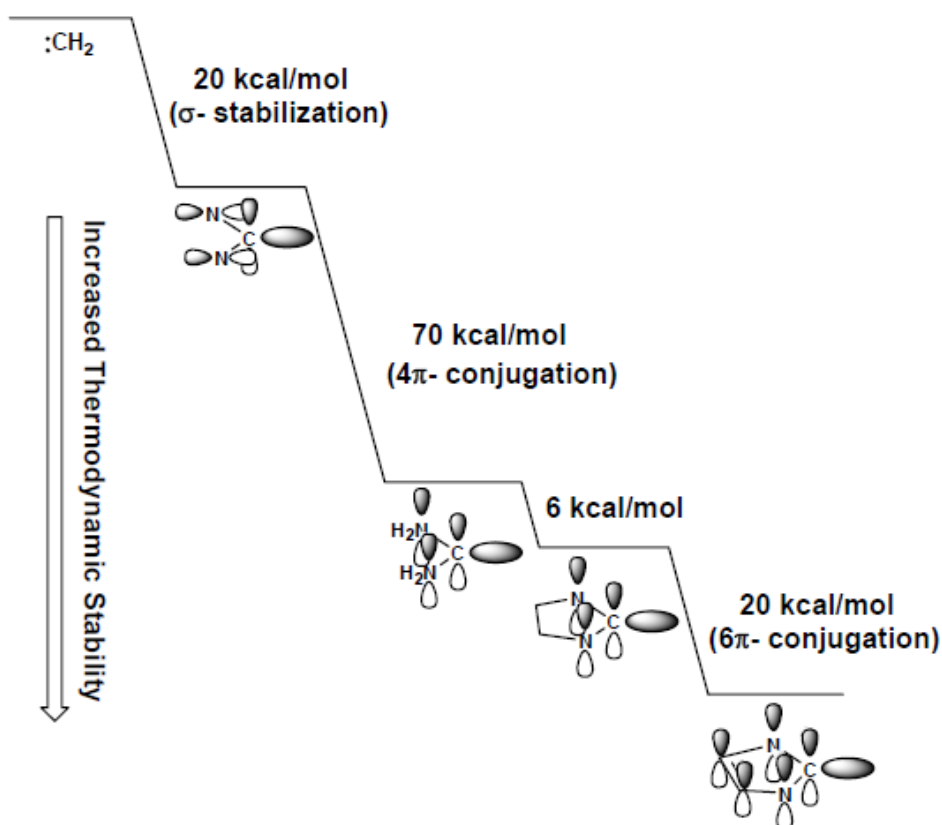


Figure 1.1-11 Diagram of thermodynamic stability of different carbenes obtained from DFT calculations.

Combining the two foregoing arguments, it can be concluded, that electron delocalization indeed occurs, nevertheless the major stabilizing effect is ascribed to the influence of the π -donors σ -attractors nitrogen atoms bonded to the carbene center. This statement is in agreement with the fact that non-aromatic aminocarbenes have also been isolated.

1.1.10 Reactivity

As it was briefly mentioned in the paragraph 1.1.5, the reactivity of singlet carbenes is determined by the potential of acting as both electrophilic and nucleophilic agents and these species can be used for a preparation of carbene-Lewis base and carbene-Lewis acid adducts, respectively.

1.1.11 Carbene dimerization

The dimerization reaction leading to the corresponding enetetramines makes a major limitation in synthesis of a stable diaminocarbenes. Two different mechanisms are proposed for the discussed reaction. The first one postulates the attack of the lone electron pair placed in the in-plane σ orbital of one carbene molecule toward the unoccupied out-of-plane p_{π} orbital of the other carbene (Figure 1.1-12). Since the carbene vacant orbital has a high energy resulting from the interaction with lone electron pairs of neighboring nitrogen atoms, the energy of the formed double bond should be high, which is in agreement with experimental data (dimerization energy 19-45 kcal/mol).

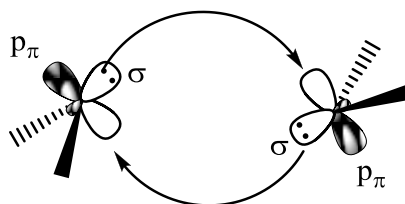


Figure 1.1-12 Schematic representation of the dimerization of singlet carbenes via interaction of lone electron pairs.

The second proposed mechanism relies on the nucleophilic attack of a carbene upon its conjugate acid (imidazolium salt) and a subsequent proton elimination.

The imidazolidinylienes (saturated ring systems) and imidazolylienes (systems containing one double bond) reveal an opposite stability with respect to the dimerization. In the case of the formers, the equilibrium is shifted towards the formation of the dimeric tetraazafulvalenes; in order to prevent the dimerization, the carbenes can be stabilized with sterically demanding substituents. On the other hand, the dimers of the imidazolylienes are unlikely to form, even in a case of the molecules with small substituents such as methyl group, (Figure 1.1-13).

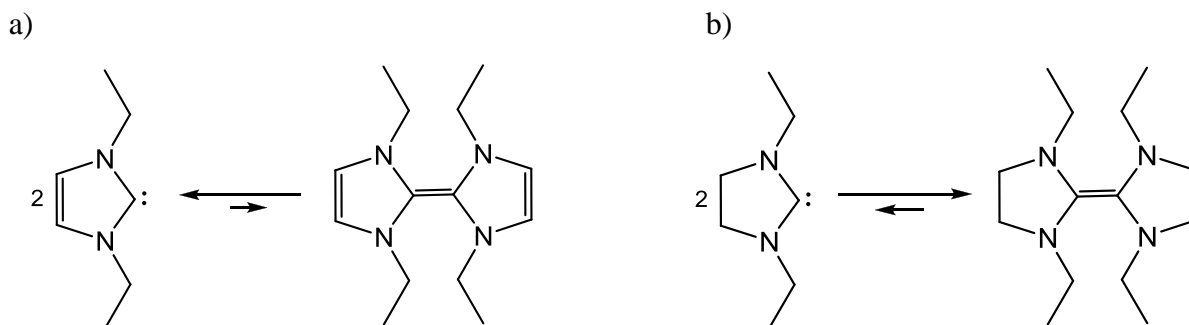
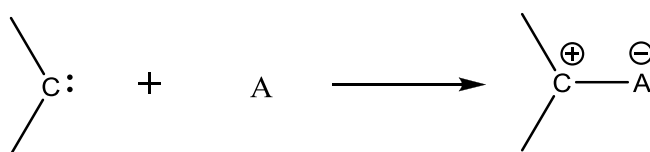


Figure 1.1-13 Stability toward dimerization of imidazolidinylienes (a) and imidazolylidenes (b).

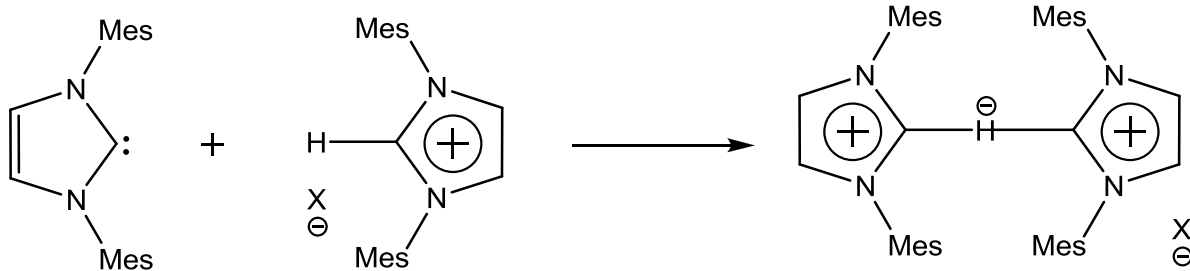
1.1.12 Carbene-Lewis acid and carbene-Lewis base adducts

a) The carbene-Lewis acid adducts (reverse ylides) result from the reaction between a nucleophilic carbene and an acid possessing an empty orbital, according to the Scheme 1.1-11;



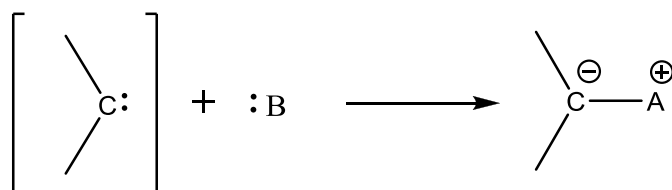
Scheme 1.1-11 Formation of reverse ylide from a free carbene and Lewis acid.

for instance adducts of carbenes with elements of groups 13, 14, 15, 16 and 17 of the periodic table are an example. Another interesting example of this kind of reaction is the protonation of a carbene. Particularly, the imidazol-2-ylidenes, being strong bases can go through the proton exchange between the free carbene and its conjugate acid as shown in Scheme 1.1-12; it is worth mentioning that the bis(carbene)-proton complex bearing significantly bulky mesityl substituents, has been isolated by Arduengo¹⁷.



Scheme 1.1-12 Protonation of a free carbene leading to unusual 3-center 4-electron biscarbene system.

b) On the other hand, the reaction between electrophilic carbenes with a lone electron pair of a donor leads to the formation of normal ylides, as reported in Scheme 1.1-13, for instance the carbene-pyridine adducts.



Scheme 1.1-13 Formation of a normal ylide from a free carbene and Lewis base.

1.2 Ionic Liquids as “Green Solvents”

In the last few decades the study and the investigation of ionic liquids (ILs) application has increased together with the interest in “Green Chemistry”. A great interest in this class of compounds has been centered on their possible use as “green” alternatives to the traditional volatile organic solvents. They have promising advantages such as an extremely low vapour pressure (generally negligible), which can match the human requirements of developing greener technologies. This is the reason why ILs are called “green solvents” in many early articles, and indeed the link between ILs and “Green Chemistry” is mainly related to the characteristic of low volatility. The “greenness” of ILs is also attributable to their non-toxicity, non-explosive and non-flammability that reduces the risk when treating fast, exothermic oxidation and also to their thermal and chemical stability.¹⁸

The ILs are salts with a melting point below 100 °C and many of them are found in liquid state at room temperature, the latter are called RTILs (Room Temperature Ionic Liquids) and this property makes them potentially useful compounds as solvents. In particular the solvents

investigated for chemical processes are typically constituted by an organic cations (examples are reported in Figure 1.2-1) and inorganic anions (examples are reported in Figure 1.2-2).

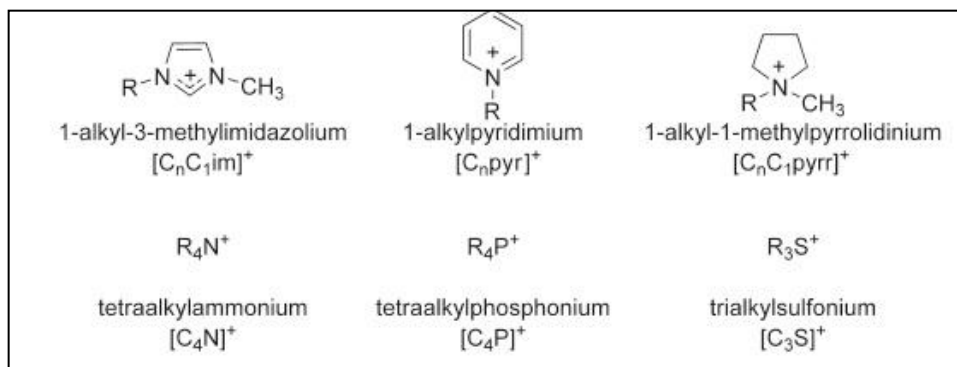


Figure 1.2-1 Some commonly used cations for ionic liquids.

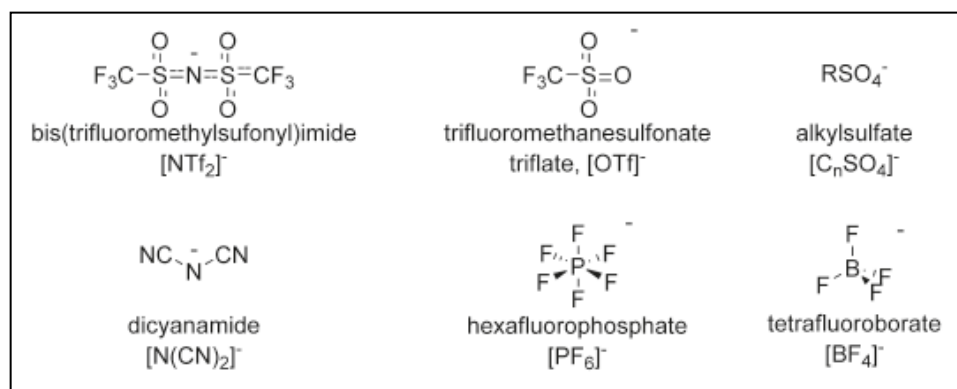


Figure 1.2-2 Some commonly used anions for ionic liquids.

In addition to their “greenness” feature, ILs are often referred as “designable solvents” mainly because their physical properties such as melting point, viscosity, density, solubility and coordination properties, can be tuned according to different reactions or processes by altering the combination of their anions and cations.¹⁹

With regard to the catalytic reaction some catalysts proved to improve their catalytic activity in ILs than in traditional solvents, moreover some catalytic reactions which do not work in common organic solvents can be performed in ILs. Another advantage of ILs in catalytic reactions is the efficient immobilization of the catalyst in the ionic liquid phase. The ILs are also able to dissolve many inorganic and organometallic compounds, therefore a large amount of catalysts having polar or ionic character can be immobilized in ILs, it means a easy separation and subsequent reuse of the catalyst.

1.3 The role of the counterion

As mentioned in the previous paragraph, the ionic liquids are particular salts liquid at room temperature and consist in a organic cation and an inorganic anion. The most widely studied ILs are composed of bulky and asymmetrical nitrogen-containing cations (e.g., imidazole, pyrrole, piperidine, and pyridine) in combination with a large variety of anions, ranging from simple halides to more complex organic species.

The ILs properties are controlled by the selection of both, so the change of cation and anion can affect many physical properties as melting point and solubility. In particular the miscibility of ionic liquids in water is a very important parameter because water is ubiquitous and even in little amounts could affect the properties of ILs.

Early investigations about water miscibility found that the behavior of ILs in water varies with the anion, for example in the case of 3-butyl-1-methyl-1*H*-imidazol-3-ium ($[C_4C_1im]^+$, Figure 4) was demonstrated that Cl^- , Br^- , $[OTf]^-$, and $[BF_4]^-$ give ionic liquids that mix with water in all compositions, whereas in the case of $[C(CN)_3]^-$, $[PF_6]^-$ and $[NTf_2]^-$ the ILS lead to a biphasic mixture with water (Figure 1.3-1).

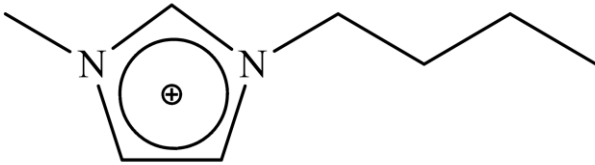
	
<u>Miscible with water</u> $[Cl]^-$, $[Br]^-$, $[OTf]^-$, $[BF_4]^-$	<u>Immiscible with water</u> $[C(CN)_3]^-$, $[PF_6]^-$, $[NTf_2]^-$

Figure 1.3-1 Solubility in water of $[C_4C_1im]^+$ with a different counterion.

For these anions of $[C_4C_1im]^+$ based ILs the octanol-water partition coefficient, K_{ow} , that quantify the hydrophobicity of a compound was measured and resulted to increase in the following order: $[OTf]^- < [BF_4]^- < Br^- < [NO_3]^-$, $Cl^- < [PF_6]^- < [NTf_2]^-$. This suggests that hydrogen bonding to the anion gives a significant contribution to the hydrophilicity of the ionic liquid. On the other hand, it was also observed that cation did not give a significant contribution to the hydrophilicity, in fact, spectroscopic studies did not evidence interactions between the water and the cation of the IL.

In presence of an increased amount of water the hydrolysis issue comes up. For water miscible-ionic liquids a self-associate dimeric structure in an “anion-water-water-anion” chain was observed. For ionic liquid that not mix fully with water the dimeric structures forms chain of

molecules and percolate through the ionic liquids' structures and cause them to break up into small ionic cluster Figure 1.3-2.

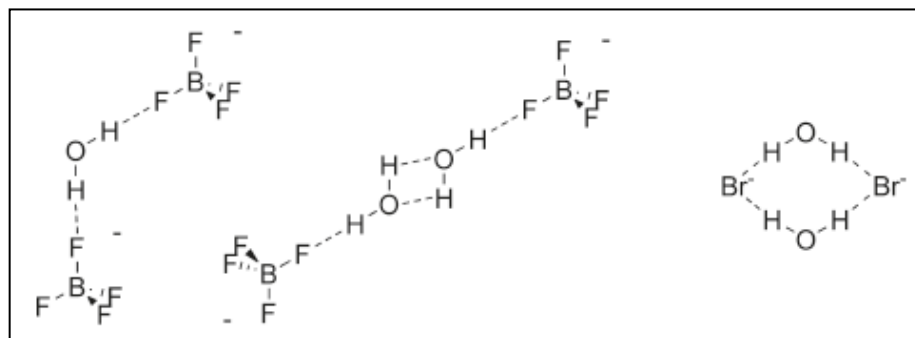


Figure 1.3-2 Some observed ionic liquid-water hydrogen-bonded structures:symmetric 2:1 anion-water, anion-water-water-anion chain, and anion-water-anion-water cyclic dimer.

1.3.1 The hexafluorophosphate problem

Imidazolium-based ILs with hexafluorophosphate anion have been the subject of extensive debates about their eventual decomposition into the toxic hydrofluoric acid. The hydrolysis of hexafluorophosphate was investigated under several experimental conditions by NMR spectroscopy and electrospray ionization mass spectrometry (ESI-MS). The results obtained show that the $[\text{PF}_6]^-$ anion decomposes under acidic conditions or high temperature to give different aggregate ions for example $[\text{F}_4\text{PO}]^-$ and $[\text{F}_2\text{PO}_2]^-$. The imidazolium cation remains unchanged but the length of the alkyl chain may increase the possibility of hydrolysis because the anion is less protected and hence more easily hydrolysable. These observations are very important for the application of ILs with hexafluorophosphate anion as reaction solvents under aqueous and acidic conditions.²⁰

1.4 N-heterocyclic carbenes–transition metal adducts

The first two metal (Cr, Hg) complexes with N-heterocyclic carbenes as ligands (Figure 1.4-1) were reported in the literature by Wanzlick²¹ and Öfele²² in 1968. Both of them were synthesized from the corresponding imidazolium salts and metal precursors containing a sufficiently basic group to deprotonate the salts.

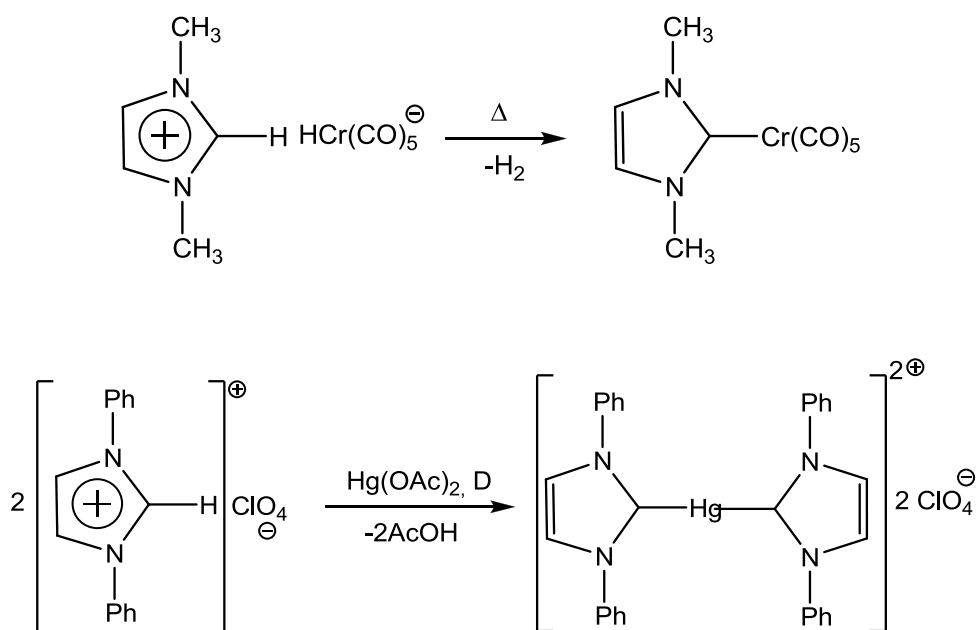


Figure 1.4-1 Two first metal complexes with N-heterocyclic carbenes as ligands.

synthesizing metal-carbene complexes due to its versatility with comparison to the first described route.²²

3. In situ deprotonation reaction of an imidazolium salt with a transition metal precursor in the presence of a base (K_2CO_3 , NEt_3 , etc.).²⁴

4. Reaction of the corresponding electron-rich olefin dimers with metal precursors leads to a imidazolidin-2-ylidene complexes.²⁵

5. Transformation of other C-bound ligands, for example inter- or intramolecular addition of N-nucleophiles to coordinated isocyanides.²⁶

6. Transfer of a carbene between different transition metal centers. The most commonly used NHC transfer reagents are Ag(I) complexes. This method is very well established for the preparation of a broad variety of transition metal-NHCs complexes such as: Au(I), Pd(II), Rh(I), Rh(III), Ir(I), Ir(III), Cu(I), Cu(II), Ru(II), Ru(III), Ru(IV), Ni(II), Pt(II).²⁷

7. Thermal decomposition of carbene adducts of alcohol, chloroform, pentafluorobenzene, CO_2 , CS_2 , cyanide and phosphonium in the presence of metal precursor.²⁸

8. Reaction of imidazolium salts and metal powders in air.²⁹

1.4.2 Electronic properties

Since the unique bonding properties of NHCs as ligands in transition metal chemistry determine the activity of the coordinated metal center, which in turn has an impact on catalytic properties of these systems, the electronic properties of the metal-carbene complexes were profoundly studied.

Two types of complexes can be distinguished according to the nature of bonding between a carbene and a metal.

1. **Fischer-type** complexes with the carbene-metal bond originating from the carbene to metal σ donation and the metal to carbene π -backdonation (donor-acceptor bond), Figure 1.4-3a.

2. **Schrock-type** complexes with the metal-carbene bond having covalent nature, resulting from the overlapping of singly occupied orbitals of triplet carbenes and triplet metal fragments, Figure 1.4-3b.

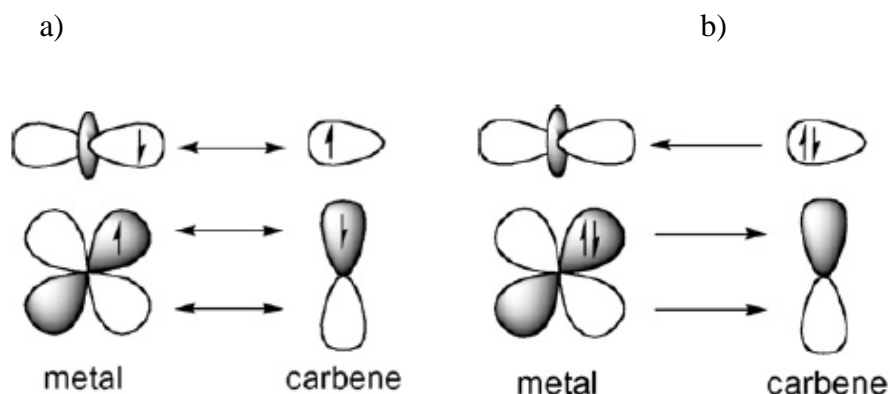


Figure 1.4-3 Metal–carbon bonding in Schrock (a) and Fischer (b) carbene complexes.

Fischer complexes are formed with electron-rich (low valent) metal atoms/cations and carbene centers stabilized by electron donation from the π -donor substituents. In contrast, Schrock complexes are formed with electron-poor metal centers (in high oxidation states) and π -withdrawing substituents.

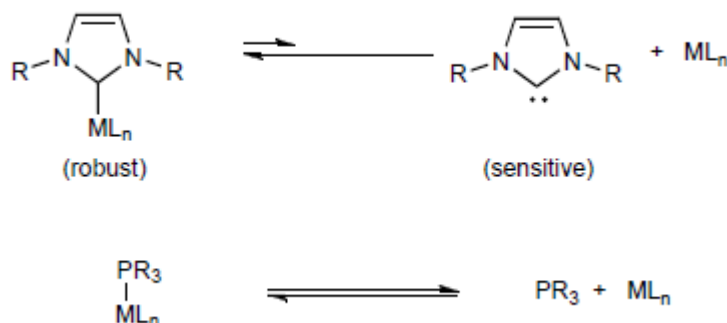
In 2000, Bertrand in his comprehensive review on stable carbenes highlighted the superiority of carbene to metal σ -donation over the metal to carbene π -donation in case of N-heterocyclic carbenes, describing the latter as negligible. The NHCs should be then considered as a non-classical Fischer complexes according to the definition given above. Bertrand at this point refers to the results obtained by photoelectron spectroscopy and DFT calculations presented by Arnold et al.³⁰ However, this point of view is not free from controversies and has been recently questioned;³¹ particularly, the π -back bonding component is reported to be significant for group 11 metals, copper, silver and gold^{5,32}. The general consensus in this affair can be formulated in a way that the π -back-donation to NHCs exists but is smaller than the π -back-donation of Fischer carbenes.

1.4.3 Comparison between phosphines and NHCs as ligands

For a long time, NHCs were considered to be so-called “mimics” of phosphines due to significant similarities in electronic properties.

In metal complexes, both of these two groups of compounds play the same role of monodentate two-electron donor ligands. The ability of phosphines and NHCs to accept electrons from orbitals of a metal was studied by the use of IR spectroscopy in a series of nickel, rhodium, iridium^{33,34} and iron³¹ complexes containing carbenes, phosphines and CO ligands. In a totally symmetric vibrational mode of CO specie, more basic ligands (better σ -donors) induce lower

vibrational frequencies. These studies showed that NHCs surpass even most basic phosphines in the electron donating ability and for this reason the bonds formed by NHCs with metals are considered to be stronger than the metal-phosphines, Scheme 1.4-1.



Scheme 1.4-1 Shift of equilibrium towards the formation of carbene-metal complexes from the free carbenes and comparison with the equilibrium for phosphines.

Another aspect differing phosphines and NHCs is the ability of the latter to form complexes with alkaline, lanthanides and high oxidation state metals in which the π -back-donation does not occur.

1.5 N-Heterocyclic carbene silver(I) complexes

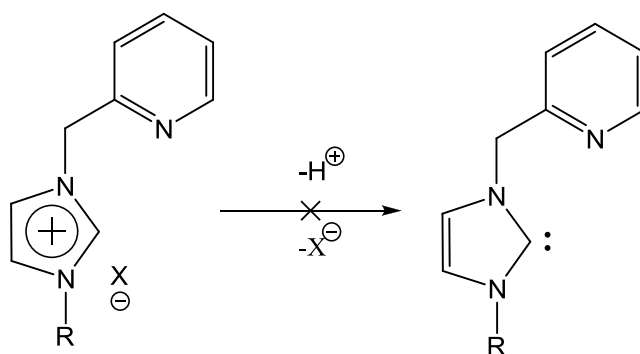
The high interest in studying Ag(I)-NHCs emerges mainly from the ease of their preparation and the transmetalation efficiency to obtain other important metal-NHCs. In addition, the silver(I) complexes hold potential applications in medicine, nanomaterials, liquid crystals and organic synthesis.

1.5.1 Synthesis

There are two general synthetic ways to obtain Ag(I)-NHCs: (1) the silver base method and (2) the free carbene method; additionally, Garrison and Youngs³¹ distinguish (3) the in-situ reaction of imidazolium salts with a base in a presence of silver salt and (4) the transmetalation between a complex of tungsten-NHC and silver precursor.

In spite of the fact that the first structurally characterized Ag(I)-NHC complex was synthesized via the free carbene and silver salt route, the use of Ag_2O both as a base and silver source in the complexes syntheses is most common among the other possibilities for few following reasons: (1) Ag_2O is relatively stable and readily accessible, (2) the reactions can be carried out in mild conditions, (3) special preparation of the solvents is not required, (4) chirality can be retained.

The free carbene route is not favorable due to the requirement of using strong bases such as KH or KO^tBu; the main risk is that the base can attack other acidic protons in the ligand. This argument is especially significant for ligands containing methylene groups in α position with respect to the nitrogen atom, where the deprotonation usually leads to the products of decomposition instead to the free carbene (Scheme 1.5-1).



Scheme 1.5-1 Unsuccessful deprotonation of methylene-linked imidazolium salt.

1.5.2 Structures.

The Ag(I)-NHC complexes reveal a great structural diversity in the solid state. Whereas the imidazolium ligands in the presence of silver source and non-coordinating anions form invariably a structural motif with two carbene moieties bound to the silver cation, the silver complexes with coordinating anions like halides, are found to form five different bonding motifs, presented in Figure 1.5-1.

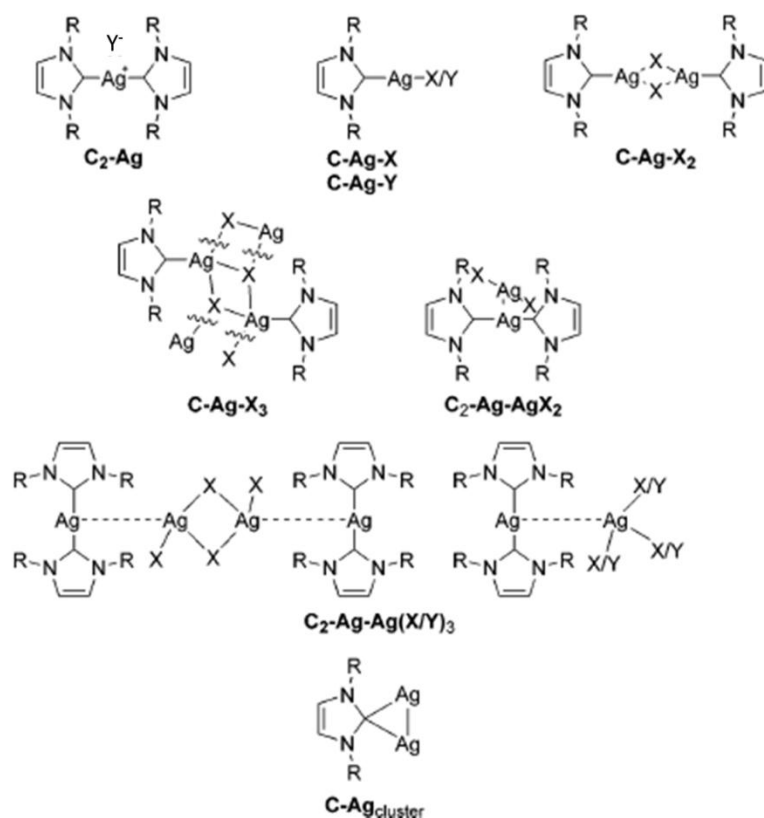


Figure 1.5-1 Bonding motifs of silver N-heterocyclic carbenes. X = halide and Y = non-halide.

These structures are described as: coordinating (C-Ag-X/Y), bridging (C-Ag-X₂), staircase (C-Ag-X₃), halogeno counterion of type [AgX₂]⁻ (C₂-Ag-AgX₂), halogeno counterions of type [Ag₂X₄]²⁻, and silver NHCs with silver-silver interactions that are stabilized by three donor groups.

1.5.3 NMR

One of the most common techniques, used for a characterization of the Ag(I)-NHCs, is ¹H and ¹³C NMR spectroscopy, which is justified by the experimental difficulty to obtain single crystals suitable for the X-Ray diffraction. In fact, the information about the presence of the silver complexes gained from the NMR experiments is immediate. The characteristic feature of ¹³C NMR spectrum is the resonance of the carbon atom of carbene coordinated to silver, appearing over a wide range of chemical shift: 213.7 – 163.2 ppm³¹. The observed signal appears as a singlet, or a doublet due to the coupling to the magnetically active silver nucleus, with a spin of 1/2. Silver has two naturally occurring isotopes, ¹⁰⁷Ag and ¹⁰⁹Ag, with a percent abundance of 51.839(7)% and 48.161(7)%, respectively. The ¹J coupling constants range from 180 to 234 Hz and 204 to 270 Hz³¹ respectively for the two isotopes. Therefore in theory, the expected splitting pattern in the cases where the coupling is observed, should be consisted of a doublet of doublets due to the presence of

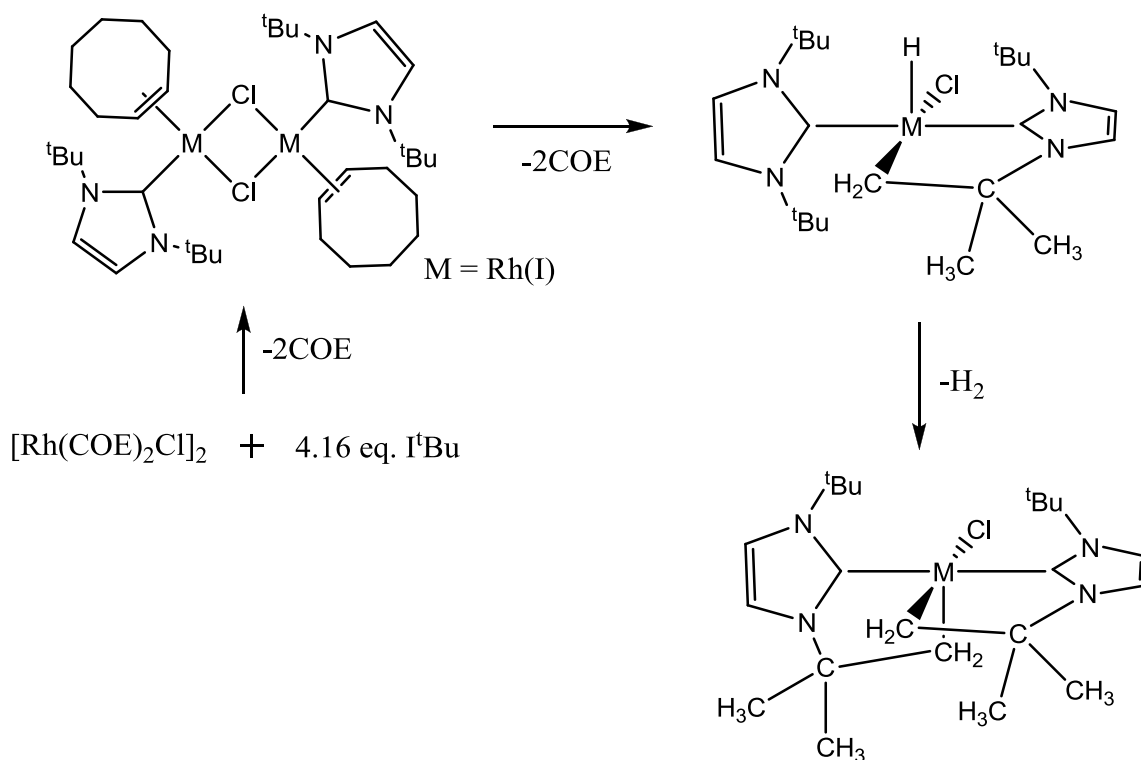
the two isotopes. However, in majority of cases the splitting is not observed. This interesting property of the spectra was attributed by Lin and coworkers³⁵ to the fluxionality of silver NHC complexes on the NMR time scale. The presence of the singlet is explained by the increase of the velocity of the exchange of the ligands, resulting in the averaged picture in ¹³C NMR spectrum. On the other hand, the presence of the doublet (or doublet of doublets) indicate either a static conformation of the complex in question, or a process which is very slow on NMR time scale.

1.6 Rhodium(I)-NHC complexes

Most of the rhodium(I) complexes with NHCs described in the literature were synthesized via transmetalation from corresponding silver(I)-NHC complexes in the presence of adequate rhodium precursor; this method has the advantage of avoiding the harsh reaction conditions provided by the use of a strong base to form the free carbene; consequently, the syntheses from silver complexes afford the rhodium compounds in high yields (70-90%). This protocol has been used for the first time in 2003.³⁴

As it was mentioned before, some rhodium-NHC complexes containing carbonyl derivatives as ligands, likewise few other transition metal complexes (Ni, Ir and Fe) have been employed as probes for the basicity of the N-heterocyclic ligand, by means of IR spectroscopy; this method allows for the determination of Tolman electronic parameters for NHCs.

Moreover, rhodium (and iridium and iron³⁶)-NHC complexes reveal unique properties (never observed before in the NHC chemistry, neither for other phosphine-related complexes³³), namely aliphatic and aromatic C-H activation^{37,38}; these (mostly) intramolecular processes lead to corresponding cyclometalated species. Specifically, a very interesting, highly unusual behavior has been reported by Nolan et al. for a rhodium dimer [Rh(COE)₂Cl]₂ (COE=cyclooctene) reacting with I^tBu = N,N-di(tert-butyl)imidazole-2-ylidene, shown in Scheme 1.6-1.



Scheme 1.6-1 Unprecedented reactivity between I^{tBu} and $\text{Rh}(\text{I})$ dimer leading to doubly cyclometalated complex.

Furthermore, some rhodium-NHC complexes, bearing a sterically demanding ligand such as COD (1,5-Cyclooctadiene) or NBD (norbornadiene), display restricted rotation about the metal-carbene bond (which is essentially single), the rate of which can be controlled by altering the steric bulk of the auxiliary ligands. For instance chiral triazolindene rhodium complexes containing an axis of chirality (Figure 1.6-1) has been described by Enders et al.^{39,40}

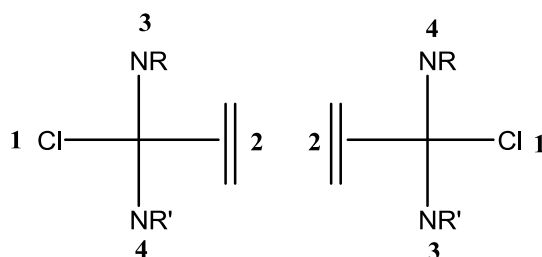


Figure 1.6-1

The latter described complexes are a kind of atropisomers which are stereoisomers resulting from hindered rotation about single bonds where the steric strain barrier to rotation is high enough to allow for the isolation of the conformers;⁴¹ they display an axial chirality which generates

enantiomers in the absence of stereogenic centers. This class of compounds has attracted considerable attention due to its potential in asymmetric syntheses and catalysis.

Formally, atropoisomers are conformers that interconvert with a half-life of more than 1000 seconds at a given temperature. Atropoisomerism was first time detected in biaryl compound 6,6'-dinitro-2,2'-diphenic acid in 1922 (Figure 1.6-2);

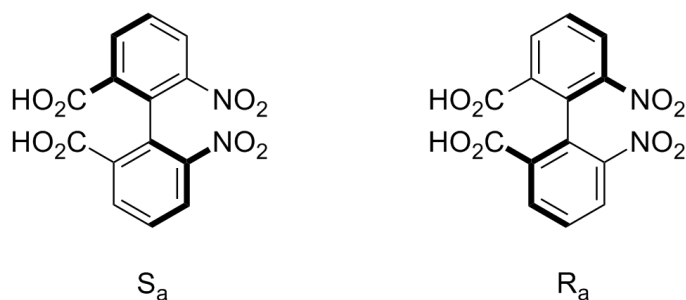


Figure 1.6-2 Atropoisomers of 6,6'-dinitro-2,2'-diphenic acid.

The equilibrium between atropoisomers can be reached thermally, as opposite to other chiral compounds, which must be treated chemically.

1.7 Iron(II)-NHCs complexes

The inquiry into *N*-heterocyclic carbene piano-stool iron(II) complexes within the framework of this thesis arises from the fact that these systems reveal particular properties.³¹ First of all they have been already investigated as a probes for the bonding of *N*-heterocyclic carbenes to transition metal complexes and this study opened a new perspectives for the interpretation of the acceptor properties of the carbenes. Additionally, the iron is an interesting alternative to other transition metals used in homogeneous catalysis, because it is cheap, non-toxic, environmentally friendly and abundant;³⁶ specifically, the iron complexes display the catalytic activity in hydrosilylation of carbonyl derivatives and hydrogen transfer reactions. However, despite the interesting chemistry behind, iron is still one of the rare transition metals which has not been intensively studied in the context of NHCs.

The particular constitution of piano-stool iron(II) complexes, which possess both the redox active Fe^{II} center and CO ligand(s), makes them to be an attractive probes for measuring the carbene basicity in a quantitative way (Figure 1.7-1).

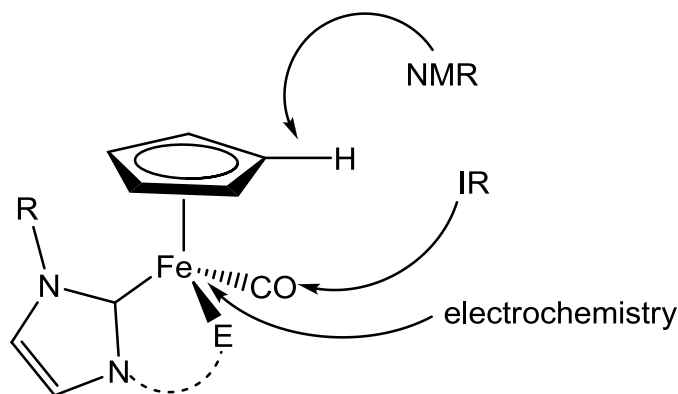


Figure 1.7-1 Direct and indirect probes for ligand tuning in Fe(II) carbene complexes.

1.7.1 Electrochemical measurements

The possibility of using electrochemical analysis for the ligand basicity determination, relies on the fact that ligands being strong σ donors can easily saturate the metal center with the electron density, which leads to the facilitated oxidation of iron(II) to iron(III). As a consequence, the $\text{Fe}^{\text{III}}/\text{Fe}^{\text{II}}$ redox potential can be used as a probe of the ligand basicity.³¹

The oxidation potential is much lower in case of the neutral iron(II) complexes than in the cationic forms. Moreover, the electronic parameters which can be derived from the electrochemical analysis indicate only a minor differences between the basicity of carbenes, pyridines and most basic phosphines.

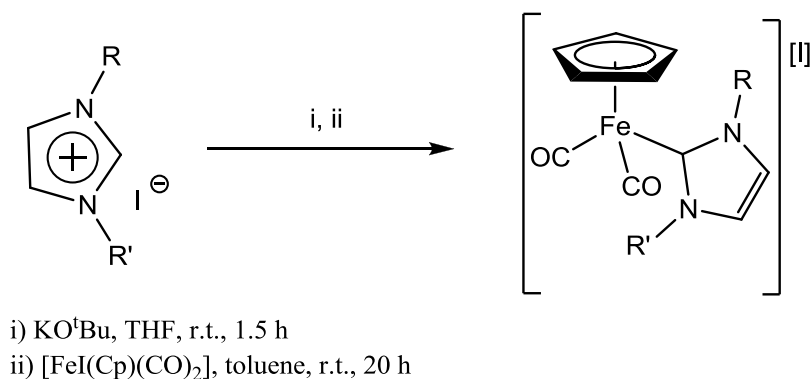
1.7.2 Nature of bonding of NHCs to iron

The information derived from the electrochemical measurements³¹ are in accordance with the ^1H NMR data, which show similar chemical shift for the cyclopentadienyl ring protons in iron complexes bearing pyridine and the ones bearing carbenes as a ligands. This suggests that there must be a significant contribution of π back-bonding from metal to carbene in order to balance the stronger effect of σ donation of carbenes when compared to pyridine. This indication is eventually confirmed by DFT and calculations of a transferred charge from metal to ligand in three iron complexes containing CO, pyridine and NHC, respectively. These results may be extrapolated for other metal-NHCs.

Finally, the orbitals which are involved in π back-bonding in the Fe-NHCs have been determined as the HOMO of the $[\text{Fe}(\text{Cp})(\text{CO})_2]^+$ fragment as a donor and the NHC's π^* antibonding orbital LUMO+1.

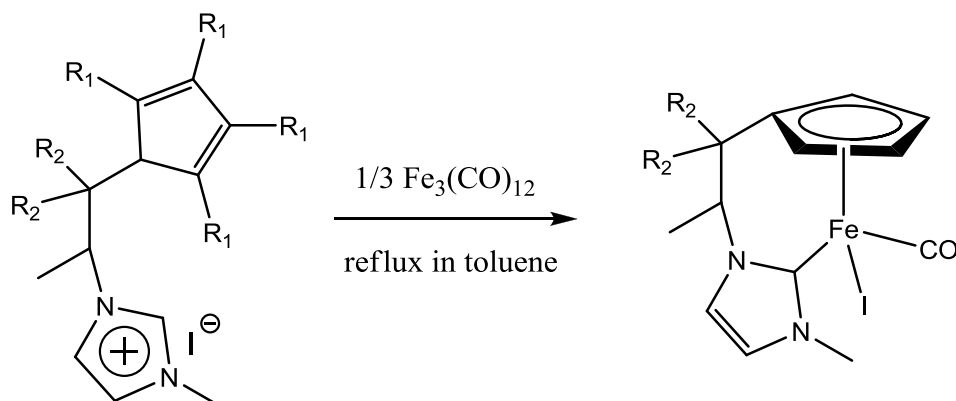
1.7.3 Synthesis

These complexes are obtained by synthetic route starting from corresponding imidazolium salts and followed by deprotonation with a strong base like KO^tBu and subsequent in situ metalation with iron(II) precursor $[\text{FeI}(\text{Cp})(\text{CO})_2]$ to form a cationic compound with a halide as a counter ion (Figure 1.8-1). Under UV irradiation, the complexes lose CO, which place is filled by the halide atom to afford neutral iron compounds.³¹



Scheme 1.7-1 Synthetic protocol leading to piano-stool iron(II) complexes

Another very interesting, unprecedented protocol has been proposed by Royo et al.³⁶ consisting in oxidative addition of the C–H bond of imidazolium to $\text{Fe}(0)$, followed by elimination of the Fe–H intermediate and the cyclopentadienyl proton, as shown in Scheme 1.7-2



Scheme 1.7-2 Synthesis of piano-stool iron(II)-NHC complexes under mild conditions.

This type of C–H activation is unique in Fe–NHC chemistry. The big advantage of this method is the lack of necessity to use a base, which can lead to the decomposition of imidazolium salts as precursors for the complexes synthesis. According to the report of Royo, the synthesis affords only one diastereoisomer in spite of the fact that the aliphatic linker between the NHC and the cyclopentadienyl ring and the metal center both possess a stereogenic centers.

1.8 Catalytic properties of transition metal-NHCs complexes

N-heterocyclic carbenes, due to their particular coordination chemistry, became recently “*broadly catalytically useful ligands*”⁴² with the potential to supplement and in part, replace the ubiquitous class of organophosphanes in a number of organometallic catalytic reactions. NHCs both stabilize and activate metal centers in different catalytic steps of organic syntheses, for example, C-H activation, C-C, C-H, C-O and C-N bond formation⁹. Nowadays, the most common NHCs used in catalysis are five-membered ring imidazolylidenes and imidazolinylienes, whose impressive versatility has been proven in many types of catalytic reactions.⁴³ Their outstanding potential as supporting ligands in metal-mediated catalytic reactions arises mainly from the remarkable stability of the formers, due to the strong σ -electron-donating properties of NHC which prevent the dissociation of the carbene from the metal center.

Additionally, N-heterocyclic carbenes have been found to be active in asymmetric catalysis. The preparation and use of enantiomerically pure complexes with a chirality introduced to different parts of the carbene molecules has been reported; the complexes can feature either chiral substituents at the nitrogen atoms, a chiral ring framework, a chiral metal center or a chiral backbone (Figure 1.8-1).

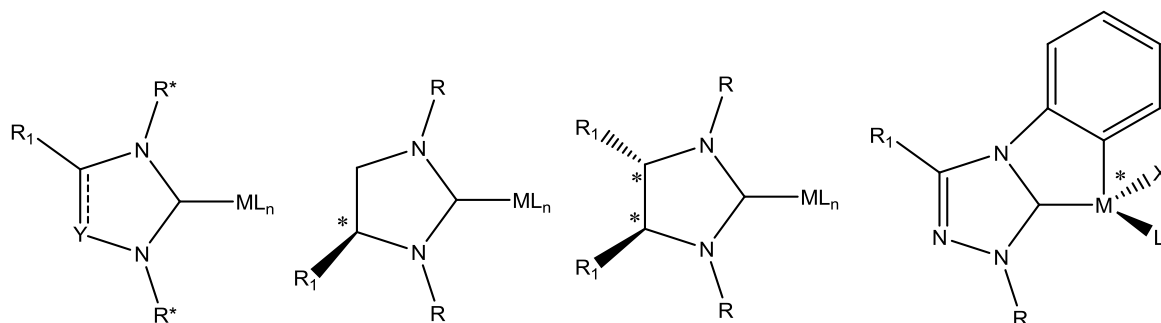
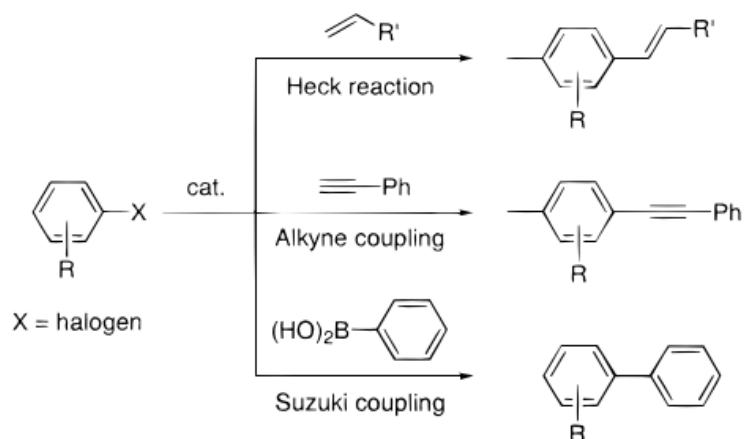


Figure 1.8-1 Different types of chiral NHCs.

In the following overview of the most investigated catalytic reactions employing transition metals-NHCs as catalysts is reported.

1.8.1 Heck-type reactions

Heck-type reactions lead to products of coupling between halide-substituted aromatic species and unsaturated compounds such as alkenes, alkynes and aromatic rings, shown in Scheme 1.8-1.



Scheme 1.8-1 Heck-type reactions.

Catalysts used for these reactions are palladium complexes with the general formula $[\text{PdL}_2\text{I}_2]$ adopting the usual square-planar geometry and bearing two NHC (namely 1,3-dimethylimidazole-2-ylidene) and two iodides as ligands (Figure 1.8-2).

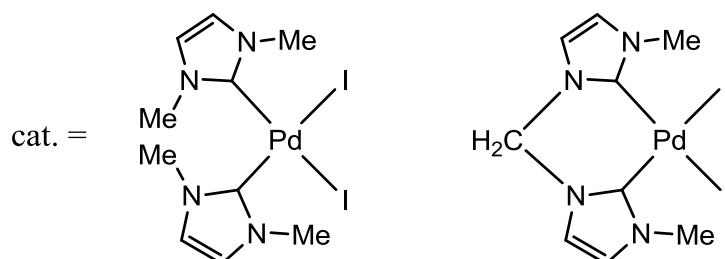
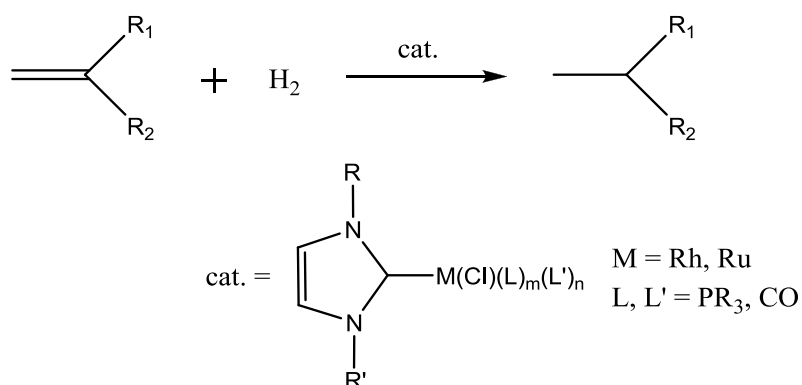


Figure 1.8-2 Palladium(II) catalysts for the Heck-type reactions.

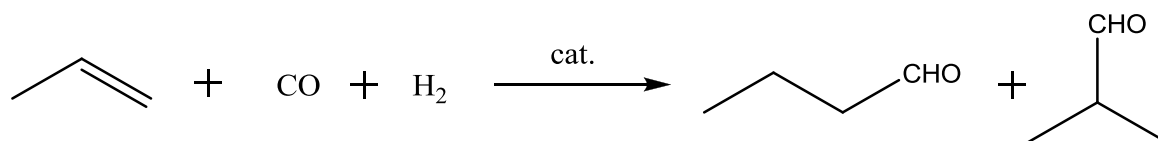
1.8.2 Hydrogenation of olefins.



Scheme 1.8-2 Hydrogenation of olefins.

The reactions between olefins and hydrogen, shown in Scheme 1.8-2 are catalyzed by rhodium(I) and ruthenium(II) complexes possessing both N-heterocyclic carbene and phosphine as ligands. The use of the mixed systems is justified by the difference in electronic properties of these ligands; due to the fact that phosphines are weaker σ -donors and stronger π -acceptors than carbenes, the electron density at the metal center is decreased when comparing with biscarbene complexes, which facilitates the reaction of the reagent with H_2 .

1.8.3 Hydroformylation of olefins.

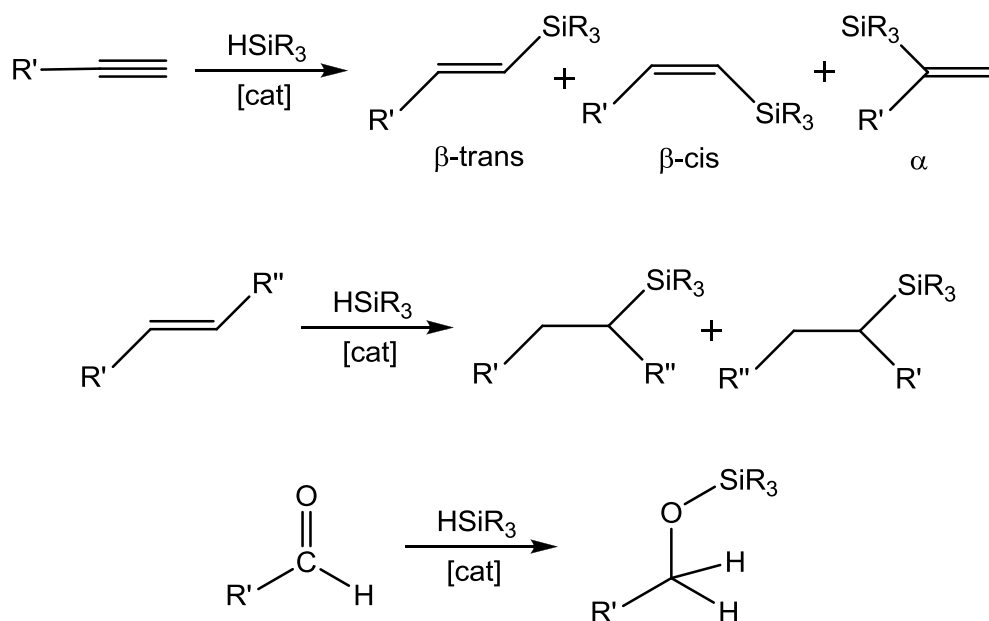


Scheme 1.8-3 Hydroformylation of olefins.

Hydroformylation of olefins relies on a reaction of an alkene with carbon oxide and hydrogen to afford corresponding aldehydes, Scheme 1.8-3. Rhodium(I)-NHC complexes have been successfully employed as catalysts in this reaction, although their activity has been found as slightly lower than with the use of triphenylphosphine complex $RhH(CO)(PPh_3)_3$, due to the increase of the electron density on metal center by the carbene. Nevertheless, the rhodium(I)-NHC complexes such as $[RhCl(COD)(NHC)]$, $[RhCl(PPh_3)_2(NHC)]$, $[RhCl(CO)(PPh_3)(NHC)]$ or $[RhCl(CO)(NHC)_2]$ are still considered as a promising alternatives for the phosphines due to the long-term stability of the N-heterocyclic carbenes.

1.8.4 Hydrosilylation reactions

Various rhodium- and ruthenium-NHC complexes have been investigated in the hydrosilylation reactions, which involve the addition of inorganic or organic silicon hydrides to multiple bonds such as alkyne, alkene and carbonyl groups (Scheme 1.8-4).⁴⁴



Scheme 1.8-4 Hydrosilylation reactions.

Regarding the hydrosilylation reactions of terminal alkenes, rhodium-NHC complexes (both the complexes possessing only NHCs and systems combining NHCs with phosphines) have been proved to be better catalysts in the anti-Markovnikov addition than complexes of a type $[\text{RhCl}(\text{PPh}_3)_3]$, bearing only the phosphines ligands, due to the increase of the electron density at the metal center in case of the NHC complexes, thanks to the remarkable donating ability of carbenes.⁴⁵

With alkynes, mixture of α -2-silyl-1-alkyl and cis and trans silylated alkenes are generally obtained but cis to trans isomerization is completely achieved by the elongation of the reaction time or alternatively by heating. The drawback of this reaction is the difficulty to obtain the desired products in good yields in a selective way; usually the increase in the yield induces a drop in the selectivity and the opposite; for instance, the rhodium complex shown in Figure 1.8-3a, synthesized by Buchmeiser,⁴⁵ was examined in the hydrosilylation of ketones, alkenes and alkynes; the reaction employing the alkynes afforded products in moderate yields but was found to be selective, even with the low catalyst loadings (i.e., as low as 0.05 mol %). On the other hand, the complex shown in Figure 1.8-3b, has been tested in the hydrosilylation reactions by Oro et al.⁴⁵, where good yields and fair to good selectivity have been found.

a)

b)

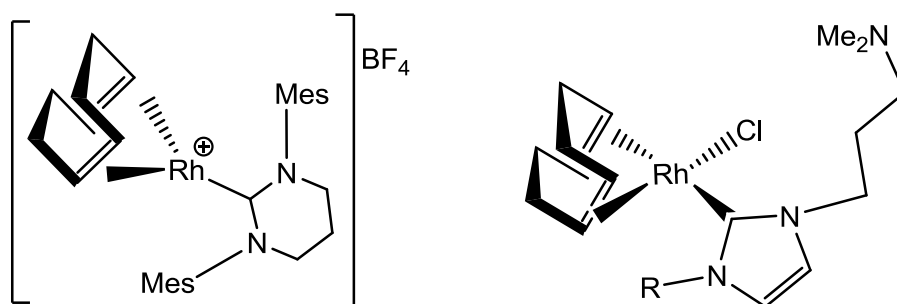
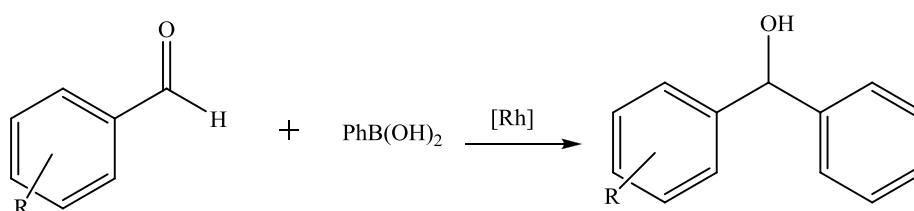


Figure 1.8-3 Structures of Rh(I)-NHC complexes active in alkyne hydrosilylation.

1.8.5 Addition of phenylboronic acid to benzaldehyde

As early as 2001, Furstner screened a number of “common” NHCs in the Rh-catalyzed addition of phenyl boronic acids to *p*-anisaldehyde (Scheme Scheme 1.8-5), making use of azolium salts in an in situ procedure.⁴⁶ The authors notably observed that unsaturated NHCs performed better than their saturated analogues. Direct comparison with trialkyl phosphines revealed that, even though both ligand classes afforded similar yields, NHCs led to reactions that were 5-8 times faster. The optimized catalytic system, comprised of IPr · HCl and RhCl₃, allowed for the arylation of numerous alkyl and aryl aldehydes in moderate to excellent yields. Over the last five years, Ozdemir and co-workers have synthesized several number of [RhCl(NBD)(NHC)] complexes and tested their catalytic activities in the addition of phenyl boronic acid to benzaldehyde derivatives. Different scaffolds, such as imidazolidinylidenes,^{47,48} benzimidazolylidenes,⁴⁹ were employed and found active in this transformation. All these rather diverse NHC architectures proved efficient at 80 °C with 1 mol % catalyst loading for differently substituted benzaldehydes.



Scheme 1.8-5

References

- 1 Fevre, M.; Pinaud, J.; Gnanou, Y.; Vignolle, V.; Taton, D., *Chem. Soc. Rev.*, **2013**, 42, 2142
- 2 Bourissou, D.; Guerret, O.; Gabbaï, P.; Bertrand, G. *Chem. Rev.* **2000**, 100, 39.
- 3 Hoffmann, R. *J. Am. Chem. Soc.* **1968**, 90, 1475.
- 4 Wanzlick, H. W.; Kleiner, H. J. *Angew. Chem.* **1961**, 73, 493-493.
- 5 Arduengo, A. J.; Harlow, R. L.; Kline, M.; *J. Am. Chem. Soc.* **1991**, 113, 361-363
- 6 de Frémont, P.; Marion, N.; Nolan, S. P. *Coord. Chem. Rev.* **2009**, 253, 862-892.

-
- 7 Dupont, J. J. *Braz. Chem. Soc.* **2004**, *15*, 341-350.
- 8 Caló, V.; Del Sole, R.; Nacci, A.; Schingaro, E.; Scordari, F. *Eur. J. Org. Chem.* **2000**, *2000*, 869-871.
- 9 Herrmann, W. a. *Angew. Chem., Int. Ed.* **2002**, *41*, 1290-1309.
- 10 Scholten, J. D.; Leal, B. C.; Dupont, J. *ACS Catalysis* **2012**, *2*, 184-200.
- 11 Ballarin, B.; Busetto, L.; Cassani, M. C.; Femoni, C. *Inorg. Chim. Acta* **2010**, *363*, 2055-2064.
- 12 http://www.scripps.edu/baran/images/grpmtgpdf/Zografos_Feb_04.pdf.
- 13 (a) Debus, H.; *Justus Liebigs Annalen der Chemie*, **1858**, *107*, 199. (b) Radzisewski, B. *Berichte der deutschen chemischen Gesellschaft*, **1882**, *15*, 2706.
- 14 Gridnev, A. A.; Mihaltseva, I. M. *Synth. Commun.* **1994**, *24*, 1547-1555
- 15 Glorius, F.; Spielkamp, N.; Holle, S.; Goddard, R.; Lehmann, C. W. *Angew. Chem., Int. Ed.* **2004**, *43*, 2850-2852.
- 16 Arduengo, A. J. *Acc. Chem. Res.* **1999**, *32*, 913.
- 17 Arduengo, A. J.; Gamper, S. F.; Tamm, M.; Calabrese, J. C.; Davidson, F.; Craig, H. A. *Structure* **1995**, *117*, 572-573.
- 18 Ranke, J.; Stolte, S.; Stormann, R.; Arning, J.; Jastorff, B.; *Chem. Rev.*, **2007**, *107*, 2183-2206
- 19 Zhang, Q.; Zhang, S.; Deng, Y.; *Green Chem.*, **2011**, *13*, 2619
- 20 Hallett, J.P.; Welton T. *Chem.Rev.*, **2011**, *111*, 3508-3576
- 21 Wanzlick, H. W.; Schönherr, H. J. *Angew. Chem.* **1968**, *80*, 154-154.
- 22 Ofele, K. *Angew. Chem., Int. Ed.* **1968**, *12*, 950.
- 23 Arduengo III, A. J.; Dias, H. V. R.; Harlow, R. L.; Kline, M. J. *Am. Chem. Soc.* **1992**, *114*, 5530-5534.
- 24 Jean-Baptiste Dit Dominique, F.; Gornitzka, H.; Hemmert, C. *Organometallics* **2010**, *29*, 2868-2873.
- 25 Lappert, M. F. *J. Organomet. Chem.* **1988**, *358*, 185-213.
- 26 Lin, T.-S.; Luo, M.-Z.; Liu, M.-C. *Tetrahedron* **1995**, *51*, 1055-1068.
- 27 Lin, I. J. B.; Vasam, C. S. *Coord. Chem. Rev.* **2007**, *251*, 642-670.
- 28 Liu, B.; Liu, X.; Chen, C.; Chen, C.; Chen, W. *Organometallics* **2012**, *31*, 282-288.
- 29 Liu, B.; Xia, Q.; Chen, W. *Angew. Chem., Int. Ed.* **2009**, *48*, 5513-6.
- 30 Green, J. C.; Scurr, R. G.; Arnold, P. L.; Cloke, G. N. *Chem. Commun.* **1997**, 1963-1964.
- 31 Mercks, L.; Labat, G.; Neels, A.; Ehlers, A.; Albrecht, M. *Organometallics* **2006**, *25*, 5648-5656
- 32 Garrison, J. C.; Youngs, W. J. *Chem. Rev.* **2005**, *105*, 3978-4008.
- 33 Kandepi, V. V. K. M.; Cardoso, J. M. S.; Peris, E.; Royo, B. *Organometallics* **2010**, *29*, 2777-2782
- 34 Chianese, A. R.; Li, X.; Janzen, M. C.; Faller, J. W.; Crabtree, R. H.; Organomet, W. A. J. *Organometallics* **2003**, *22*, 1663-1667.
- 35 Wang, H. M. J.; Lin, I. J. B.; *Organometallics*, **1998**, *17*, 972
- 36 Cardoso, J. M. S.; Royo, B. *Chem. Commun.* **2012**, *48*, 4944-4946.
- 37 Corbera, R.; Sanau, M.; Peris, E. *Organometallics* **2006**, *25*, 4002-4008.
- 38 Scott, N. M.; Dorta, R.; Stevens, E. D.; Correa, A.; Cavallo, L.; Nolan, S. P. *J. Am. Chem. Soc.* **2005**, *127*, 3516-26.
- 39 Enders, D.; Gielen, H.; Runsink, J.; Breuer, K.; Brode, S.; Boehn, K. *Eur. J. Inorg. Chem.* **1998**, 913-919.
- 40 Enders, D.; Gielen, H. J. *Organomet. Chem.* **2001**, *618*, 70-80.
- 41 Bringmann, G.; Price Mortimer, A. J.; Keller, P. A.; Gresser, M. J.; Garner, J.; Breuning, M. *Angew. Chem., Int. Ed.* **2005**, *44*, 5384-5427.
- 42 Crabtree, R. J. *Organomet. Chem.* **2005**, *690*, 5451-5457.
- 43 Díez-González, S.; Marion, N.; Nolan, S. P. *Chem. Rev.* **2009**, *109*, 3612-76.
- 44 Imlinger, N.; Wurst, K.; Buchmeiser, M. R. *J. Organomet. Chem.* **2005**, *690*, 4433-4440
- 45 Jiménez, M. V.; Pérez-Torrente, J. J.; Bartolomé, M. I.; Gierz, V.; Lahoz, F. J.; Oro, L. A. *Organometallics* **2008**, *27*, 224-234
- 46 Furstner, A.; Krause, H. *Adv. Synth. Catal.* **2001**, *343*, 343-350.
- 47 (a) Ozdemir, I.; Demir, S.; C, etinkaya, B. *J. Mol. Catal. A: Chem.* **2004**, *215*, 45-48. (b) Yigit, M.; O'zdemir, I.; C, etinkaya, E.; C, etinkaya, B. *Heteroat. Chem.* **2005**, *16*, 461-465. (c) Kilincarslan, R.; Yigit, M.; O'zdemir, I.; C, etinkaya, E.; C, etinkaya, B. *J. Heterocycl. Chem.* **2007**, *44*, 69-73.
- 48 (a) Ozdemir, I.; Yigit, M.; C, etinkaya, E.; C, etinkaya, B. *Heterocycles* **2006**, *68*, 1371-1379. (b) Yigit, M.; Ozdemir, I. *Transition Met. Chem.* **2007**, *32*, 536-540.
- 49 Ozdemir, I.; Gu'rbu'z, N.; Go'k, Y.; C, etinkaya, B.; C, etinkaya, E. *Transition Met. Chem.* **2005**, *30*, 367-371.

2 Synthesis and Characterization of Imidazolium Salts Incorporating the NHBoc functionalization

2.1 Introduction

The novel imidazolium salts [BocNHCH₂CH₂ImR]⁺X⁻ (**1a**, R = Methyl, X = I⁻; **1b**, R = Benzyl, X = Br⁻; **1c**, R = Trityl, X = Cl⁻) bearing increasingly bulky N-alkyl substituents were prepared in high yields by alkylation of the (2-imidazol-1-yl-ethyl)-carbamic acid *tert*-butyl ester¹ respectively with benzyl bromide and trityl chloride in dichlorometane at room temperature (Chart 2.1-1).

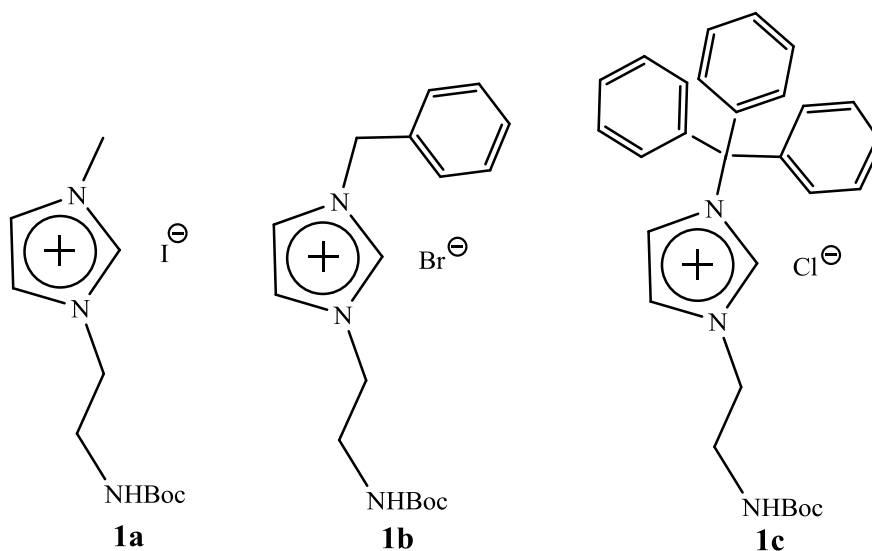
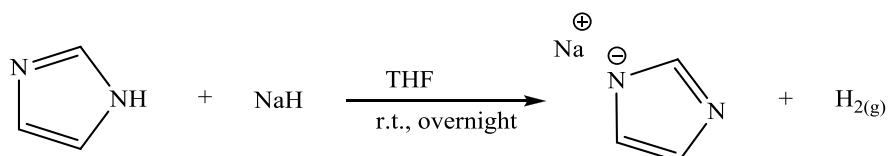


Chart 2.1-1

2.2 Results and discussion

2.2.1 Synthesis

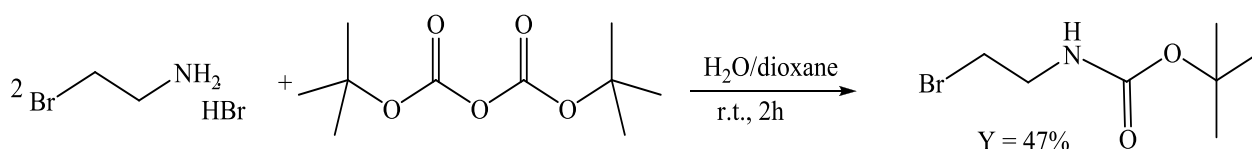
The reduction reaction of the imidazole by sodium hydride was performed under inert and dry atmosphere following a procedure available in literature.² The reaction takes place overnight at room temperature in dry THF to obtain the sodium imidazolide salt in quantitative yield (Scheme 2.2-1).



Scheme 2.2-1

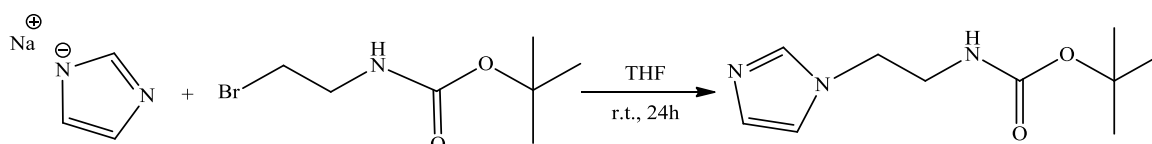
Some variations on the literature procedure have been done in order to make easier and safer the preparation of large amount of the product. In particular the operations of filtration and separation were effected by cannula and the time of dropping of imidazole in NaH was increased; the white solid obtained was kept in the glove box.

The protection reaction was performed reacting the 2-bromoethylamine-hydrobromide with di-*tert*-butyldicarbonate (Scheme 2.2-2) for 2 hours at room temperature in a 1:1 mixture H₂O/dioxane by following a procedure reported in literature.¹



Scheme 2.2-2

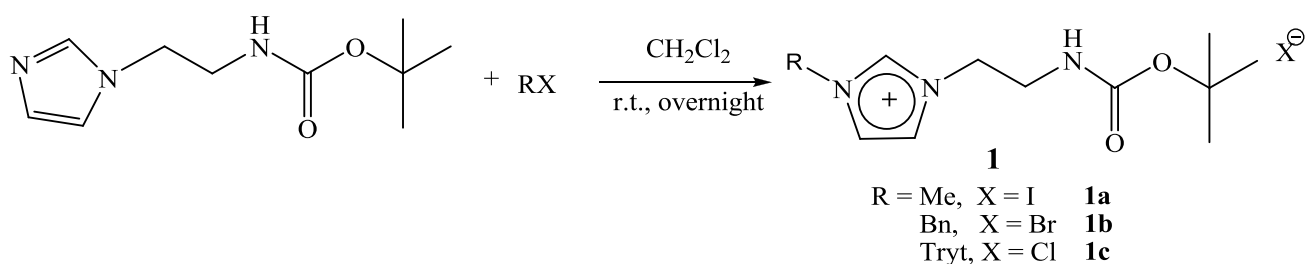
The 2-Bromoethylamine-*t*-butylcarbamate was reacted with the sodium imidazolide salt synthesized (Scheme 2.2-3)³



Scheme 2.2-3

The product was purified by chromatography on silica gel, eluting with $\text{CH}_2\text{Cl}_2/\text{CH}_3\text{OH}/\text{NH}_4\text{OH}$ (100:5:1), and it was obtained with 55% yield as a yellow oil.

The alkylation reaction of the second nitrogen was performed by an excess of alkyl halide stirring overnight in CH_2Cl_2 solution (Scheme 2.2-4) following a synthetic method reported in literature.¹



Scheme 2.2-4

The result is a quantitative yield in the corresponding alkylated imidazolium salt with the halide as counterion.

Likewise **1a**, the salt **1b** was isolated as a colourless to pale yellow viscous liquid whereas **1c** is a crystalline solid;¹ they are soluble in chlorinated solvents, and were fully characterized by elemental analysis, NMR spectroscopy, electrospray ionization mass spectrometry (ESI-MS) and in case of **1c** also by X-ray diffraction. The NMR resonances of the imidazolium fragment were observed at chemical shifts typical for imidazolium salts and it is worth noting, that to the best of our knowledge, substitution at the 1,3-positions of the imidazole unit with the trityl group has been reported only in one case regarding rhodium-catalyzed hydrosilylation/cyclization reactions.⁴

Crystals of **1c** suitable for single crystal X-ray diffraction were grown from a double layer of dichloromethane and petroleum ether (1:4). The molecular structure is shown in Figure 2.2-1, crystal data and experimental details are presented in Table 2.2-1. The single crystals selected for X-ray analysis crystallize in the centrosymmetric $P2_1/c$ space group ($Z = 4$), and the unit cell also contains four water molecules. The bond distances and angles are in the expected range compared to those of known imidazolium salts⁵ and also the N(1)-C(19) distance for the N-C(trityl) bond of 1.5016(16) Å is in keeping with literature data.⁶ In the latter group two phenyl rings (C(7)-C(12) and C(13)-C(18)) are linked in an helical shape, whereas the third phenyl (C(1)-C(6)) generates a second helical system with imidazole.⁷ The NH group is not involved in hydrogen bonds with the

carbenic hydrogen but, on the contrary, it acts as donor with one of the chloride counteranions ($N(3)\dots Cl(1) = 3.262 \text{ \AA}$). Each of the four water molecules has also hydrogen bonds with two chloride anions (3.182 and 3.233 \AA) and with the carbenic hydrogen (3.034 \AA).

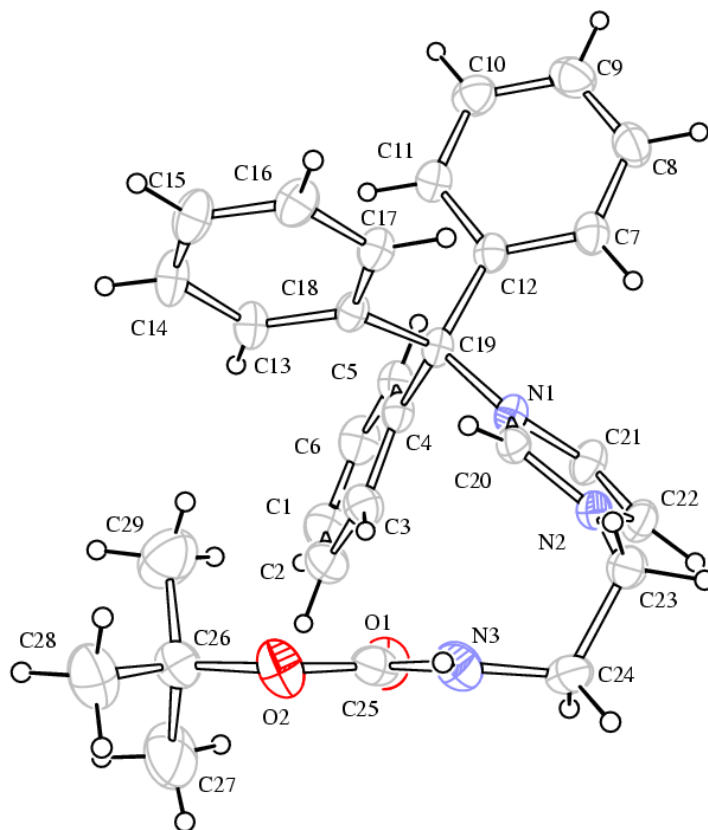


Figure 2.2-1 ORTEP diagram of **1c** depicted with displacement ellipsoids at 30% probability level. The counterion and water molecules have been omitted for clarity.

Table 2.2-1 Crystal Data, Data Collection and Refinement Parameters for **1c**

Compound	1c·H₂O
Formula	$C_{29}H_{34}ClN_3O_3$
Fw	508.04
T, K	296(2)
λ , \AA	0.71073
Crystal system	Monoclinic
Space group	$P2_1/c$
a, \AA	8.5286(9)
b, \AA	17.2903(18)
c, \AA	18.910(2)

α , °	90
β , °	93.2710(10)
γ , °	90
Cell Volume, Å ³	2751.8(5)
Z	4
D _c , g cm ⁻³	1.226
μ , mm ⁻¹	0.173
F(000)	1080
Crystal size, mm	0.80 x 0.70 x 0.60
θ limits, °	1.61 to 28.71
Index ranges	-10 ≤ h ≤ 11, -22 ≤ k ≤ 21, -24 ≤ l ≤ 25
Reflections collected	31214
Independent reflections	6711 [R(int) = 0.0219]
Completeness to $\theta = 25.00^\circ$	100.0%
Data / restraints / parameters	6711 / 0 / 348
Goodness on fit on F ²	0.903
R ₁ (I > 2σ(I))	0.0419
wR ₂ (all data)	0.1139
Largest diff. peak and hole, e Å ⁻³	0.235 and -0.289

2.3 Deprotonation of the imidazolium salts

Herrmann and co-workers have already reported that the deprotonation of the similar 1-(2-ethylaminoethyl)-3-methylimidazolium chloride system [EtNHCH₂CH₂ImMe][Cl] in THF/CH₃CN smoothly proceeds without side reactions.⁸ On this light, we initially performed the reaction between **1a** and a slight excess of KOBu^t at room temperature in two parallel NMR-scale experiments in CDCl₃ and CD₃CN. In both solvents the ¹H NMR spectra, registered immediately after the preparation of the samples, only showed the disappearance of the NCHN singlet (δ 9.70 in CDCl₃, δ 8.70 in CD₃CN) indicating the successful deprotonation, whereas in the ¹³C NMR a 1:1:1 triplet at δ 137.0 (J_{C,D} = 31.4 Hz) was attributed to the deuteration (D) of the imidazolium salt at the C(2) position to give [**1a-D**]**I**. The ESI-MS(+) analyses in methanol of the solution showed a peak

at 227 m/z confirming the formation of **[1a-D]⁺**. Successively the same reaction was carried out in bulk in THF and monitored by transferring, after 10 min., under strict anhydrous conditions, part of the solution in a NMR tube that after removal of the solvent under vacuum and addition of dry CDCl_3 (or CD_3CN) was flame-sealed under argon. The ^1H and ^{13}C NMR spectra of the thus prepared samples were more complex compared to those described above and showed, together with the resonances earlier attributed to **[1a-D]⁺**, the presence of substantial amounts of at least one more product that we haven't identified so far. In our opinion these results clearly showed that the deprotonation reaction leads to the immediate formation of the sought NHC carbene however, due to its high reactivity, it can be used only *in situ* reactions.

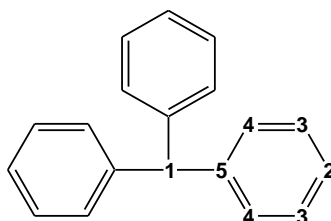
2.4 Experimental Section

Materials and Procedures. All reactions were carried out under Argon using standard Schlenk techniques. Solvents were dried and distilled under nitrogen prior to use; the deuterated solvents used after being appropriately dried and degassed were stored in ampoules under argon on 4Å molecular sieves. The prepared derivatives were characterized by elemental analysis and spectroscopic methods. The IR spectra were recorded with a FT-IR spectrometer Perkin Elmer Spectrum 2000. The NMR spectra were recorded using Varian Inova 300 (^1H , 300.1; ^{13}C , 75.5 MHz), Varian MercuryPlus VX 400 (^1H , 399.9; ^{13}C , 100.6 MHz). The spectra were referenced internally to residual solvent resonances, and unless otherwise stated, they were recorded at 298 K for characterization purposes; full ^1H and ^{13}C NMR assignments were done. J.Young valve NMR tubes (Wilmad) were used to carry out NMR experiments under inert conditions. ESI-MS analyses were performed by direct injection of methanol solutions of the metal complexes using a WATERS ZQ 4000 mass spectrometer. Elemental analyses were performed on a ThermoQuest Flash 1112 Series EA Instrument. The chemicals 2-bromoethylamine hydrobromide, imidazole (ImH), benzyl bromide, were used as purchased from Aldrich; the starting building blocks: 2-*t*-Boc-aminoethylbromide (carbamic acid 2-bromoethyl-*t*-butyl ester),⁹ (2-Imidazol-1-yl-ethyl)-carbamic acid *tert*-butyl ester (BocNHCH₂CH₂Im),^{7,10} 1-(2-BocNH-ethyl)-3-methylimidazolium iodide (**1a**) were prepared according to literature procedures. Petroleum ether (Etp) refers to a fraction of b.p. 60-80 °C. Melting points were taken with a Stuart Scientific Melting point apparatus SMP3 and were uncorrected. Crystal data were collected at room temperature on a Bruker APEX II diffractometer equipped with a CCD detector operating at 50 kV and 30 mA, using graphite monochromated MoK_α radiation ($\lambda = 0.71073 \text{ Å}$). An empirical absorption correction was applied on both structures by using SADABS.¹¹ They were solved by direct methods and refined by full-

matrix least-squares based on all data using F^2 with SHELXL97.¹² All non-hydrogen atoms were refined anisotropically, with the exception of the hydrogen atoms which were set geometrically and given fixed isotropic thermal parameters.

2.4.1 Synthesis of triphenylchloromethane (Trityl Chloride)

This product was synthesized using a modified literature method.¹³ A three-neck dry round bottom flask was charged with triphenylmethanol (4.0 g, 15.4 mmol) and dry toluene (10 mL) under argon. A condenser was attached and the mixture was heated to 80 °C. Acetyl chloride (1.1 mL, 15.4 mmol) was added with a dropping funnel whilst stirring vigorously with a magnetic stirrer. Once the solid had dissolved, additional acetyl chloride (1.90 mL, 27.8 mmol) was added over the course of 10 minutes. The solution was heated for 30 minutes and then cooled in an ice bath, and petroleum ether (80 mL) was added. This mixture was left in the ice bath for 2 hours at which point a dark brown product separated out and discarded. Volatiles were removed from the filtrate under vacuum to give a pale yellow solid that after washing with petroleum ether (3 x 5mL) and dried afforded the title compound as a off white powder (3.34 g, 78 %) that must be stored under argon. ¹H NMR: (300.1 MHz, CDCl₃): δ 7.34-7.25 (m, Ph); ¹³C NMR (75.50 MHz, CDCl₃): δ 145.25 (C₅), 129.67 (C₄), 127.76 (C₂), 127.71 (C₃), 81.34 (C₁).



Trityl and phenyl group numbering scheme

2.4.2 Synthesis of sodium salt of imidazolium¹

The reaction is performed under nitrogen atmosphere. In a 250mL flask NaH (3.80g, 0.158mol) (we usually employ NaH 60% in mineral oil, previously washed three times with petroleum ether in order to enhance NaH activity, and kept under nitrogen) and dry THF (20mL) was added. Subsequently imidazole (11.73g, 0.1726mol), dissolved in THF (50mL), was added dropwise in 30min. The reaction mixture was stirred at room temperature overnight. At the end of the reaction the mixture was filtered and washed with dry THF. The residual solvent removed under vacuum leading to a white solid with a quantitative yield. The product is kept under inert atmosphere. This reaction was performed also in larger quantities attempting a small scale-up, in a 1L flask was added 32.0g (1.35mol) of NaH in dry THF (170mL) and 100g (1.47mol, 1.09eq.) of imidazole in dry THF (420mL), the dripping has lasted 2 hours while the reaction time was the same. ¹H-NMR (D₂O): δ(ppm): 7.64 (s, 1H), 7.00 (s, 2H).

2.4.3 Synthesis of 2-Bromoethylamine-*t*-butylcarbamate ¹

In a 1L three necked flask 12.30g (0.06mol) of 2-bromoethylamine-hydrobromide were dissolved in 60mL of a 1:1 di H₂O/dioxane mixture. The solution was cooled in an ice bath. Other two solutions (NaOH 1M in 60mL of water, 0.06mol) and (6.54g of di-*tert*-butyldicarbonate in 70mL of dioxane, 0.03mol) were prepared and separately added in two dropping funnel. NaOH solution was dropped in 15min while the di-*tert*-butyldicarbonate solution in 30min. Then the ice bath was removed and the mixture stirred for 2h at room temperature. Then the solution was extracted with CH₂Cl₂ (200mL) and the aqueous phase washed once more with 100mL of CH₂Cl₂. The organic phase was washed with citric acid 5% (2x100mL) and sodium chloride 10% (2x100mL). CH₂Cl₂ was dried with sodium sulphate, the solution filtered and the solvent removed under vacuum. 3.16g of a yellow oil was obtained and identified as 2-Bromoethylamine-*t*-butylcarbamate (Y = 47%).

This reaction was then carried with five times the amount of the above procedure. In these condition the dripping times double and the reaction lasts 3 hours. After the filtration by cannula and the purification was obtained the product in the same yield.

¹H-NMR (CDCl₃): δ(ppm): 4.95 (s, NH), 3.69 (s, 8H, dioxane), 3.52 (m, 2H), 3.44 (m, 2H).

2.4.4 Synthesis of (2-Imidazol-1-yl-ethyl) *t*-butylcarbamate ¹

In a 1L flask, to a suspension of imidazolium salt 31.25g (0.28mol, 2eq) in dry THF (300mL) kept under inert atmosphere, was added with a cannula 2-Bromoethylamine-*t*-butylcarbamate (31.44g, 0.14mol) already dissolved in dry THF (200mL). The reaction mixture was stirred at room temperature for 24 hours. The crude reaction was filtered on celite and washed with dry THF, then the solvent was removed under vacuum. The yellow oil thus obtained was dissolved in CH₂Cl₂ and purified by column chromatography on silica. At first eluted with CH₂Cl₂, then with a mixture of CH₂Cl₂/CH₃OH (100:5) and finally with a mixture of CH₂Cl₂/CH₃OH/NH₄OH (100:5:1). 12.27g of a yellow oil was isolated and identified as (2-Imidazol-1-yl-ethyl) *t*-butylcarbamate. (Y = 55%,).

¹H NMR (CDCl₃): δ(ppm): 7.50 (s, 1H, NCHN), 7.05 (s, 1H, CH_{im}), 6.90 (s, 1H, CH_{im}), 4.90 (br s, 1H, NH), 4.07 (t, 2H, NCH₂, J = 5.6Hz), 3.42 (m, 2H, CH₂NH), 1.42 (s, 9H, CH₃). ¹³C NMR (CDCl₃): δ(ppm): 155.8 (C=O), 137.1 (NCHN), 129.2 (CH_{im}), 118.8 (CH_{im}), 79.6 (Cq, *t*-Bu), 46.4 (NCH₂), 41.3 (CH₂NH), 28.1 (CH₃). IR (THF) ν (CO): 1714 cm⁻¹

2.4.5 Synthesis of 1-(2-*t*-Butoxycarbonylamino-ethyl)-3-methyl-3H-imidazolium iodide (1a)¹

In a 250mL flask, kept under inert atmosphere, 5.30g (0.024mol) of (2-Imidazol-1-yl-ethyl) *t*-butylcarbamate was dissolved in 10mL of dry CH₂Cl₂, subsequently an excess of CH₃I (5mL, 0.080mol, 3eq.) was added. The reaction mixture was stirred at room temperature overnight. The

product was washed with Et₂O (3x10mL) and, after having removed the washing water, the residual solvent and methyl iodide in excess were removed under vacuum. 1-(2-*t*-Butoxycarbonylaminoethyl)-3-methyl-3*H*-imidazolium iodide, **1a**, was obtained with a quantitative yield. ¹H NMR (CDCl₃): δ(ppm): 9.92 (s, 1H, NCHN), 7.19 (s, 1H, CH_{im}), 7.08 (s, 1H, CH_{im}), 5.75 (br s, 1H, NH), 4.28 (t, 2H, NCH₂, J = 5.6Hz), 3.93 (s, 3H, NCH₃), 3.59 (m, 2H, CH₂NHBoc), 1.28 (s, 9H, CH₃). ¹³C NMR (CDCl₃): δ(ppm): 156.2 (C=O), 137.0 (CH, NCHN), 123.1 (2CH, CH_{im}), 79.9 (Cq, *t*-Bu), 46.7 (NCH₂), 40.2 (CH₂NH), 37.2 (NCH₃), 28.6 (CH₃, *t*-Bu). IR (CH₂Cl₂) v (CO): 1708 cm⁻¹; (NaCl) v (CO): 1703 cm⁻¹. ESI-MS (MeOH, *m/z*): 226 (100) [M]⁺, 127 (100) [M]⁻.

2.4.6 Synthesis of 1-(2-BocNH-ethyl)-3-benzyl-imidazolium bromide **1b** ⁴

In a 100 mL round bottom flask to a solution of BocNHCH₂CH₂Im (1.02 g, 4.80 mmol) in CH₂Cl₂ (10 mL) an excess of benzylbromide (7.20 mmol) was added. After stirring for 12 h at room temperature, the solvent was removed under vacuum and the resulting pale yellow viscous oil was thoroughly washed with diethyl ether (3 x 10 mL). After separation from the washings the oil was kept under vacuum at 40 °C for several hours to yield 1.87 g (100 %) of **1b**. ¹H NMR (399.9 MHz, CDCl₃): δ 10.20 (s, 1H, NCHN), 7.45 (s, 1H, CH_{im}), 7.35 – 7.27 (m, 5H, Ph), 7.22 (s, 1H, CH_{im}), 6.12 (br s, 1H, NH), 5.52 (s, 2H, PhCH₂N), 4.56 (br t, 2H, NCH₂), 3.69 (br t, 2H, CH₂NH), 1.36 (s, 9H, CH₃). ¹³C NMR (100.6 MHz, CDCl₃): δ 156.1 (C=O), 137.9 (CH, NCHN), 132.7 (Ph, C₅), 128.9 (Ph, 2C₄), 128.8 (Ph, 2C₃), 128.3 (Ph, C₂), 123.3 (CH_{im}), 121.4 (CH_{im}), 79.4 (Cq, ^tBu), 53.3 (PhCH₂), 49.5 (NCH₂), 40.2 (CH₂NH), 28.6 (CH₃, ^tBu). IR (CH₂Cl₂, cm⁻¹): 1706 (vs, ν_{CO}); (neat, cm⁻¹): 3399 (vs, ν_{NH}), 3136, 3068, 2977, 1701 (vs, ν_{CO}), 1560, 1509, 1457, 1366, 1255, 1164. ESI-MS (MeOH, *m/z*): 302 (100) [M]⁺; 79 (97), 81 (100) [Br]⁻. Analysis calcd. (%) for C₁₇H₂₄BrN₃O₂: C, 53.41; H, 6.33; N, 10.99. Found: C, 53.80; H, 6.62; N, 11.33.

2.4.7 Synthesis of 1-(2-BocNH-ethyl)-3-trityl-imidazolium chloride, **1c** ⁴

In a 100 ml round bottom flask to a solution of BocNHCH₂CH₂Im (0.93 g, 4.41 mmol) dissolved in CH₂Cl₂ (20 mL) trityl chloride (1.30 g, 4.66 mmol) was added. After stirring for 16 h at room temperature, the solvent was removed under vacuum and the resulting solid was thoroughly washed with diethyl ether (3 x 10 mL) to yield 2.05 g (95 %) of a white solid identified as **1c**. ¹H NMR (399.9 MHz, CDCl₃): □ 9.12 (s, 1H, NCHN), 8.01 (s, 1H, CH_{im}), 7.39 (m, 9H, Ph), 7.13 (m, 6H, Ph), 6.96 (s, 1H, CH_{im}), 6.61 (br s, 1H, NH), 4.78 (t, 2H, J_{H,H} = 5.5 Hz, NCH₂), 3.61 (m, 2H, J_{H,H} = 5.4 Hz, CH₂NH), 1.31 (s, 9H, CH₃). ¹³C NMR (100.6 MHz, CDCl₃): δ 156.6 (C=O), 139.5 (C₅), 137.3 (NCHN), 129.5 (C₄), 129.3 (C₂), 128.9 (C₃), 123.5 (CH_{im}), 123.3 (CH_{im}), 79.5 (Cq, ^tBu), 79.2 (C₁), 49.9 (NCH₂), 40.5 (CH₂NH), 28.3 (CH₃, ^tBu). IR (CH₂Cl₂, cm⁻¹): 1707 (vs, ν_{CO}); (KBr, cm⁻¹): 3368 (vs, ν_{NH}), 3166, 3144, 3061, 2977, 1702 (vs, ν_{CO}), 1493, 1446, 1365, 1252, 1168. ESI-

MS (MeOH, m/z): 454 (100) $[M]^+$. Analysis calcd. (%) for $C_{29}H_{32}ClN_3O_2$: C, 71.09; H, 6.58; N, 8.58. Found: C, 71.16; H, 6.50; N, 8.65. M.p. = 68 °C. Crystals of **1c** suitable for single crystal X-ray diffraction were grown from a double layer of dichloromethane and petroleum ether (1:4) at room temperature.

2.4.8 Reaction of **1a** with KOBut

The NMR experiments carried out in deuterated chloroform and acetonitrile gave identical results therefore only the data for the experiment in $CDCl_3$ is reported. To a NMR tube containing **1a** (0.030 g, 0.085 mmol) and KOBut^t (0.012 g, 0.11 mmol) *ca.* 0.6 mL of $CDCl_3$ was added. The tube was flame-sealed under Argon and the 1H NMR spectrum run immediately afterwards showed the quantitative formation of the imidazolium salt deuterated at the C2 position [**1a-D**]**I**. 1H NMR (399.9 MHz, $CDCl_3$): δ 7.34 (s, 1H, CH_{imid}), 7.26 (s, 1H, CH_{imid}), 5.82 (br s, 1H, NH), 4.53 (t, Im CH_2 , 2H, $^3J_{H,H} = 5.6$ Hz), 4.05 (s, 3H, N- CH_3), 3.68 (m, CH_2NHBoc , 2H), 1.39 (s, 9H, CH_3). ^{13}C NMR (100.6 MHz, $CDCl_3$): δ 156.3 (C=O), 137.2 (t, CD, Im, $J_{D,C} = 31.4$ Hz), 123.0, 122.7 (2CH, CH_{imid}), 79.9 (Cq, *t*-Bu), 49.7 (N CH_2), 40.1 (CH_2NH), 37.0 (N CH_3), 28.3 (CH_3). **ESI-MS** (MeOH, m/z): 226 (100), $[M]^+$, 227 (67%) $[M-D]^+$, 127 (100) $[M]^-$.

To a solution of **1a** (0.053 g, 0.150 mmol) dissolved in anhydrous THF (*ca.* 10 mL), KOBut^t (0.017 g, 0.150 mmol) was added. The reaction was stirred at room temperature. After 10 min part of the solution was transferred under strict anhydrous conditions with a filtering cannula in a NMR tube. After removal of the solvent under vacuum and addition of dry $CDCl_3$ the tube was flame-sealed under argon. The 1H NMR spectra of the thus prepared sample showed the complete disappearance of the signal at δ 9.70 for the NCHN proton. The rest of the spectra indicate the presence of [**1a-D**]**I** together with at least another set of signals due to unidentified side products. The same experiment, repeated after 3 h, did not show significant changes in the NMR spectra.

3 Counterion exchange

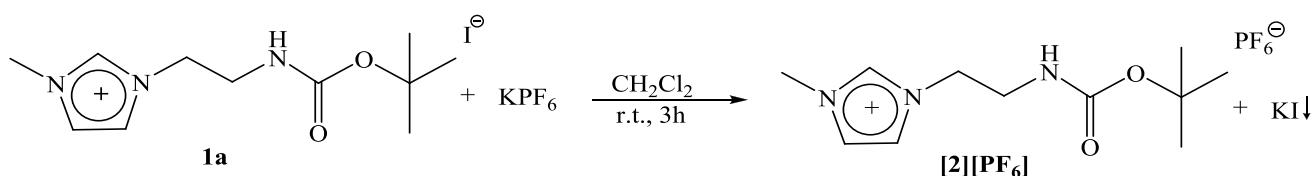
3.1 Introduction

Imidazolium salt with the cation $[BocNHCH_2CH_2ImMe]^+$ [**2**] and X = $[PF_6]$, $[ClO_4]$, $[NTf_2]$, $[NO_3]$ are from hereon termed and have been prepared by means of metathesis reactions.¹⁴ Its potential as ionic liquid (IL) was investigated.

3.2 Results and Discussion

3.2.1 Synthesis of 1-(2-*t*-Butoxycarbonylamino-ethyl)-3-methyl-3*H*-imidazolium hexafluorophosphate ([2][PF₆]):

The precursor **1a** was reacted with the salt KPF₆ to obtain the exchange of the counterion with a quantitative yield (Scheme 3.2-1).



Scheme 3.2-1

The product 1-(2-*t*-Butoxycarbonylamino-ethyl)-3-methyl-3*H*-imidazolium hexafluorophosphate ([2][PF₆]) was characterized by NMR spectroscopy and ESI-MS analysis. The ¹H-NMR spectrum in CDCl₃ of [2][PF₆] shows a shift if compared to the precursor regards the imidazole ring protons (δ 9.92 (NCHN), 7.19 (CH) and 7.08 (CH) for **1a**) that shift to 9.54, 7.25 and 7.17 ppm respectively for [2][PF₆]. The chemical shift relative to methylene groups and CH₃ are comparable with those of the precursor **1a**. However the pattern of the ¹H-NMR spectrum confirms that the imidazolium cation remain unaltered. The ¹⁹F-NMR spectrum (Figure 2.1-1) shows the presence of 6 F as a doublet at δ = -72.75 (J_{P-F} = 710Hz) typical of a PF₆ anion. The ESI-MS analysis confirms the product formation, the spectrum shows the molecular ion at 226 *m/z* [C₁₁H₂₀N₃O₂⁺] for the positive ions and only one peak at 145 *m/z* for the negative ions corresponding to the ion hexafluorophosphate [PF₆⁻]. The product appears as a yellow oil with a density of 1.06 g/mL at 25°C, stable in air and with the same solubility behaviour of the precursor **1a**.

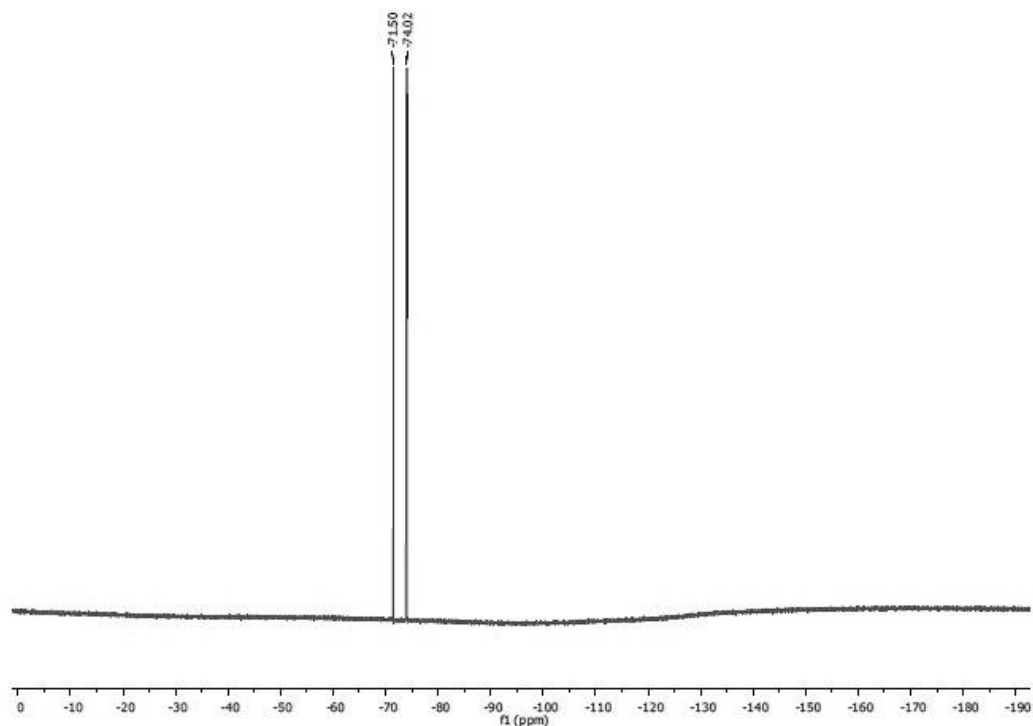


Figure 3.2-1 ^{19}F -NMR spectrum of $[\mathbf{2}][\text{PF}_6]$ in CDCl_3 .

Crystals of $[\mathbf{2}][\text{PF}_6]$ suitable for single crystal X-ray diffraction were grown by cooling down the reaction product at -20°C . The molecular structure is presented in Figure 3.1-2 with crystal data (Table 3.2-1).¹⁵

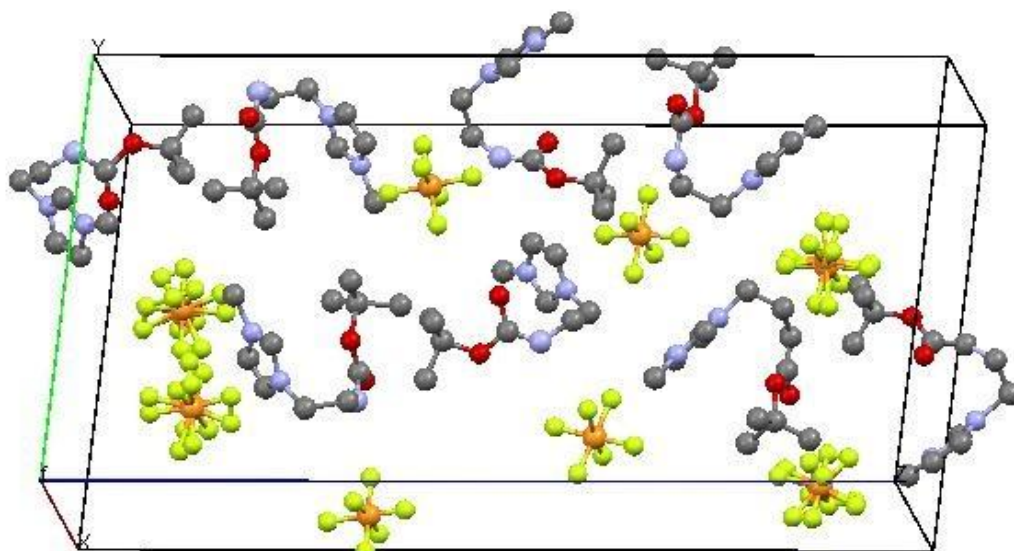


Figure 3.2-2 Unity cell of [2][PF₆].

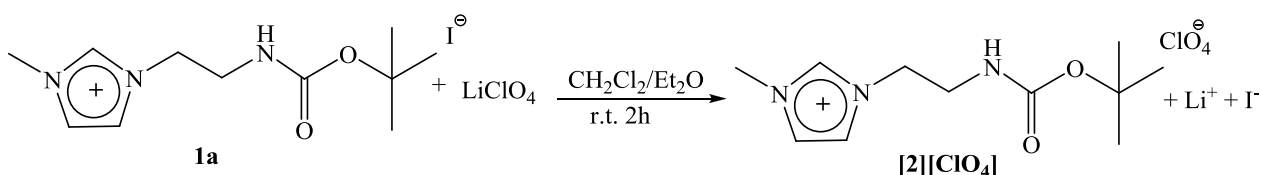
Table 3.2-1 Crystal data of [2][PF₆]

Formula	C ₁₈ H ₂₀ F ₆ N ₂ O ₃ P
FW	371.26
T, K	298
cryst syst	Monoclin
space group	P2 ₁
a, Å	6.261(3)
b, Å	16.889(7)
c, Å	32.354(13)
α, deg	90.00
β, deg	92.033
γ, deg	90.00
cell volume, Å ³	3419.02
Z	8

The ionic liquid [2][PF₆] in aqueous solution gives hydrolysis problems. In the Introduction (Paragraph 1.2) the mechanism of the hydrolysis in ILs was explained: the water forms a dimeric structure with the anion and in presence of a great amount of H₂O chains of molecules which seep in the ILs structure and break them into small ionic cluster influence also the cation behaviour. In our particular case we could observe from the ¹H-NMR performed after the addition of water at [2][PF₆] the disappearance of the signal relative to the Boc group which probably corresponds to the deprotection of NH₂ group together with decomposition products.¹²

Synthesis of 1-(2-*t*-Butoxycarbonylamino-ethyl)-3-methyl-3H-imidazolium perchlorate ([2][ClO₄])

From the reaction between the precursor **1a** in CH₂Cl₂ and a solution of salt LiClO₄ in Et₂O was performed the anion exchange from iodide to perchlorate (Scheme 3.2-2). The reaction mixture was dried, dissolved in distilled water and finally purified from the inorganic salt by an extraction in CH₂Cl₂. It was obtained a yellow oil, with a yield of 76%, identified as 1-(2-*t*-Butoxycarbonylamino-ethyl)-3-methyl-3H-imidazolium perchlorate ([2][ClO₄]) from IR, NMR and ESI-MS characterizations.



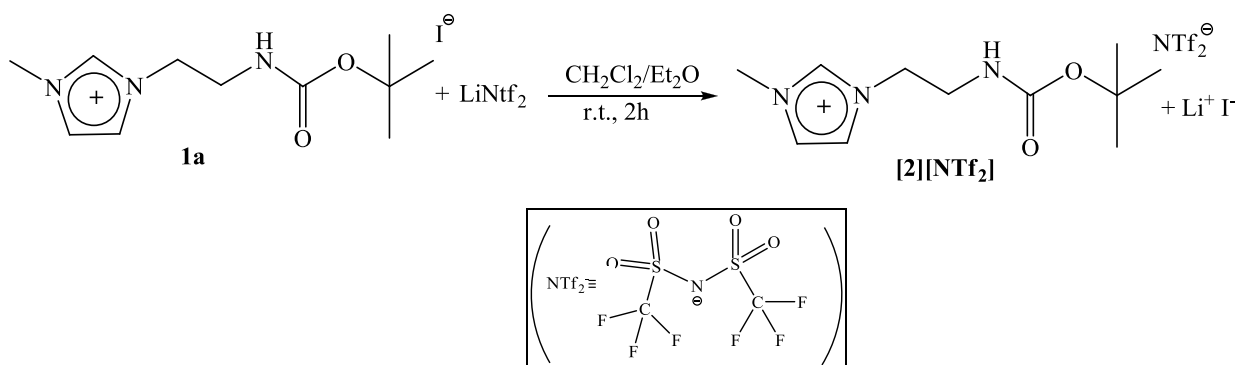
Scheme 3.2-2

The ¹H-NMR spectrum shows the signals shift of the imidazole ring protons, the acid proton (NCHN) was found at δ 8.83 ppm and the backbone protons of the imidazole ring respectively at 7.31 ppm and 7.26 ppm. The chemical shift relative to methylene groups, CH₃ and *t*-Bu resonate to 4.36, 3.58 3.96 and 1.39 ppm for [2][ClO₄]. The counterion exchange was confirmed by ESI-MS analysis that shows, from negative ions, only one peak at 99 *m/z* corresponding to the perchlorate anion. The presence of [ClO₄] ion was also identified by IR spectrum that displays broad peaks at 1097 cm⁻¹ and at 1167 cm⁻¹, by comparison with typical IR stretching of [ClO₄] reported in literature (1090, 1100 cm⁻¹).¹⁶ The stretching of the C=O group of the imidazolium cation was also identified at ν (CO) = 1710 cm⁻¹.

Synthesis of 1-(2-*t*-Butoxycarbonylamino-ethyl)-3-methyl-3H-imidazolium bis(trifluoromethylsulfonyl)imide ([2][NTf₂])

The counterion [NTf₂] has been chosen assuming that the corresponding ionic liquid would had to be insoluble in water, an important characteristic to avoid hydrolysis problems. In spite of what it was just affirmed, the partial solubility of [2][NTf₂] was observed.

A solution of the precursor **1a** in CH₂Cl₂ was reacted with the salt LiNTf₂ dissolved in Et₂O (Scheme 3.2-3) to obtain 1-(2-*t*-Butoxycarbonylamino-ethyl)-3-methyl-3H-imidazolium bis(trifluoromethylsulfonyl)imide, [2][NTf₂], as a thick, yellow oil with a density of 2.30g/mL at 25°C with a yield of 82%. The product was treated and characterized in the same way described for [2][ClO₄].



Scheme 3.2-3

The $^1\text{H-NMR}$ spectrum indicates the shift of the aromatic protons NCHN and the two CH_{im} respectively to δ 8.74, 7.31 and 7.22 ppm. The chemical shift relative to methylene groups, CH_3 and t-Bu resonate to 4.31, 3.55 3.93 and 1.38 ppm for $[\mathbf{2}][\text{NTf}_2]$. The $^{19}\text{F-NMR}$ (Figure 3.2-3) shows the presence of the counterion as a singlet at -79.1 ppm.

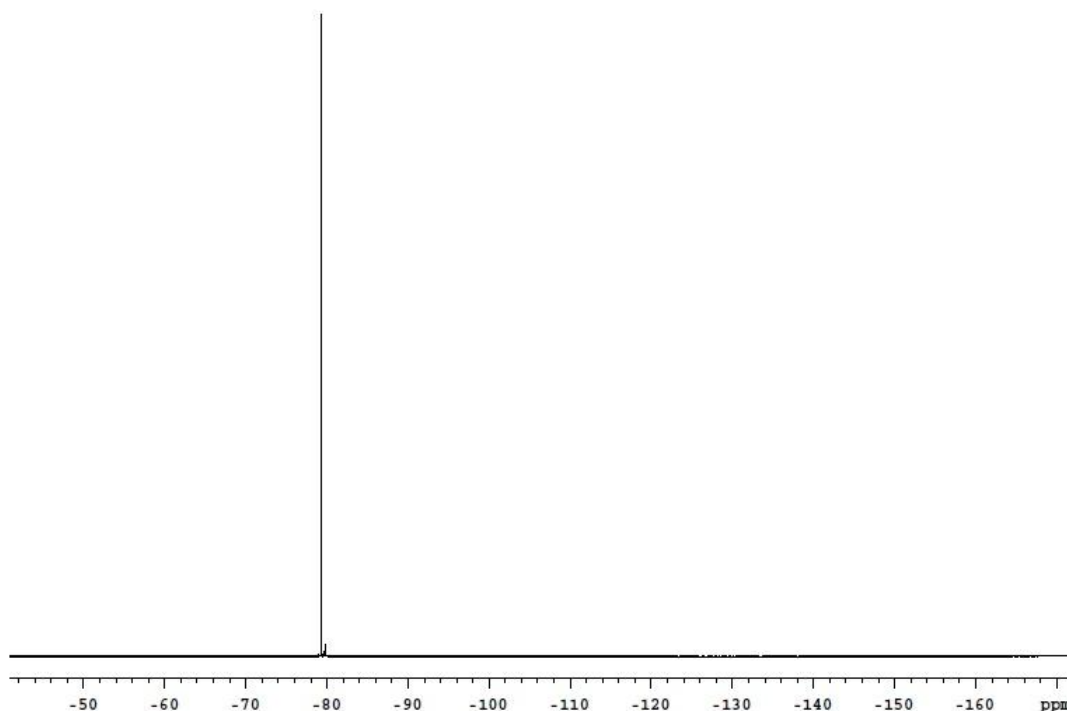


Figure 3.2-3 $^{19}\text{F-NMR}$ spectrum of $[\mathbf{2}][\text{NTf}_2]$.

The ESI-MS analysis (Figure 3.2-4) confirms the counterion exchange in fact in the spectrum was noted only one peak at 280 m/z for the negative ions corresponding to $[\text{C}_2\text{F}_6\text{NO}_4\text{S}_2]$ and the molecular ion at 226 m/z $[\text{C}_{11}\text{H}_{20}\text{N}_3\text{O}_2^+]$. In the IR spectrum were observed the peaks of the major

functional group of the counterion, R-SO₂-N, SO₂ and CF₃, respectively at 1351, 1191 and 790 cm⁻¹,¹⁷ the stretching of the C=O group of the imidazolium cation was also identified at $\nu(\text{CO}) = 1711 \text{ cm}^{-1}$.

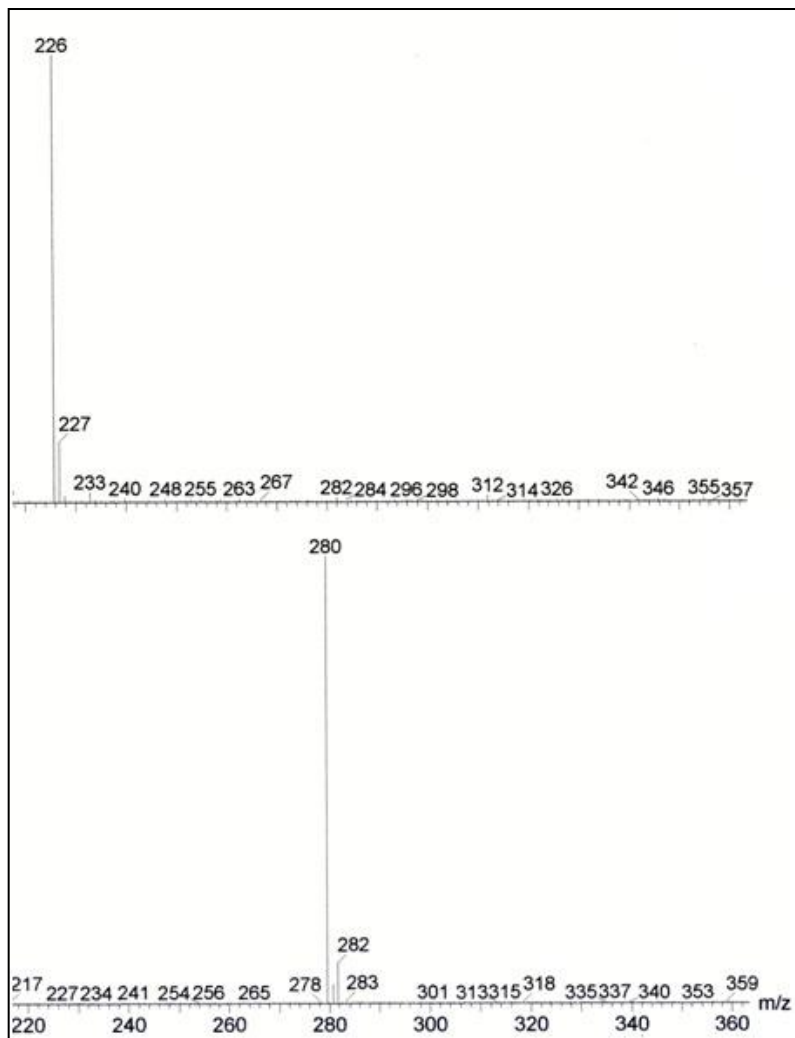
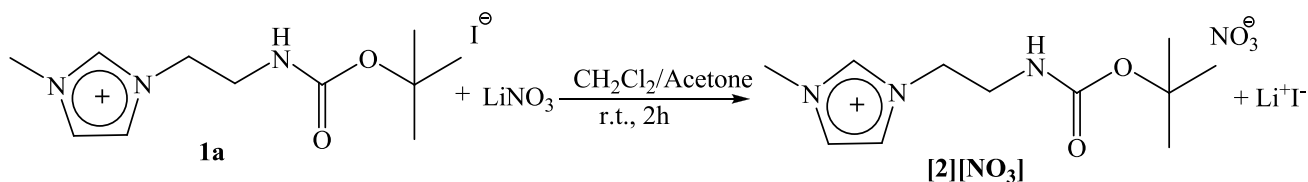


Figure 3.2-4 ESI-MS spectrum of [2]NTf₂, above is shown the peak of the molecular cation and below the negative ion.

Synthesis of 1-(2-*t*-Butoxycarbonylamino-ethyl)-3-methyl-3*H*-imidazolium nitrate ([2][NO₃])

A solution of **1a** in CH₂Cl₂ was reacted with a solution of LiNO₃ in acetone (Scheme 3.2-4) to perform the counterion exchange and obtain the ionic liquid 1-(2-*t*-Butoxycarbonylamino-ethyl)-3-methyl-3*H*-imidazolium nitrate, [2][NO₃], as a thick yellow oil in a quantitative yield. It was used the acetone as a reaction solvent because the salt results not completely soluble neither in dichlorometane nor in diethyl ether. Unfortunately the product was soluble in water, for this reason

it was impossible to purify $[2][\text{NO}_3]$ from the inorganic salts by the extraction with $\text{CH}_2\text{Cl}_2/\text{H}_2\text{O}$. The product appears as a yellow oil with a density of 1.14 g/mL at 25°C.



Scheme 3.2-4

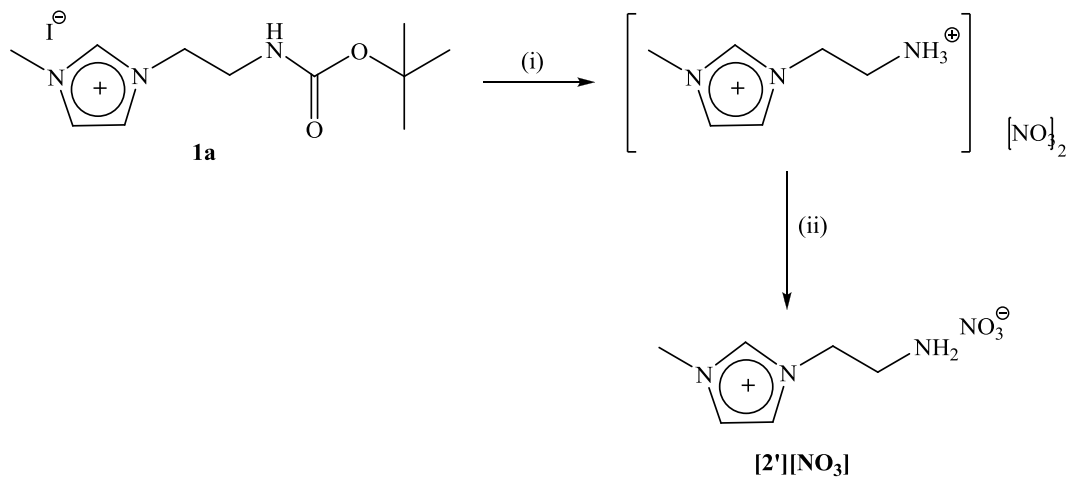
$[2][\text{NO}_3]$ was characterized by NMR and IR spectroscopy. The NMR analysis was performed in deuterated water for its solubility characteristics. The ^1H -NMR spectrum shows a shift of the acid proton (NCHN) to δ 8.61 and the imidazole backbone protons to 7.35 and 7.30 ppm. The peak of NH is not detectable. By IR spectroscopy the presence of the nitrate was observed as a peak at 1368 cm^{-1} ,¹⁸ the protective group BOC shows a broad peak at 3416 cm^{-1} corresponding to NH and a peak at 1694 cm^{-1} for the carbonyl. The ESI-MS analysis of this product was not developed due to the impossibility to remove the I from the reaction mixture, purification of $[2][\text{NO}_3]$ will be matter of further studies.

Synthesis of 3-(2-aminoethyl)-1-methyl-1H-imidazol-3-ium nitrate ($[2'][\text{NO}_3]$)

Once obtained a series of NHBoc functionalized imidazolium salts we also prepared a deprotected form, following a procedure reported in the literature.¹⁹

The precursor, **1a**, was deprotected by acid treatment of the amine group (Scheme 3.2-5). In the first step a dichloromethane solution of 1-(2-*t*-Butoxycarbonylamino-ethyl)-3-methyl-3*H*-imidazolium iodide was treated with HNO_3 65% at room temperature leading to the insoluble dicationic salt, $[\text{NH}_3(\text{CH}_2)_2\text{ImMe}][\text{NO}_3]_2$. On addition of nitric acid the pale yellow solution immediately turns to dark violet due to the concomitant oxidation of the iodide to iodine. After removal of the solvent and iodine under vacuum and washing with acetonitrile, $[\text{NH}_3(\text{CH}_2)_2\text{ImMe}][\text{NO}_3]_2$ ($[2'][\text{NO}_3]$) was obtained as an air-stable white solid. This salt is soluble in DMSO, water and partially soluble in methanol and ethanol. The dicationic species was characterized by NMR and IR spectroscopy. In the ^1H -NMR spectrum in DMSO solvent the NCHN resonance was found at δ 9.10 (137.25 in ^{13}C -NMR spectrum), the imidazole backbone protons (CH_{im}) appear as a singlet at 7.73 ppm, whereas the resonance of the ammonium group was found

as a broad singlet at δ 8.06 (this resonance was not observed when the spectra was carried out in D_2O). The methylene protons of the side chain give rise to a triplet at 4.40 ppm and a multiplet at 3.35 ppm (corresponding at δ 46.31 for NCH_2 and δ 38.41 for $CH_2NH_3^+$ in the ^{13}C -NMR spectrum).



Scheme 3.2-5

Subsequent treatment of $[NH_3(CH_2)_2ImMe][NO_3]_2$ in methanol with NaOH led to the formation of 3-(2-aminoethyl)-1-methyl-1*H*-imidazol-3-ium nitrate, **[2']** $[NO_3]$, with a yield of 33%. After evaporation of the solvent, the product can be separated from the saline byproduct by extraction with acetonitrile to afford a pale yellow oil. In the 1H -NMR in DMSO, the NH_2 resonance was not observed whereas the signals corresponding to the ethylamino side chain protons are upfield shifted with respect to $[NH_3(CH_2)_2ImMe][NO_3]_2$, in particular the directly bound amino-methylene protons (CH_2NH_2) are shifted and appear as a triplet at δ 2.89. The ESI-MS analysis indicates the presence of the cation $[NH_2(CH_2)_2ImMe]^+$ with a single peak at $m/z = 126$ and the nitrate anion at $62 m/z$.

Table 3.2-2 Most significant chemical shifts in $^1\text{H-NMR}$ spectra of the functionalized imidazolium salts 1-(2-*t*-Butoxycarbonylamino-ethyl)-3-methyl-3*H*-imidazolium (1).

Compounds	NCHN $\delta(\text{ppm})$	CHim $\delta(\text{ppm})$	NCH ₂ $\delta(\text{ppm})$	NCH ₃ $\delta(\text{ppm})$
1a (CDCl ₃)	9.92	7.19 7.08	4.28	3.93
[2][PF ₆] (CDCl ₃)	9.54	7.25 7.15	4.39	3.92
[2][ClO ₄] (CDCl ₃)	8.83	7.31 7.26	4.36	3.96
[2][NTf ₂] (CDCl ₃)	8.74	7.31 7.22	4.31	3.93
[2][NO ₃] (D ₂ O)	8.61	7.35 7.30	4.12	3.74
[2'] [NO ₃] (D ₂ O)	9.08	7.73 7.71	4.09	3.86

3.3 Experimental Section

Materials and General Procedure. All reactions were carried out under argon using standard Schlenk techniques. The solvents dichloromethane (CH₂Cl₂) and tetrahydrofuran (THF) were degassed and distilled on appropriate drying agent (Na on benzophenone for THF, CaH₂ for CH₂Cl₂) and kept on molecular sieves in a inert atmosphere. The other solvents employed: dioxane, methanol (MeOH), hexane and diethyl ether (Et₂O) were used without further purification. The deuterated solvents, used after being dried on appropriate drying agents and degassed, were stored in ampules under argon on 4Å molecular sieves. Reagents: potassium hexafluorophosphate, lithium perchlorate, lithium bis(trifluoromethan)-sulfonimide, lithium nitrate, silver nitrate were used as purchased from Sigma Aldrich. All reactions were followed, and the products characterized through

IR and NMR spectroscopy. The IR spectra were recorded with a FT-IR Perkin-Elmer Spectrum 2000 spectrometer using a NaCl cell (thickness 1mm) for liquids compounds and KBr or NaCl pellets (neat or nujol) for solids and oils. The accuracy on the wave number is ± 1 cm⁻¹. The NMR spectra were recorded using Varian Inova 300 (1H, 300.1; 13C, 75.5 MHz), Varian MercuryPlus VX 400 (1H, 399.9; 13C, 100.6 MHz), Varian Inova 600 (1H, 599.7; 13C, 150.8 MHz) instruments. The spectra were referenced internally to residual solvent resonances, and unless otherwise stated, they were recorded at 298 K for characterization purposes. All chemical shift values are reported in ppm (δ scale), using, as an internal standard, the residual proton resonance of the non-deuterated: CDCl₃ (7.26, 77.0) D₂O (4.80). ESI-MS analyses were performed by direct injection of methanol solutions of the metal complexes using a Waters ZQ 4000 mass spectrometer. Elemental analyses were performed on a Thermo-Quest Flash 1112 Series EA instrument. Crystal data were collected at room temperature on a Bruker APEX II diffractometer equipped with a CCD detector operating at 50 kV and 30 mA, using graphite monochromated MoK α radiation ($\lambda = 0.71073$ Å). An empirical absorption correction was applied on both structures by using SADABS.¹¹ They were solved by direct methods and refined by full-matrix least-squares based on all data using F^2 with SHELXL97.¹² All non-hydrogen atoms were refined anisotropically, with the exception of the hydrogen atoms which were set geometrically and given fixed isotropic thermal parameters.

3.3.1 Synthesis of 1-(2-*t*-Butoxycarbonylamino-ethyl)-3-methyl-3*H*-imidazolium hexafluorophosphate ([2][PF₆])

To a solution of 1-(2-*t*-Butoxycarbonylamino-ethyl)-3-methyl-3*H*-imidazolium iodide, **1a**, (4.42g, 0.012mol) in CH₂Cl₂ (20mL) 2.54g (0.013mol, 1.1eq) of KPF₆ solid was added. The reaction mixture was stirred for 3h, at the end of the reaction, the reaction mixture was filtered on a celite pad and the solvent was removed under vacuum. A yellow oil identified as 1-(2-*t*-Butoxycarbonylamino-ethyl)-3-methyl-3*H*-imidazolium hexafluorofosphate, [2][PF₆] was obtained in quantitative yield. The density was estimated as 1.06g/mL at 25°C. ¹H NMR (CDCl₃) δ (ppm): 9.54 (s, 1H, NCHN); 7.25 (s, 1H, CHim), 7.17 (s, 1H, CHim); 5.62 (br s, 1H, NH); 4.39 (t, 2H, NCH₂, J = 5.6Hz); 3.92 (s, 3H, NCH₃); 3.56 (m, 2H, CH₂NHBoc); 1.28 (s, 9H, CH₃). ¹³C NMR (CDCl₃) δ (ppm): 156.40 (C=O); 137.23 (CH, NCHN); 123.02 (2CH, CHim); 49.78 (NCH₂); 40.20 (CH₂NH); 37.01 (NCH₃); 28.28 (CH₃). ¹⁹F NMR (CDCl₃) δ (ppm): -72.75 (d, 6F, J = 710 Hz). ESI-MS (MeOH, *m/z*): 226 (100) [M]⁺, 145 (100) [M]⁻.

3.3.2 Synthesis of 1-(2-*t*-Butoxycarbonylamino-ethyl)-3-methyl-3*H*-imidazolium perchlorate ([2][ClO₄])

In a 50mL flask 0.22g (62mmol) of **1a** was dissolved in CH₂Cl₂ (20mL), to this a solution of LiClO₄ (0.33g, 5eq, 3.12mmol) was added in Et₂O (15mL). The reaction mixture was stirred for 2h. At the end of the reaction the product was filtered and, after removing the solvent under reduced pressure, was dissolved in H₂O. The product can be separated from salts by extraction in CH₂Cl₂, the organic phase was dried with sodium sulphate anhydrous and filtered on filter paper. Removed the solvent, a yellow oil with a yield of 76% was obtained. ¹H NMR (CDCl₃) δ(ppm): 8.83 (s, 1H, NCHN); 7.31 (s, 1H, Him), 7.26 (s, 1H, CHim); 5.46 (br s, 1H, NH); 4.36 (t, 2H, NCH₂, J = 5.4Hz); 3.96 (s, 3H, NCH₃); 3.58 (m, 2H, CH₂NHBoc); 1.39 (s, 9H, CH₃). ESI-MS (MeOH, *m/z*): 226 (100) [M]⁺, 99 (100) [M]⁻. IR (CH₂Cl₂) v (ClO₄): 1097 cm⁻¹; v (ClO₄): 1167 cm⁻¹ v (C=O): 1710 cm⁻¹.

3.3.3 Synthesis of 1-(2-*t*-Butoxycarbonylamino-ethyl)-3-methyl-3*H*-imidazolium bis(trifluoromethylsulfonyl)imide ([2][NTf₂])

To a solution of **1a** (5.27g, 0.015mol) in CH₂Cl₂ (35mL) 7.01g (0.024mol, 1.6eq) of C₂F₆LiNO₄S₂ dissolved in 25mL of Et₂O was added. The reaction mixture was stirred for 2h. At the end of the reaction the solvent was removed under reduced pressure and then the product was dissolved in H₂O and extracted with CH₂Cl₂. The organic phase was dried with sodium sulphate anhydrous and filtered on filter paper. After removing the solvent 6.22g of a yellow oil identified as -(2-*t*-Butoxycarbonylamino-ethyl)-3-methyl-3*H*-imidazolium bis(trifluoromethane) sulfinimide, [2][NTf₂], were obtained. Yield: 82%. The density was estimated as 2.30g/mL at 25°C. ¹H NMR (CDCl₃) δ(ppm): 8.74 (s, 1H, NCHN); 7.31 (s, 1H, CHim), 7.22 (s, 1H, CHim); 5.29 (br s, 1H, NH); 4.31 (t, 2H, NCH₂, J = 5.6Hz); 3.93 (s, 3H, NCH₃); 3.55 (m, 2H, CH₂NHBoc); 1.38 (s, 9H, CH₃). ¹⁹F NMR (CDCl₃) δ(ppm): -79.10 (s, 6F) ESI-MS (MeOH, *m/z*): 226 (100) [M]⁺, 280 (100) [M]⁻. IR ;(NaCl) v (CO): 1711 cm⁻¹ v (R-SO₂-N): 1351 cm⁻¹; v (SO₂): 1191 cm⁻¹; v (CF₃): 790 cm⁻¹.

3.3.4 Synthesis of 1-(2-*t*-Butoxycarbonylamino-ethyl)-3-methyl-3*H*-imidazolium nitrate ([2][NO₃])

In a 100mL flask was dissolved 3.67g (10.4mmol) of **1a** in CH₂Cl₂ (30mL), to this a solution of LiNO₃ (1.43g, 2eq, 20.7mmol) in acetone (15mL) was added. The reaction mixture was stirred for 2h. Unlike to the previous procedure the extraction CH₂Cl₂/H₂O was not made because this ionic liquid results soluble in water. At the end of the reaction the product was filtered and the solvent removed under reduced pressure, a yellow oil with a quantitative yield was obtained, [2][NO₃]. The

density was estimated as 1.14g/mL at 25°C. **¹H NMR** (D₂O) δ(ppm): 8.61 (s, ¹H, NCHN); 7.35 (s, 1H, CHim), 7.30 (s, 1H, CHim); 4.12 (t, 2H, NCH₂, J = 5.6Hz); 3.74 (s, 3H, NCH₃); 3.35 (m, 2H, CH₂NHBoc); **IR** (NaCl) ν (NH): 3413 cm⁻¹; ν (CO): 1694 cm⁻¹; ν (NO₃): 1368 cm⁻¹.

4 Synthesis and Characterization of Imidazolium Salts incorporating a Benzyl Group

4.1 Introduction

The novel imidazolium salts [BzImR]X (**1d**, R = Methyl, X = I; **1e**, R = Benzyl, X = Br; **1f**, R = Ph₂CH, X = Cl; **1g**, R = Trityl, X = Cl; **1h**, R = *t*-butyl, X = Br) bearing increasingly bulky N-alkyl substituents were prepared in high yields. (Figure 4.1-1). Four of them (**1d**, **1e**, **1g**, **1h**) have been employed as precursors for the synthesis of Rh(I) complexes.

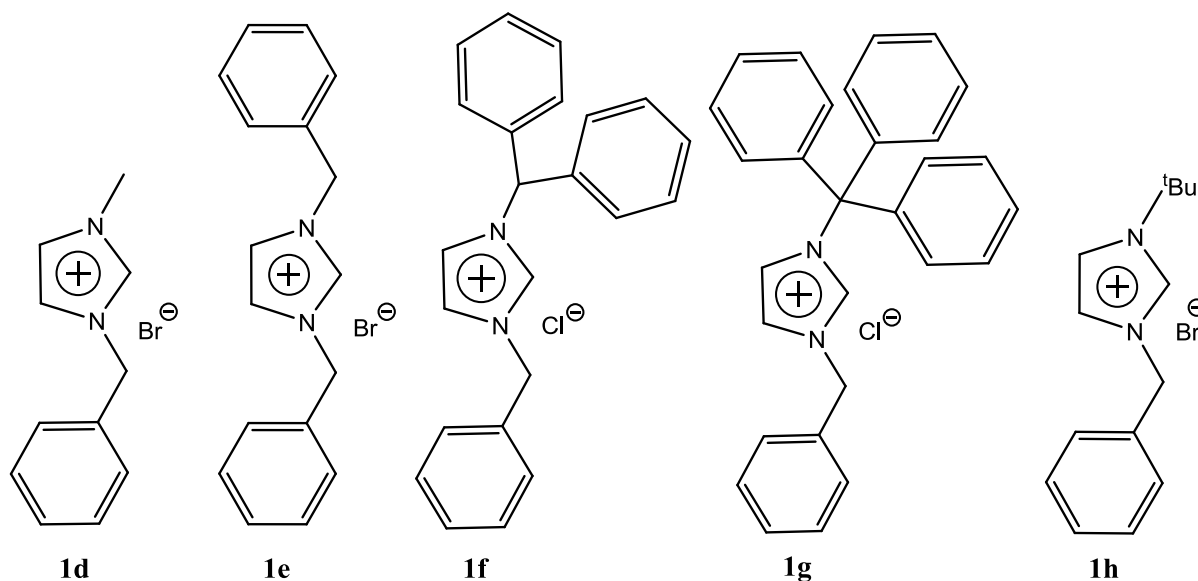


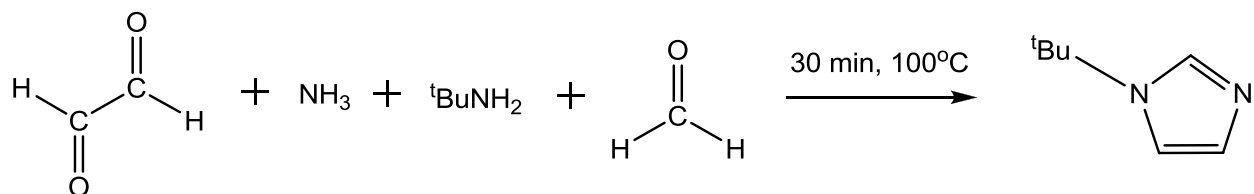
Figure 4.1-1 The imidazolium salts [BzImR]X **1d-h**, bearing increasingly bulky N-alkyl substituents.

4.2 Results and discussion

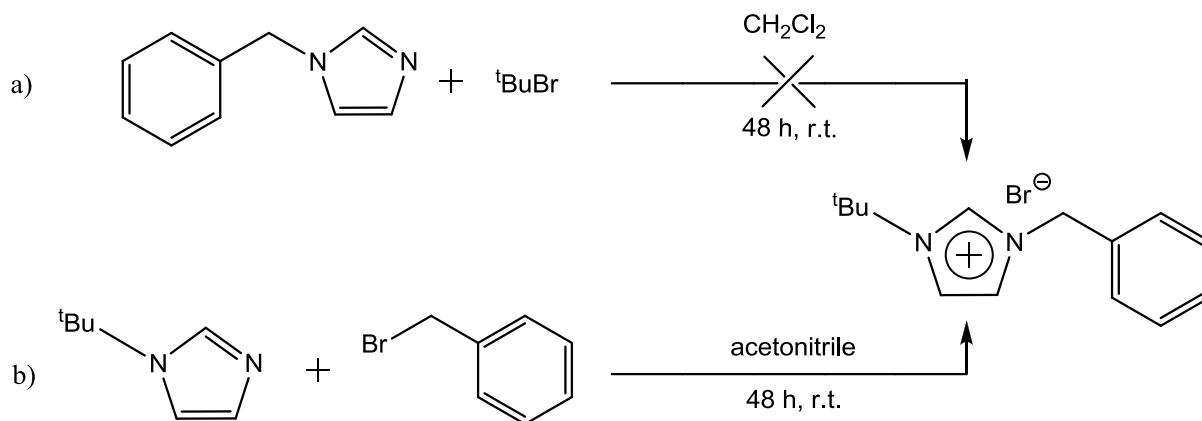
4.2.1 Synthesis

The imidazolium salts [BzImR]X (**1d**, R = methyl, X = Br; **1e**, R = benzyl, X = Br) were prepared in quantitative yields following published procedures²⁰ by alkylation of 1-benzylimidazole with the pertinent alkyl halide in dichloromethane or/and acetonitrile at room temperature. A similar synthetic procedure was also employed for the preparation of the novel imidazolium salts **1f**, **1g** and **1h** (**1f**, R = Ph₂CH-, X = Cl; **1g**, R = trityl, X = Cl; **1h**, R = *t*-butyl, X = Br). However, while in the case of **1g** this procedure led to the desired product in a straightforward way, in case of **1f** the product was obtained but the purification proved to be a lengthy and time-consuming process and for **1g** the alkylation of 1-benzylimidazole with 1-*tert*-butyl bromide did not afford the desired

product. The most likely explanation of this failure is the occurrence of a E1 elimination reaction, in which the *tert*-butyl bromide in the presence of 1-benzylimidazole, which is a weak base ($pK_a = 7.3$) releases a molecule of HBr (with evolution of isobutene gas) which further reacts with benzylimidazole to form the corresponding imidazolium bromide salt. This hypothesis has been confirmed by the ^1H NMR analysis of the crude material, which showed the presence of 2-methylpropene with chemical shifts at 4.58 and 1.56 ppm, in perfect agreement with simulated spectra²¹; in contrast, for the 1-benzylimidazolium bromide salt a full peak assignment was not possible to be made²²; furthermore, the most intense signal appearing in the spectrum in a low field with the chemical shift $\delta = 1.73$ ppm was attributed to unreacted *tert*-butyl bromide. Eventually, the salt **1h** was obtained by an alkylation of *tert*-butylimidazole (prepared using the Debus-Radziszewski reaction²³ shown in Scheme 4.2-1) with benzyl bromide²⁴ (Scheme 4.2-2).



Scheme 4.2-1 Debus-Radziszewski reaction employed in the synthesis of *tert*-butylimidazole



Scheme 4.2-2 (a) The unsuccessful synthesis of **1h** by alkylation of 1-benzylimidazole with *tert*-butyl bromide, thwarted by the E1 elimination and (b) the alkylation of *tert*-butylimidazole with benzyl bromide leading to the desired product.

The imidazolium salt **1d** was isolated as a pale yellow viscous liquid, whereas the salts **1e-h** are very hygroscopic crystalline solids. Moreover, it has been observed, that the use of acetonitrile as a solvent favored the formation of crystalline solid products, whereas the syntheses carried out in CH_2Cl_2 usually led to the formation of viscous liquids. This behavior can be explained either by the different physical properties of these two solvents (much bigger dipole moment and lower density

of acetonitrile with respect to CH_2Cl_2), which can cause different intermolecular interactions; or the difference can derive from the presence of some impurities often present in the CH_2Cl_2 , such as hydrogen chloride or methanol. All the salts **1d-h** are soluble in chlorinated solvents and were fully characterized by elemental analysis, NMR spectroscopy and electrospray ionization mass spectrometry (ESI-MS). The NMR resonances of the imidazolium salts were observed at chemical shifts typical for compounds of this kind. The most significant chemical shifts and coupling constants in ^1H and ^{13}C NMR spectra of the **1d-h** compounds are presented in Table 4.2-1. As regards the ^1H NMR spectra, the acidic protons NCHN of the imidazole fragment were found in the range 10.66 – 9.92 ppm; the resonances of the imidazole backbone protons were observed in the aromatic region of the spectra for all of the salts, as two singlets in the spectra of **1d**, **1f** and **1g**, as a doublet with a coupling constant $^2J_{\text{H,H}} = 1.5$ Hz in case of the symmetric **1e** (Figure 4.2-1), and as two multiplets (namely two not resolved doublet of doublets) with a coupling constant $^1J_{\text{H,H}} = 1.8$ Hz and $^2J_{\text{H,H}} \approx ^1J_{\text{H,H}}$ for **1h** (Figure 4.2-2). In case of **1g** the two signals were significantly shifted one from the other ($\Delta\delta = 0.72$ ppm); the benzylic protons resonate in the range 5.36-5.21 ppm and appear as a singlet.

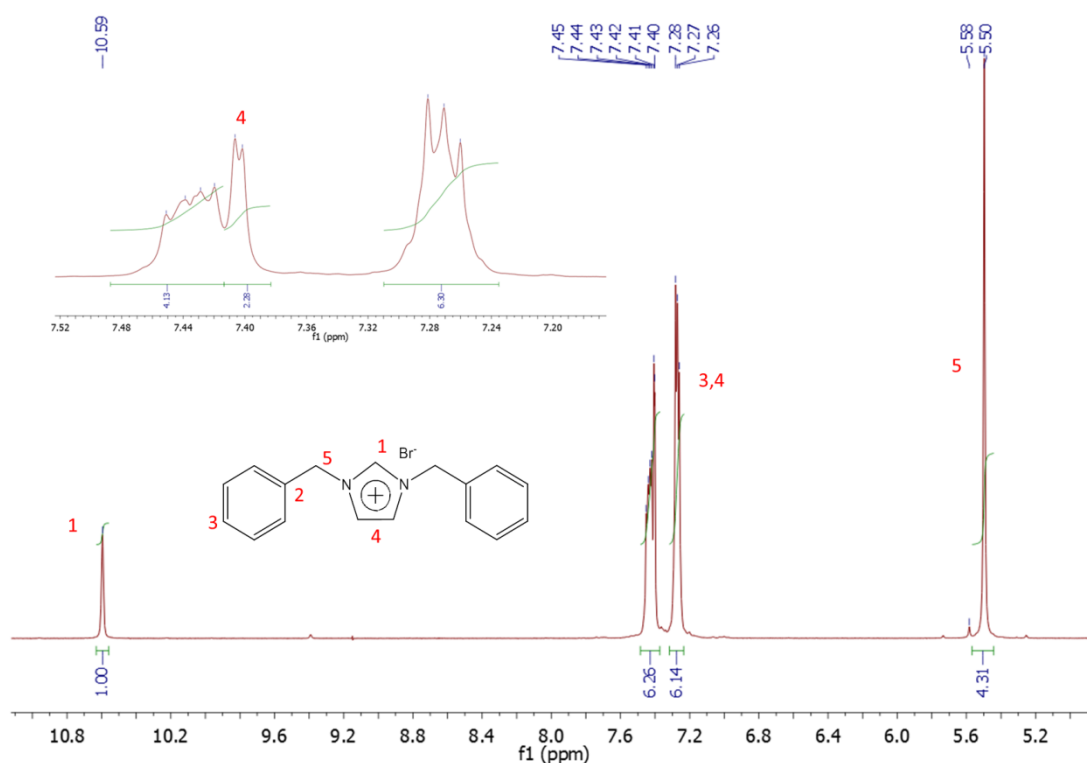


Figure 4.2-1 ^1H NMR spectrum of **1e** with the inset showing signals deriving from imidazole backbone protons.

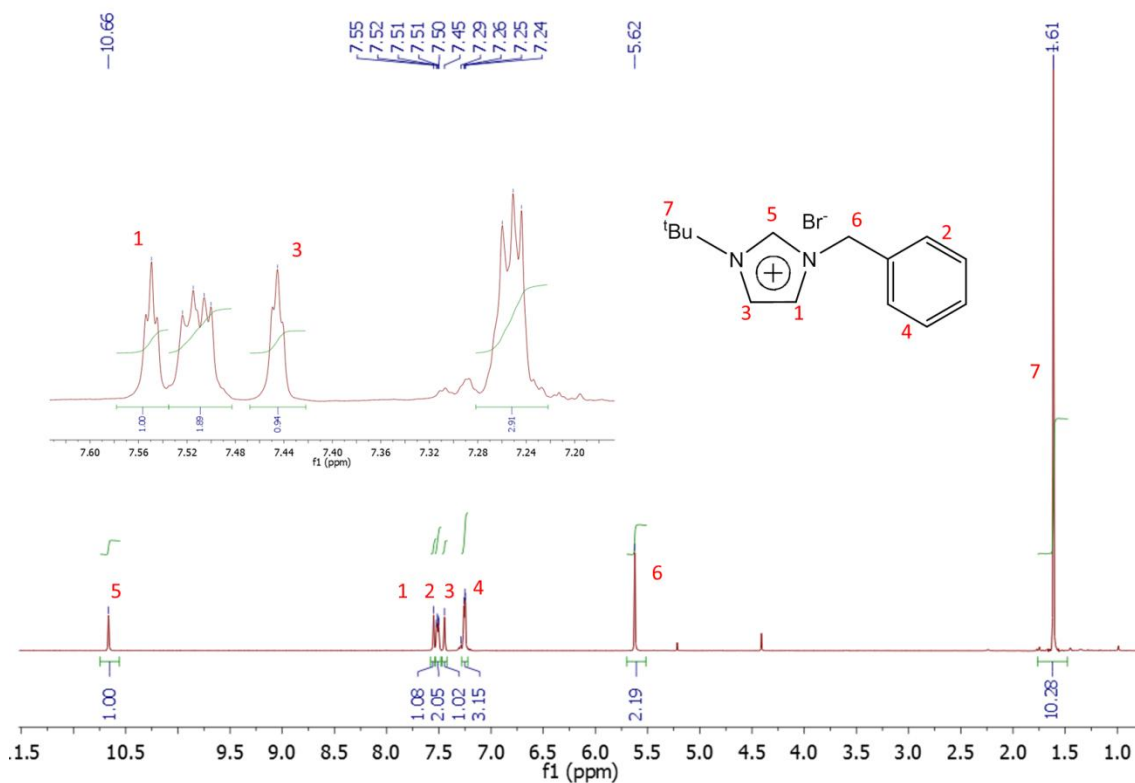


Figure 4.2-2 ^1H NMR spectrum of **1h** with the inset showing signals deriving from imidazole backbone protons.

Table 4.2-1 The most significant chemical shifts in ^{13}C and ^1H NMR spectra of the **1d-h**.

Compounds	δ (ppm) NCHN	δ (ppm) CH_{im}	δ (ppm) NCHN	δ (ppm) CH_{im}
1d	10.58	7.48 (s)	137.9	123.2 121.6
1e	10.59	7.41 d, $J_{\text{H,H}} = 1.5$ Hz	136.3	122.0
1f	10.74	Not detected	140.8	122.0 121.1
1g	9.92	7.65 (s)	146.8	123.7 121.8

1h	10.66	7.55 m, $^1J_{\text{H,H}} = 1.82 \text{ Hz}$ 7.45 m, $^1J_{\text{H,H}} = 1.88 \text{ Hz}$	137.4	121.9 119.7
----	-------	--	-------	----------------

4.2.2 Deprotonation of imidazolium salts

The preparation of free carbenes from the imidazolium salts **1d** and **1e** have been tried without a success. The deprotonation reactions were carried out under strictly anhydrous conditions in a variety of dry solvents, including acetonitrile, THF and toluene, using 1.2 molar equivalent of the base KO^tBu with respect to the imidazolium salt. In most of the cases, after the addition of the base, the reaction mixture turned bright yellow, but the NMR analysis indicated only the presence of unidentified decomposition products. Eventually, we succeeded in deprotonating the salts **1d** and **1e**, without decomposition, in the reaction of the respective imidazolium salt with only 0.9 molar equivalent of the KO^tBu . The choice of this proportion salt/base seems to be rational in a light of the risk to deprotonate other acidic sites in a molecule by a strong base; however, since the reaction was carried out in CDCl_3 , an immediate deuteration occurred (**1'e**), which was unambiguously confirmed by the ^{13}C NMR experiment; in this spectrum, a downfield triplet deriving from the carbenic carbon coupling to the deuterium atom appeared at 135.94 ppm with coupling constant $^1J(^{13}\text{C-D}) = 33.0 \text{ Hz}$ (Figure 4.2-3).

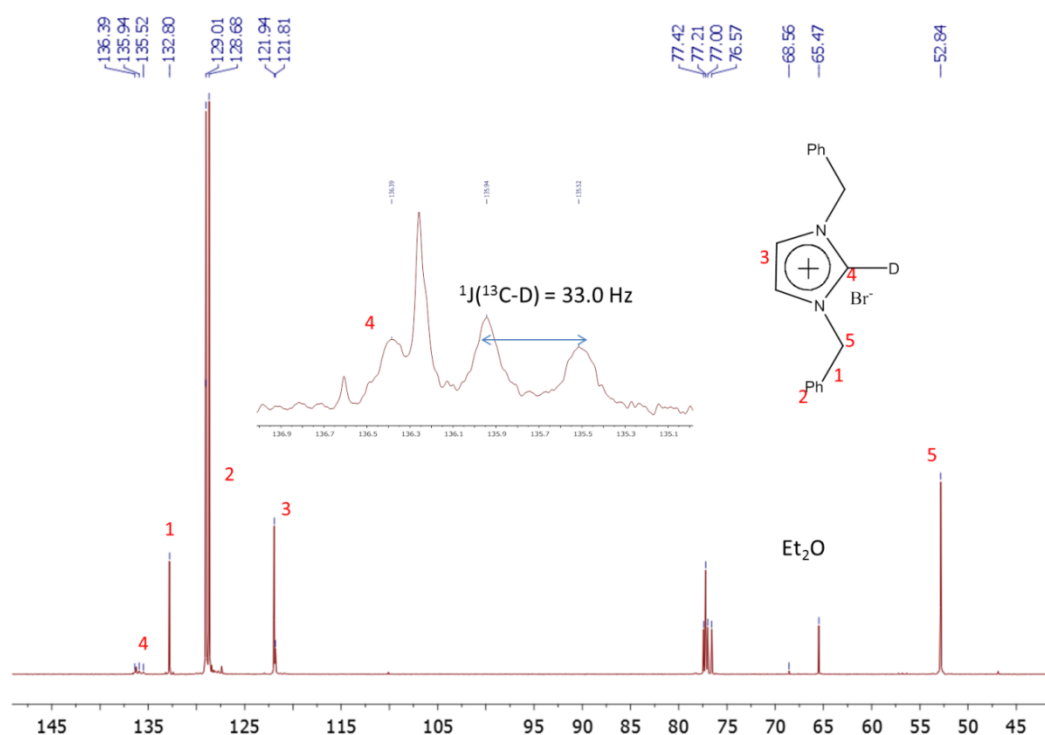


Figure 4.2-3 ^{13}C NMR spectrum of deuterated **1'e** with the inset showing the 1:1:1 triplet at 135.94 ppm.

These results indicate that the deprotonation reaction leads to the immediate formation of the desired NHC carbene, but due to its high reactivity, it can be used only *in situ* reactions.

4.3 Experimental Part

Materials and Procedures. All reactions were carried out under argon using standard Schlenk techniques. Solvents were dried and distilled under nitrogen prior to use; the deuterated solvents, used after being appropriately dried and degassed, were stored in ampules under argon on 4Å molecular sieves. The prepared derivatives were characterized by elemental analysis and spectroscopic methods. The IR spectra were recorded with a FT-IR Perkin-Elmer Spectrum 2000 spectrometer. The NMR spectra were recorded using Varian Inova 300 (^1H , 300.1; ^{13}C , 75.5 MHz), Varian MercuryPlus VX 400 (^1H , 399.9; ^{13}C , 100.6 MHz). The spectra were referenced internally to residual solvent resonances, and unless otherwise stated, they were recorded at 298 K for characterization purposes; full ^1H and ^{13}C NMR assignments were done, when necessary, by gCOSY, gHSQC, gHMBC, NOESY and DEPT-135 NMR experiments using standard Varian pulse sequences; J.Young valve NMR tubes (Wilmad) were used to carry out NMR experiments under inert conditions. ESI-MS analyses were performed by direct injection of methanol solutions of the metal complexes using a Waters ZQ 4000 mass spectrometer. Elemental analyses were performed on a Thermo-Quest Flash 1112 Series EA instrument. The chemicals 1-methylimidazole, 1-benzylimidazole, benzyl bromide, *tert*-butyl bromide, the chemicals glyoxal and formaldehyde were used as purchased from Farmitalia Carlo Erba; *tert*-butylamine was purchased from Merck. The starting building blocks 1-*tert*-butylimidazole, trityl chloride, 1-benzyl-3-methyl-imidazolium bromide (**1d**), 1,3-dibenzyl-imidazolium bromide (**1e**), were prepared according to literature procedures or modified literature methods.

4.3.1 Synthesis of 1-benzyl-3-methyl-imidazolium bromide (**1d**)

This product was synthesized using a literature method.^{17 (a),(b)} In a 100 mL round-bottom flask to a solution of 1-methylimidazole (0.24 mL, 3.0 mmol) in acetonitrile (15 mL), an equivalent molar amount of benzyl bromide (0.36 mL, 3.0 mmol) was added. After stirring for 12 h at room temperature, the solvent was removed under vacuum, and the resulting pale yellow, viscous oil was thoroughly washed with diethyl ether (3 x 10 mL), Et₂O and hexane. After separation from the washings the oil was kept under vacuum at 40 °C for several hours to yield 0.720 g (Y = 94%) of **1d**. Anal. Calc.d for C₁₁H₁₃BrN₂: C, 52.19; H, 5.18; Br, 31.57; N, 11.07. Found: C, 52.01; H, 5.30; Br, 31.52; N, 11.01. **ESI-MS** (MeOH, m/z): 173 (100) [C₁₁H₁₃N₂]⁺; 79 (100), 81 (97) [Br]⁻. **^1H NMR** (400 MHz, CDCl₃): δ 10.58 (s, 1H, NCHN), 7.48 (s, 1H, CH_{im}), 7.47-7.46 (m, 1H, Ph),

7.41-7.39 (m, 3H, CH_{im} + Ph), 7.30 (s, 1H, Ph), 7.23 (s, 1H, Ph), 5.57 (s, 2H, CH₂Ph), 4.08 (s, 3H, CH₃). ¹³C NMR (100 MHz, CDCl₃): δ 137.93 (NCHN), 132.68 (C_q, Ph), 129.62 (Ph), 129.51 (Ph), 129.02 (Ph), 123.22 (CH_{im}), 121.63 (CH_{im}), 53.57 (CH₂Ph), 36.86 (CH₃).

4.3.2 Synthesis of 1,3-dibenzyl-imidazolium bromide (1e)

This product was synthesized using a literature method ^{17(c)}. In a 100 mL round-bottom flask to a solution of 1-benzylimidazole (0.48 g, 3.0 mmol) in acetonitrile (15 mL), an equivalent molar amount of benzyl bromide (0.36 mL, 3.0 mmol) was added. After stirring for 12 h at room temperature, the solvent was removed under vacuum, and the resulting pale yellow, viscous oil was thoroughly washed with diethyl ether (10 mL) and Etp (10 mL). After separation from the washings the oil was kept under vacuum at 40 °C for several hours to yield 0.98 g (Y = 99%) of **1e**. ¹H NMR (400 MHz, CDCl₃): δ 10.59 (s, 1H, NCHN), 7.43 (m, 4H, Ph), 7.41 (d, 2H, J_{H,H} = 1.5 Hz, CH_{im}), 7.28 (m, 6H, Ph), 5.50 (s, 4H, CH₂Ph). ¹³C NMR (100 MHz, CDCl₃): δ 136.34 (NCHN), 132.76 (C_q, Ph), 129.21 (Ph), 129.15 (Ph), 128.78 (Ph), 122.01 (CH_{im}), 53.01 (CH₂Ph). **ESI-MS** (MeOH, m/z): 249 (100) [C₁₇H₁₇N₂]⁺; 79 (97), 81 (100) [Br]⁻. Anal. Calc.d for C₁₇H₁₇BrN₂: C, 62.02; H, 5.20; Br, 24.27; N, 8.51. Found: C, 61.79; H, 5.03; Br, 24.39; N, 8.28.

4.3.3 Synthesis of 1-benzyl-3-diphenylmethylimidazolium chloride (1f)

This product was synthesized using a modified literature method.²¹ In a Schlenk to a solution of 1-benzylimidazole (0.25 g, 1.58 mmol) in CH₂Cl₂ (10 mL), diphenylmethyl chloride (0.28 mL, 4.74 mmol) was added. After stirring for 48 h at room temperature, the solvent was removed under vacuum, and the resulting pale yellow viscous oil was thoroughly washed with diethyl ether (3 x 10 mL). After separation from the washings the oil was kept under vacuum for several hours to yield **1f**.

4.3.4 Synthesis of 1-benzyl-3-trityl-imidazolium chloride (1g)

In a Schlenk tube to a solution of trityl chloride (0.18 g, 0.64 mmol) dissolved in CH₂Cl₂ (10 mL), 1-benzylimidazole (0.10 g, 0.65 mmol) was added. After stirring for 16 h at room temperature, the solvent was removed under vacuum and the resulting solid was thoroughly washed with diethyl ether (3 x 10 mL) to yield 0.25 g (89%) of a white solid identified as **1g**. ¹H NMR (300 MHz, CDCl₃): δ 9.92 (s, 1H, NCHN), 7.65 (s, 1H, CH_{im}), 7.49-7.11 (m, 20H, Ph), 6.93 (s, 1H, CH_{im}), 5.97 (s, 2H, CH₂Ph). ¹³C NMR (100 MHz, CDCl₃): δ 139.56 (C₅), 138.28 (NCHN), 133.54 (C₁₀), 129.63-127.66 (Ph), 123.69 (CH_{im}), 121.84 (CH_{im}), 79.77 (C₁), 53.92 (CH₂Ph). Anal. Calc.d for C₂₉H₂₅ClN₂: C, 79.71; H, 5.77; Cl, 8.11; N, 6.41. Found: C, 79.52; H, 5.43; Cl, 8.32; N, 6.05. **ESI-MS** (MeOH, m/z): 401 (100) [C₂₉H₂₅N₂]⁺; In the ESI-MS(-) spectrum, no peaks were observed.

4.3.5 Synthesis of 1-benzyl-3-tertbutylimidazolium bromide (1h)

In a Schlenk to a solution of 1-benzylimidazole (0.25 g, 1.58 mmol) in CH₂Cl₂ (5 mL), *tert*-butyl bromide (0.53 ml, 4.74 mmol) was added. After stirring for 48 h at room temperature, the solvent was removed under vacuum, and the resulting pale yellow viscous oil was thoroughly washed with diethyl ether (3 x 10 mL). After separation from the washings the oil was kept under vacuum for several hours to yield crude product.

4.3.6 Synthesis of 1-*tert*-butylimidazole (Debus-Radziszewski reaction)

This product was synthesized using a literature method.²¹ In a 100 mL three-necked flask connected to two dropping funnels and a condenser, was placed 50 mL of distilled water. One dropping funnel contained a mixture of 40% aqueous glyoxal (11.5 mL, 0.10 mol) and 40% aqueous formaldehyde (8.1 mL, 0.10 mol), the other *tert*-butylamine (10.6 mL, 0.10 mol) and 25% aqueous ammonia (6.8 mL, 0.10 mol). The water was heated until boiling, and then both solutions were added simultaneously. The reaction mixture turned brown and was stirred for 30 min at 100°C after complete addition and then cooled to room temperature. After removal of the water by rotatory evaporator, the crude product was purified via vacuum distillation (bp. 53°C/0.9mbar) and 1-*tert*-butylimidazole was obtained as a very pale yellow liquid (1.49 g, 12%). ¹H NMR (400 MHz, CDCl₃): δ 7.60 (s, 1H, NCHN), 7.05 (s, 1H, CH_{im}), 7.03 (s, 1H, CH_{im}), 1.57 (s, 9H, CH₃, ^tBu). ¹³C NMR (100 MHz, CDCl₃): δ 134.33 (NCHN), 129.06 (C_{im}), 116.27 (Cq^tBu), 30.62 (CH₃, ^tBu).

4.3.7 Synthesis of 1-benzyl-3-*tert*-butylimidazolium bromide (1h)

This product was synthesized using a modified literature method.²¹ In a Schlenk to a solution of 1-*tert*-butylimidazole (0.17 g, 1.40 mmol) in acetonitrile (5 mL), an equivalent molar amount of benzyl bromide (0.15 mL, 1.40 mmol) was added. After stirring for 48 h at room temperature, the solvent was removed under vacuum, and the resulting white solid was thoroughly washed with diethyl ether (2 x 4 mL). After separation from the washings the solid was kept under vacuum for 1 hour to yield 0.33 g (83%) of **1h**. ¹H NMR (400 MHz, CDCl₃): δ 10.66 (s, 1H, NCHN), 7.55 (dd, 1H, ³J_{H,H} ≈ ⁴J_{H,H} = 1.82 Hz, CH_{im}), 7.51 (m, 2H, Ph), 7.45 (dd, 1H, ³J_{H,H} ≈ ⁴J_{H,H} = 1.80 Hz, CH_{im}), 5.62 (s, 2H, CH₂Ph), (s, 9H, CH₃, ^tBu). ¹³C NMR (100 MHz, CDCl₃): δ 137.47 (NCHN), 133.28 (Cq, Ph), 129.00 (Ph), 128.14 (Ph), 121.96 (CH_{im}), 119.75 (CH_{im}), 60.21 (Cq, ^tBu), 52.66 (CH₂Ph), 29.91 (CH₃, ^tBu). Anal. Calcd (%) for C₁₄H₁₉BrN₂: C, 56.96; H, 6.49; Br, 27.07; N, 9.49. Found: C, 56.68; H, 6.26; Br, 26.86; N, 9.20. ESI-MS (MeOH, m/z): 215 (100) [C₁₄H₁₉N₂]⁺; 79 (100), 81 (97) [Br]⁻.

4.3.8 Synthesis of 1,3-dibenzyl-imidazolium triflate (1j)

In a Schlenk to a solution of 1,3-dibenzyl-imidazolium bromide (0.440 g, 1.34 mmol) in dichloromethane (3 mL) stirred for 5 min, silver triflate (0.346 g, 1.34 mmol) was added. After stirring for 24 h at room temperature, the solvent was removed under vacuum, and the resulting white solid was thoroughly washed with diethyl ether (3 x 10 mL). After separation from the washings the solid was kept under vacuum at 40 °C for several hours to yield 0.720 g (Y = 99%) of 1,3-dibenzyl-imidazolium triflate. ¹H NMR (400 MHz, CDCl₃): δ 9.52 (s, 1H, NCHN), 7.39-7.31 (m, 10H, Ph), 7.22 (d, 2H, J_{H,H} = 1.47 Hz, CH_{im}), 5.33 (s, 4H, CH₂Ph). ¹³C NMR (100 MHz, CDCl₃): δ 136.1 (NCHN), 132.6 (C_q, Ph), 129.4 (Ph), 129.3 (Ph), 128.8 (Ph), 122.1 (CH_{im}), 53.4 (CH₂Ph).

4.3.9 Reaction of 1e with KO^tBu (1'e)

Removal of the acidic proton with a strong base (0.9 equivalents).

The salt **1e** was dissolved in deuterated CDCl₃, then the KO^tBu base was added to the reaction mixture and stirred for 5 min. After this time, the above reaction was checked by NMR. ¹H NMR (600 MHz, CDCl₃): δ 7.38 (m, 6H, Ph + CH_{im}), 7.20 (m, 6H, Ph + CH_{im}), 5.43 (s, 4H, CH₂Ph). ¹³C NMR (150 MHz, CDCl₃): δ 132.80 (C_q, Ph), 129.01 (Ph), 128.79 (Ph), 128.42 (Ph), 121.94 (CH_{im}), 52.84 (CH₂Ph).

References

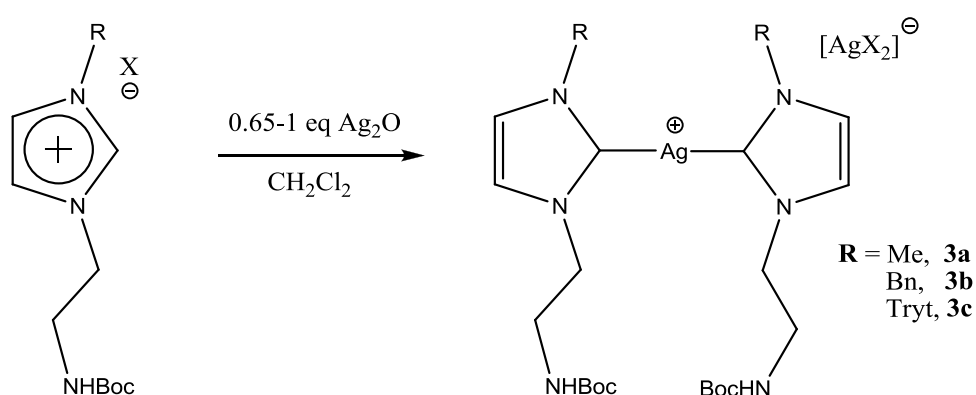
-
- 1 Busetto, L.; Cassani, M. C.; Femoni, C.; Macchioni, A.; Mazzoni, R.; Zuccaccia, D. *J. Organomet. Chem.* **2008**, 693, 2579.
 - 2 Sigler, G. F.; Rouhani, R.; *PCT Int. Appl.* **2000**, WO 2000078763, A2 20001228
 - 3 Bridger, G. J.; Skerlj, R. T.; Kaller, A.; Harwig, C.; Bogucki, D.; Wilson, T.; Crawford, J.; McEachern, E. J.; Atsma, B.; Nan, S.; Zhou, Y.; Schols, D.; Smith, Christopher D.; Di Fluri, R. M.; *Patent*, **2003**, WO2003055876
 - 4 Park, K. H.; Kim, S. Y.; Son, S. U.; Chung, Y. K. *Eur. J. Org. Chem.*, **2003**, 4341.
 - 5 Lough, W. W. N. O, A. J.; Morris, R. H. *Organometallics* **2009**, 28, 6755 and references cited therein.
 - 6 Navarro, M.; Cisneros-Fajardo, E. J.; Lehmann, T.; Sanchez-Delgado, R. A.; Atencio, R.; Silva, P.; Lira, R.; Urbina, J. A. *Inorg. Chem.* **2001**, 40, 6879.
 - 7 (a) Casarini, D.; Femoni, C.; Grilli, S.; Lunazzi, L.; Mazzanti, A. *J. Org. Chem.* **2001**, 66, 488. (b) Gust, D.; Mislow, K. *J. Am. Chem. Soc.* **1973**, 95, 1535. (c) Focante, F.; Leardini, R.; Mazzanti, A.; Mercandelli, P.; Nanni, D. *Organometallics* **2006**, 25, 2166.
 - 8 Herrmann, W. A.; Lukas, K. C.; Gookn, J.; Artus, G. R. J.; *Chem. Eur. J.* **1996**, 17, 1627.
 - 9 Sigler, G. F.; Riaz, R. *Patent* WO2000078763, **2000**.
 - 10 Bridger, G. J.; Skerlj, R. T.; Kaller, A.; Harwig, C.; Bogucki, D.; Wilson, T.; Crawford, J.; McEachern, E. J.; Atsma, B.; Nan, S.; Zhou, Y.; Schols, D.; Smith, C. D.; Di Fluri, R. M. *Patent* WO2003055876, **2003**.
 - 11 Sheldrick, G. M., SADABS, 1996, University of Göttingen, Germany.
 - 12 Sheldrick, G. M., SHELXL97, University of Göttingen, Germany.
 - 13 Neumann, W. P.; Uzick, W.; Zarkadis, Antonios, K. *J. Am. Chem. Soc.* **1986**, 108, 3762.

-
- 14 Cesari C. "Oxidiperoxomolybdenum catalyzed olefin epoxidation: the role of Ionic Liquids" Master degree in Industrial Chemistry A.Y. 2011-2012 University of Bologna.
- 15 Lough, W. W. N. O, A. J.; Morris, R. H. *Organometallics*, **2009**, *28*, 6755, and references therein
- 16 Pal S.; Nath Poddar S.; Gosh, S.; *Polyhedron*, **1995**, *14*, 325-328
- 17 Silverstein, R.W.; Webster, F.X.; *Identificazione spettroscopica di composti organici*, Casa Editrice Ambrosiana
- 18 Khloprogge, J.T.; Wharton, D.; Hickey, L.; Frost, R.L.; *Am. Mineral.*, **2002**, *87*, 623-629
- 19 Ballarin, B.; Busetto, L.; Cassani, M.C.; Femoni, C.; *Inorg. Chim. Act.*, **2010**, *363*, 2055-2064
- 20 ^(a) Patil, S.; Deally, A.; Gleeson, B.; Helge, M.; Paradisi, F.; Tacke, M. *Appl.Organometal.Chem.* **2010**, *24*, 781-793.
^(b) Moret, M.-etienne; Chaplin, A. B.; Lawrence, A. K.; Scopelliti, R.; Dyson, P. J. *Organometallics* **2005**, *24*, 4039-4048. ^(c) Patil, S.; Claffey, J.; Deally, A.; Hogan, M.; Gleeson, B.; Miguel, L.; Méndez, M.; Müller-bunz, H.; Paradisi, F.; Tacke, M. *Organometallics* **2010**, 1020-1031.
- 21 <http://www.personal.psu.edu/the1/sn1ande.htm>.
- 22 Elango, K.; Srirambalaji, R.; Anantharaman, G. *Tetrahedron Letters* **2007**, *48*, 9059-9062.
- 23 Sauerbrey, S.; Majhi, P. K.; Daniels, J.; Schnakenburg, G.; Brändle, G. M.; Scherer, K.; Streubel, R. *Inorganic Chemistry* **2011**, *50*, 793-9.
- 24 Corbera, R.; Sanau, M.; Peris, E. *Organometallics* **2006**, *25*, 4002-4008.

5 Synthesis and Characterization of Silver(I) Complexes with N-Heterocyclic Carbene Bearing the NHBoc Functionalization

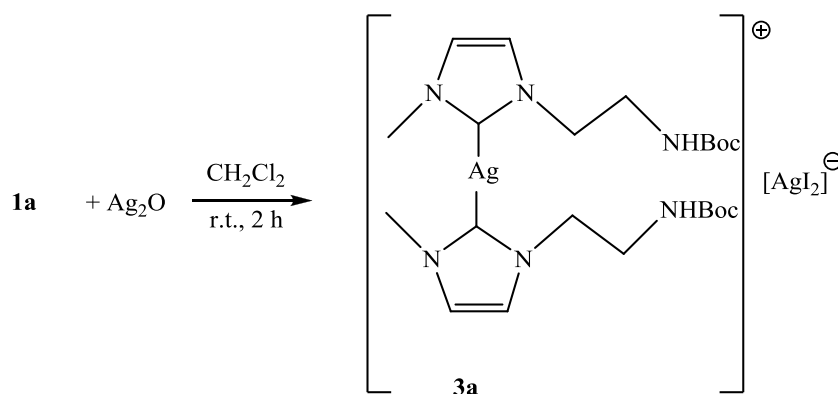
5.1 Introduction

Silver(I)-NHC complexes **3a-c** were obtained in quantitative yields via the most common silver base route,¹ by the reaction of the corresponding imidazolium salts with a small excess of Ag₂O in a 2:1.3 stoichiometric ratio Scheme 5.1-1. These particular compounds are precursors of Rh(I)-NHC complexes.



5.2 Results and Discussion

The imidazolium **1a** was hence treated with a slurry of Ag₂O in dichloromethane in a 2:1 molar ratio and stirred at room temperature for 2 h in the dark and under argon. The resulting grey suspension was filtered and the volatiles removed under reduced pressure to afford in quantitative yields the silver complex **3a** as a white solid that was analyzed by different spectroscopic techniques (Scheme 5.2-1).



Scheme 5.2-1

In the ^1H NMR spectrum in CDCl_3 the complete disappearance of the high frequency peak for the imidazolium proton was coupled with the appearance in the ^{13}C NMR spectrum of a sharp singlet at δ 184.9 assigned to a $\text{Ag-C}_{\text{carbene}}$ carbon (no ^{13}C - $^{107}\text{Ag}/^{109}\text{Ag}$ coupling was observed); the CH_{imid} carbons at δ 121.7 and 121.4 ppm, are, like the $\text{Ag-C}_{\text{carbene}}$ chemical shift, perfectly in keeping with the values reported in the literature for other imidazol-2-ylidene-silver complexes.¹ The electrospray ionization mass spectrometry analysis in methanol indicated the presence in solution of the silver salt $[\text{Ag}(\text{NHC-NHBoc})_2]^+[\text{AgI}_2]^-$ with peaks at 557 (100) m/z for $[\text{M}]^+$ ($\text{C}_{22}\text{H}_{38}\text{AgN}_6\text{O}_4$) and at 361 (100) m/z for $[\text{AgI}_2]^-$ with the observed isotopic distribution in perfect agreement with the calculated one. The carbonyl stretching frequency (ν_{CO}) of the carbamate group appeared at 1716 cm^{-1} in the IR spectrum in THF whilst the IR-Microscopy showed a strong N-H stretching absorption at 3339 cm^{-1} and a ν_{CO} at 1701 cm^{-1} . The silver complex is completely soluble in halogenated solvents, THF, acetone but insoluble in diethyl ether and petroleum ether.

Colourless crystals suitable for an X-ray crystal structure determination were obtained from a double layer acetone/hexane at $-20\text{ }^\circ\text{C}$. As illustrated in Figure 2.2-1 (selected bonds and angles are indicated in Table 2.2-1) the crystal structure consists of a $[\text{Ag}_2\text{I}_4]^{2-}$ fragment sandwiched between two identical $[\text{Ag}(\text{NHC-NHBoc})_2]^+$ complexes (**3a**) and it is analogous to the one reported by Chen and Liu.²

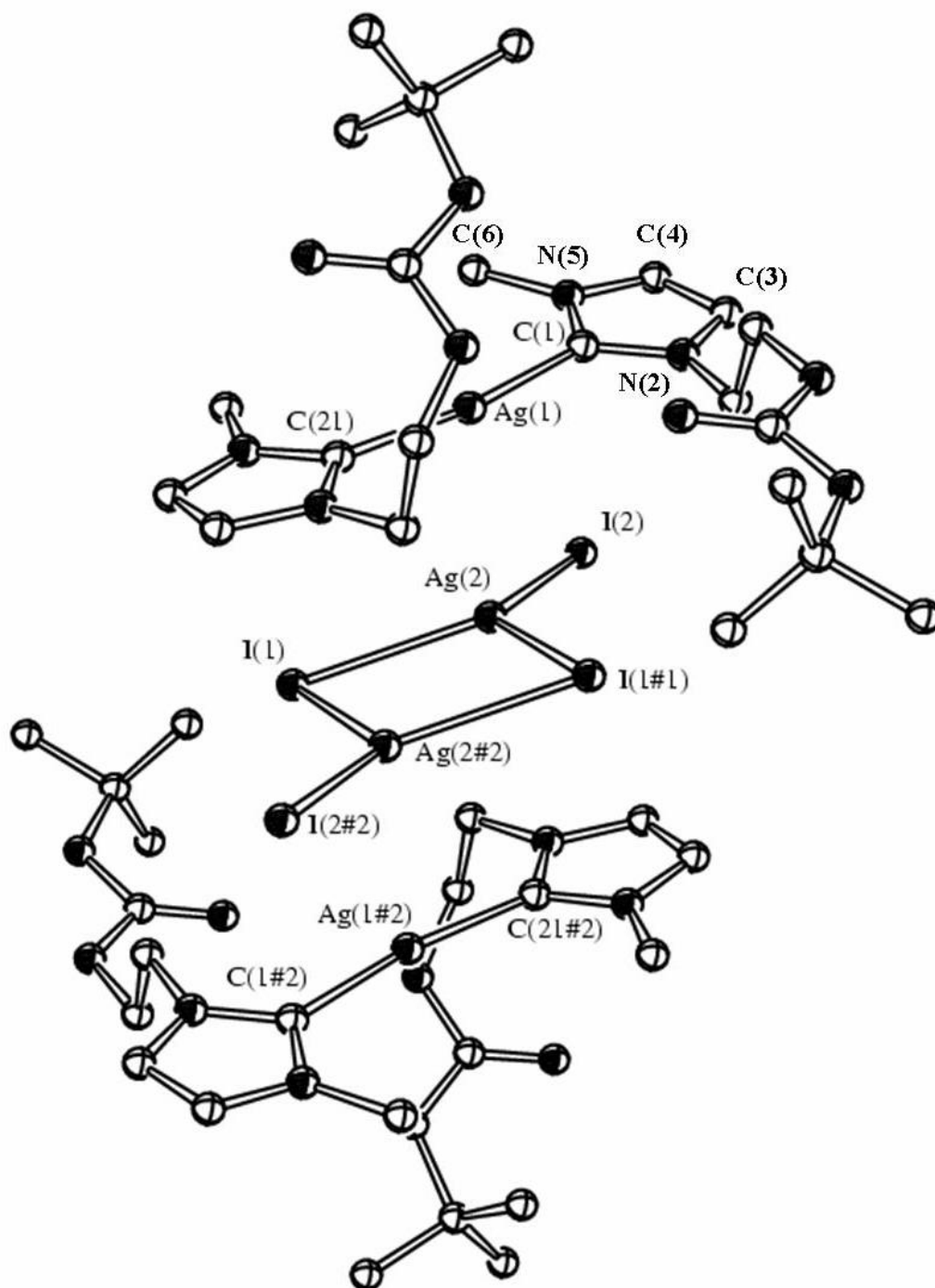


Figure 5.2-1 ORTEP diagram (30% probability thermal ellipsoids) of **3a** (for sake of clarity hydrogen atoms have been omitted).

The similarities are found in the quasi-planar geometry showed by the imidazolic rings, connected through Ag(1), as well as in their almost linear arrangement as indicated by the C-Ag(1)-C angle of 170.9(3)°. Furthermore, the Ag(1)-C bonds are 2.081(7) and 2.077(9) Å. The Ag-I distances within the [Ag₂I₄]²⁻ anion, namely 2.6902(9) Å for I(2)-Ag(2), 2.7871(9) Å for I(1#1)-Ag(2) and 2.8390(9) Å for I(1)-Ag(2), are also comparable. There are, however, major differences

with regard to the Ag-Ag bond distances, the intermolecular interactions and the crystal packing. As a matter of fact the Ag(1)-Ag(2) contact connecting the complex to the anionic fragment is 3.2873(10) Å long, and a second long distance of 3.2421(14) Å is found between the two Ag(2) atoms of the latter, while the values Chan and Liu report are 3.042 Å and 2.9643(16) Å, respectively. This might be due to the fact that, unlike theirs, the structure we present displays important intermolecular hydrogen bonds that build an arrangement of infinite [Ag(NHC-NHBoc)₂]⁺ chains and, consequently, weaken the Ag(1)-Ag(2) interactions. The elongation of the Ag-Ag distance within the [Ag₂I₄]²⁻ anion seems to be another consequence of the network assembled by the intermolecular interactions. More specifically, hydrogen bonds involve the intermolecular NH.....O=C donor...acceptor carbamic couples, with values between 2.890(8) and 2.821(8) Å.

In order to obtain suitable crystals for X-ray diffractions different crystallization attempts were necessary. During these procedures, and already after the first crystallization from acetone-hexane, we noticed the presence of a white solid material only soluble in CDCl₃ warmed at 65 °C. The NMR spectra run on the heterogeneous sample at room temperature showed one single set of resonances identical to those observed for the crude material **3a** whereas the NMR of the same sample made homogeneous after heating at 65 °C, revealed the presence of a second, identical but higher frequency shifted, set of signals attributed to a second NHC-Ag species **3a'**. The relative intensity of these new resonances increased with the number of re-crystallization steps: after two steps the presence of **3a'**, estimated by NMR of ca. 8% raised up to ca. 50% after four times.

During one of these re-crystallization steps we obtained crystals whose morphology appeared different from **3a** and whose structure, shown in Figure 5.2-2 and Figure 5.2-3 (selected bonds and angles are indicated in the Table 5.2-1, represents a rare example of multinuclear, polymeric silver complex with a staircase-type structure composed of Ag₄I₄ cluster fragments that aggregate to give an infinite ribbon stair structure, to which the carbene units are coordinate on both sides via C-Ag bonds.³

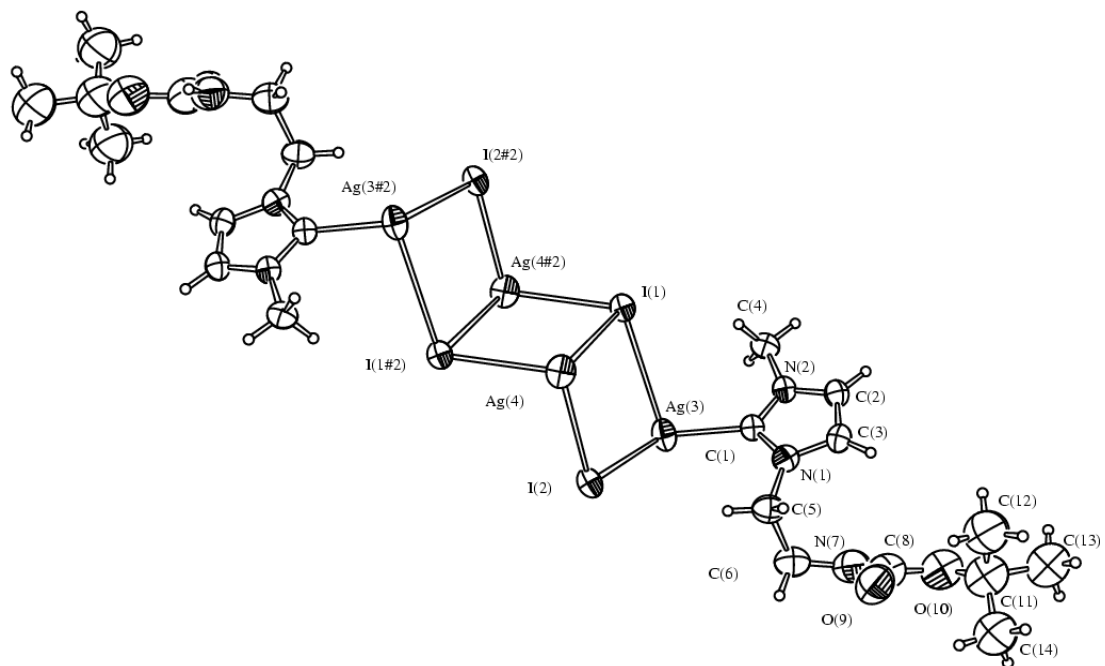


Figure 5.2-2 ORTEP diagram (30% probability thermal ellipsoids) of **3a'**.

The perspective view shown in Figure 5.2-2 highlights the complex step structure of the AgI polymer, which propagates along the *b* axis.

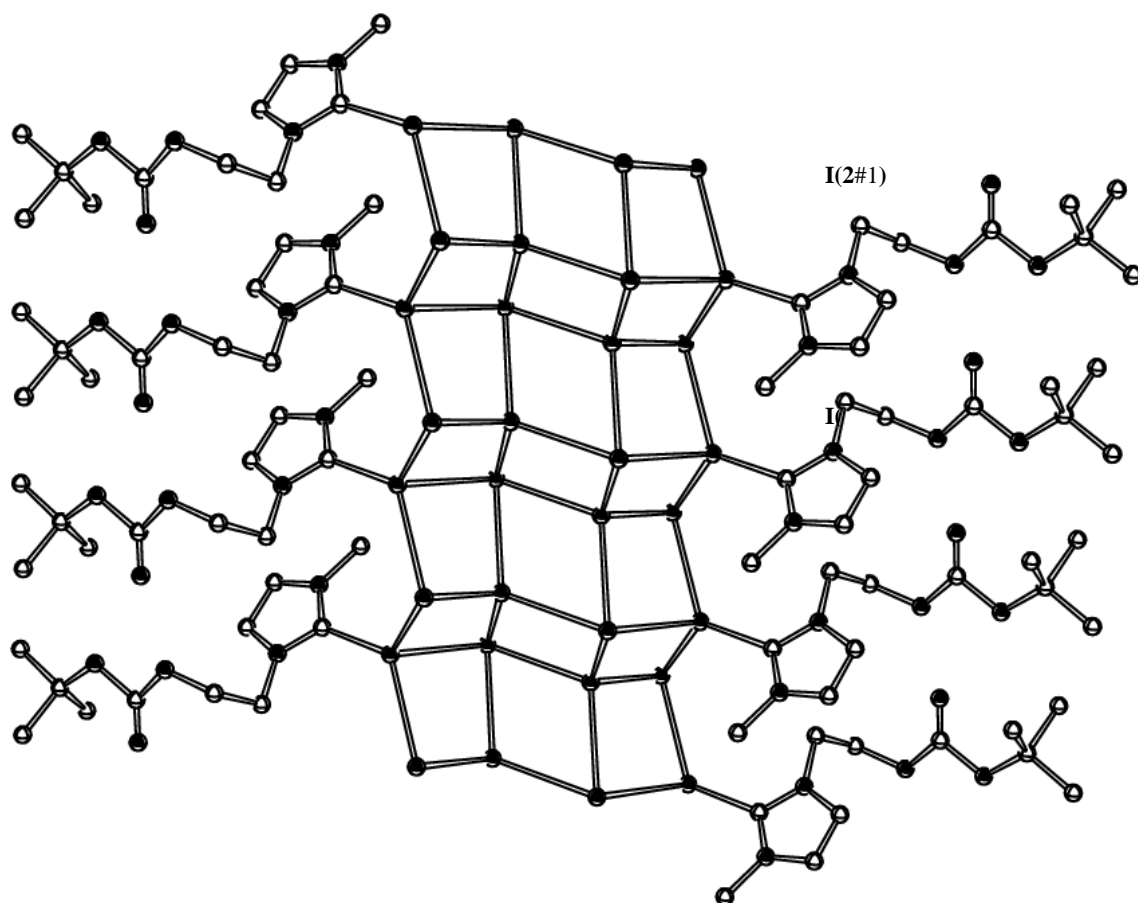


Figure 5.2-3 ORTEP diagram (30% probability thermal ellipsoids) of **3a''**. For sake of clarity hydrogen atoms have been omitted.

The unit cell contains an independent carbene molecule, two independent silver atoms [Ag(3) and Ag(4)] and two independent iodine atoms [I(1) and I(2)]. The silver atom Ag(3) shows a quasi-planar trigonal coordination, if we exclude the long Ag(3)-Ag(4) interaction [3.132(3)], being directly bonded to the carbenic C1 atom [2.167(16) Å] and to two I(2) atoms with bond lengths equal to 2.855(2) and 2.868(2) Å (Figure 5.2-2). There is also a fourth long contact of 3.306 Å between Ag(3) and I(1) that would give a pseudo tetrahedral coordination to Ag(3) if kept into account. The other Ag atom, Ag(4), indeed possesses this last type of coordination, being completely internal to the cluster structure and bonded to four I atoms through contacts whose lengths vary from 2.816(3) to 2.919(2) Å. There is also an additional, fairly long Ag(4)-Ag(4) contact [3.117(3) Å]. The wide range observed for the Ag-I bond distances [2.816(3)-2.919(2) Å] is comparable to what found in the literature for analogous compounds. The relatively long Ag-Ag distances observed [3.117(3) and 3.132(3) Å] suggest that they are quite weak and the ribbon stair frame is mainly stabilized by the multiple bridging iodides. These distances are less than the sum of

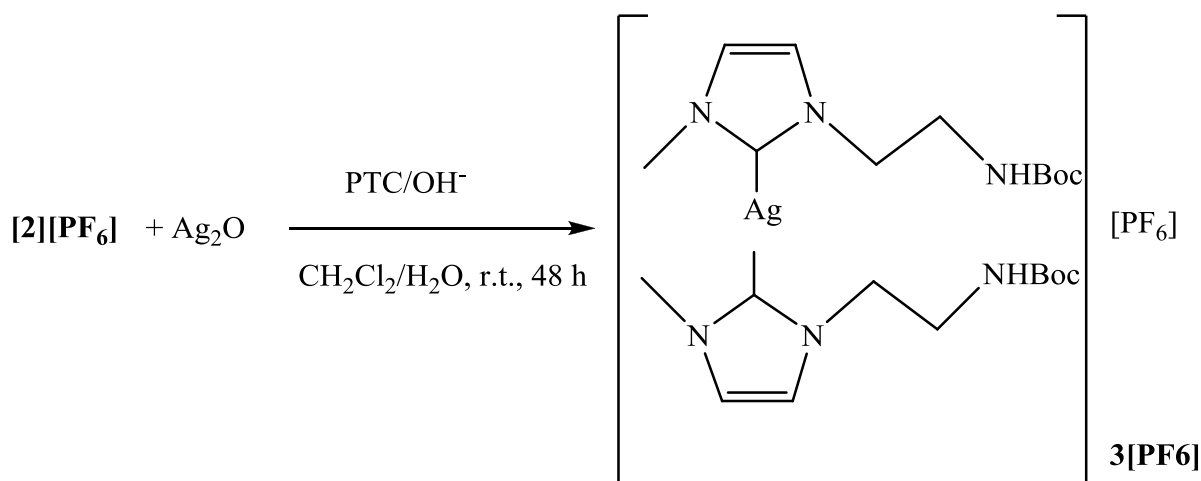
the van der Waals radii of 3.44 Å for silver,⁴ but are in the range observed for ligand-unsupported Ag^I-Ag^I distances (2.80 to 3.30 Å).⁵ As far as the iodine atoms are concerned, they all are tri-coordinated to Ag atoms and the main difference stands in their position: I(1) is internal to the Ag₄I₄ cluster unit and has also got an additional fourth long contact with Ag(3), I(2) is peripheral. The carbene molecules are positioned onto both sides of the ribbon stair structure, bonded to every peripheral Ag atoms. The rings protrude outward along the polymeric AgI chain and the X-ray crystal packing pattern (Figure 5.2-3) showed that although they are not stacked, they lay on parallel planes distant 3.362 Å from each other. The Ag-C bond distance of 2.167(16) Å is somewhat longer than those of known silver carbene complexes (2.052-2.090Å).⁶ With regard to the carbamic moiety, the X-ray analysis showed a positional disorder hence in the solid state it can be found in two different regions of the unit cell, one occupied for about 69%, the other for the remaining 31%. This is reasonable if we consider that the carbamic moiety is actually the most external fraction of the structure, nevertheless the disorder is partially controlled by intermolecular N-H...O hydrogen bonds [2.480 Å in the prevailing isomer, 2.794 Å in the minor one].

Table 5.2-1 Selected bond lengths (Å) and angles (°) for **3a**, **3a'** and **3[PF₆]**

3a		3a'		3[PF₆]	
Ag(1)-C(21)	2.077(7)	I(1)-Ag(4#2)	2.882(2)	Ag(1)-C(1)	2.062(7)
Ag(1)-C(1)	2.081(7)	I(1)-Ag(4)	2.919(2)	Ag(1)-C(17)	2.088(6)
Ag(1)-Ag(2)	3.2873(10)	I(2)-Ag(4)	2.816(3)	C(1)-N(5)	1.348(8)
Ag(2)-I(2)	2.6902(9)	I(2#1)-Ag(3)	2.855(2)	C(1)-N(2)	1.374(8)
Ag(2)-I(1#1)	2.7871(9)	I(2)-Ag(3)	2.868(2)	N(2)-C(3)	1.378(9)
Ag(2)-I(1)	2.8390(9)	Ag(3)-C(1)	2.167(16)	C(3)-C(4)	1.300(11)
Ag(2)-Ag(2#2)	3.2421(14)	Ag(4)-I(1#2)	2.882(2)	C(4)-N(5)	1.393(9)
Ag(2#2)-I(1)	2.7871(9)	Ag(4)-Ag(3)	3.132(3)	N(5)-C(6)	1.454(9)
C(1)-N(2)	1.354(8)	Ag(4)-Ag(4#2)	3.117(3)	C(1)-Ag(1)-C(17)	177.8(2)
C(1)-N(5)	1.348(9)	C(1)-N(1)	1.31(2)	N(5)-C(1)-N(2)	103.4(5)
C(4)-N(5)	1.373(9)	C(1)-N(2)	1.32(2)	N(5)-C(1)-Ag(1)	130.7(5)
C(3)-C(4)	1.327(11)	C(2)-N(2)	1.32(2)	N(2)-C(1)-Ag(1)	125.7(5)
C(3)-N(2)	1.360(9)	C(2)-C(3)	1.37(3)	C(1)-N(2)-C(3)	110.6(6)
C(21)-Ag(1)-C(1)	170.9(3)	C(3)-N(1)	1.37(2)	C(1)-N(2)-C(7)	125.5(5)
C(21)-Ag(1)-Ag(2)	91.48(18)	Ag(4#2)-I(1)-Ag(4)	64.99(6)	C(3)-N(2)-C(7)	123.6(6)

C(1)-Ag(1)-Ag(2)	90.99(19)	Ag(4)-I(2)-Ag(3)	88.47(6)	C(4)-C(3)-N(2)	107.7(7)
I(2)-Ag(2)-I(1#1)	123.97(3)	C(1)-Ag(3)-I(2)	124.6(5)	C(3)-C(4)-N(5)	107.4(6)
I(2)-Ag(2)-I(1)	124.56(3)	I(2)-Ag(4)-I(1)	100.96(6)	C(1)-N(5)-C(4)	110.9(6)
I(1#1)-Ag(2)-I(1)	109.63(3)	I(2)-Ag(4)-Ag(4#2)	121.05(9)	C(1)-N(5)-C(6)	123.9(6)
I(2)-Ag(2)-Ag(2#2)	167.71(4)	I(1#3)-Ag(4)-Ag(4#2)	114.52(10)	C(4)-N(5)-C(6)	125.2(6)
I(1#1)-Ag(2)-Ag(2#2)	55.57(2)	I(1#2)-Ag(4)-Ag(4#2)	58.08(6)		
I(1)-Ag(2)-Ag(2#2)	54.07(2)	I(1)-Ag(4)-Ag(4#2)	56.93(6)		
I(2)-Ag(2)-Ag(1)	100.49(3)				

The reaction of **[2][PF₆]** (paragraph 3.2-1) with Ag₂O in a 2:1 molar ratio, under basic PTC (phase transfer catalyst)/OH⁻ conditions in the presence of [NBu₄]⁺PF₆⁻ and NaOH⁷ formed the simple biscarbene salt **3[PF₆]** (Scheme 5.2-2) in 71% yield (NMR).



Scheme 5.2-2

The ¹H and ¹³C NMR spectra are not significantly different from those of **3a'** but unlike this latter the carbene carbon signal at δ 180.3 appears as a broad doublet with C-^{107/109}Ag coupling constant of 185.4 Hz.

Suitable crystals for X-Ray diffraction of **3[PF₆]** have been obtained by slow evaporation from a CDCl₃ solution at room temperature. The crystal packing and structure of **3[PF₆]**·2CDCl₃ are respectively shown in Figure 5.2-2 and Figure 5.2-3 respectively (selected bonds and angles are indicated in

Table **5.2-1**), and the latter consists of two independent silver biscarbene molecules in a 1:1 enantiomeric mixture. Within the same molecule, the two carbenes coordinated to the same silver

atom are absolutely identical and carry the carbamic chain on the same side of the five-member ring with respect to the silver position. Furthermore, the *cis* position of the substituents allows the enantiomers to face one another in pairs, with the carbene units not staggered but laying on parallel planes distant about 3.219 Å from each other. The space between the two groups of isomers is filled by the anion and solvent molecules.

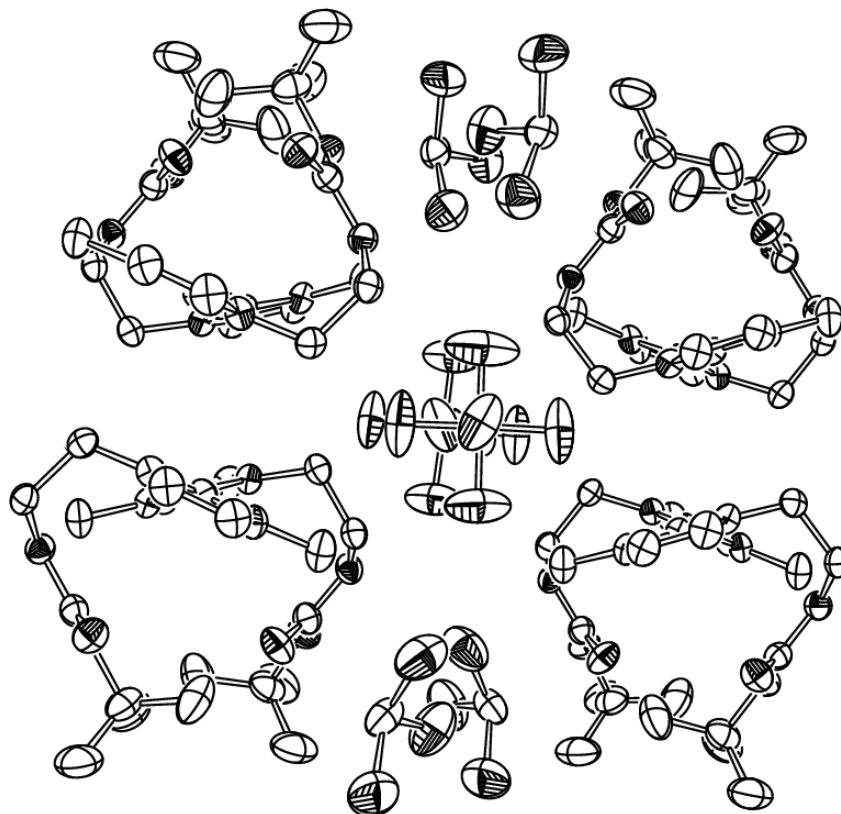


Figure 5.2-4 Crystal packing of **3**[PF₆]⁻ (30% probability thermal ellipsoids). For sake of clarity hydrogen atoms have been omitted.

The sterical hindrance caused by the carbamic chains, which are not linear but bent inwards within the same space region, causes the two five-member rings to adopt a non-coplanar geometry and their torsion angle is about 39°. The Ag-C bond distances 2.062(7) and 2.088(6) Å are shorter than those found in **3a'** but comparable with **3a** and totally in agreement with what reported for other analogous cationic biscarbene complexes. The C(1)-Ag(1)-C(17) angle is close to linearity with an angle of 177.8(2)°.

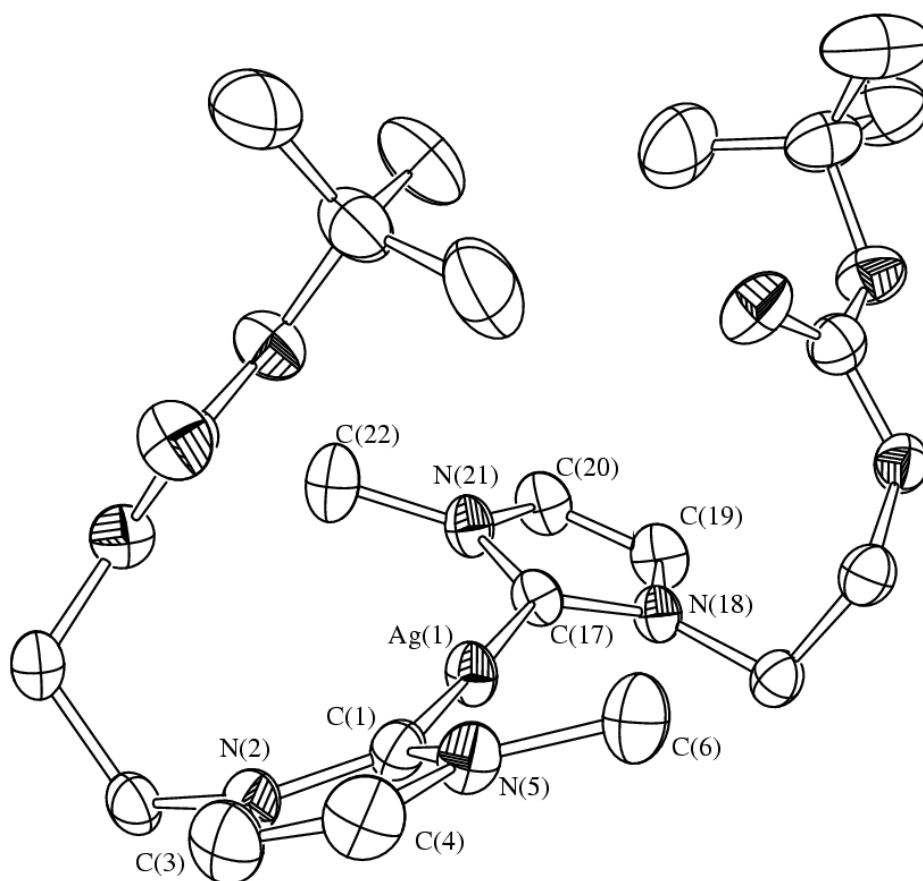


Figure 5.2-5 ORTEP diagram (30% probability thermal ellipsoids) of **3**[PF₆]. For sake of clarity hydrogen atoms have been omitted.

We finally studied the reactivity of [NH₂CH₂CH₂ImMe][I], toward Ag₂O under a variety of conditions. Our investigations started carrying the reaction between [NH₂CH₂CH₂ImMe][I] and Ag₂O in a 2:1 ratio in two parallel experiments: i) in a flask containing anhydrous DMSO-*d*₆ and 4 Å molecular sieves with the filtered, colourless reaction mixture successively transferred into a NMR tube and ii) by direct addition of all the reagents in a NMR tube. In both cases the analysis of the NMR spectra indicated that [NH₂CH₂CH₂ImMe][I] rapidly reacts with Ag₂O to give a single silver-containing product: in the ¹H NMR the peak at δ 9.10 disappears and the resonances of the imidazole CHs backbone are shifted upfield from 7.74 and 7.71 to 7.46 and 7.42, respectively while nothing can be said on the fate of the NH₂ group, whose resonance is never observed even in the starting proligand. In the ¹³C NMR spectra the original resonance at δ 136.9 for the NCHN carbon is replaced by a singlet at δ 179.8, analogous to the Ag-C_{carbene} found for the silver complexes **3a**. However continuous monitoring by NMR showed that this product is rather unstable and rapidly decomposes: the solution turned yellow and a silver mirror together with a brown powdery solid coated the NMR tube whilst the proton and carbon NMR spectra showed that the peaks assigned to

the silver adduct weaken in intensity while the resonances of the starting imidazolium salt reappear. When the same reaction was carried in bulk, the black suspension stirred for 2 h was filtered on a celite pad and after addition of acetonitrile a light brown precipitate was obtained. The ESI-MS(+) spectrum of the freshly filtered solution showed peaks for the $[(M+Na)]^+$ cation at 382 (100) and 384 (90) m/z and peaks at 366 (42) 368 (38) m/z that we tentatively attributed to the presence in solution of the neutral species $(NHC-NH_2)AgI$ (**7**, $NHC-NH_2 = 1-(2\text{-aminoethyl})\text{-3-methylimidazolin-2-ylidene}$) that in the ESI-MS conditions easily loose the NH_2 fragment.⁹

Silver complexes **3b** and **3c** (Scheme 5.1-1) have been obtained from **1b** and **1c** as previously described for the complex **3a**. The reaction has been followed by NMR and ESI-MS spectroscopy and the silver complex reacted in situ with $[RhCl(NBD)]_2$ as transmetallant agent (vide infra chapter 7).

5.3 Experimental section

Materials and Procedures. All reactions were carried out under Argon using standard Schlenk techniques. Solvents were dried and distilled under nitrogen prior to use; the deuterated solvents used after being appropriately dried and degassed were stored in ampoules under argon on 4Å molecular sieves. The prepared derivatives were characterized by elemental analysis and spectroscopic methods. The IR spectra were recorded with a FT-IR spectrometer Perkin Elmer Spectrum 2000. The NMR spectra were recorded using Varian Inova 300 (1H , 300.1; ^{13}C , 75.5 MHz), Varian MercuryPlus VX 400 (1H , 399.9; ^{13}C , 100.6 MHz), Varian Inova 600 (1H , 599.7, ^{13}C , 150.8 MHz) instruments. The spectra were referenced internally to residual solvent resonances, and unless otherwise stated, they were recorded at 298 K for characterization purposes; full 1H and ^{13}C NMR assignments were done, when necessary, by gCOSY, gHSQC, gHMBC, NOESY and DEPT-135 NMR experiments using standard Varian pulse sequences; J.Young valve NMR tubes (Wilmad) were used to carry out NMR experiments under inert conditions. ESI-MS analysis were performed by direct injection of methanol solutions of the metal complexes using a WATERS ZQ 4000 mass spectrometer. Elemental analyses were performed on a ThermoQuest Flash 1112 Series EA Instrument. The Ag_2O were used as purchased from Aldrich. Petroleum ether (Etp) refers to a fraction of bp 60-80 °C. Crystal data were collected at room temperature on a Bruker APEX II diffractometer equipped with a CCD detector operating at 50 kV and 30 mA, using graphite monochromated MoK_{α} radiation ($\lambda = 0.71073 \text{ \AA}$). An empirical absorption correction was applied on both structures by using SADABS.⁸ They were solved by direct methods and refined by full-matrix least-squares based on all data using F^2 with SHELXL97.⁹ All non-hydrogen atoms were

refined anisotropically, with the exception of the hydrogen atoms which were set geometrically and given fixed isotropic thermal parameters.

5.3.1 Synthesis of 1-(2-NHBoc-ethyl)-3-methyl-imidazolin-2-ylidene silver bromide (**3a**)

To a solution of **1** (0.380 g, 1.80 mmol) dissolved in THF (ca.10 mL) an excess of MeI (0.5 mL) was added. The reaction was stirred overnight and the solvent removed under vacuum to yield 0,623 g (98%) of a yellow oil identified as **3a**. $^1\text{H NMR}$ (399.9 MHz, CDCl_3): d 9.70 (s, 1H, NCHN), 7.45 (s, 1H, CHimid), 7.39 (s, 1H, CHimid), 5.78 (t, 1H, $^3J_{\text{H,H}} = 5.8$ Hz, NH), 4.55 (t, 2H, $^3J_{\text{H,H}} = 5.6$ Hz, NCH_2), 4.07 (s, 3H, NCH_3), 3.68 (m, 2H, CH_2NHBoc), 1.40 (s, 9H, CH_3). $^{13}\text{C}\{^1\text{H}\}\text{NMR}$ (100.6 MHz, CDCl_3): d 156.2 (C=O), 137.0 (CH, NCHN), 123.1 (2CH, CHimid), 79.9 (Cq, t-Bu), 46.7 (NCH_2), 40.2 (CH_2NH), 37.2 (NCH_3), 28.6 (CH_3 , t-Bu). $^1\text{H NMR}$ (399.9 MHz, CD_3CN): d 8.70 (s, 1H, NCHN), 7.42 (s, 1H, CHimid), 7.37 (s, 1H, CHimid), 5.78 (br s, 1H, NH), 4.25 (t, 2H, $^3J_{\text{H,H}} = 5.6$ Hz, NCH_2), 3.85 (s, 3H, NCH_3), 3.45 (m, 2H, CH_2NHBoc), 1.36 (s, 9H, CH_3). $^1\text{H NMR}$ (399.9 MHz, D_2O): d 7.52 (s, 1H, CHimid), 7.48 (s, 1H, CHimid), 4.30 (t, 2H, $^3J_{\text{H,H}} = 6.0$ Hz, NCH_2), 3.92 (s, 3H, NCH_3), 3.54 (m, 2H, CH_2NHBoc), 1.39 (s, 9H, CH_3). IR (THF, cm^{-1} 1708 (vs, mCO). ESI-MS (MeOH, m/z): 226 (100) $[\text{M}]^+$, 127 (100). For the synthesis of complexes **3a'** and **3a''** see ref.⁹

5.3.2 Synthesis of 1-(2-NHBoc-ethyl)-3-benzyl-imidazolin-2-ylidene silver bromide (**3b**)

To a solution of **1b** (0.500 g, 1.31 mmol) in CH_2Cl_2 (30 mL), Ag_2O (0.154 g, 0.66 mmol) was added. The suspension was stirred for 2 h, filtered on celite and the solvent was removed under reduce pressure to give the product ready for trans-metallation. The silver intermediate of 1-(2-BocNH-ethyl)-3-benzyl-imidazolin-2-ylidene silver bromide **3b** was not isolated but a NMR and ESI-MS analysis was carried out on the crude material to confirm its formation. $^1\text{H NMR}$ of **3b** (399.9 MHz, CDCl_3): δ 7.21-6.98 (m, 5H, Ph), 7.02 (s, 1H, CH_{im}), 6.81 (s, 1H, CH_{im}), 5.74 (br s, 1H, NH), 5.14 (s, 2H, PhCH_2N), 4.16 (br t, 2H, NCH_2), 3.39 (br t, 2H, CH_2NH), 1.28 (s, 9H, CH_3). $^{13}\text{CNMR}$ (100.6 MHz, CDCl_3): δ 181.5 (s, C-Ag), 155.9 (C=O), 135.7 (Ph, C_5); 128.7 (Ph, C_4); 128.1 (Ph, C_3); 127.3 (Ph, C_2), 122.0 (CH_{im}), 120.9 (CH_{im}), 78.9 (Cq, ^tBu), 55.2 (CH_2 , PhCH_2), 51.1 (CH_2 , NCH_2), 41.2 (CH_2 , CH_2NH), 28.1 (CH_3 , ^tBu). IR (CH_2Cl_2 , cm^{-1}): 1707 (vs, ν_{CO}). ESI-MS (MeOH, m/z): 709 (100) $[\text{C}_{34}\text{H}_{46}\text{AgN}_6\text{O}_4]^+$; 79 (100), 81 (97) $[\text{Br}]^-$. $^1\text{H NMR}$ (400 MHz, CDCl_3): δ 7.29 – 7.18 (m, 10H, Ph), 6.99 (s, 2H, CH_{im}), 5.21 (s, 4H, CH_2Ph). $^{13}\text{C NMR}$ (100 MHz, CDCl_3): δ 180.60 (s, C-Ag), 135.50 (Cq, Ph), 128.80 (Ph), 128.25 (Ph), 127.55 (Ph), 121.62 (C_{im}), 55.33 (CH_2Ph).

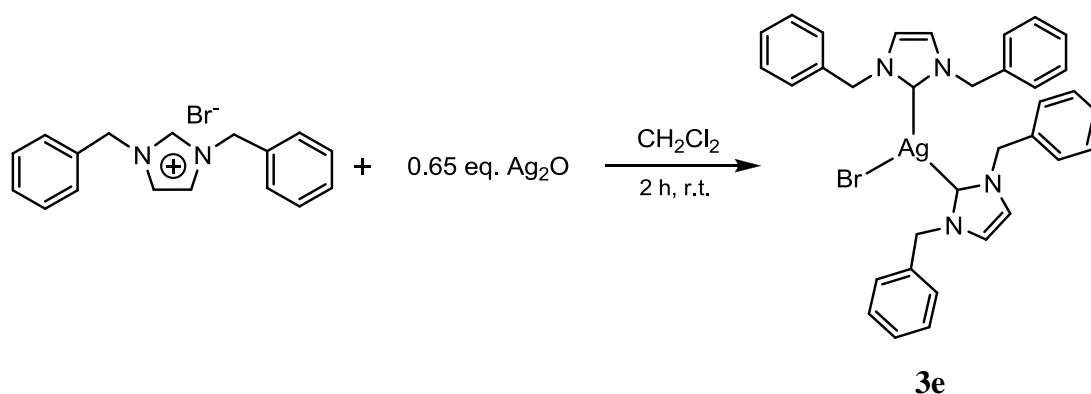
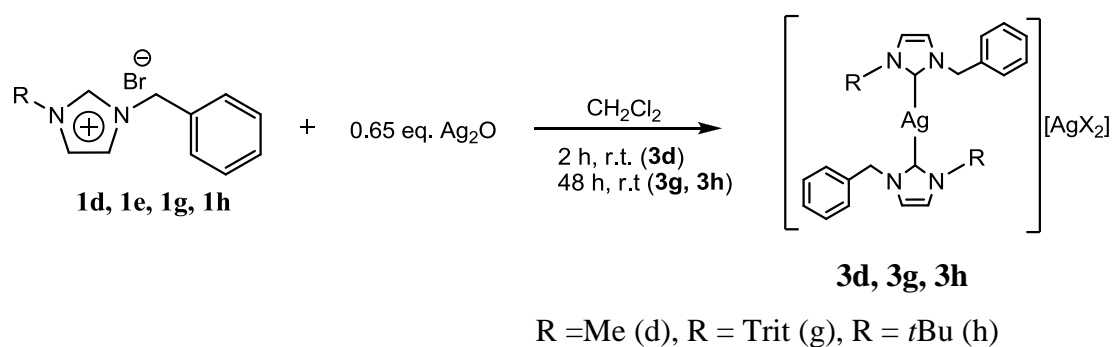
5.3.3 Synthesis of 1-(2-NHBoc-ethyl)-3-trityl-imidazolin-2-ylidene silver bromide (3c)

To a solution of **1c** (0.200 g, 0.41 mmol) in CH₂Cl₂ (20 mL), Ag₂O (0.050 g, 0.21 mmol) was added. The suspension was stirred for 48 h then, solid [Rh(NBD)Cl]₂ (0.092 g, 0.20 mmol) was directly added to the reaction mixture. The silver intermediate **3c** was not isolated but a ¹H NMR and ESI-MS analysis was carried out on the crude material to confirm its formation. ¹H NMR (399.9 MHz, CDCl₃): δ 7.36-7.21 (m, 15H, Ph), 7.29 (s, 1H, CH_{im}), 7.03 (s, 1H, CH_{im}), 4.24 (t, 2H, J_{H,H} = 6.0 Hz, NCH₂), 3.51 (t, 2H, J_{H,H} = 6.0 Hz, CH₂NH), 1.43 (s, 9H, ^tBu), the NH resonance was not observed. ¹³C NMR (100.6 MHz, CDCl₃): δ 183.9 (s, C-Ag), 156.8 (C=O), 142.0 (C₅), 130.0 (C₄), 128.4 (C₂, C₃), 123.5 (CH_{im}), 119.5 (CH_{im}), 80.0 (C1), 79.9 (Cq, ^tBu), 52.6 (NCH₂), 41.4 (CH₂NH), 28.3 (CH₃, ^tBu). ESI-MS (MeOH, *m/z*): 1015 (50) [C₅₈H₆₄AgN₆O₄]⁺, 243 (100) [Ph₃C]⁺.

6 Synthesis and Characterization of Silver(I) Complexes with N-Heterocyclic Carbene Bearing a Benzyl Group

6.1 Introduction

Silver(I)-NHC complexes **3d-h** were obtained in quantitative yields under the conditions described in the previous chapter (Scheme 6.1-1). These Ag-NHC complexes have been employed as precursors for the formation of [RhCl(NBD)(NHC)] complexes.



Scheme 6.1-1 Synthesis of silver(I)-NHC complexes **3d-h**.

6.2 Results and discussion

All the reactions were carried out in dichloromethane at room temperature with the exclusion of light and afforded the less bulky **3d** and **3e** complexes after 2 h and the **3d** and **3e** after 48 h.

The formation of **3d**, **3e**, **3g** and **3h** was unambiguously confirmed by elemental analysis, NMR spectroscopy, electrospray ionization mass spectrometry (ESI-MS) and in case of **3e** also by X-ray diffraction.

As regards the NMR data, the common features in the spectra for all of the complexes were the disappearance of the acidic imidazolium NCHN proton resonance in the ^1H NMR spectra,

coupled with appearance of a highly deshielded singlet (doublet in case of **3g**, deriving from the silver-bonded C_{carbene}) in the ¹³C NMR spectra (Figure 6.2-1).

As can be seen from these data, the chemical shift δ for the Ag-C resonance for the different Ag(I) complexes is found between 185.0 and 177.5 ppm. Only in the case of the complex **3g**, the coupling of the carbon nucleus to the silver one was observed as a doublet with a coupling constant $^1J(^{13}\text{C}-^{107/109}\text{Ag}) = 236$ Hz, which expresses the average of coupling to the two naturally occurring isotopes of silver ¹⁰⁷Ag and ¹⁰⁹Ag (both isotopes with I=1/2). This value of the ¹J(C-Ag) constant lies in the range reported²⁸ for silver(I)-NHC complexes, specifically, the C_{carbene} couples to ¹⁰⁷Ag with a coupling constant in the range 180 to 234 Hz, whereas this constant ranges from 204 to 270 Hz when C_{carbene} couples to ¹⁰⁹Ag. Particularly Nolan¹⁰ and colleagues observed for a 1,3-diisopropyl-imidazolin-2-ylidene silver chloride (IPr)AgCl and a 1,3-dimesityl-imidazolin-2-ylidene silver chloride (IMes)AgCl a downfield signal of carbonic carbon resonating at 184.6 ppm as a doublet of doublets with an observable coupling between carbon and silver of $^1J(^{13}\text{C}-^{109}\text{Ag}) = 253$ Hz and $^1J(^{13}\text{C}-^{107}\text{Ag}) = 219$ Hz.

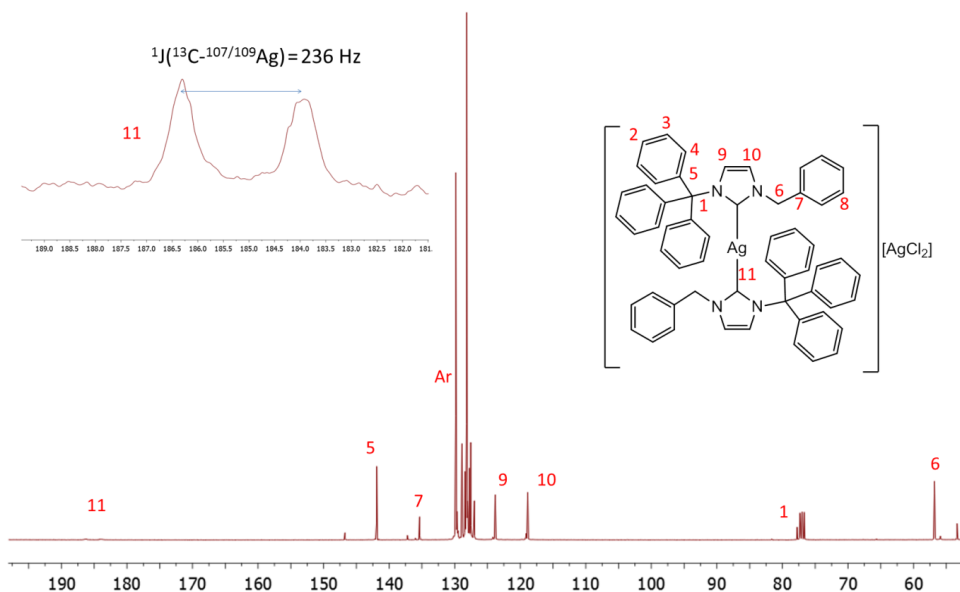
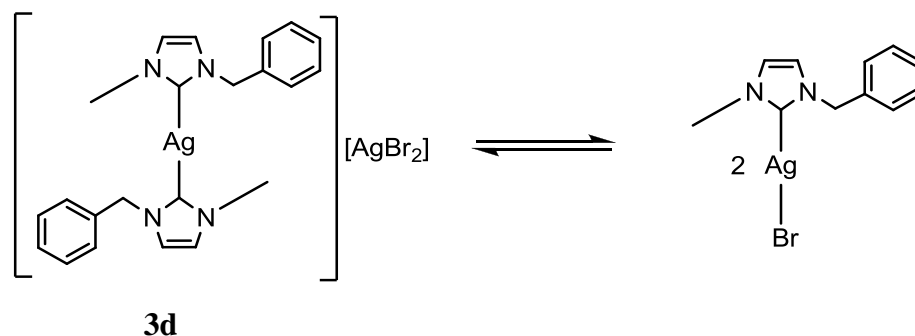


Figure 6.2-1 ¹³C NMR spectrum of **3g** with the inset showing the downfield doublet.

The observation of the doublet at 185 ppm in the ¹³C NMR spectrum of **3g** indicates that the bulkiness of the substituent at the imidazolium nitrogen atom influences the dynamic behavior within the structure of the silver complex. The absence of the doublet of doublets splitting pattern in the case of **3g** suggests that the steric hindrance caused by the trityl group on the one N-side of the imidazole is not enough high to consider its quasi-static behavior as it can be done for the

mentioned examples of (IPr)AgCl and (IMes)AgCl. Nevertheless, the presumable exchange process⁴ between the ligands and the metal center is slower on the NMR time scale for the **2d** than for the other three characterized complexes. The dynamic behavior of silver(I)-NHC complexes has been reported.¹¹ Due to the similarity structure the dynamic behavior shown in Scheme 6.2-1 can be proposed also for **4d**. Also in the case of the reported silver complex, no ^{13}C - $^{107/109}\text{Ag}$ coupling was observed, exactly as in the cases of complexes **3d**, **3e** and **3h**.



Scheme 6.2-1 Proposed dynamic behavior within the structure of **3d**.

Moreover, according to Nolan⁵, the highly deshielded proton at $\delta = 185.0$ ppm may indicate a stronger donation to the silver, which means a stronger Ag-C bond. This in turn leads to the decrease of the lability of the carbene ligands with respect to the metal center. Indeed, the carbenic carbene resonance in the group of all the silver complexes **3d-h** is most deshielded in the case of the complex **3h**.

In keeping with previous observations,⁶ in the ^1H NMR spectra, the resonances of imidazole backbone protons CH_{im} in the silver complexes are shifted upfield with respect to the corresponding imidazolium precursors, whereas no significant shift has been observed in the ^{13}C NMR spectra. Additionally, the chemical shift of these CH_{im} protons is solvent-dependent. The use of $\text{DMSO-}d_6$ caused the downfield shift of the signals with comparison to their position in spectra acquired for the sample in CDCl_3 , namely the signals were shifted from 7.16 and 6.90 ppm to 7.62 and 7.53 ppm. This behavior can be explained by the fact that DMSO is a H-bonding solvent, and some electrostatic interactions between the analyzed compound and the solvent are likely to form.¹²

The discussed above resonances of the imidazolium backbone protons have been observed as two doublets (AB system) in case of the complexes **3d**, **3g** and **3h** with coupling constants $^1J_{\text{H,H}} = 1.80$ Hz, $^1J_{\text{H,H}} = 1.90$ Hz and $^1J_{\text{H,H}} = 1.87$ Hz, respectively. In case of the complex **3e**, the protons appear as a singlet.

Crystals of **3e** suitable for single crystal X-ray diffraction were grown from a double layer of dichloromethane and petroleum ether (1:4). The molecular structure with selected bond distances

and angles is presented in Figure 6.2-2. Complex **3e** exists as a biscarbene compound with the two neutral carbene moieties bound to the silver cation in the presence of the anion to balance the charge.

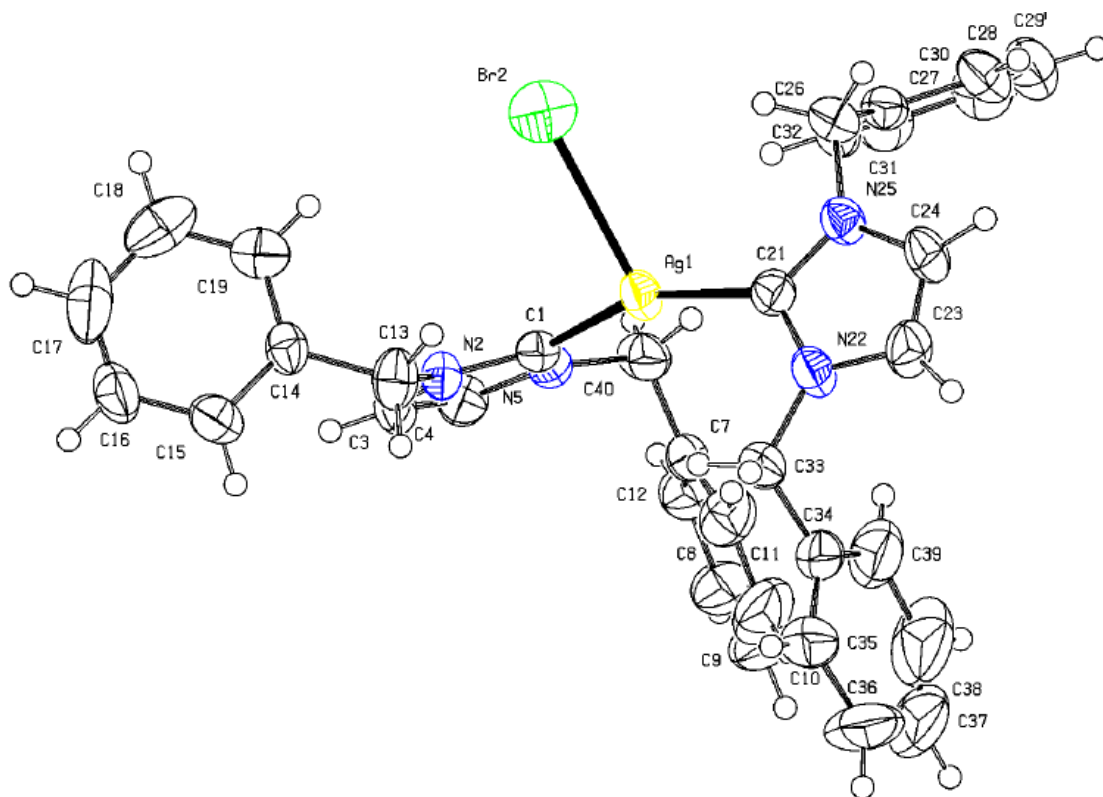


Figure 6.2-2 ORTEP diagram of **3e** depicted with thermal ellipsoids at 50% probability. Selected bond distances (Å) and bond angles (deg): Ag(1)-C(21) 2.118(7); Ag(1)-C(1) 2.125(7); Ag(1)-Br(2) 2.8609(12); C(21)-Ag(1)-C(1) 156.7(3); C(21)-Ag(1)-Br(2) 104.84(18); C(1)-Ag(1)-Br(2) 98.43(17).

The compound **3e** crystallizes in the $P2_1/n$ space group of the monoclinic crystal system ($Z = 4$). This particular structure for a Ag(I)-NHC complex was reported for a first time in 2007 by Newman and co-workers;¹³ this finding was quite surprising at that time, since most of the silver products resulting from the reaction of imidazolium halide and Ag_2O exist in one of the two structural motifs shown in Figure 6.2-2, with formulas: $(NHC)AgX$ and $(NHC)_2Ag^+/AgX_2^-$, both of them having a stoichiometry of 1 NHC:1 Ag:1 halide. The formation of one of these two structures depends mainly on the degree of polarity of a solvent used in the synthesis; the more polar solvents favor the latter, cationic silver salt. For Newman, unexpectedly, a reaction of 1,3-dibenzyl-imidazolium bromide with 5 equivalents of Ag_2O in dichloromethane afforded, in a reproducible manner, the new structure of stoichiometry 2 NHC:1 Ag:1 halide.

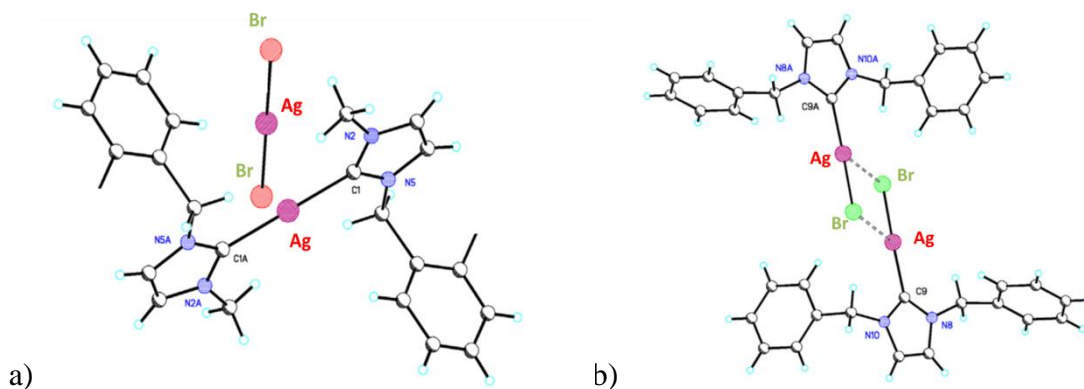


Figure 6.2-3 Two most commonly formed structures of bis-carbene silver(I) complexes with a stoichiometry of 1 NHC:1 Ag:1 halide.

The X-ray data obtained for **3e** from the reaction of 1,3-dibenzyl-imidazolium bromide **1e** with 0.65 molar equivalents of the Ag_2O in dichloromethane are in a perfect agreement (within the experimental error) with the reported ones.⁸

As can be seen from the ORTEP diagram shown in Figure 6.2-3, the structure shows almost planar geometry formed by the two coordinating carbons, the bromide and the silver with the C–Ag–C angle being 156.7° . The distance between Ag and Br atoms is quite long (2.86 Å), longer than for the usual structure shown in the Figure 6.2-2.

The reason for which the unusual bonding motif is formed is not yet explained. The same synthetic reaction was also tried⁸ with different proportions of silver oxide and dibenzylimidazolium bromide affording invariably crystals with the same structure.

The complexes **3d**, **3g** and **3h**, authenticated by means of NMR and ESI-MS spectroscopy are described, for sake of simplicity, as a bis-carbene salts of the type: $[\text{Ag}(\text{carbene})_2][\text{AgX}_2]$.

Moreover, the electrospray ionization mass spectrometry analysis in methanol indicated the presence in solution of the cations $[(\text{NHC})_2\text{Ag}]^+$ with the observed isotopic distributions in perfect agreement with the calculated ones.

6.3 Experimental section

Materials and Procedures. All reactions were carried out under Argon using standard Schlenk techniques. Solvents were dried and distilled under nitrogen prior to use; the deuterated solvents used after being appropriately dried and degassed were stored in ampoules under argon on 4Å molecular sieves. The prepared derivatives were characterized by elemental analysis and spectroscopic methods. The IR spectra were recorded with a FT-IR spectrometer Perkin Elmer Spectrum 2000. The NMR spectra were recorded using Varian Inova 300 (^1H , 300.1; ^{13}C , 75.5

MHz), Varian MercuryPlus VX 400 (^1H , 399.9; ^{13}C , 100.6 MHz). The spectra were referenced internally to residual solvent resonances, and unless otherwise stated, they were recorded at 298 K for characterization purposes; full ^1H and ^{13}C NMR assignments were done, when necessary, by gCOSY, gHSQC, gHMBC, NOESY and DEPT-135 NMR experiments using standard Varian pulse sequences; J.Young valve NMR tubes (Wilmad) were used to carry out NMR experiments under inert conditions. ESI-MS analysis were performed by direct injection of methanol solutions of the metal complexes using a WATERS ZQ 4000 mass spectrometer. The Ag_2O were used as purchased from Aldrich. Petroleum ether (Etp) refers to a fraction of bp 60-80 °C. Crystal data were collected at room temperature on a Bruker APEX II diffractometer equipped with a CCD detector operating at 50 kV and 30 mA, using graphite monochromated MoK_α radiation ($\lambda = 0.71073 \text{ \AA}$). An empirical absorption correction was applied on both structures by using SADABS.⁸ They were solved by direct methods and refined by full-matrix least-squares based on all data using F^2 with SHELXL97.⁹ All non-hydrogen atoms were refined anisotropically, with the exception of the hydrogen atoms which were set geometrically and given fixed isotropic thermal parameters.

6.3.1 Synthesis of 1-benzyl-3-methyl-imidazolin-2-ylidene silver bromide (3d)

To a solution of **1d** (0.25 g, 0.97 mmol) in CH_2Cl_2 (10 mL) stirred in a Schlenk, Ag_2O (0.15 g, 0.63 mmol) was added. The reaction mixture was stirred for 2 h at room temperature; in the end of the reaction a colorless solution and a small amount of the black solid of Ag_2O was found in the Schlenk, which was subsequently filtered on Celite and the solvent was removed under vacuum to afford 0.32 g (82%) of a white solid identified as **3d**. $^1\text{H NMR}$ (400 MHz, CDCl_3): δ 7.34 (m, 3H, Ph), 6.98 (d, 1H, $J_{\text{H,H}} = 1.79 \text{ Hz}$, CH_{im}), 6.93 (d, 1H, $J_{\text{H,H}} = 1.80 \text{ Hz}$, CH_{im}), 5.28 (s, 2H, CH_2Ph), 3.84 (s, 3H, CH_3). $^{13}\text{C NMR}$ (100 MHz, CDCl_3): δ 181.87 (s, C-Ag), 135.45 (Cq, Ph), 129.11 (Ph), 128.65 (Ph), 127.81 (Ph), 122.53 (CH_{im}), 121.08 (CH_{im}), 55.87 (CH_2Ph), 38.73 (CH_3). **ESI-MS** (MeOH, m/z): 173 (100) [$\text{C}_{11}\text{H}_{13}\text{N}_2$] $^+$; 451 (45) [$\text{C}_{22}\text{H}_{24}\text{N}_4\text{Ag}$] $^+$. In the ESI-MS(-) spectrum, no peaks were observed

6.3.2 Synthesis of 1,3-dibenzyl-imidazolin-2-ylidene silver bromide (3e)

To a solution of **1e**, (0.20 g, 0.61 mmol) in DCM (ca. 10 mL) stirred in a Schlenk, Ag_2O (0.09 g, 0.39 mmol) was added. The reaction mixture was stirred for 2 h at room temperature; in the end of the reaction a colorless solution and a small amount of the black solid of Ag_2O was found in the Schlenk, which was subsequently filtered on Celite and the solvent was removed under vacuum to afford 0.28 g (95%) of a white solid identified as **3e**. $^1\text{H NMR}$ (400 MHz, CDCl_3): δ 7.29 – 7.18

(m, 10H, Ph), 6.99 (s, 2H, CH_{im}), 5.21 (s, 4H, CH₂Ph). ¹³C NMR (100 MHz, CDCl₃): δ 180.60 (s, C-Ag), 135.50 (Cq, Ph), 128.80 (Ph), 128.25 (Ph), 127.55 (Ph), 121.62 (C_{im}), 55.33 (CH₂Ph).

6.3.3 Synthesis of 1-benzyl-3-trityl-imidazolin-2-ylidene silver bromide (3g).

To a solution of **1g**, (0.05 g, 0.17 mmol) in CH₂Cl₂ (ca. 10 mL) stirred in a Schlenk, Ag₂O (0.03 g, 0.11 mmol) was added. The reaction mixture was stirred for 48 h at room temperature; in the end of the reaction a colorless solution and a small amount of the black solid of Ag₂O was found in the Schlenk, which was subsequently filtered on Celite and after characterizing the crude material by NMR, it was instantaneously used for the preparation of the corresponding rhodium complex **4g**. ¹H NMR (300 MHz, CDCl₃): δ 7.34-7.21 (m, 20H, Ph), 7.03 (d, 1H, J_{H,H} = 1.90 Hz, CH_{im}), 6.91 (d, 1H, J_{H,H} = 1.90 Hz, CH_{im}), 5.25 (s, 2H, CH₂Ph). ¹³C NMR (100 MHz, CDCl₃): δ 185 (d, J_{Ag-C} = 236 Hz, C-Ag), 141.91 (C₅), 135.36 (C₇), 129.84 (Ph), 128.90 (Ph), 128.42 (Ph), 128.18 (Ph), 127.76 (Ph), 127.68 (Ph), 127.55 (Ph), 126.99 (Ph), 123.82 (CH_{im}), 118.86 (CH_{im}), 77.75 (Cq^{Trit}), 56.81 (CH₂Ph). ESI-MS (MeOH, m/z): 907 (100) [C₅₈H₄₈AgN₄]⁺.

6.3.4 Synthesis of 1-benzyl-3-tert-butyl-imidazolin-2-ylidene silver bromide (3h)

To a solution of **1h**, (0.066 g, 0.22 mmol) in CH₂Cl₂ (5 mL) stirred in a Schlenk, (0.026 g, 0.11 mmol) of Ag₂O was added. The suspension was stirred for 48 h. In the end of the reaction, a colorless solution and a small amount of the black solid of Ag₂O was found in the Schlenk and a silver mirror on its walls. The solvent was removed under vacuum and deuterated chloroform was added for NMR analysis. ¹H NMR (300 MHz, CDCl₃): δ 7.32 (m, 3H, Ph), 7.21 (m, 2H, Ph), 7.16 (d, 1H, J_{H,H} = 1.88 Hz, CH_{im}), 6.90 (d, 1H, J_{H,H} = 1.88 Hz, CH_{im}), 5.32 (s, 2H, CH₂Ph), 1.72 (s, 9H, ^tBu). ¹H NMR (400 MHz, DMSO-*d*₆): δ 7.62 (s, 1H, CH_{im}) 7.53 (s, 1H, CH_{im}), 7.42-7.30 (m, 5H, Ph), 5.35 (s, 2H, CH₂Ph), 1.64 (s, 9H, ^tBu). ¹³C NMR (100 MHz, CDCl₃): δ 178.24 (s, C-Ag), 135.41 (Cq, Ph), 129.04 (Ph), 128.58 (Ph), 127.76 (Ph), 119.35 (CH_{im}), 57.90 (Cq ^tBu), 56.92 (CH₂Ph), 31.78 (^tBu). ESI-MS (MeOH, m/z): 537 (30) [C₂₈H₃₈AgN₄]⁺; 321 (18) [C₁₄H₁₈AgN₂]⁺. In the ESI-MS(-) spectrum, no peaks were observed.

References

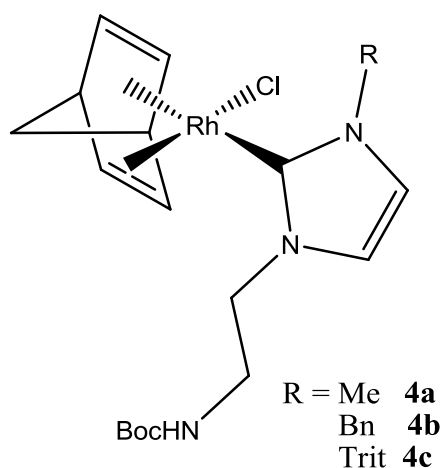
-
- 1 (a) de Frémont, P.; Scott, N. M.; Stevens, E. D.; Ramnial, T.; Lightbody, O.C.; Macdonald, C. L. B.; Clyburne, J. A. C.; Abernethy, C. D.; Nolan, S. P.; *Organometallics*, **2005**, 24, 6301; (b) Schneider, S. K.; Herrmann, W. A.;

-
- Herdtwack, E.; *Z. Anorg. Allg. Chem.* **2003**, 629, 2363; (c) Arduengo, A. J.; Dias, H. V. R.; Calabrese, J. C.; Davidson, F.; *Organometallics*, **1993**, 12, 3405.
- 2 Chen, W.; Liu, G.; *J. Organomet. Chem.* **2003**, 673, 5.
- 3 (a) Chiu, P.L.; Chen, C.Y.; Zeng, J.Y.; Lu, C.Y.; Lee, H.M.; *J. Organomet. Chem.* **2005**, 690, 1682; (b) Liu, Q.-X.; Xu, F.-B.; Li, Q.-S.; Zeng, X.-B.; Leng, X.-B.; Chou, Y.L.; Zhang, Z.-Z.; *Organometallics* **2003**, 22, 309; (c) Lee, K. M.; Wang, H.M.J.; Lin, I.J. B.; *J. Chem. Soc., Dalton Trans.* **2002**, 2852; (d) Guerret, O.; Sole, S.; Gornitzka, H.; Teichert, M.; Trinquier, G.; Bertrand, G.; *J. Am. Chem. Soc.* **1997**, 119, 6668.
- 4 Bondi, A.; *J. Phys. Chem.* **1964**, 68, 441.
- 5 (a) Pyykkö, P.; Mendizabal, F.; *Inorg. Chem.* **1998**, 37, 3018; (b) Singh, K.; Long, J.R.; Stavropoulos, P.; *J. Am. Chem. Soc.* **1997**, 119, 2942; (c) Forniés, J.; Martínez, F.; Navarro, R.; Urriolabeitia, E.P.; *Organometallics* **1996**, 15, 1813; (d) Marsich, N.; Pellizer, G.; Camus, A.; Lanfredi, A.M.M.; Ugozzoli, F.; *Inorg. Chim. Acta* **1990**, 169, 171; (e) Hartman, E.; Straehle, J.; *Z. Anorg. Allg. Chem.* **1990**, 583, 31; (f) Jansen, M.; *Angew. Chem., Int. Ed. Engl.* **1987**, 26, 1098; (g) Uson, R.; Forniés, J.; Tomás, M.; Catton, F.A.; Falvello, L.R.; *J. Am. Chem. Soc.* **1984**, 106, 2482; (h) Baenziger, N.C.; Struss, A.W.; *Inorg. Chem.* **1976**, 15, 1807.
- 6 (a) Lee, C.K.; Lee, K.M.; Lin, I.J.B.; *Organometallics* **2002**, 21, 10; (b) Caballero, A.; Díez-Barra, E.; Jalón, F.A.; Merino, S.; Tejada, J.; *J. Organomet. Chem.* **2001**, 617-618, 395; (c) Garrisen, J.C.; Simons, R.S.; Talley, J.M.; Wesdemiotis, C.; Tessier, C.A.; Youngs, W.J.; *Organometallics* **2001**, 20, 1276; (d) Ku, R.Z.; Huang, J.C.; Cho, J.Y. Kiang, F.M.; Reddy, K.R.; Chen, Y.C.; Lee, K.J.; Lee, J.H.; Lee, G.H.S.; Peng, M.; Liu, S.T.; *Organometallics* **1999**, 18, 2145.
- 7 Bildstein, B.; Malaun, M.; Kopacka, H.; Wurst, K.; Mitterböck, M.; Ongania, K.H.; Opromolla, G.; Zanello, P.; *Organometallics*, **1999**, 18, 4325.
- 8 Sheldrick, G. M., SADABS, 1996, University of Göttingen, Germany.
- 9 Sheldrick, G. M., SHELXL97, University of Göttingen, Germany.
- 10 Fre, P. D.; Scott, N. M.; Stevens, E. D.; Ramnial, T.; Lightbody, O. C.; Macdonald, C. L. B.; Clyburne, J. A. C.; Abernethy, C. D.; Nolan, S. P. *Organometallics* **2005**, 24, 6301-6309.
- 11 Busetto, L.; Cristina Cassani, M.; Femoni, C.; Macchioni, A.; Mazzoni, R.; Zuccaccia, D. *J. Organomet. Chem.* **2008**, 693, 2579-2591.
- 12 Newman, C. P.; Clarkson, G. J.; Rourke, J. P. *J. Organomet. Chem.* **2007**, 692, 4962-4968.
- 13 Kline, M.; Harlow, R. L. *J. Am. Chem. Soc.* **1991**, 113, 363-365.

7 Synthesis and Characterization of NHCs Rhodium Complexes with the NHBoc Functionalization

7.1 Introduction

We herein describe the synthesis and characterization of novel functionalized NHC metal complexes of rhodium(I) of the type $[\text{RhCl}(\text{NBD})(\text{NH}(\text{Boc})\text{CH}_2\text{CH}_2\text{ImR})]$ (**4a**, R = Me **4b**, R = Benzyl; **4c** Trityl) (Scheme 7.1-1). Their dynamic behavior of the rhodium systems has been investigated by means of VT NMR studies and DFT calculations.

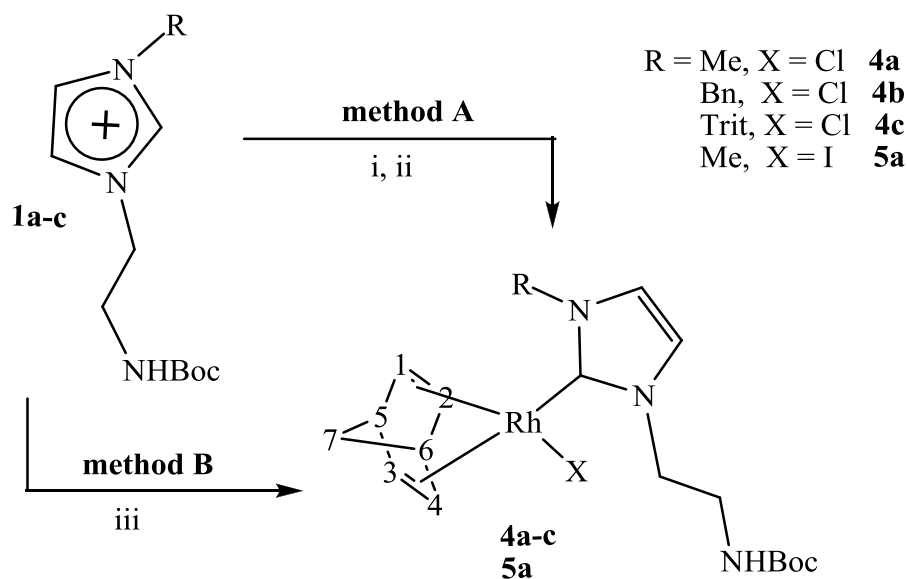


Scheme 7.1-1

7.2 Results and Discussion

7.2.1 Synthesis of Rhodium(I) complexes and solution NMR studies.

The rhodium complexes $[\text{RhCl}(\text{NBD})(\text{NHC})]$ (NBD = 2,5-Norbornadiene; **4a**, R = Me; **4b**, R = Benzyl; **4c**, R = Trityl) were synthesized by transmetallation from the NHC-Ag complexes **3a-c** (paragraph 2.2.1) in dichloromethane (Scheme 7.2-1, method A). The iodide analogue $[\text{RhI}(\text{NBD})(\text{NHC})]$ (**5a**, R = Me) was instead prepared either by reaction with the *in situ* generated carbene in THF (Scheme 7.2-1 method B, reaction conditions iii) or by ion exchange methatesis from **4a** with an excess of NaI.¹



Scheme 7.2-1 Synthesis of Rhodium(I) complexes. Reactions and conditions for **4a-c**: i) Ag_2O , CH_2Cl_2 , R.T.; ii) $[\text{RhCl}(\text{NBD})]_2$, CH_2Cl_2 , R.T., 2 h. Reaction and conditions for **5a**: iii) $[\text{Rh}(\text{NBD})(\text{O}^t\text{Bu})]_2$, THF, R.T., 3 h.

We found that whereas the transmetallation reaction with $[\text{RhCl}(\text{NBD})]_2$ always gave the yellow neutral mononuclear metallocarbene complexes **4** in a very efficient and selective way (70-90% yield), with the synthetic procedure **B** the iodide complex **5a** was always isolated in lower yields (30-40%). This is probably due to the erratic oxidation of tetrahydrofuran to γ -butyrolactone catalyzed by Rh(I) (either the starting $[\text{RhCl}(\text{NBD})]_2$) in the presence of trace amounts of water.² With the transmetallation method **A**, after filtering off any unreacted Ag_2O or any formed AgX followed by gradient column chromatography under argon on anhydrous silica gel, complexes **4** were isolated as yellow microcrystalline solids. They are completely soluble in chlorinated solvents, acetonitrile, partially soluble in diethyl ether and completely insoluble in petroleum ether. Complexes **4a,b** and **5a** are air-sensitive in the solid state and in solution but not moisture-sensitive: continuous monitoring of the NMR samples in CDCl_3 showed that decomposition to unidentified products rapidly occurs after exposure to air (ca. 1 h) but not after controlled additions of degassed water either at room temperature (over two weeks) or 55 °C (30 min.). On the contrary **4c** is perfectly air stable and NMR monitoring for over 10 days of a sample prepared in air with not anhydrous chloroform did not present any significant decomposition.

They have been fully characterized by elemental analysis, ESI-MS mass spectrometry and ^1H and ^{13}C NMR using gCOSY, gHSQC and gHMBC experiments for full resonances assignments.

The ^1H NMR (CDCl_3) spectra for **4a** show a broad signal at 6.74 ppm assigned to the =CH backbone protons, whilst in the ^{13}C NMR spectra the coordination of the carbene to the rhodium center becomes evident as a doublet resonance at 184.2 ppm (d, $J_{\text{C,Rh}} = 57.1$ Hz). These chemical

shifts and coupling constant values lie in the usual range for related Rh(I)-NHC complexes.³ The olefinic protons of the norbornadiene ligand feature three 1:1:1 resonances (2 protons each) at 4.86, 3.82 and 3.49 ppm respectively and three doublets in the ¹³C NMR spectra at 63.6 ($J_{C,Rh} = 4.8$ Hz), 51.0 ($J_{C,Rh} = 4.8$ Hz), 48.1 ($J_{C,Rh} = 12.3$ Hz). This observation can be explained by the lack of an effective symmetry plane in the molecules as the result of the hindered rotation about the carbene-rhodium bond. Due to the steric hindrance exerted by the two sidearms, the norbornadiene moiety and the chlorine atom are displaced in a out-of-plane disposition with respect to the imidazole ring. If the two sidearms are different the molecule has C₁ symmetry, therefore a pair of conformational enantiomers is generated.

The ¹H spectra of compound **4b**, bearing a benzyl group, are displayed in Figure 7.2-1. The spectrum recorded at room temperature (middle trace) shows very broad signals and, in particular, the signal of the benzylic CH₂ is close to the coalescence point. When the temperature is raised to +55°C all the signals sharpen, whereas on lowering the temperature the benzylic CH₂ decoalesces into an AB system (5.58 and 6.02 ppm), and the methylenic protons of the amide sidearm splits into diastereotopic signals too.

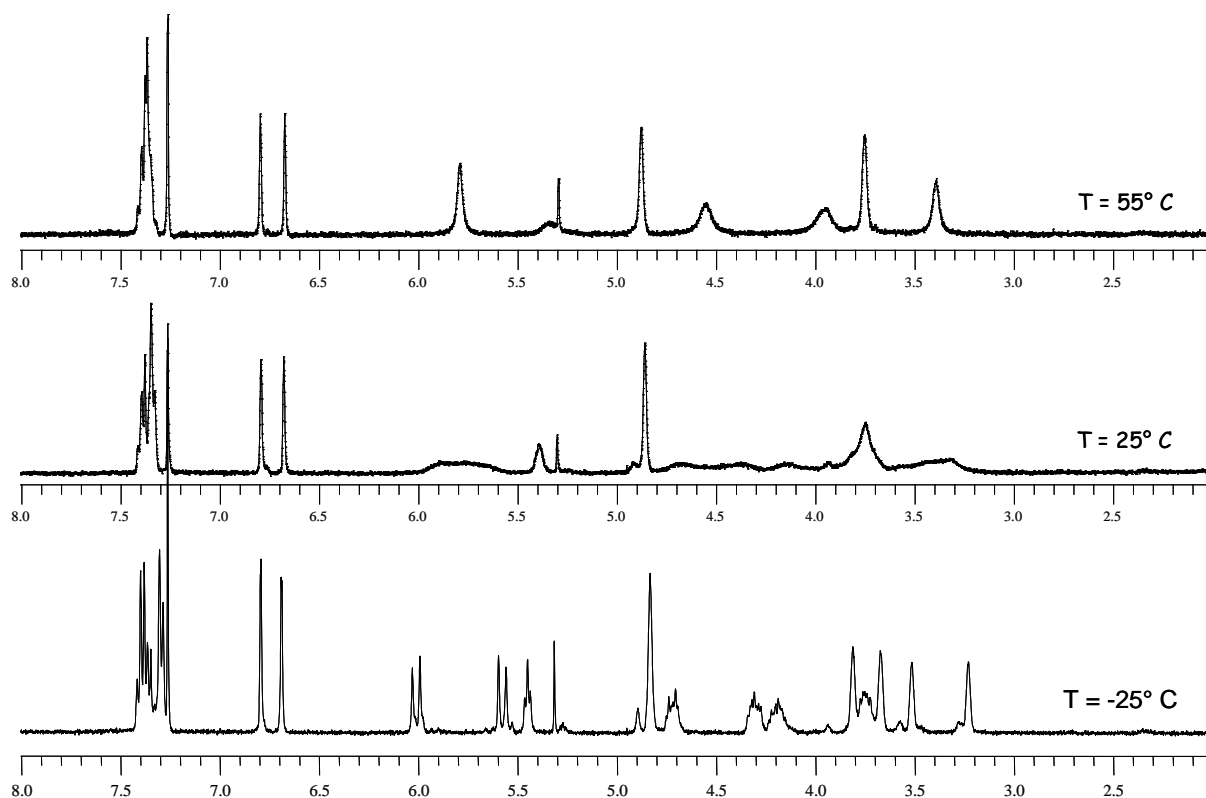


Figure 7.2-1 ¹H-NMR at 600 MHz in CDCl₃ of **4b**.

The carbonyl stretching frequency (ν_{CO}) of the carbammic group $-\text{NHC(O)O}-$ does not give any information on the kind of coordination and is similar to that of the starting imidazolium precursor always appearing at about 1710 cm^{-1} for the rhodium complexes and although the complexes are neutral, positive ESI-MS analyses for the complexes **4a-c** and **5a** always showed a major m/z peak corresponding to the $[\text{M} - \text{X}]^+$ fragment.

All attempts to facilitate a κN coordination of the amine nitrogen by removing the halide ligand as AgX resulted in decomposition products even when the reactions were performed in coordinating solvents (acetone or acetonitrile) and/or in the presence of poorly coordinating anions (triflate).

7.3 Stereodynamics

The stereodynamics and the rotation barriers about the Rh-carbene bond have been determined by making use of variable temperature NMR spectroscopy,⁴ on increasing the steric hindrance of N-alkyl substituent and by varying the halogen atom.

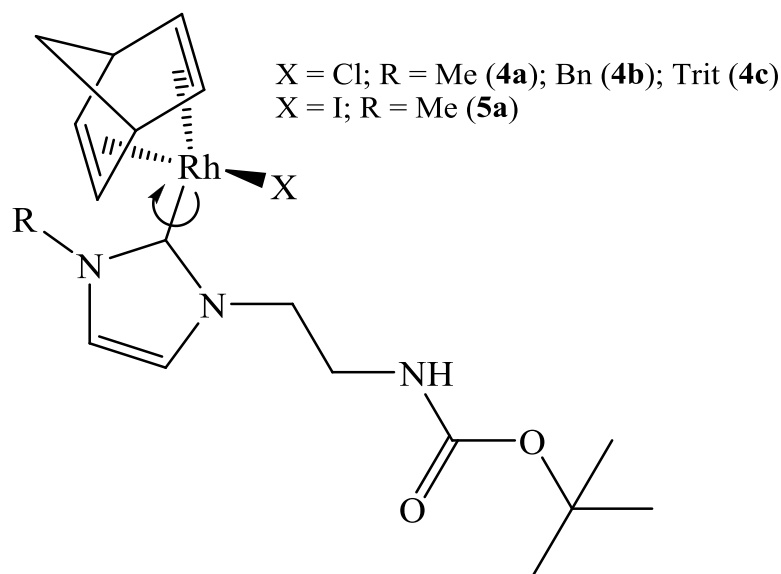


Chart 7.3-1

In the case of **4b**, the signal of the benzylic CH_2 shows the typical shape of the coalescence at $+25\text{ }^\circ\text{C}$. As shown in Figure 7.3-1, the signal sharpens at high temperature whereas it decoalesces into an AB-system at low temperature. Line shape simulation at various temperatures yielded the rate constants for the enantiomerization, from which an activation energy of 58.6 kJ mol^{-1} was derived by the Eyring equation. The activation energy was found to be constant with respect to the temperature, indicating a negligible value of the activation entropy. This implies that the observed

barrier should be due to steric effects only. When the steric hindrance on one sidearm is reduced, like in compound **4a**, the rotational barrier is lower (55.3 kJ mol^{-1}), and the enantiomerization process could be monitored by observing the splitting of a CH signal of norbornadiene.

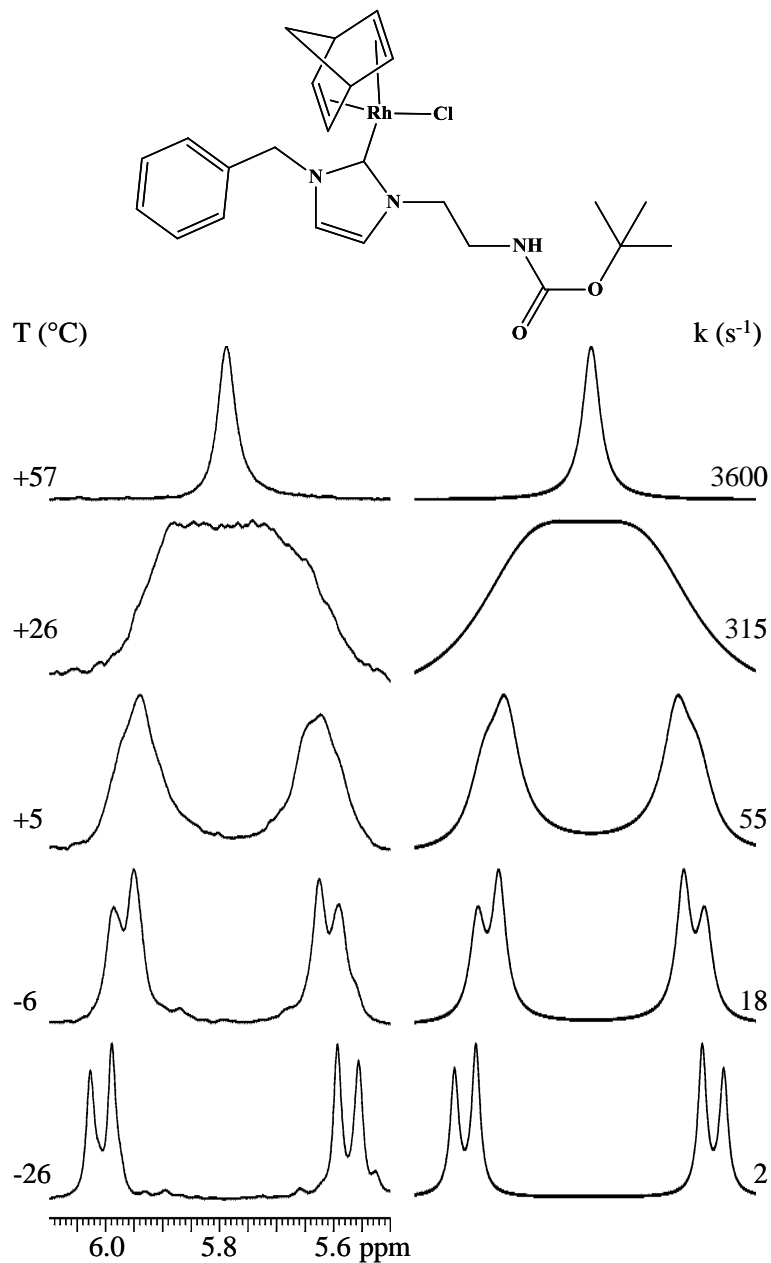


Figure 7.3-1 Variable temperature spectra of **4b** showing the evolution of the benzylic CH_2 signal. (^1H NMR at 400 MHz in CDCl_3). On the right the simulations with the corresponding rate constants are reported.

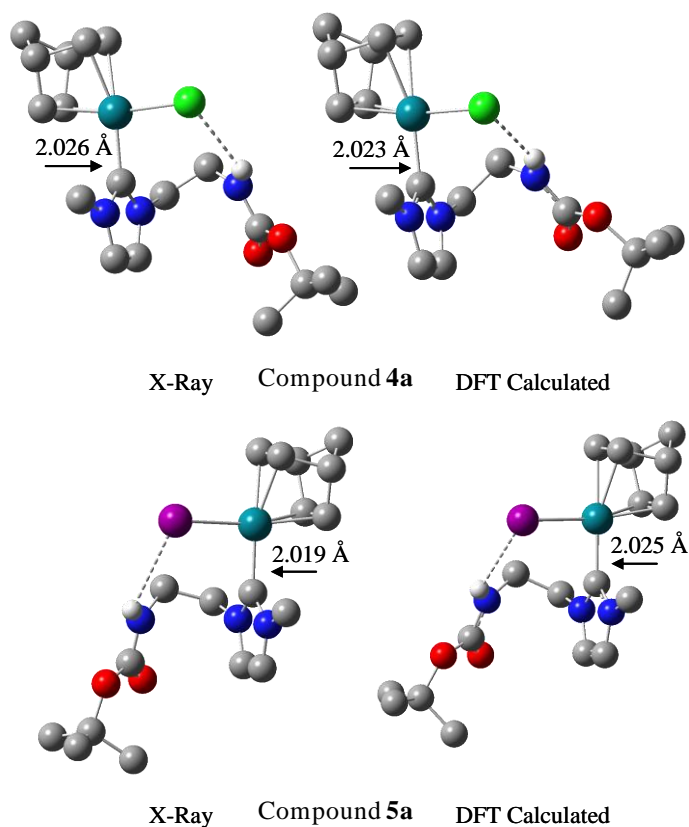
On the contrary, when the chlorine atom of **4a** is exchanged with iodine (as in compound **5a**), the rotational barrier is increased, and the signals of norbornadiene are split at room temperature. On raising the temperature the coalescence point is reached at $+57 \text{ }^\circ\text{C}$, and a single broad signal was observed at $+90 \text{ }^\circ\text{C}$ (spectra at higher temperatures cannot be recorded due to decomposition). The

rotational barrier was derived to be 72.4 kJ mol⁻¹. These data agree very well with those of Enders and Gielen confirming a steric origin of the rotation barrier.⁵

An analogous behavior is observed for **4c** moreover the presence of the three phenyl rings of the trityl group causes a ring current effect that leads to a significant upfield shift of one of the NCH₂- wingtip diastereotopic protons that is found at 6.02 ppm whereas on the opposite, a proton of the norbornadiene is highfield shifted to an unusually low 2.1 ppm.

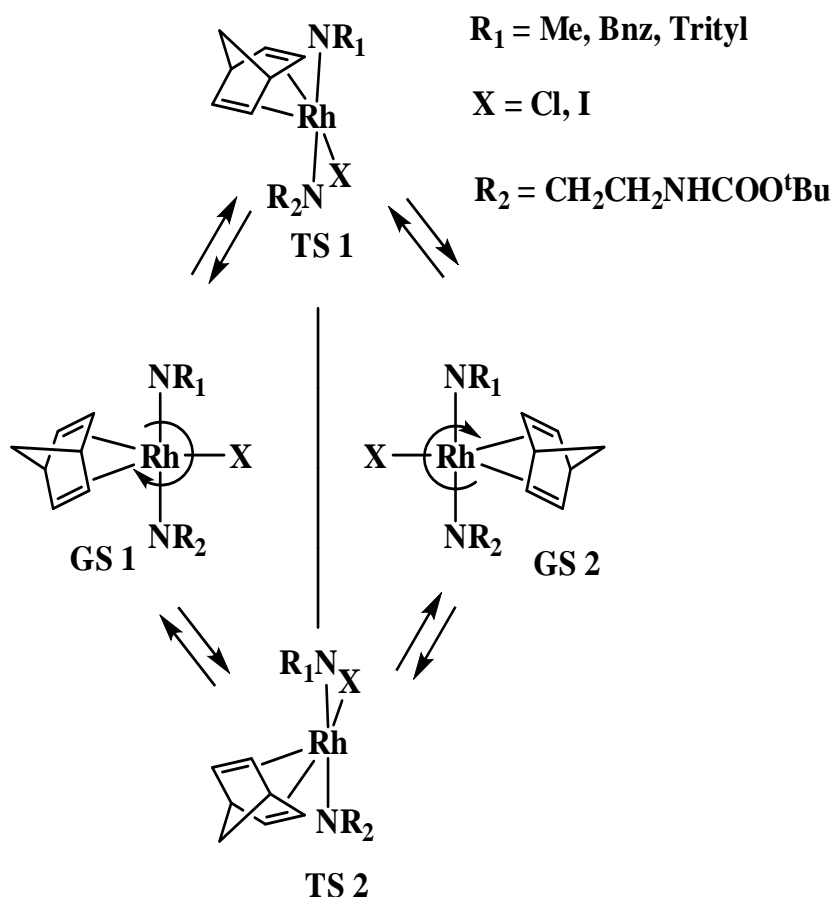
The variable temperature spectra taken in the case of compound **4c** showed that the rotational barrier (58.8 kJ mol⁻¹) was identical, within errors, to that obtained in the case of the benzyl-substituted compound **4b** however, the spectra simulations show a noticeable increase of the free energy of activation on raising the temperature, therefore indicating a negative entropic activation.

DFT calculations of compounds **4a-c** and **5a** were performed at the B3LYP/LANL2DZ level. The geometry of the calculated ground states of **4a** and **5a** were almost identical to that observed in the solid state (Figure 7.3-2). In particular the calculations correctly reproduced the Rh-C, Rh-Cl and Rh-I bond lengths. In addition, the torsion angles that generate the two conformational enantiomers observed in solution were also correctly reproduced (Cl(2)-Rh(1)-C(8)-N(2) = 89.15°; I(1)-Rh(1)-C(8)-N(9) = 96.72°). These results actually show that the theoretical level employed in the calculations is suitable to tackle the conformational analysis of these complexes.



Scheme 7.3-1 Left: experimental X-ray structures of **4a** and **5a**. Right: calculated structures.

The two enantiomeric ground states can interconvert into each other by two possible transition states due to the rotation around the carbene-Rhodium bond (Scheme 7.3-1). The first one (TS-1) corresponds to the crossing of the halogen atom on the CH₂ of the amide-ethyl moiety (denoted as R₂), whereas the second transition state (TS-2) takes place when the halogen crosses the second alkyl sidearm group (R₁) on the imidazole. The nature of the halogen and of R₁ obviously influence the value of the rotational barrier. DFT calculations of the two possible transition states (Table 7.3-1) suggested that in all the cases the threshold pathway (i.e. that with the lowest transition state energy) corresponded to the passage of the halogen atom on the amide-ethyl group (TS-1), with the simultaneous crossing of the norbornadiene on the second sidearm. The calculations also suggested that the energy barrier is strongly related to the steric hindrance of R₁, and for this reason the barrier calculated for compound **4c** is predicted to be quite high (100.0 kJ mol⁻¹).



Scheme 7.3-2 Enantiomerization pathway for compounds **4a-c** and **5a**.

Table 7.3-1 Calculated and experimental energy barriers for the enantiomerization of **4a-4c** and **5a**. (Energies in kJ mol^{-1} , calculations at the B3LYP/LANL2DZ level).

Compd.	TS-1	TS-2	Exp. (kJ mol^{-1})
4a	58.8	67.8	55.3
4b	67.9	77.7	58.6
4c	100.0	126.4	58.8
5a	79.2	83.3	72.4

Whilst the rotation barriers calculated for **4a,b** matched the experimental values, this was not true in the case of **4c**, where the experimental value was equal to that obtained for compound **4b** and much smaller with respect to the calculated one. In addition, the energy barrier derived for **4c** from lineshape simulation showed a strong dependence from the temperature, whilst the barriers measured for **4a,b** did not show this effect. In particular, the large negative activation entropy derived from simulations (-40 ± 10 e.u.) indicates that a strongly organized transition state and a

different interconversion pathway takes place in the case of compound **4c**. The inversion process may proceed either via a cleavage of the Rh-Cl bond before or during the rotation⁶ or by partial dissociation of the trityl group into a contact ionic pair, followed by the rotation of the Rh-Cl moiety and subsequent reformation of nitrogen-trityl carbon bond.⁷ The experimental evidence that the replacement of chlorine with iodine raises the rotational barrier in the case of **4a** and **5a** (as correctly indicated also by the calculations) suggests that the latter hypothesis should be considered more likely. In addition, the possible coordination of a phenyl ring of the trityl moiety to rhodium⁸ in the transition state might be responsible for the partial dissociation of trityl group and for lowering the energy of the transition state. In this framework the value obtained for compound **4c** is a threshold value for the true steric rotational barrier.

7.3.1 Crystal Structure determination for **4a**, **5a**, **4c**

The molecular structures of the rhodium(I) complexes **4a**, **5a**, **4c** were determined via X-ray diffraction and are reported in Figure 7.3-2, Figure 7.3-3 Figure 7.3-4, respectively. The crystal data and experimental details are reported in Table 7.3-2. The structural analysis confirmed that the Boc protection removes most of the nucleophilicity of the amide nitrogen that is never involved in any coordinative bond. The crystals of **4a** and **5a** suitable for diffraction were grown by slow evaporation of a mixture of CH₂Cl₂ and petroleum ether.

The structure of **4a**, which crystallized in a centric space group (*P*2₁/*c*), consists of separated C₁₈H₂₇ClN₃O₂Rh molecules arranged in eclipsed, alternated columns of enantiomers. There are, in fact, two possible orientations of the BocNHCH₂CH₂- and -CH₃ substituents on the functionalized imidazolium ring and both are generated by the cell symmetry operators from the unique Rh complex in the asymmetric unit. Rhodium shows a classic square-planar coordination and is bonded to Cl(2) atom, the carbenic C(8) atom and the bi-dentate norbornadiene fragment. The stronger trans effect that the carbene exercises comparing with the chlorine ligand is inferable from the distances between Rh and C atoms on the norbornadiene unit: the Rh-C(1) and Rh-C(2) contacts in trans with the carbene are 2.204(2) and 2.206(2) Å respectively, the Rh-C(3) and Rh-C(4) bond lengths in trans with Cl atom are remarkably shorter, both 2.083(2) Å. Despite the presence of donor chlorides anions, there are not significant intra- or intermolecular hydrogen bonds in the solid state, with the exception of a very weak intermolecular interaction between Cl(2) and N(3) (3.366 Å). In addition there is no evidence of a positional disorder in the structure even at room temperature, and this is an index of the very high efficient solid packing of the molecules, which is mainly stabilized by steric effects.

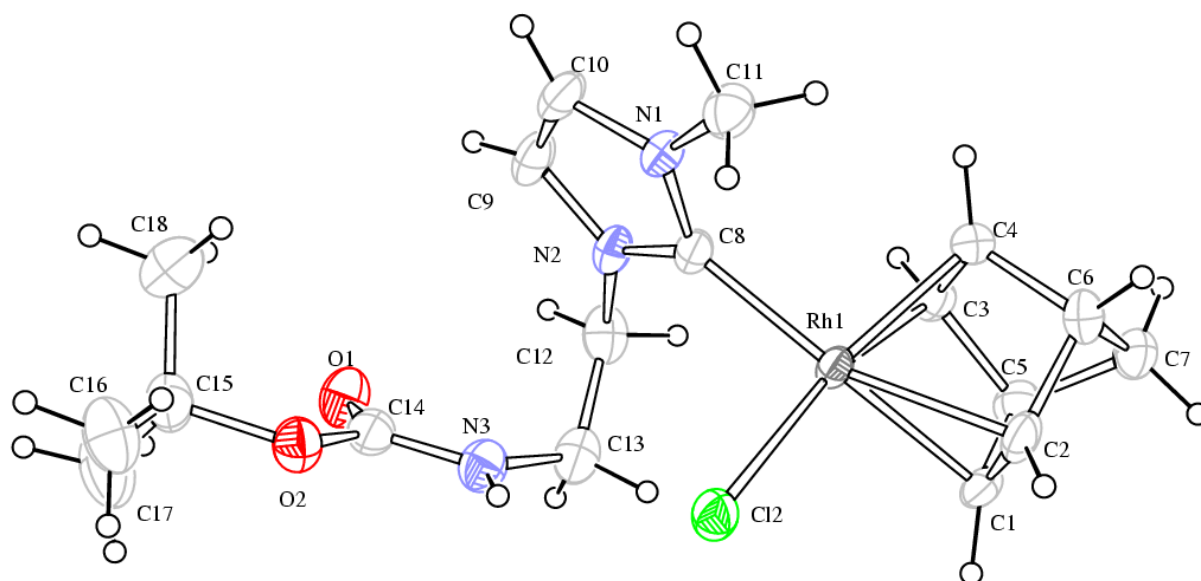


Figure 7.3-2 ORTEP diagram of **4a** depicted with displacement ellipsoids at 30% probability level.

The structure of **5a** (Figure 7.3-2), which crystallized in the same centric space group as its chloride congener, does not significantly differ from the latter in terms of solid-state packing and atomic coordination, the only exception being a slight positional disorder found in the terminal *tert*-butyl group of the ligand. Again the complex crystallized in a racemic mixture with both enantiomers present in a 1:1 ratio. The same strong trans effect of the carbenic atom C(8) is also observed, as revealed by the Rh-C bond lengths: the Rh-C(1) e Rh-C(2) distances, in trans position with respect to C(8), are both 2.207(4) Å, while the Rh-C(4) e Rh-C(5) bonds, in trans to the I atom, are 2.103(4) e 2.105(4) Å in that order. There is a positional disorder in the structure of C₁₈H₂₇IN₃O₂Rh (**5a**), more specifically in the *t*Bu group, so the involved carbon atoms were split in two positions and anisotropic displacement parameter restraints were applied.

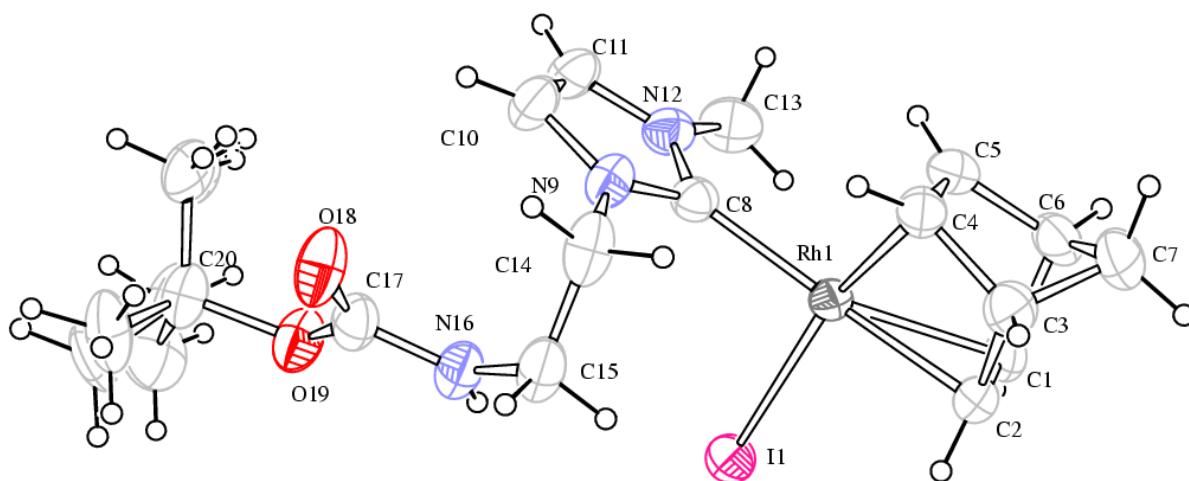


Figure 7.3-3 ORTEP diagram of **5a** depicted with displacement ellipsoids at 30% probability level.

Crystals of **4c** suitable for X-ray diffraction were obtained from a concentrated acetonitrile solution at $-20\text{ }^{\circ}\text{C}$.

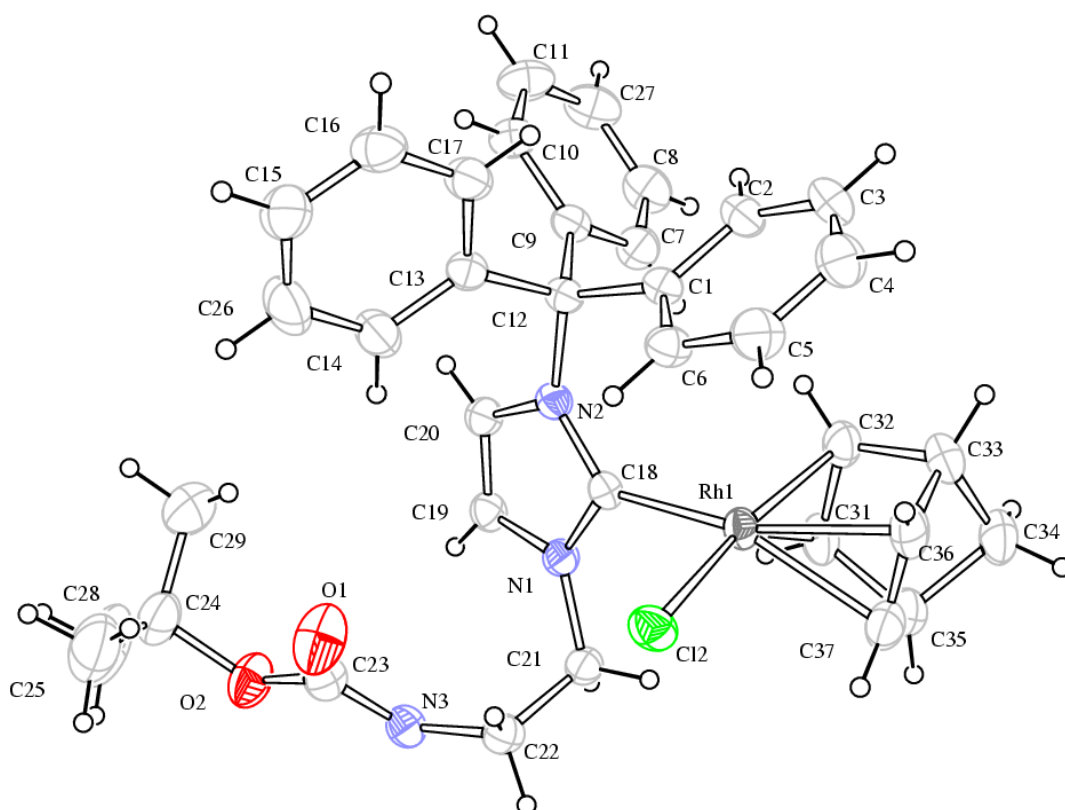


Figure 7.3-4 ORTEP diagram of **4c** depicted with displacement ellipsoids at 30% probability level.

Compound **4c** crystallizes in the centrosymmetric $P2_1/n$ group, and both enantiomers are generated by the centre of symmetry, as in the previous cases. At a variance with **4a** and **5a**, the unit

cell contains also 8 molecules of acetonitrile, that makes the crystal package less efficient. As in the case of **4a** and **5a**, the Rhodium has a square-planar coordination, with the Rh-Cl and Rh-C bond distances slightly longer with respect to **4a** (2.055 Å for Rh(1)-C(18) and 2.428 Å for Rh(1)-Cl(2)). This could be ascribed to the steric hindrance exerted by the large trityl group. The dihedral angle Cl(2)-Rh(1)-C(18)-N(2) that yields the two enantiomers whose barrier was observed in solution is 111°, to be compared with that of 92.47° observed for Cl(2)-Rh(1)-C(8)-N(1) in **4a**.

Table 7.3-2 Crystal Data, Data Collection and Refinement Parameters for 1c, 4a, 5a, 4c

Compound	4a	5a	4c·2CH₃CN
Formula	C ₁₈ H ₂₇ ClN ₃ O ₂ Rh	C ₁₈ H ₂₇ IN ₃ O ₂ Rh	C ₄₀ H ₄₅ ClN ₅ O ₂ Rh
Fw	455.79	547.24	766.17
T, K	298(2)	296(2)	296(2)
λ, Å	0.71073	0.71073	0.71073
Crystal system	Monoclinic	Monoclinic	Monoclinic
Space group	<i>P</i> 2 ₁ / <i>c</i>	<i>P</i> 2 ₁ / <i>c</i>	<i>P</i> 2 ₁ / <i>n</i>
a, Å	11.9725(7)	12.0829(13)	13.1294(13)
b, Å	18.1627(10)	15.0838(16)	9.7921(10)
c, Å	9.9190(5)	12.2761(13)	29.874(3)
α, °	90	90	90
β, °	112.3730(10)	108.2450(10)	93.5440(10)
γ, °	90	90	90
Cell Volume, Å ³	1994.55(19)	2124.7(4)	3833.4(7)
Z	4	4	4
D _c , g cm ⁻³	1.518	1.711	1.328
μ, mm ⁻¹	1.006	2.272	0.555
F(000)	936	1080	1592
Crystal size, mm	0.30 x 0.25 x 0.20	0.20 x 0.15 x 0.10	0.60 x 0.40 x 0.20
θ limits, °	1.84 to 25.00	1.77 to 25.00	1.37 to 28.72
Index ranges	-14 ≤ h ≤ 14, -21 ≤ k ≤ 21, -11 ≤ l ≤ 11	-14 ≤ h ≤ 14, -17 ≤ k ≤ 17, -14 ≤ l ≤ 14	-17 ≤ h ≤ 17, -13 ≤ k ≤ 13, -40 ≤ l ≤ 39
Reflections collected	18769	20041	43389
Independent reflections	3513 [R(int) = 0.0209]	3740 [R(int) = 0.0449]	3740 [R(int) = 0.0276]
Completeness to θ = 25.00°	100.0 %	100.0 %	100.0 %
Data / restraints / parameters	3513 / 0 / 226	3740 / 24 / 255	9350 / 0 / 459
Goodness on fit	1.030	1.009	0.998

on F^2			
R_1 ($I > 2\sigma(I)$)	0.0217	0.0303 and 0.0623	0.0319
wR_2 (all data)	0.0617	0.0503 and 0.0717	0.0759
Largest diff. peak and hole, e \AA^{-3}	0.388 and -0.283	0.639 and -0.634	0.519 and -0.277

7.4 Conclusion

We have described the synthesis of novel imidazolium salts that are precursors for rhodium(I) complexes $[\text{RhX}(\text{NBD})(\text{NHC})]$ ($\text{NHC} = 1-(2\text{-NHBoc-ethyl})\text{-3-R-imidazolin-2-ylidene}$; $\text{X} = \text{Cl}$, $\text{R} = \text{Me}$ (**4a**), $\text{R} = \text{Benzyl}$ (**4b**), $\text{R} = \text{Trityl}$ (**4c**); $\text{X} = \text{I}$, $\text{R} = \text{Me}$ (**5a**)) in which the NHC ligands bear an amide-functional group on one nitrogen and increasing bulky N-alkyl substituents (Me, Benzyl, Trityl) on the other. All the complexes display restricted rotation about the metal-carbene bond however whilst the rotation barriers calculated for the complexes in which $\text{R} = \text{Me}$, Benzyl (**4a,b** and **5a**) matched the experimental values, this was not true in the trityl case **4c**, where the experimental value was equal to that obtained for compound **4b**, and much smaller with respect to the calculated one. In addition, the energy barrier derived for **4c** from lineshape simulation showed a strong dependence from the temperature, whilst the barriers measured for **4a,b** did not show this effect. In particular, the large negative activation entropy derived from simulations (-40 ± 10 e.u.) indicates that a strongly organized transition state and a different interconversion pathway takes place in the case of compound **4c**. We believe that these observations may bring important implications in further research in NHC-M formation and studies in this direction are in progress.

7.5 Experimental Section

Materials and Procedures. All reactions were carried out under Argon using standard Schlenk techniques. Solvents were dried and distilled under nitrogen prior to use; the deuterated solvents used after being appropriately dried and degassed were stored in ampoules under argon on 4\AA molecular sieves. The prepared derivatives were characterized by elemental analysis and spectroscopic methods. The IR spectra were recorded with a FT-IR spectrometer Perkin Elmer Spectrum 2000. The NMR spectra were recorded using Varian Inova 300 (^1H , 300.1; ^{13}C , 75.5 MHz), Varian MercuryPlus VX 400 (^1H , 399.9; ^{13}C , 100.6 MHz), Varian Inova 600 (^1H , 599.7, ^{13}C ,

150.8 MHz) instruments. The spectra were referenced internally to residual solvent resonances, and unless otherwise stated, they were recorded at 298 K for characterization purposes; full ^1H and ^{13}C NMR assignments were done, when necessary, by gCOSY, gHSQC, gHMBC, NOESY NMR experiments using standard Varian pulse sequences; J.Young valve NMR tubes (Wilmad) were used to carry out NMR experiments under inert conditions. ESI-MS analysis were performed by direct injection of methanol solutions of the metal complexes using a WATERS ZQ 4000 mass spectrometer. Elemental analyses were performed on a ThermoQuest Flash 1112 Series EA Instrument. The chemicals $[\text{RhCl}(\text{NBD})]_2$ was purchased from Strem and used as received; the starting building blocks: 1-(2-BocNH-ethyl)-3-methyl-imidazolin-2-ylidene silver iodide (**2a**),⁷ were prepared according to literature procedures. Petroleum ether (Etp) refers to a fraction of b.p. 60-80 °C. The reactions were monitored by thin-layer chromatography (TLC) on highly purified silica gel on polyester (w/UV indicator) and visualized using UV light (254 nm). Column chromatography were carried out under argon on silica gel previously heated at about 200 °C while a slow stream of a dry nitrogen was passed through it;⁹ celite was dried in an oven at 150 °C. Melting points were taken with a Stuart Scientific Melting point apparatus SMP3 and were uncorrected. Crystal data were collected at room temperature on a Bruker APEX II diffractometer equipped with a CCD detector operating at 50 kV and 30 mA, using graphite monochromated MoK_α radiation ($\lambda = 0.71073 \text{ \AA}$). An empirical absorption correction was applied on both structures by using SADABS.¹⁰ They were solved by direct methods and refined by full-matrix least-squares based on all data using F^2 with SHELXL97.¹¹ All non-hydrogen atoms were refined anisotropically, with the exception of the hydrogen atoms which were set geometrically and given fixed isotropic thermal parameters.

7.5.1 Synthesis of $[\text{RhCl}(\text{NBD})\{1-(2-\text{NHBoc-ethyl})-3\text{-methyl-imidazolin-2-ylidene}\}]$. (**4a**)

To a solution of **1a** (0.258 g 0.73 mmol) in CH_2Cl_2 (ca. 30 mL), Ag_2O (0.107 g, 0.37 mmol) was added. The suspension was stirred for 2 h, filtered on celite and the filtrate added to a solution of $[\text{Rh}(\text{NBD})\text{Cl}]_2$ (0.168 g 0.37 mmol) in CH_2Cl_2 . After stirring for 3 h the yellow AgI was filtered off and the solvent was removed under vacuum. The crude material was purified by column chromatography on silica gel using first CH_2Cl_2 and then $\text{CH}_2\text{Cl}_2:\text{MeOH} = 100:3$ (v/v) as eluent to afford 0.23 g (71 %) of **4a** as a yellow solid. R_f : 0.60 ($\text{CH}_2\text{Cl}_2:\text{MeOH} = 100:5$). $^1\text{H-NMR}$ (300.1 MHz, CDCl_3): δ 6.76 (br s, 2H, CH_{im}), 5.34 (br s, 1H, NH), 4.86 (m, 2H, NBD), 4.49 (m, 2H, NCH_2), 4.10 (s, 3H, NCH_3), 3.92 (m, 2H, CH_2NH), 3.82 (m, 2H, NBD), 3.49 (m, 2H, NBD), 1.41 (s, 9H, ^tBu), 1.36 (t, 2H, $J_{\text{H,H}} = 1.4 \text{ Hz}$, C^7H_2 NBD). $^{13}\text{C}\{-^1\text{H}\}$ NMR (75 MHz, CDCl_3): δ 184.2 (d, $J_{\text{C,Rh}} = 57.1 \text{ Hz}$), 156.3 (C=O), 121.8 (CH_{im}), 121.6 (CH_{im}), 79.4 (d, $J_{\text{C,Rh}} = 4.6 \text{ Hz}$, NBD), 79.2 (Cq,

^tBu), 63.6 (d, $J_{C,Rh} = 4.8$ Hz; NBD), 51.0 (d, $J_{C,Rh} = 2.4$ Hz, NBD), 49.6 (NCH₂), 48.1 (d, $J_{C,Rh} = 12.3$ Hz, NBD), 41.3 (CH₂NH), 37.9 (NCH₃), 28.4 (CH₃, ^tBu). **IR** (CH₂Cl₂, cm⁻¹): 1712 (vs, ν_{CO}); IR (KBr, cm⁻¹): 3386 (s, ν_{NH}), 3156, 3120, 3104, 3056, 3041, 2981, 2922, 1700 cm⁻¹ (vs, ν_{CO}), 1500, 1364, 1254, 1173. **ESI-MS** (MeOH, m/z): 478 (11) [M + Na]⁺, 420 (100) [M - Cl]⁺; 490 (100) [M + Cl]⁻. Analysis calcd. (%) for C₁₈H₂₇ClN₃O₂Rh: C, 47.43; H, 5.97; N, 9.22. Found: C, 47.10; H, 6.04; N, 9.23. M.p. = 136 °C (dec.). Suitable crystals of **4a** for X-Ray diffraction have been obtained by slow evaporation from a mixture of CH₂Cl₂ and petroleum ether.

7.5.2 Synthesis of [RhCl(NBD){1-(2-NHBoc-ethyl)-3-benzyl-imidazolin-2-ylidene}]. (**4b**)

To a solution of **1b** (0.500 g, 1.31 mmol) in CH₂Cl₂ (30 mL), Ag₂O (0.154 g, 0.66 mmol) was added. After stirring for 2 h at room temperature, the suspension was filtered on celite and the filtrate added to a solution of [Rh(NBD)Cl]₂ (0.301 g, 0.65 mmol) in CH₂Cl₂. After 3 h, AgBr was filtered off and the solvent was removed under vacuum. The crude material was purified by column chromatography on silica gel using first CH₂Cl₂ and then CH₂Cl₂:MeOH = 100:1 (v/v) as eluent to afford 0.67 g (78 %) of **4b** as a yellow solid. R_f: 0.65 (CH₂Cl₂:MeOH = 100:5). The silver intermediate of 1-(2-BocNH-ethyl)-3-benzyl-imidazolin-2-ylidene silver bromide **2b** was not isolated but a NMR and ESI-MS analysis was carried out on the crude material to confirm its formation. **¹H NMR** of **4b** (599.7 MHz, CDCl₃, 228.18 K): δ 7.35 (m, 5H, Ph), 6.79 (d, 1H, $J_{H,H} = 1.8$ Hz, CH_{im}), 6.68 (d, 1H, $J_{H,H} = 1.8$ Hz, CH_{im}), 6.01 (d, 1H, $J_{H,H} = 15.2$ Hz, CH₂Ph), 5.57 (d, 1H, $J_{H,H} = 15.2$ Hz, CH₂Ph), 5.45 (t, 1H, $J_{H,H} = 5.6$ Hz, NH), 4.83 (m, 2H, NBD), 4.70 (m, 1H, NCH₂); 4.31 (m, 1H, NCH₂), 4.18 (m, 1H, CH₂NH), 3.81 (m, 1H, NBD), 3.76 (m, 1H, CH₂NH), 3.67 (m, 1H, NBD), 3.51 (m, 1H, NBD), 3.23 (m, 1H, NBD), 1.39 (s, 9H, CH₃), 1.31 (d, 1H, $J_{H,H} = 8.1$ Hz, C⁷H₂, NBD), 1.26 (d, 1H, $J_{H,H} = 8.1$ Hz, C⁷H₂, NBD). **¹³C-{¹H} NMR** (150.8 MHz, CDCl₃, 228.2 K): δ 185.2 (d, $J_{C,Rh} = 55.2$), 156.3 (C=O), 136.8 (Ph, C₅); 128.9 (Ph, C₄); 128.6 (Ph, C₃); 128.1 (Ph, C₂), 122.3 (CH_{im}), 120.5 (CH_{im}), 79.3 (Cq, ^tBu), 79.2 (CH, NBD), 63.6 (d, $J_{C,Rh} = 4.8$ Hz, C⁷H₂, NBD), 54.5 (CH₂, CH₂Ph), 51.1 (d, $J_{C,Rh} = 15.7$ Hz, CH, NBD), 49.4 (d, $J_{C,Rh} = 12.1$ Hz, CH, NBD), 49.2 (NCH₂), 48.6 (d, $J_{C,Rh} = 11.5$ Hz, CH, NBD), 41.8 (CH₂NH), 28.3 (CH₃, ^tBu). **IR** (CH₂Cl₂, cm⁻¹): 1710 (vs, ν_{CO}); IR (KBr, cm⁻¹): 3340 (s, ν_{NH}), 3167, 3123, 3091, 3060, 3032, 2978, 2928, 1708 cm⁻¹ (vs, ν_{CO}), 1509, 1365, 1250, 1173. **ESI-MS** (MeOH, m/z): 554 (12) [M + Na]⁺, 496 (100) [M - Cl]⁺; 530 (100) [M - H]⁻. Analysis calcd. (%) for C₂₄H₃₁ClN₃O₂Rh: C, 54.19; H, 5.87; N, 7.90. Found: C, 54.21; H, 5.89; N, 7.87.. M.p. = 97 °C.

7.5.3 Synthesis of [RhCl(NBD){1-(2-NHBoc-ethyl)-3-trityl-imidazolin-2-ylidene}]. (4c)

To a solution of **1c** (0.200 g, 0.41 mmol) in CH₂Cl₂ (20 mL), Ag₂O (0.050 g, 0.21 mmol) was added. The suspension was stirred for 48 h then, solid [Rh(NBD)Cl]₂ (0.092 g, 0.20 mmol) was directly added to the reaction mixture. After stirring for further 2 h the crude material was filtered on a celite pad, the insoluble material was thoroughly washed with CH₂Cl₂ and the solvent removed under vacuum. The residue was purified by column chromatography on silica gel treated with 5% v/v triethylamine in Et₂O, using Et₂O:CH₂Cl₂ = 1:3 (v/v) as to afford 0.22 g (78 %) of **4c** as a yellow solid. R_f: 0.71 (CH₂Cl₂:MeOH 100:5); R_f: 0.22 (Et₂O). Suitable crystals for a X-ray diffraction analysis were obtained from a concentrated solution of **4c** in CH₃CN at -20 °C. The silver intermediate **3c** was not isolated but a ¹H NMR and ESI-MS analysis was carried out on the crude material to confirm its formation. ¹H NMR of **4c** (599.7 MHz, CDCl₃, 243.2 K): δ 7.38-7.17 (m, 15H, Ph), 6.98 (s, 1H, CH_{im}), 6.46 (s, 1H, CH_{im}), 6.02 (br s, 1H, NCH₂), 6.14 (t, J_{H,H} = 5.1 Hz, 1H, NH), 4.60 (br s, 1H, NCH₂), 4.53 (s, 1H, NBD), 3.88 (br s, 1H, CH₂NH), 3.72 (br s, 1H, CH₂NH), 3.62 (s, 1H, CH, NBD), 3.57 (s, 1H, CH, NBD), 3.23 (s, 1H, CH, NBD), 2.82 (s, 1H, CH, NBD), 2.1 (s, 1H, CH, NBD), 1.41 (s, 9H, ^tBu), 0.98 (m, 2H, NBD). ¹³C-¹H NMR (150.8 MHz, CDCl₃, 243.2 K): δ 185.4 (d, J_{C,Rh} = 56.1 Hz), 156.6 (C=O), 142.1 (C₅), 128.7 (C₄), 128.3 (C₂), 127.4 (C₃), 124.8 (CH_{im}), 119.7 (CH_{im}), 79.1 (C_q, ^tBu), 77.3 (C₁), 73.5 (CH, NBD), 64.3 (CH, NBD), 61.9 (C⁷H₂, J_{C,Rh} = 5.1 Hz, NBD), 51.2 (NCH₂), 49.3 (CH, NBD), 48.7 (CH, NBD), 45.1 (CH, NBD), 44.7 (CH, NBD), 40.8 (CH₂NH), 28.8 (CH₃, ^tBu). IR (CH₂Cl₂, cm⁻¹): 1702 (vs, ν_{CO}); IR (KBr, cm⁻¹): 3319 (s, ν_{NH}), 3141, 3089, 3058, 3032, 2975, 2930, 1707 (vs, ν_{CO}), 1492, 1445, 1250, 1170. ESI-MS (MeOH, m/z): 648 (100) [M - Cl]⁺; 682 [M - H]⁻. Analysis calcd. (%) for C₃₆H₃₉ClN₃O₂Rh: C, 63.21; H, 5.75; N, 6.14. Found: C, 63.51; H, 5.98; N, 6.04. M.p. = 108 °C.

7.5.4 Synthesis of [RhI(NBD){1-(2-NHBoc-ethyl)-3-methyl-imidazolin-2-ylidene}], (5a) by method B.

[RhCl(NBD)]₂ (0.050 g, 0.11 mmol) and KO^tBu (0.024 g, 0.22 mmol) were reacted in THF (10 mL) for 3 h. Successively the imidazolium salt **1a** (0.076 g, 0.212 mmol) was added and after stirring for further 3 h the solid was removed by filtration and the resulting orange solution was evaporated to dryness. After washing with Et₂O 0.049 g (41 %) of **5a** were obtained and suitable crystals of **5a** for X-Ray diffraction have been obtained by slow evaporation from a mixture of CH₂Cl₂ and petroleum ether.

7.5.5 Synthesis of 5a by ion exchange.

Alternatively to a solution of **4a** (0.050 mg, 0.11 mmol) in degassed methanol (2 mL) an excess of NaI (0.030 g, 0.2 mmol) was added. After stirring for 20 h the suspension was filtered and after removal of the volatiles in vacuo the product was used without further workup. **¹H NMR** (399.9 MHz, CDCl₃): δ 6.78 (s, 2H, CH_{im}), 5.25 (br s, 1H, NH), 5.09 (m, 1H, CH, NBD), 4.98 (m, 1H, CH, NBD), 4.64 (m, 1H, NCH₂), 4.26 (m, 1H, NCH₂), 3.98 (s, 3H, CH₃), 3.89 (m, 1H, CH₂NH), 3.82 (m, 2H, CH, NBD), 3.72 (m, 1H, CH₂NH), 3.63 (m, 2H, CH, NBD), 1.42 (s, 9H, ^tBu), 1.26 (m, 2H, CH₂, NBD). **¹³C-{¹H}NMR**: δ 183.7 (d, $J_{C,Rh} = 56.2$ Hz), 122.0 (CH_{im}), 121.9 (CH_{im}), 78.9 (Cq, ^tBu), 76.8 (CH, NBD), 76.4 (CH, NBD), 64.9 (⁷CH₂, NBD), 49.2 (NCH₂), 37.7 (CH₃), 40.3 (CH₂NH), 51.2 (CH, NBD), 50.6 (CH, NBD), 28.0 (^tBu). **IR** (THF, cm⁻¹): ν(C=O): 1715; IR (KBr, cm⁻¹): 3354 (s, ν_{NH}), 3165, 3094, 3052 (m, CH_{im}), 2975, 2924 (broad vs, CH), 1700 (vs, ν_{CO}). **ESI-MS(+)** (MeOH, m/z): = 420 (100) [M - I]⁺; 127 (100) [I]. Analysis calcd. (%) for C₁₈H₂₇IN₃O₂Rh: C, 39.51; H, 4.97; N, 7.68. Found: C, 40.00; H, 5.14; N, 7.61. M.p. = 148 °C (dec.).

7.6 DFT Calculations

Conformational searches were performed by Molecular Mechanics (MMFF force Field as implemented in Titan 1.0.5, Wavefunction inc.). Final geometry optimizations were carried out at the B3LYP/LanL2DZ level¹² by means of the Gaussian 09 series of programs.¹³ The standard Berny algorithm in redundant internal coordinates and default criteria of convergence were employed in all the calculations. Harmonic vibrational frequencies were calculated for all the stationary points. For each optimized ground state the frequency analysis showed the absence of imaginary frequencies, whereas each transition state showed a single imaginary frequency. Visual inspection of the corresponding normal mode was used to confirm that the correct transition state had been found. All the reported energy values represent total electronic energies. In general, these give the best fit with experimental DNMR data.¹⁴ Therefore, the computed numbers have not been corrected for zero-point energy contributions or other thermodynamic parameters. This avoids artefacts that might result from the ambiguous choice of the adequate reference temperature, from the empirical scaling¹⁵ and from the treatment of low-frequency vibration as harmonic oscillators.¹⁶

8 Synthesis and Characterization of NHCs Rhodium complexes with a Benzyl Group Functionalization

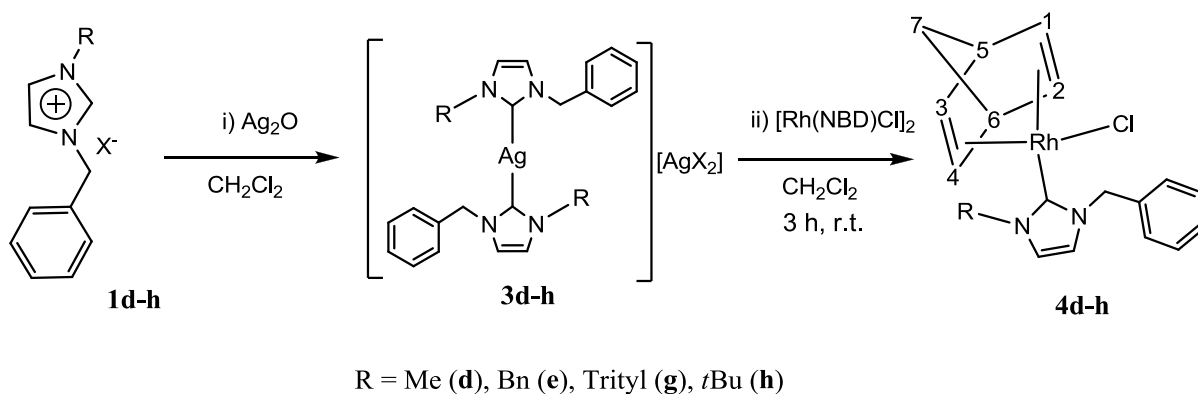
8.1 Introduction

The synthesis and characterization of novel functionalized NHC metal complexes of rhodium(I) of the type $[\text{RhCl}(\text{NBD})([\text{BnzCH}_2\text{CH}_2\text{ImR}])]$ (**4d**, R = Methyl; **4e**, R = Benzyl; **4g**, R = Trityl; **4h**, R = *t*Butyl) has been also developed. The dynamic behavior of the rhodium systems has been investigated by means of VT NMR studies and DFT calculations. Following the previous chapter the aim of this work were: a) to understand what happen in the transition state of the rotational barrier of **4g** and b) to increase the steric hindrance in order to try to isolate a pure racemate in solid and in solution state stopping the rotational barrier.

8.2 Results and discussion

8.2.1 Synthesis of Rhodium(I) Complexes and Solution NMR Studies

The rhodium complexes $[\text{RhCl}(\text{NBD})(\text{NHC})]$ (NBD = 2,5-norbornadiene; NHC = 1-benzyl-3-R-imidazolin-2-ylidene; **4d**, R = Me; **4e**, R = benzyl; **4g**, R = trityl; **4h**, R = *tert*-butyl) were synthesized in high yields (70–95%) by transmetalation from the Ag(I)-NHC complexes **3d-h** in dichloromethane (Scheme 8.1-1).



Scheme 8.1-1 Synthesis of rhodium(I)-NHC complexes **4d-h**

Complexes **4d-h** were isolated as yellow microcrystalline solids, after filtering off any unreacted Ag_2O or any formed AgX by gradient column chromatography under argon on anhydrous silica gel. They are completely soluble in chlorinated solvents and acetonitrile, partially soluble in diethyl ether, and completely insoluble in petroleum ether. Complexes **4d-h** are air stable in the solid state and in solution confirmed by continuous monitoring of the NMR samples in CDCl_3 over

2 weeks, in opposite to the structurally similar but amide-functionalized rhodium(I)-NHC complexes containing a Boc-protected 1-(2-aminoethyl) group on a side chain. The melting point has been determined only for the complex **4d** (m.p. = 142 °C) due to the fact that in the case of **4e**, a thermal decomposition occurred before the melting has been observed (at 210 °C) and the complex **4h** is hygroscopic, which made impossible the measurement of the melting temperature.

Complexes **4d-h** have been fully characterized by ESI-MS mass spectrometry, and ^1H and ^{13}C NMR using gCOSY, gHSQC, and gHMBC experiments for full resonance assignments. The most significant chemical shifts and coupling constants in ^1H and ^{13}C NMR spectra of the complexes **4d-h** are presented in Table 8.1-1 and

Table 8.1-2, respectively.

Table 8.1-1 The most significant chemical shifts in ^1H NMR spectra of the rhodium(I)-NHC complexes **4d-h**, acquired at room temperature.

Compounds	CH_2Ph δ (ppm)	CH_{NBD} δ (ppm)	C^7H_2 δ (ppm)	CH_{im} δ (ppm)	
4d (Me)	5.73 (s)	4.84 (s)	1.30 (m)	6.76 (s)	
		3.73 (s)			
		3.36 (br s)			6.65 (s)
4e (Bz)	5.73 (br s)	4.78 (s)	1.20 (br d, $J_{\text{H,H}} = 1.4$ Hz)	6.61 (s)	
		3.60 (s)			
		3.20 (br s)			
4g (Trit.)	6.84 (d, $J_{\text{H,H}} = 15.06$ Hz)	4.61 (s)	0.95 (m)	6.76 (d, $J_{\text{H,H}} = 2.06$ Hz)	
		3.59 (s)		6.56	
		3.44 (s)		(d, $J_{\text{H,H}} = 1.97$ Hz)	
		6.17 (d, $J_{\text{H,H}} = 14.79$ Hz)		2.87 (s)	
		1.94 (s)			
4h (^tBu)	6.41 (d, $J_{\text{H,H}} = 15.09$ Hz)	4.84 (m)	1.36 (d, $J_{\text{H,H}} = 8$ Hz)	7.06 (d, $J_{\text{H,H}} = 1.97$ Hz)	
		4.70 (m)			
		3.81 (br s)		6.72	
		6.27 (d, $J_{\text{H,H}} = 15.09$ Hz)		3.78 (br s)	(d, $J_{\text{H,H}} = 2.03$ Hz)
		3.47 (m)			

The general trend which can be observed for all of the compounds **4d-h** is the increasing complexity of their ^1H NMR spectra (acquired at room temperature) with the increasing bulkiness of the N-substituents. The bigger is the steric hindrance, the higher the activation energy of the rotation about the Rh-carbene bond and the less symmetric is the specie in terms of the magnetic equivalency of the nuclei. As an example, the signals attributed to the imidazole backbone protons appear as two singlets at 6.76 and 6.65 ppm for **4d** and one singlet at 6.61 ppm for the symmetric **3b**, but in case of the more hindered **4g** and **4h** the discussed protons appear as two doublets with the $^3J_{\text{H,H}} = 2$ Hz. A similar behavior was observed at room temperature for the benzylic CH_2 protons; they are found as singlets for the complexes **4d** and **4e**, whereas in cases of **4g** and **3h** the CH_2 decoalesces into AB system, showing two doublets with the $^2J_{\text{H,H}} = 15$ Hz (Figure 8.1-1 and Figure 8.1-2). Moreover, the imidazole backbone protons resonate in a slightly lower field with respect to the corresponding imidazolium salts and the silver complexes.

The olefinic protons of the norbornadiene ligand in cases of **4d** and **4e** complexes feature three resonances (2 protons each), whereas the C^7H_2 (CH_2NBD) appears as a multiplet (**4d**) or a doublet (**4b**) in a low field at 1.30 and 1.20 ppm, respectively; for the compound **4g** and **4h** there are seven signals corresponding to the eight protons of the norbornadiene; for **4g** all of them are singlets except the C^7H_2 , which appear as a multiplet at 0.95 ppm, whereas in the case of the complex **4h** the protons C^7H_2 were exceptionally found as two doublets with the coupling constant $^2J_{\text{H,H}} = 8$ Hz. The spectroscopic data are in accordance with the reported ones³¹. These observations suggest the absence of an effective symmetry plane in the molecules resulting from the hindered rotation about the carbene – rhodium bond.

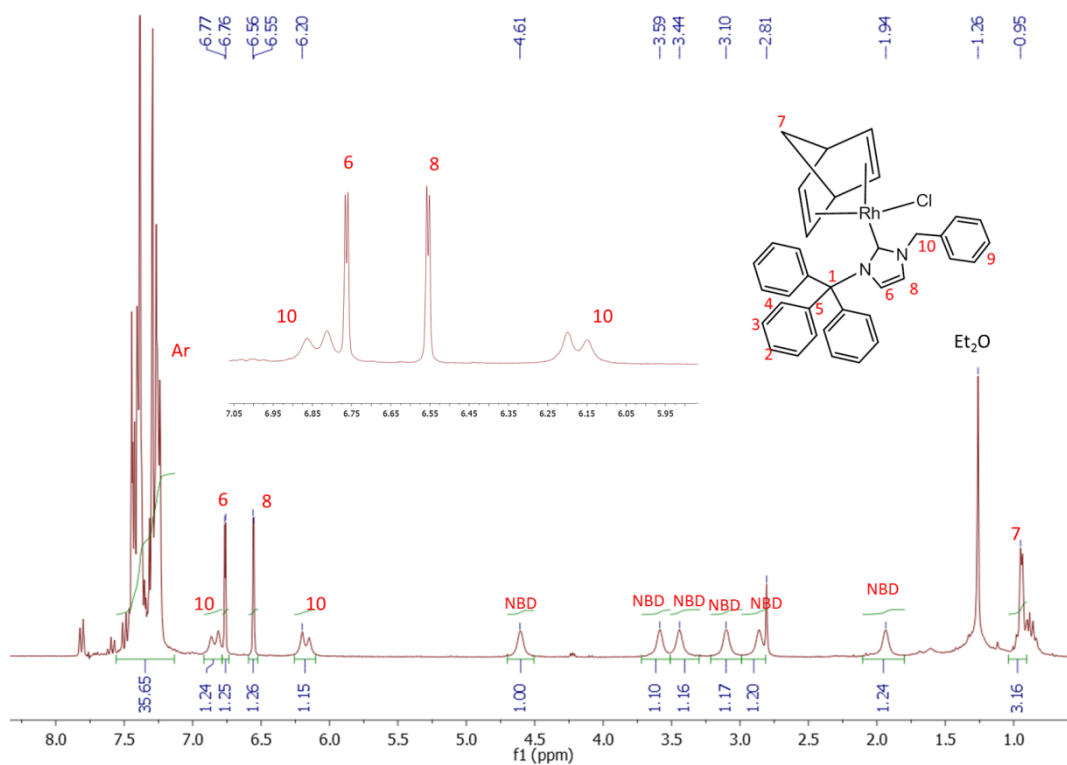


Figure 8.1-1 ^1H NMR spectrum of **4g** with the inset showing the deconvoluted benzylic and imidazole backbone protons.

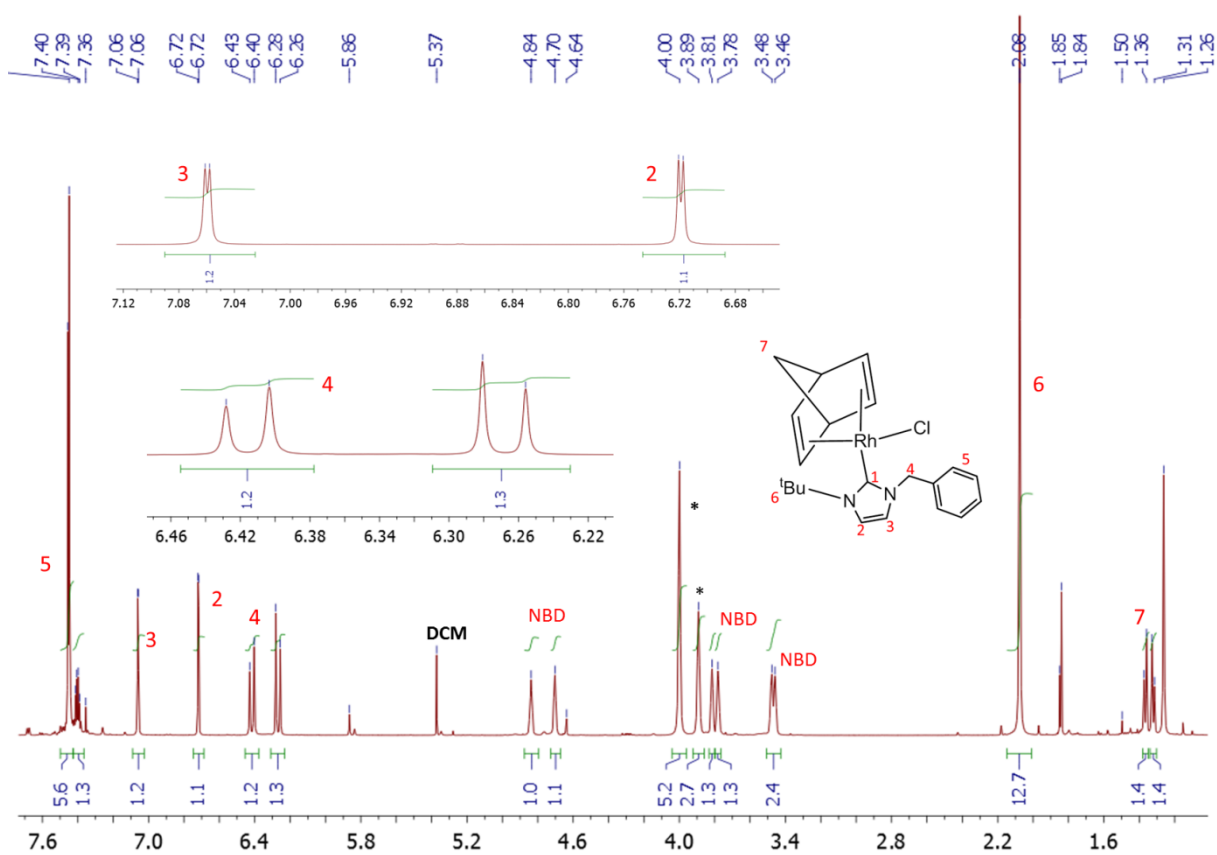
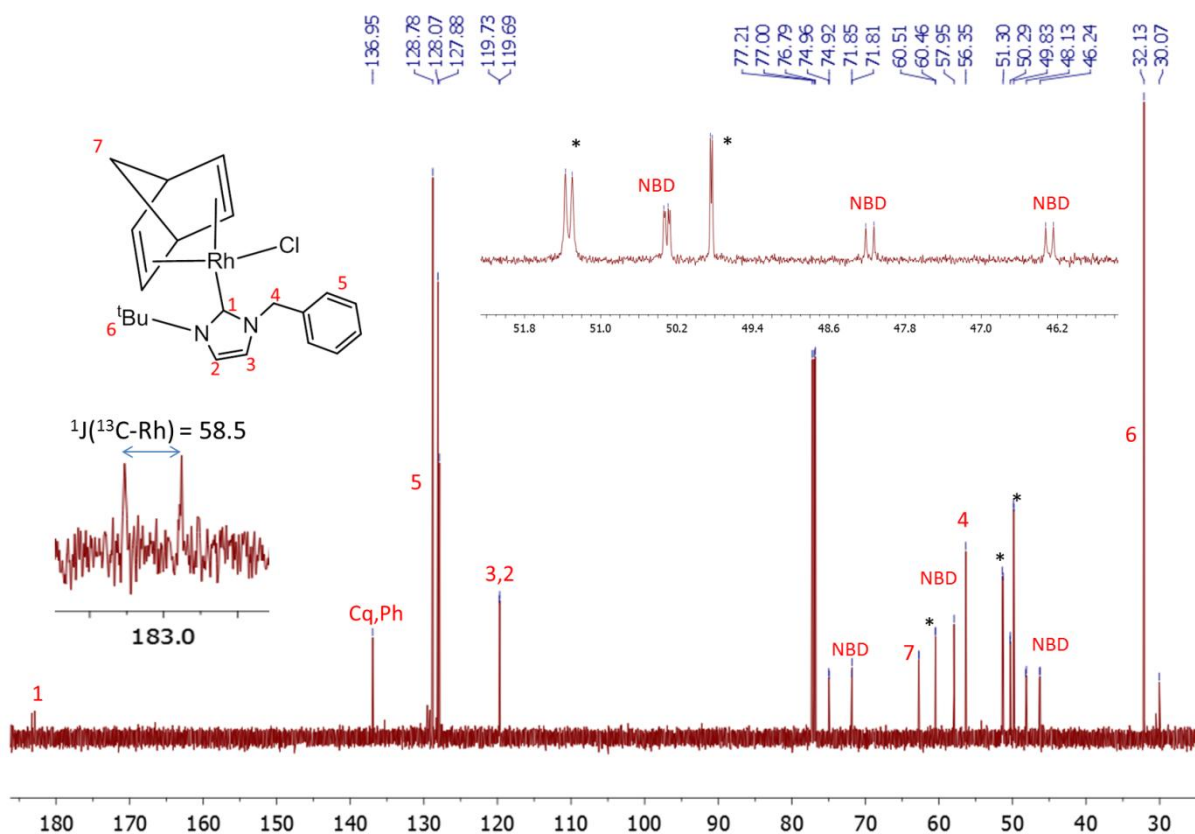


Figure 8.1-2 ^1H NMR spectrum of **4h** with the inset showing the deconvoluted benzylic and imidazole backbone protons.

All of the complexes **4d-h** show a common feature in the ^{13}C NMR spectra, namely, the appearance of the downfield doublet with the one-bond coupling constants: $^1J(^{13}\text{C}-^{103}\text{Rh}) = 57.8$ Hz for **4d**, $^1J(^{13}\text{C}-^{103}\text{Rh}) = 76.8$ Hz for **4e**, $^1J(^{13}\text{C}-^{103}\text{Rh}) = 57.8$ for **4g** and $^1J(^{13}\text{C}-^{103}\text{Rh}) = 58.5$ Hz for **4h** resulting from the coupling of the carbenic carbon nucleus to the rhodium nucleus, occurring naturally as almost entirely one isotope ^{103}Rh with a nuclear spin $I = 1/2$ ¹⁷.

The carbon atoms of the norbornadiene ligand appear as four doublets (including the C^7H_2) in the ^{13}C NMR spectra of **4d** and **4e**, whereas more sophisticated pattern has been found for **4g**: three singlets and three doublets (including the C^7H_2) and for **4h**, where the resonances appear as doublets and one doublet of doublet (including the C^7H_2), resulting from the coupling to the metal center, with coupling constants $J(^{13}\text{C}-^{103}\text{Rh})$ ranging from 2.5 to 13 Hz (Figure 8.1-3-2). The increasing complexity of the splitting patterns in the ^{13}C NMR spectra going from **4d** to **4h** confirms the influence of the steric encumbrance on the rate of the dynamic processes with respect to the NMR time scale.



* residue of starting material $[\text{Rh}(\text{NBD})\text{Cl}]_2$

Figure 8.1-3 ^{13}C NMR spectrum of **4h**.

Table 8.1-2 Most significant chemical shifts in ^{13}C NMR spectra of the rhodium(I)-NHC complexes **4d-h**.

Compounds	NCHN δ (ppm)	CH_{NBD} δ (ppm)	C^7H_2 δ (ppm)
4d	184.8 (d, $J_{\text{C-Rh}} = 57.82$ Hz)	79.0 (d, $J_{\text{H,H}} = 6.0$ Hz) 51.0 (d, $J_{\text{H,H}} = 2.5$ Hz) 48.3 (d, $J_{\text{H,H}} = 12.77$ Hz)	63.4 (d, $J_{\text{H,H}} = 5.22$ Hz)
	185.4 (d, $J_{\text{C-Rh}} = 76.80$ Hz)	79.1 (d, $J_{\text{H,H}} = 5.70$ Hz) 51.0 (d, $J_{\text{H,H}} = 5.70$ Hz) 48.5 (d, $J_{\text{H,H}} = 17.00$ Hz)	63.3 (d, $J_{\text{H,H}} = 5.30$ Hz)
4g	186.5 (d, $J_{\text{C-Rh}} = 55.00$ Hz)	73.1 (s) 49.7 (s) 49.0 (s) 45.7 (d, $J_{\text{H,H}} = 13.00$ Hz) 44.7 (d, $J_{\text{H,H}} = 10.80$ Hz)	61.8 (d, $J_{\text{H,H}} = 5.80$ Hz)
	183.0 (d, $J_{\text{C-Rh}} = 58.5$ Hz)	74.9 (d, $J_{\text{H,H}} = 6.1$ Hz) 71.8 (d, $J_{\text{H,H}} = 6.3$ Hz) 57.9 (s) 50.3 (dd, $J_{\text{H,H}} = 2.5$ Hz, $J_{\text{H,H}} = 7.0$ Hz) 48.1	62.7 (d, $J_{\text{H,H}} = 5.2$ Hz)

		(d, $J_{H,H} = 13.0$ Hz) 46.2 (d, $J_{H,H} = 12.2$ Hz)	
--	--	--	--

8.3 Stereodynamics

The stereodynamics and the rotation barriers about the Rh-carbene bond have been determined by means of variable-temperature NMR spectroscopy; the rotation barrier was modulated by increasing the steric hindrance of the N-alkyl substituent (Figure 8.3-1).

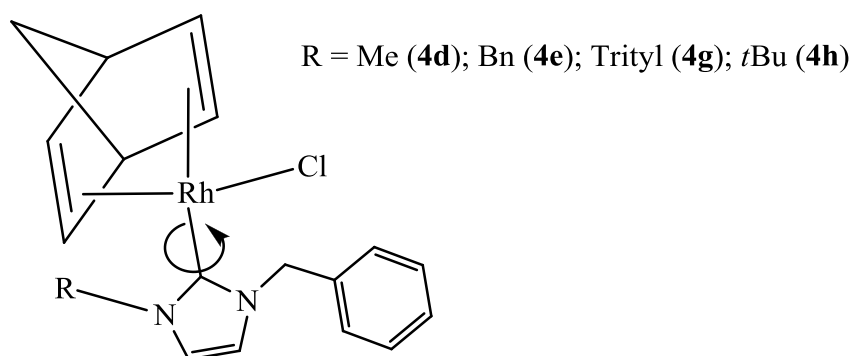


Figure 8.3-1 The hindered rotation about the Rh-carbene bond.

As it was briefly mentioned before, the direct consequence of the hindered rotation about the Rh – carbene bond is the lack of the symmetry plane in these complexes; in fact, the norbornadiene moiety and the chlorine atom are displaced in an out-of-plane disposition with respect to the imidazole ring. If the two side arms are different, the molecule has C_1 symmetry; therefore a pair of conformational enantiomers is generated, as presented in Figure 8.3-2 .

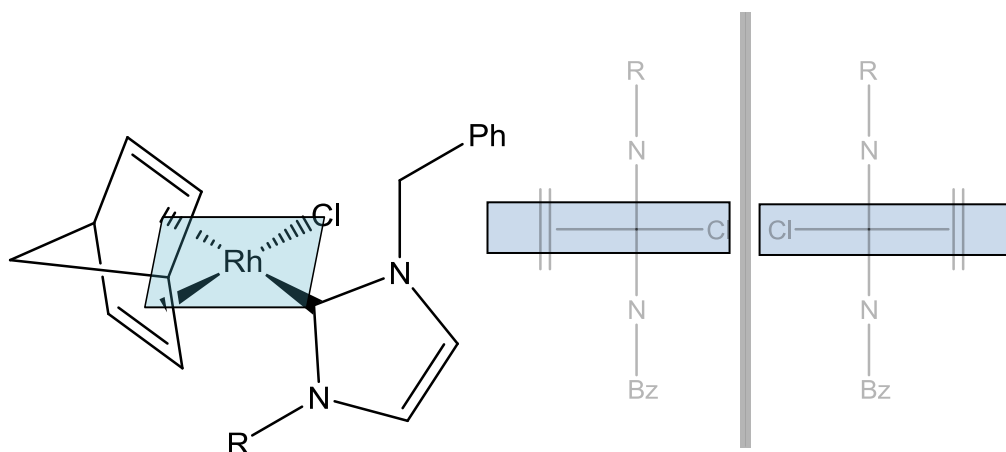


Figure 8.3-2 Coordination plane of the rhodium(I) in the complexes **4d-h** and the two enantiomers generated by the axis of chirality along the Rh-carbene bond.

The ^1H NMR spectra of the complex **4d** recorded at a series of temperatures ranging from -30 to 25 $^\circ\text{C}$ in 1,1,2,2-tetrachloroethane- d_2 (boiling point 146.5°C) are shown in Figure 8.3-3. The singlet at 5.73 ppm observed at room temperature, deriving from the benzylic geminal protons broadens on decreasing the temperature and reaches the typical shape of the coalescence at 10 $^\circ\text{C}$. On further lowering the temperature, the resonance decoalesces into AB system, showing sharp lines at -30°C (5.60 and 5.85 ppm, see Figure 8.3-3). A similar behavior is also observed for the signals attributed to the protons of the norbornadiene ligand; the signals broaden on lowering the temperature until coalescence at ~ 10 $^\circ\text{C}$, and then sharpen again in the range of the temperature between 10 and -30 $^\circ\text{C}$.

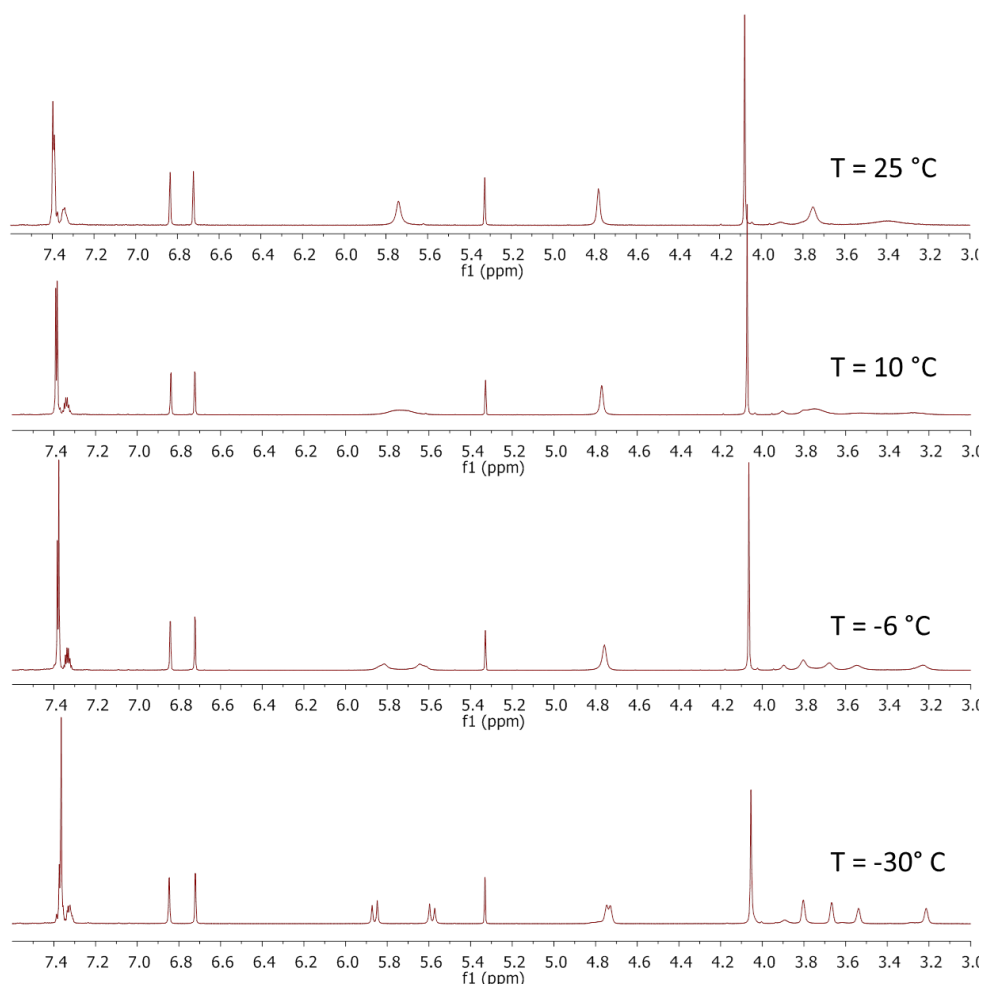


Figure 8.3-3 ^1H NMR spectra of **4d** at various temperatures (600 MHz, $\text{C}_2\text{D}_2\text{Cl}_4$).

The VT NMR experiment in case of complex **4e** bearing the two benzyl groups on the N-side arms of the imidazole, which cause a bigger steric hindrance with respect to the previously

discussed **4d**, shows that the anisochronous benzylic protons appear as a broad doublet at room temperature, whereas the coalescence is reached at 32 °C. Subsequently, on further raising the temperature, the resonance sharpens and at 75°C appears as a very sharp, intense singlet. On the other hand, at -10 °C, the splitting pattern characteristic for an AB system has been observed, although the two doublets were not well resolved. In this case, the coalescence of the olefinic norbornadiene protons has not been reached in the range of temperature investigated (Figure 8.3-4).

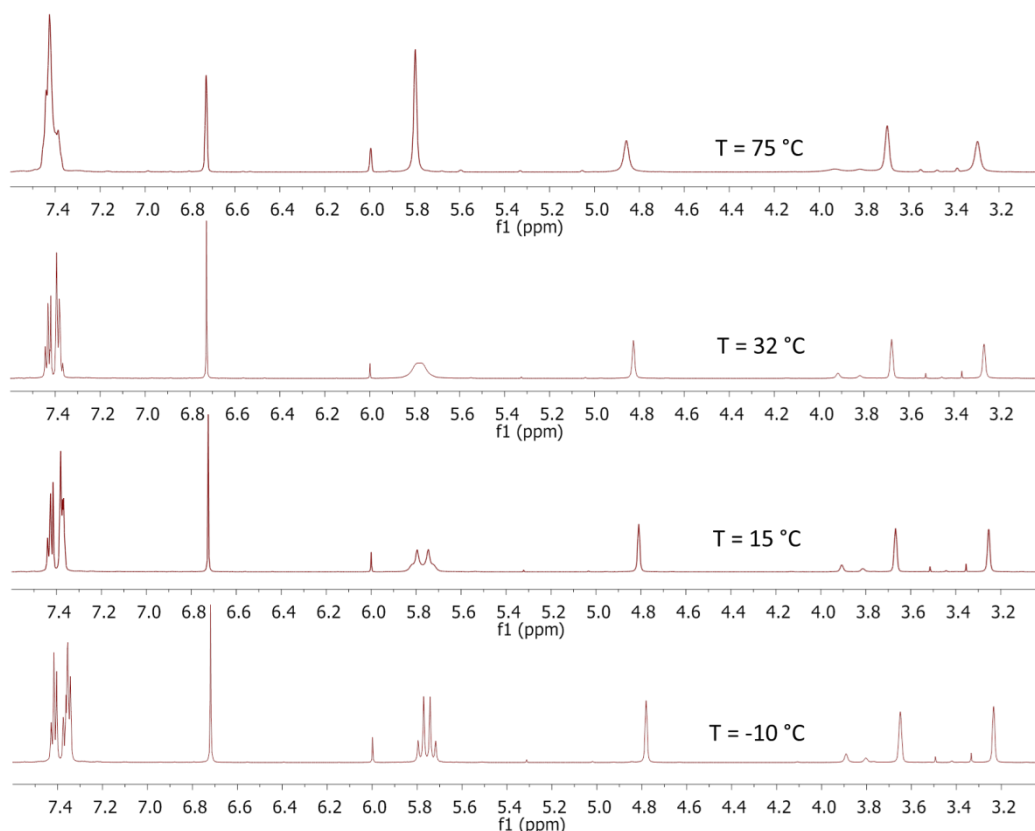


Figure 8.3-4 ^1H NMR spectra of **4d** at various temperatures (600 MHz, $\text{C}_2\text{D}_2\text{Cl}_4$).

For the complex **4g**, bearing the trityl group, two VT experiments were performed, in CDCl_3 (boiling point 61-62 °C) and in 1,1,2,2-Tetrachloroethane- d_2 , respectively. In the first experiment, due to low boiling point of the CDCl_3 , spectra at temperatures higher than 50 °C could not be acquired and coalescence was not observed. In the second experiment, the obtained spectra indicated some decomposition processes of the investigated complex. A likely explanation of this behavior can be a presence of traces of acid in chlorinated solvents, which, as reported, often lead to the partial regeneration of NHC complexes¹⁸.

The VT NMR analysis was also carried out for the complex **4h** in toluene- d_8 (boiling point 110 °C), but due to the high activation energy of the hindered rotation about the Rh-carbene bond, the coalescence of the benzylic protons was not reached.

Thus, in order to determine the stereodynamics of these two complexes **4g,h** and to calculate the energy barrier, an exchange spectroscopy (EXSY) experiment has been employed. However, the required information was obtained only for the complex **4g**; in case of the **4h**, the means of the dynamic NMR (both VT and EXSY) appeared to be not suitable for the experimental determination of the thermodynamic data, which is in accordance with limitations of this technique reported in the literature,¹⁹ namely, that only energy barriers over the range 4.5 – 23 kcal mol⁻¹ (18.8 – 96.2 kJ mol⁻¹) can be determined. In **4h** the rotational energy barrier is stopped at room temperature, it can be used, after enantiomeric separation in a chiral column chromatography, as a precursor in asymmetric catalysis.

8.4 Kinetics

The benzylic signals in the spectra of the complexes **4d** and **4e** show coalescence at 10 and 32 °C, respectively. At this temperatures, the kinetic constants for the enantiomerization were accurately determined by calculations from the below equation:

$$k = \frac{\pi|\nu_A - \nu_B|}{\sqrt{2}} \quad \text{Eq. 8.1}$$

where ν_A and ν_B are the resonant frequencies (expressed in Hz) of nuclei A and B in the absence of the exchange. The kinetic constants for the temperatures above and below the coalescence temperature were derived by the means of the lineshape simulation performed over the entire range of temperatures (Figure 8.4-1).

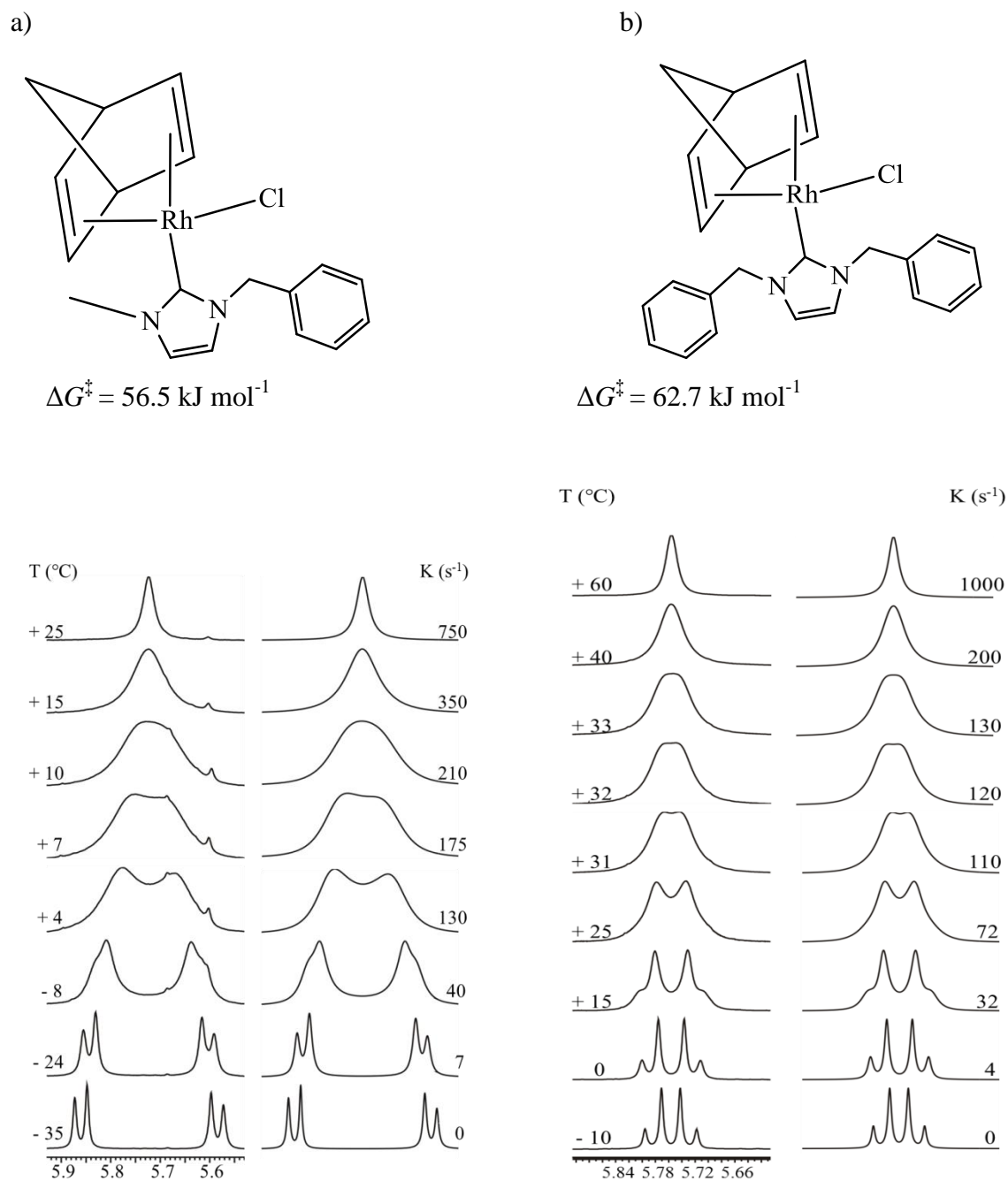


Figure 8.4-1 Variable-temperature spectra of **4d** (a) and **4e** (b) showing the evolution of the benzylic CH₂ signals (¹H NMR at 600 MHz, C₂D₂Cl₄). On the right side of each plot the simulations with the corresponding rate constants are reported.

Subsequently, an activation energies of 56.5 and 62.7 kJ mol⁻¹ for **4d** and **4e** respectively, were derived from the Eyring equation. The activation energy was found to be constant with respect to the temperature, indicating a negligible value of the activation entropy. This observation indicates that the observed barrier should be due to steric effects only and it is consistent with the increase of the activation energy between less steric hindered **4d** and the more steric hindered **4e**

($\Delta\Delta G^\ddagger = 6.2 \text{ kJ mol}^{-1}$). These data agree very well with those reported by Enders and Gielen,⁵ who proposed a steric origin of the rotational barrier.

The 1D EXSY experiment carried out at four different temperatures: -10, -15, -20 and -25 °C on the complex **4g**, allowed for a determination of kinetic constants for the rotation around the carbon-metal bond. The linear functions of $\ln([A]_{eq} - [A]_t)$ vs. the used array of mixing times: 0.025, 0.05, 0.075 and 0.1 s were plotted for each temperature (Figure 8.4-2a), affording the kinetic constants, which, as expected, increase with the increment of the temperature. For each temperature, the activation energy was derived by the use of the Eyring equation.

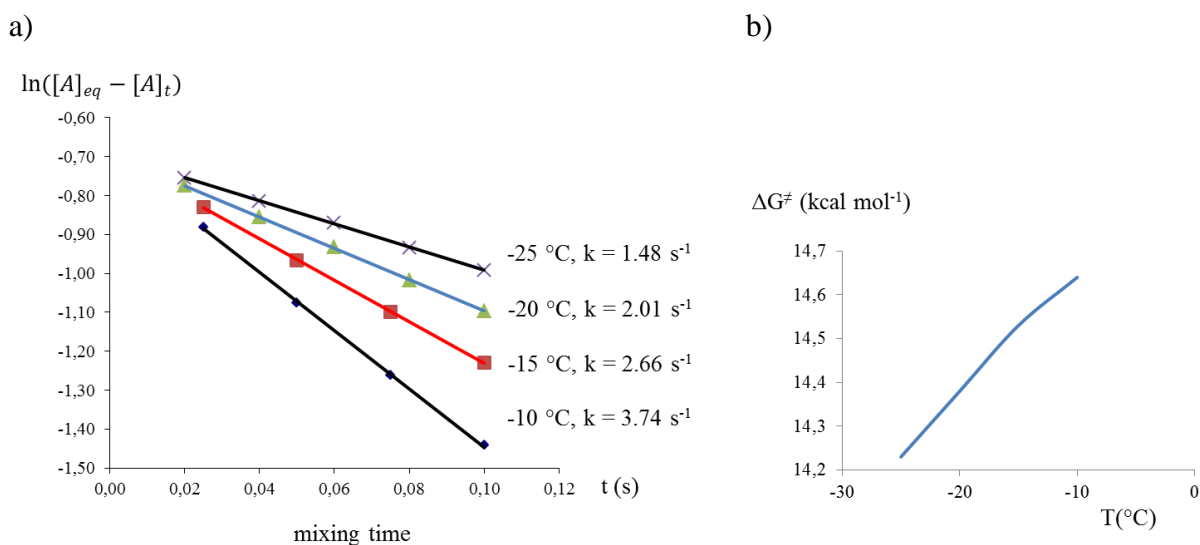
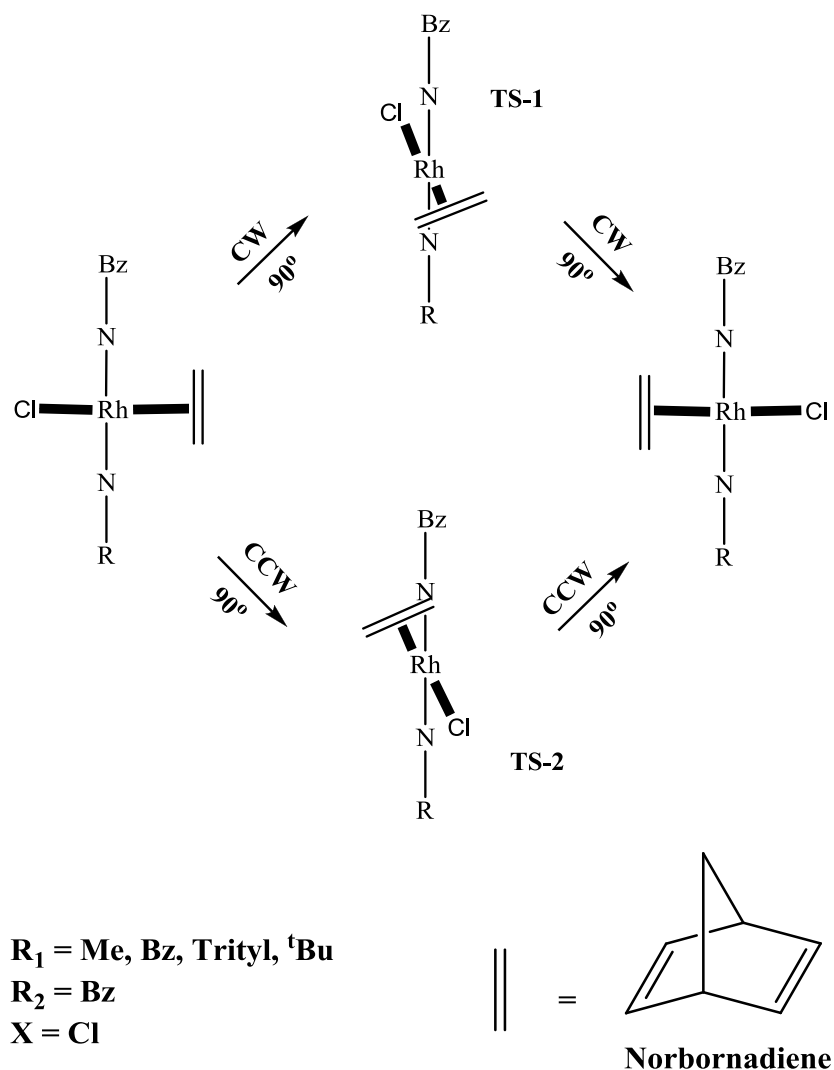


Figure 8.4-2 The plots of $\ln([A]_{eq} - [A]_t)$ vs. mixing time at different temperatures (a) and the dependence of the activation energy on the temperature (b).

The EXSY experiment showed that the rotational barrier (61.9 kJ mol^{-1}) was identical, within the experimental error, to that obtained in the case of the dibenzyl-substituted compound **4e**; however the plot of the ΔG^\ddagger against the temperature (Figure 8.4-2b) shows a variation of the former, indicating a negative entropic activation.

As shown in Scheme 8.4-1, the two enantiomeric ground states GS and GS' can interconvert into each other by two possible transition states due to the rotation around the carbene-rhodium bond.



Scheme 8.4-1 Enantiomerization pathway for compounds **4d-h**.

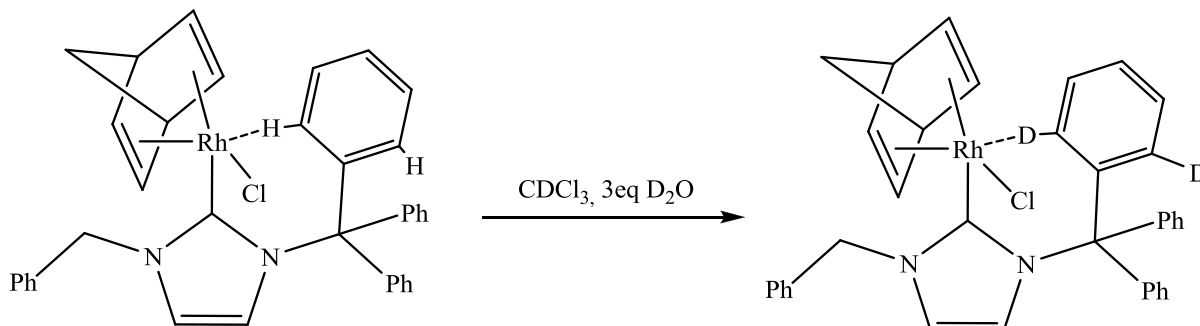
The first one (TS-1) is reached by a 90° clockwise rotation starting from GS and corresponds to the crossing of the chloride atom on the benzylic CH₂ of one of the side arms of the imidazole (denoted as R₂), whereas the second transition state (TS-2) takes place when a counterclockwise rotation forces the chloride atom to cross the second alkyl side arm group (R₁) on the imidazole. The steric hindrance of the R₁ obviously influence the activation energy of the rotational barrier. DFT calculations of the two possible transition states (Table 8.4-1) suggested that the threshold pathway (i.e., that with the lowest transition-state energy) corresponded in all the cases to the passage of the halogen atom on the benzyl group (TS-1), with the simultaneous crossing of the norbornadiene on the second side arm (R₁). The calculations also suggested that the energy barrier is strongly related to the steric hindrance of R₁, and for this reason the barrier calculated for compound **4c** is predicted to be very high (100.0 kJ mol⁻¹).

Table 8.4-1 Calculated and experimental energy barriers for the enantiomerization of **4d-h** (energies in kJ mol^{-1} , calculations at the B3LYP/LANL2DZ level).

Compound	TS-1	TS-2	Experimental (kJ mol^{-1})
4d	55.0	58.5	56.5
4e	65.3	78.7	62.7
4g	101.7	115.9	61.9
4h	96.7	119.7	not calculable

As can be seen from Table 8.4-1, the rotation barriers calculated for **4d** and **4e** were consistent with the experimental values, whereas it was not true in the case of **4c**, where the experimental value was equal to that obtained for compound **4e** and much smaller with respect to the calculated one; moreover, as it was already mentioned, the energy barrier derived for **4g** from the data obtained from the EXSY experiment, showed a strong dependence on the temperature, whereas for the two other complexes, the quantity did not vary with the temperature. In particular, the big negative activation entropy derived from simulations (-27 ± 10 eu) indicates that a strongly organized transition state or a different interconversion pathway could take place in the case of compound **4g**. It is very important to highlight that all the discussed here data related to stereodynamics and kinetics of the complexes **4d-h** are in keeping with data reported in the previous chapter; this agreement indicates that the influence of the functionalization on the dynamic behavior of the investigated systems is negligible. Hence, as it has been reported in the previous case, the possible explanations for this behavior are: the inversion process may proceed either via a cleavage of the Rh-Cl bond before or during the rotation or by partial dissociation of the trityl group into a contact ionic pair, followed by the rotation of the Rh-Cl moiety and subsequent re-formation of nitrogen-trityl carbon bond; another hypothesis arises from a studies performed by Peris²⁰ and Nolan²¹ and very recently also by Royo²² on aromatic and aliphatic intramolecular C-H activation in transition metal complexes bearing NHC ligands, mentioned in Section 1.6 of the introduction. As a consequence of this reactivity, cyclometalated species are formed. In our case, the coordination of one of the carbon atoms of the trityl ligand to the metal center did not occur, which was confirmed

by NMR analysis. Nevertheless, it is worth to consider the possible interactions between hydrogen atoms in ortho positions of the aromatic rings in trityl ligand with the rhodium center. In order to investigate these interactions, the following reaction was tried: (Scheme 8.4-2);



Scheme 8.4-2 Possible reaction between the rhodium(I)-NHC complex and D₂O.

The hypothesized interactions would weaken the C-H bonds in all the three aromatic rings, enabling the exchange between the proton and deuterium nuclei, but unfortunately this reaction didn't give the expected result, only decomposition products.

Others texts were made with AgPF₆ and AgBF₄ in a solution of deuterated chloroform of **4g** to understand if it could be possible to see a potential agostic interaction between the activated cationic Rhodium specie with one of the proton of the aromatic rings, also in these cases decomposition products were observed.

8.5 Crystal Structure Determination for **4d** and **4e**.

The molecular structures of the rhodium(I) complexes **4d** and **4e** were determined via X-ray diffraction and are reported in Figure 8.5-1-1 and Figure 8.5-2. Crystals of **4d,e** suitable for diffraction were grown from a double layer of dichloromethane and petroleum ether (1:4).

The structure of **4d**, which crystallized in a centric space group (P21/c) of the monoclinic crystal system ($Z = 4$), consists of separated C₂₀H₂₇ClN₂Rh molecules arranged in eclipsed, alternating columns of enantiomers in a 1:1 ratio. The two possible orientations of the benzyl and the CH₃ substituents on the imidazolium ring result from the axial chirality present in the molecule of **4d**. Rhodium shows a classic square-planar coordination and is bonded to the Cl(2) atom, the carbenic C(1) and the bidentate norbornadiene fragment. There is a stronger trans effect observed for the carbene moiety when compared to the chlorine ligand, relying on the difference in bond lengths between the Rh atom and the carbon atoms of the norbornadiene moiety situated in the trans orientation with respect to the chlorine and the carbene, respectively; the Rh-C(16) and Rh-C(20)

contacts trans to the chlorine are 2.083(4) and 2.098(4) Å, respectively, and the Rh-C(14) and Rh-C(15) bond lengths trans to Cl atom are remarkably longer: 2.194(4) and 2.213(4) Å, respectively. It is worth to note that despite the presence of donor chlorides anions, there are not significant intra- or intermolecular hydrogen bonds in the solid state.

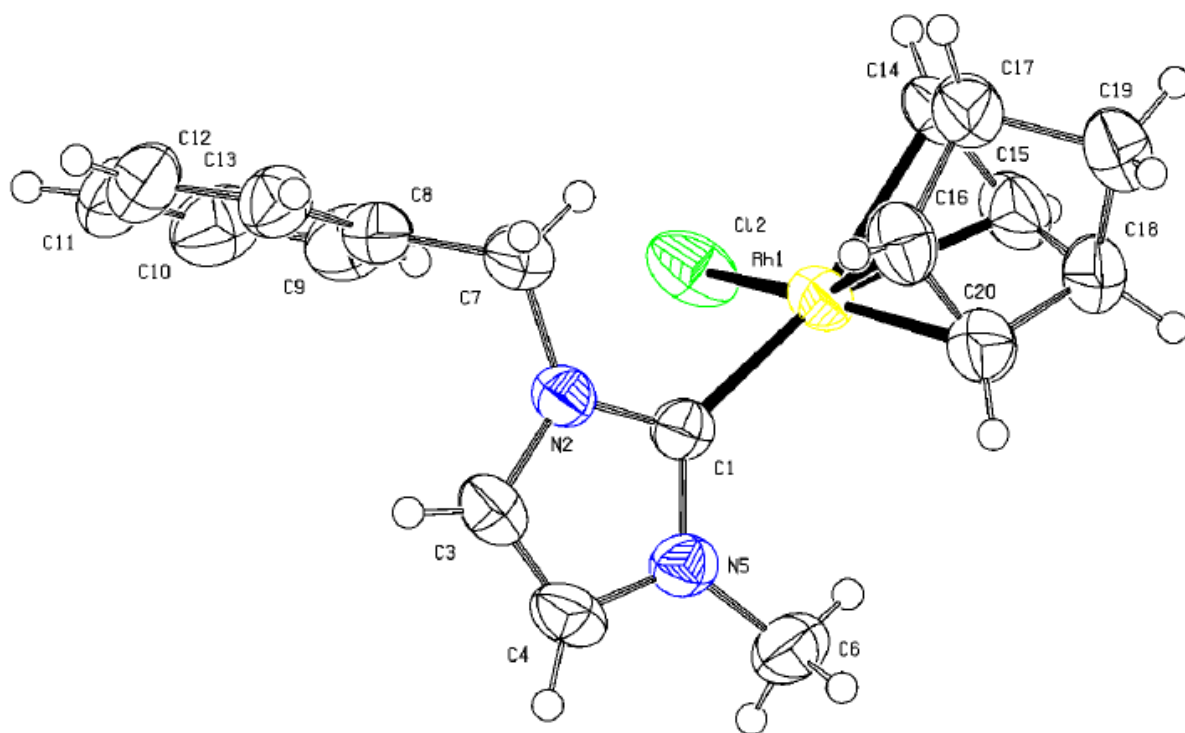


Figure 8.5-1 ORTEP diagram of **4d** depicted with thermal ellipsoids at 50% probability. Selected bond distances (Å) and bond angles (deg): Rh(1)-C(1), 2.019(4); Rh(1)-C(16), 2.083(4); Rh(1)-C(20), 2.098(4); Rh(1)-C(14), 2.194(4); Rh(1)-C(15), 2.213(4); C(1)-N(2), 1.353(4); C(1)-N(5), 1.354(4); N(2)-C(1)-N(5), 104.0(3); C(1)-Rh(1)-Cl(2), 90.57(10); C(1)-Rh(1)-C(16), 97.00(15); C(1)-Rh(1)-C(20), 99.27(15); C(1)-Rh(1)-C(14), 156.71(16); C(1)-Rh(1)-C(15), 161.52(16), C(1)-Rh(1)-C(1)-N(2), 101.0(3).

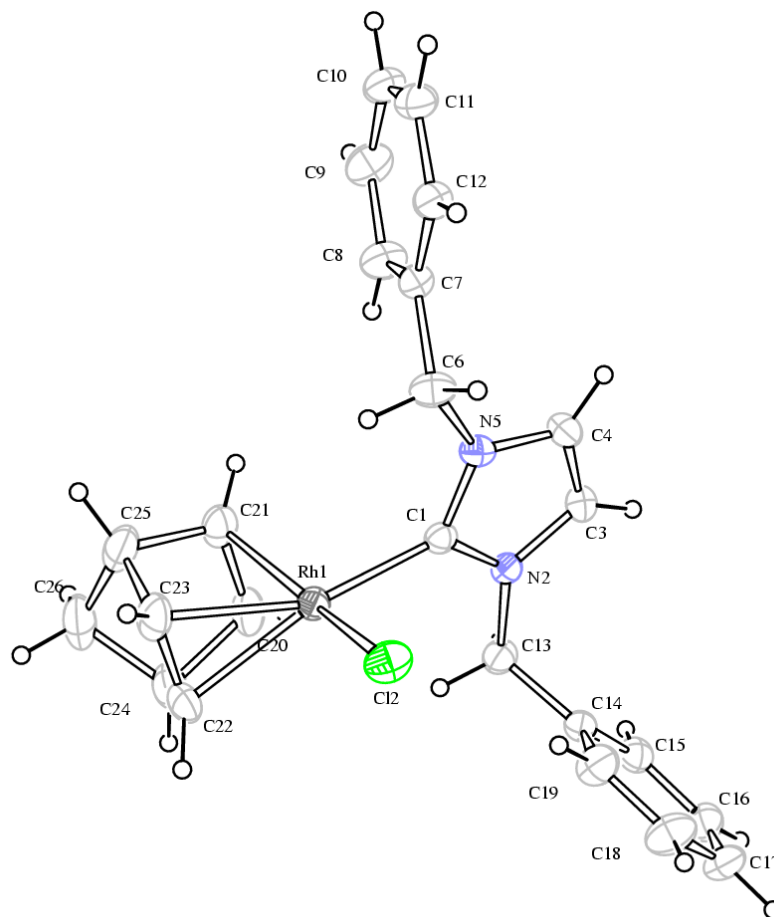


Figure 8.5-2 ORTEP diagram of **4e** depicted with thermal ellipsoids at 50% probability. Selected bond distances (Å) and bond angles (deg): Rh(1)-C(1), 2.023(2); Rh(1)-Cl(2), 2.3618(6); Rh(1)-C(20), 2.084(2); Rh(1)-C(21), 2.091(2); Rh(1)-C(22), 2.185(2); Rh(1)-C(23), 2.195(2); C(1)-N(5), 1.353(3); C(1)-N(2), 1.360(3); N(5)-C(1)-N(2), 104.19(17); C(1)-Rh(1)-Cl(2), 90.83(6); C(1)-Rh(1)-C(20), 99.49(9); C(1)-Rh(1)-C(21), 98.63(9); C(1)-Rh(1)-C(22), 161.04(10); C(1)-Rh(1)-C(23), 158.45(9), C(1)-Rh(1)-C(1)-N(2), 102.59(18).

The complex **4d** crystallizes in the centrosymmetric P21/n group of the monoclinic crystal system ($Z = 4$) and both enantiomers are generated by the center of symmetry, as in the previous case. Similarly, there is also the trans effect observable in the structure of **4e**, with the Rh- $C_{\text{norbornadiene}}$ distances shorter when in orientation trans with respect to the carbene moiety than those being trans with respect to the chloride ligand; namely the Rh-C(20) and Rh-C(21) contacts are 2.084(2) and 2.091(2), respectively, whereas Rh-C(22) and Rh-C(23) distances are longer: 2.185(2) and 2.195(2), respectively.

Generally, the crystallographic data are very similar for these two complexes **4d** and **4e** as regards the bond and angle distances and the crystal package. The relevant data are compared in Table 8.5-1.

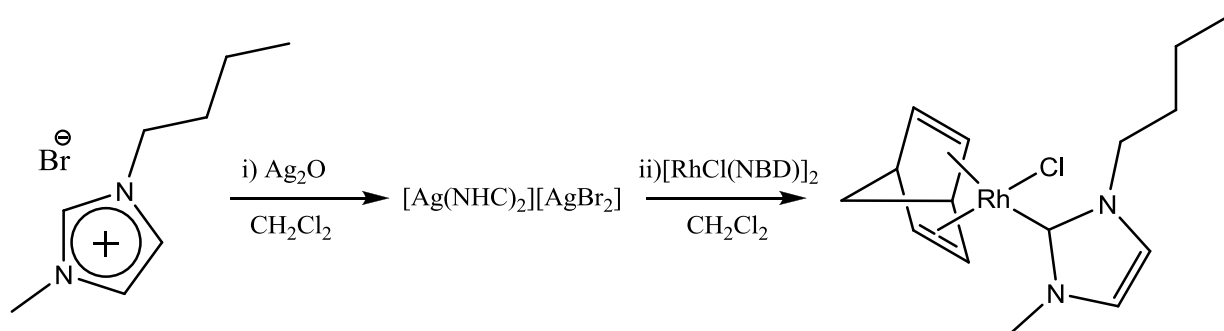
Table 8.5-1 Crystal data for **4d** and **4e**.

	4d	4e
Rh-C bond length (Å)	2.019(3)	2.023 (2)
Rh-X bond length (Å)	2.3800(11)	2.3618 (6)
C(1)-Rh(1)-C(1)-N(2)	101.0(3)	102.59 (18)

It is worth to mention that both the Rh-C_{carbene} bond distance and the dihedral angle C(1)-Rh(1)-C(1)-N(2) that yields the two enantiomers, whose barrier was observed in solution, are slightly bigger in the case of the more encumbered **4e** complex with comparison to **4d**.

8.5.1 RhCl(NBD)(1-*n*Butyl,3-Methyl-Imidazolin-2-ylidene)

Another rhodium(NHC) complex **4i** (1-*n*Butyl,3-Methyl-Imidazolin-2-ylidene) has been finally prepared in order to better understand the role of NHBoc functionalization (complexes **4a-c** paragraph 7.2.1) on the catalytic activity of complexes **4a-h** (chapter 7 and 8) in the hydrosilylation of terminal alkynes fully described in chapter 9. **4i** has been isolated by reacting the commercial imidazolium salts (1-*n*butyl, 3-methyl-imidazolium bromide) with Ag₂O in CH₂Cl₂, the silver [Ag(NHC)₂]⁺ complex obtained as transmetalating agent toward the synthesis of **4i** (Figure 8.5-3).

**Figure 8.5-3** RhCl(NBD)(1-*n*Butyl,3-Methyl-Imidazolin-2-ylidene)

The complex has been purified by column chromatography on silica gel eluting with Et₂O:CH₂Cl₂ 1:3 and isolated as a yellow solid identified as **4i** (Y = 82%) by means of ¹H NMR and ¹³C NMR spectroscopy which leads to patterns of chemical shift in line with a similar compound reported in the literature bearing a COD ancillary ligand instead of NBD.²³

8.6 Conclusion

We have described the synthesis of novel rhodium(I) complexes [RhX(NBD)(NHC)] (NHC = 1-Benzyl-3-R-imidazolin-2-ylidene; X = Cl, R = Me (**4d**), R = Benzyl (**4e**), R = Trityl (**4g**); X = I, R = *t*Butyl (**4h**)) in which the NHC ligands bear a benzyl group on one nitrogen and increasing bulky N-alkyl substituents (Me, Benzyl, Trityl, *t*Butyl) on the other. Complexes **4d-g** display restricted rotation about the metal-carbene bond however whilst the rotation barriers calculated for the complexes in which R = Me, Benzyl (**4d,e**) matched the experimental values, this was not true in the trityl case **4g**, where the experimental value was equal to that obtained for compound **4e**, and much smaller with respect to the calculated one. In addition, the energy barrier derived for **4g** from lineshape simulation showed a strong dependence from the temperature, whilst the barriers measured for **4d,e** did not show this effect. In particular, the large negative activation entropy derived from simulations (-40 ± 10 e.u.) indicates that a strongly organized transition state and a different interconversion pathway takes place in the case of compound **4g**. We believe that these observations may bring important implications in further research in NHC-M formation and studies in this direction are in progress.

In **4h** the rotational energy barrier is stopped at room temperature, hence it could be employed, after enantiomeric separation in a chiral column chromatography, as a precursor in asymmetric catalysis: preliminary results which need of further studies indicated that the separation should be possible by means of chiral HPLC.

8.7 EXPERIMENTAL SECTION

Materials and Procedures. All reactions were carried out under argon using standard Schlenk techniques. Solvents were dried and distilled under nitrogen prior to use; the deuterated solvents, used after being appropriately dried and degassed, were stored in ampules under argon on 4Å molecular sieves. The prepared derivatives were characterized by elemental analysis and spectroscopic methods. The IR spectra were recorded with a FT-IR Perkin-Elmer Spectrum 2000 spectrometer. The NMR spectra were recorded using Varian Inova 300 (^1H , 300.1; ^{13}C , 75.5 MHz), Varian MercuryPlus VX 400 (^1H , 399.9; ^{13}C , 100.6 MHz), Varian Inova 600 (^1H , 599.7; ^{13}C , 150.8 MHz) instruments. The spectra were referenced internally to residual solvent resonances, and unless otherwise stated, they were recorded at 298 K for characterization purposes; full ^1H and ^{13}C NMR assignments were done, when necessary, by gCOSY, gHSQC, gHMBC, NOESY and DEPT-135 NMR experiments using standard Varian pulse sequences; J.Young valve NMR tubes (Wilmad) were used to carry out NMR experiments under inert conditions. ESI-MS analyses were performed

by direct injection of methanol solutions of the metal complexes using a Waters ZQ 4000 mass spectrometer. Elemental analyses were performed on a Thermo-Quest Flash 1112 Series EA instrument. The chemical Ag₂O was used as purchased from Aldrich; [Rh(NBD)Cl]₂ was purchased from Strem and used as received; petroleum ether (Etp) refers to a fraction of bp 60-80 °C. The reactions were monitored by thin-layer chromatography (TLC) on highly purified silica gel on polyester (w/UV indicator) and visualized using UV light (254 nm). Column chromatography was carried out under argon on silica gel previously heated at about 200 °C while a slow stream of a dry nitrogen was passed through it; Celite was dried in an oven at 150 °C. Melting points were taken with a Stuart Scientific SMP3 melting point apparatus and were uncorrected. Sonication was performed on Elma S10H device with ultrasound frequency: 37 kHz and effective power (30W). Crystal data were collected at room temperature on a Bruker APEX II diffractometer equipped with a CCD detector operating at 50 kV and 30 mA, using graphite monochromated MoK_α radiation ($\lambda = 0.71073 \text{ \AA}$). An empirical absorption correction was applied on both structures by using SADABS.¹⁰ They were solved by direct methods and refined by full-matrix least-squares based on all data using F^2 with SHELXL97.¹¹ All non-hydrogen atoms were refined anisotropically, with the exception of the hydrogen atoms which were set geometrically and given fixed isotropic thermal parameters.

8.7.1 Synthesis of [RhCl(NBD){1-benzyl-3-methyl-imidazolin-2-ylidene}] (4d).

The silver complex **3d** was prepared according to the procedure described in the paragraph 4.2.1 and instantaneously used for a preparation of the rhodium(I) complex. The suspension of **3d** was filtered on Celite, and the filtrate was added to a solution of [Rh(NBD)Cl]₂ (0.12 g, 0.53 mmol) in CH₂Cl₂. After stirring for 3 h at room temperature, the pale yellow solid of AgBr was filtered off, and the solvent was removed under vacuum. The crude material was purified by column chromatography on silica gel using first CH₂Cl₂ and then CH₂Cl₂/MeOH [100:3 (v/v)] as eluent to afford 0.281 g (72 %) of **4d** as a yellow solid. Rf: 0.33 (CH₂Cl₂/MeOH, 100:3). ¹H NMR (300 MHz, CDCl₃): δ 7.35 (m, 5H, Ph), 6.76 (s, 1H, CH_{im}), 6.65 (s, 1H, CH_{im}), 5.72 (s, 2H, CH₂Ph), 4.84 (s, 2H, CH_{NBD}), 4.08 (s, 3H, CH₃), 3.72 (s, 2H, CH_{NBD}), 3.36 (br s, 2H, CH_{NBD}), 1.30 (m, 2H, C⁷H₂). ¹³C NMR (100 MHz, CDCl₃): δ 184.8 (d, J_{C-Rh} = 57.82 Hz), 136.92 (C_q, Ph), 128.80 (Ph), 128.27 (Ph), 128.09 (Ph), 122.24 (CH_{im}), 120.72 (CH_{im}), 79.00 (d, J = 6,04 Hz, CH_{NBD}), 63.4 (d, J = 5.22 Hz, CH_{NBD}), 54.33 (CH₂Ph), 51.02 (d, J = 2.49 Hz, CH_{NBD}), 48.3 (d, J = 12.77 Hz, CH_{NBD}), 37.77 (CH₃). Anal. Calc.d for C₁₈H₂₀ClN₂Rh: C, 53.68; H, 5.01; Cl, 8.80; N, 6.96; Rh, 25.55. Found: C, 53.25; H, 5.30; Cl, 8.62; N, 6.73; Rh, 25.38. ESI-MS (MeOH, m/z): 367 (28) [C₁₈H₂₀N₂Rh]⁺; 539 (100) [C₂₉H₃₂N₄Rh]⁺; In the ESI-MS(-) spectrum, no peaks were observed.

8.7.2 Synthesis of [RhCl(NBD){1,3-dibenzyl-imidazolin-2-ylidene}] (4e)

Silver complex **3e** was prepared according to the procedure described in the paragraph 4.2.1 and instantaneously used for a preparation of the rhodium(I) complex. The suspension of **3e** was filtered on Celite, and the filtrate was added to a solution of [RhCl(NBD)]₂ (0.14 g, 0.30 mmol) in CH₂Cl₂. After stirring for 3 h the pale yellow precipitate of AgBr was filtered off, and the solvent was removed under vacuum. The crude material was purified by column chromatography on silica gel using first CH₂Cl₂ and then CH₂Cl₂/MeOH [100:3 (v/v)] as eluent to afford 0.25 g (86%) of **4e** as a yellow solid. Rf: 0.45 (CH₂Cl₂/MeOH, 100:3). ¹H NMR (300 MHz, CDCl₃): δ 7.31 (m, 10H, Ph), 6.61 (s, 2H, CH_{im}), 5.73 (br s, 4H, CH₂Ph), 4.78 (s, 2H, CH_{NBD}), 3.60 (s, 2H, CH_{NBD}), 3.20 (d, 2H, J_{H,H} = 1.9 Hz, CH_{NBD}), 1.20 (br d, 2H, J_{H,H} = 1.4 Hz, C⁷H₂). ¹³C NMR (100 MHz, CDCl₃): δ 185.45 (d, J_{C-Rh} = 76.8 Hz), 136.87 (C_q, Ph), 128.86 (Ph), 128.61 (Ph), 128.03 (Ph), 121.08 (CH_{im}), 120.72 (CH_{im}), 79.11 (d, J = 5.7 Hz, CH_{NBD}), 63.30 (d, J = 5.3 Hz, C⁷H₂), 54.55 (CH₂Ph), 51.01 (d, J = 2.0 Hz, CH_{NBD}), 48.5 (d, J = 17 Hz, CH_{NBD}). (overnight) Anal. Calc.d for C₂₄H₂₄ClN₂Rh: C, 60.20; H, 5.05; Cl, 7.40; N, 5.85; Rh, 21.49. Found: C, 59.75; H, 5.32; Cl, 8.62; N, 6.73, Rh, 21.26. ESI-MS (MeOH, m/z): 443 (100) [C₂₄H₂₄N₂Rh]⁺. In the ESI-MS(-) spectrum, no peaks were observed.

8.7.3 Synthesis of [RhCl(NBD){1-benzyl-3-trityl-imidazolin-2-ylidene}] (4g)

Silver complex **3g** was prepared according to the procedure described in the paragraph 4.2.1 and instantaneously used for a preparation of the rhodium(I) complex. The suspension of **3g** was filtered on Celite, and the filtrate was added to a solution of [Rh(NBD)Cl]₂ (0.04 g, 0.17 mmol) in CH₂Cl₂. After stirring for 3 h the white AgCl was filtered off, and the solvent was removed under vacuum. The crude material was purified by column chromatography on silica gel treated with 5% v/v triethylamine in diethyl ether, using diethyl ether/CH₂Cl₂, 1:1 v/v, to afford 0.07 g (66 %) of **4g** as a yellow solid. Rf: 0.55 (Et₂O/CH₂Cl₂, 50:50). ¹H NMR (300 MHz, CDCl₃): δ 7.45 – 7.24 (m, 20H, Ph), 6.84 (d, 1H, J_{H,H} = 15.06 Hz, CH₂Ph), 6.76 (d, 1H, J_{H,H} = 2.06 Hz, CH_{im}), 6.56 (d, 1H, J_{H,H} = 1.97 Hz, CH_{im}), 6.17 (d, 1H, J_{H,H} = 14.79 Hz, CH₂Ph), 4.61 (br s, 1H, CH_{NBD}), 3.59 (br s, 1H, CH_{NBD}), 3.44 (br s, 1H, CH_{NBD}), 3.10 (br s, 1H, CH_{NBD}), 2.87 (br s, 1H, CH_{NBD}), 1.94 (br s, 1H, CH_{NBD}), 0.87 (m, 2H, C⁷H₂). ¹³C NMR (100 MHz, CDCl₃): δ 186.57 (d, J_{C-Rh} = 55 Hz), 142.39 (C₅), 137.51 (C₁₂), 129.07 (Ph), 128.86 (Ph), 128.26 (Ph), 128.09 (Ph), 127.91 (Ph), 127.53 (Ph), 127.24 (Ph), 124.29 (CH_{im}), 120.70 (CH_{im}), 82.01 (C_q^{trityl hydroxide}), 76.58 (C_q^{Trit}), 73.13 (s, CH_{NBD}), 61.82 (d, C⁷H₂, J_{H,H} = 5.8 Hz), 57.23 (CH₂Ph), 49.72 (CH_{NBD}), 49.01 (CH_{NBD}), 45.72 (d, C_{NBD}, J_{H,H} = 13 Hz), 44.74 (d, CH_{NBD}, J_{H,H} = 10.8 Hz), (overnight). ESI-MS (MeOH, m/z): 595 (100) [C₃₆H₃₂N₂Rh]⁺. In the ESI-MS(-) spectrum, no peaks were observed. Anal. Calc.d for

C₃₆H₃₂ClN₂Rh: C, 68.52; H, 5.11; Cl, 5.62; N, 4.44; Rh, 16.31. Found: C, 68.39; H, 4.94; Cl, 5.36; N, 4.22; Rh, 16.25.

8.7.4 Synthesis of [RhCl(NBD){1-benzyl-3-tert-butyl-imidazolin-2-ylidene}] (4h)

Silver complex **3h** was prepared according to the procedure described in section: in the paragraph 4.2.1 and instantaneously used for a preparation of the rhodium (I) complex. The suspension of **3h** was filtered in Pasteur plug (cotton + celite), and the filtrate was added to a solution of [Rh(NBD)Cl]₂ (0.025 g, 0.05 mmol) in CH₂Cl₂. After stirring for 4 h the white AgBr was filtered off, and the solvent was removed under vacuum. The resulting yellow solid of **4h** was dissolved in deuterated dimethyl sulfoxide with a few drops of deuterated chloroform and analysed by NMR. ¹H NMR (600 MHz, CDCl₃): δ 7.46 – 7.45 (m, 4H, Ph), 7.41 – 7.39 (m, 1H, Ph), 7.06 (d, 1H, J_{H,H} = 1.97 Hz, CH_{im}), 6.72 (d, 1H, J_{H,H} = 2.03 Hz, CH_{im}), 6.41 (d, 1H, J_{H,H} = 15.09 Hz, CH₂Ph), 6.27 (d, 1H, J_{H,H} = 15.09 Hz, CH₂Ph), 4.84 (m, 1H, CH_{NBD}), 4.70 (m, 1H, CH_{NBD}), 3.81 (br s, 1H, CH_{NBD}), 3.78 (br s, 1H, CH_{NBD}), 3.47 (m, 2H, CH_{NBD}), 2.08 (s, 9H, ^tBu), 1.36 (d, 1H, C⁷H₂, J_{H,H} = 8.00 Hz), 1.31 (d, 1H, C⁷H₂, J_{H,H} = 7.99 Hz). ¹³C NMR (600 MHz, CDCl₃): δ 183.0 (d, J_{C-Rh} = 58.5 Hz), 136.9 (C_q,Ph), 128.7 (Ph), 128.0 (Ph), 127.8 (Ph), 119.7 (CH_{im}), 119.6 (CH_{im}), 74.9 (d, C_{NBD}, J_{H,H} = 6.1 Hz), 71.8 (d, C_{NBD}, J_{H,H} = 6.3 Hz), 62.7 (d, C⁷H₂, J_{H,H} = 5.2 Hz), 57.9 (s, C_{NBD}), 56.3 (CH₂Ph), 50.3 (dd, C_{NBD}, J_{H,H} = 2.5 Hz, J_{H,H} = 7.0 Hz), 48.1 (d, C_{NBD}, J_{H,H} = 13.0 Hz), 46.2 (d, CH_{NBD}, J_{H,H} = 12.2 Hz), 32.1 (^tBu). Anal. Calc.d for C₂₁H₂₆ClN₂Rh: C, 56.70; H, 5.89; Cl, 7.97; N, 6.30; Rh, 23.14. Found: C, 56.51; H, 5.57; Cl, 8.12; N, 6.03, Rh, 22.92.

8.7.5 Synthesis of [RhCl(NBD){1-benzyl-3-*n*-butyl-imidazolin-2-ylidene}] (4i)

To a solution of 1-*n*-butyl-3-methyl-imidazolium bromide (0.020 g, 0.09 mmol) in CH₂Cl₂ (10 mL), Ag₂O (0.016 g, 0.06 mmol) was added. The suspension was stirred for 48 h then, solid [Rh(NBD)Cl]₂ (0.027 g, 0.09 mmol) was directly added to the reaction mixture. After stirring for further 24 h the crude material was filtered on a celite pad, the insoluble material was thoroughly washed with CH₂Cl₂ and the solvent removed under vacuum. The residue was purified by column chromatography on silica gel Et₂O, using Et₂O:CH₂Cl₂ = 1:3 (v/v) as to afford 0.027 g (82 %) of **4i** as a yellow solid. R_f: 0.68 (CH₂Cl₂:MeOH 100:5). ¹H NMR (300 MHz, CDCl₃): δ 6.70 (bd, 2H, CH_{im}), 6.69 (m, 2H, CH_{NBD}), 6.27 (m, 2H, CH_{NBD}), 4.82 (m, 2H, CH₂), 4.41 (t, 2H, CH₂), 4.03 (s, 3H, CH₃) 3.74 (br s, 2H, CH_{NBD}), 1.39 (m, 2H, CH₂), 1.30 (m, 2H, NBD, CH₂), 0.98 (s, 3H, CH₃) ¹³C NMR (300 MHz, CDCl₃): δ 181.7 (d, J_{C-Rh} = 57.5 Hz), 120.9 (CH_{im}), 119.2 (CH_{im}), 77.1 (d, C_{NBD}, J_{H,H} = 6.0 Hz), 62.8 (d, C⁷H₂, J_{H,H} = 5.1 Hz), 50.1 (s, C_{NBD}), 49.3 (br C_{NBD}), 48.3 (br, C_{NBD}), 45.3 (br, CH_{NBD}), 36.7 (CH₂), 32.4 (CH₂), 19.0. (CH₂), 12.8 (CH₃).

References

- 1 Herrmann, W. A.; Gooßen, L. J.; Spiegler, M. *J. Organomet. Chem.*, **1997**, *547*, 357.
- 2 (a) Hirai, K.; Nutton, A.; Maitlis, P. *J. Mol. Catal.* **1981**, *10*, 203. (b) Lei, A.; He, M.; Zhang, X. *J. Am. Chem. Soc.* **2002**, *124*, 8198 and references cited therein.
- 3 Jong, H.; Patrick, B. O.; Fryzuk, M. D. *Can. J. Chem.*, **2008**, *86*, 803.
- 4 For a review see: Casarini, D.; Lunazzi, L.; Mazzanti, A. *Eur. J. Org. Chem.* **2010**, 2035.
- 5 (a) Enders, D.; Gielen, H.; Runsink, J.; Breuer, K.; Brode, S.; Boehn, K. *Eur. J. Inorg. Chem.* **1998**, 913. (b) Enders, D.; Gielen, H. *J. Organomet. Chem.* **2001**, *617*, 70.
- 6 (a) Korenaga, T.; Aikawa, K.; Terada, M.; Kawauchi, S.; Mikami, K. *Adv. Synth. Catal.* **2001**, *343*, 284. (b) Mikami, K.; Aikawa, K.; Yusa, Y.; Jodry, J. J.; Yamanaka, M. *Synlett* **2002**, *10*, 1561. (c) Fjellander, E.; Szabó, Z.; Moberg, C. *J. Org. Chem.* **2009**, *74*, 9120.
- 7 (a) Oki, M. *Pure & Appl. Chem.* **1989**, *61*, 699. (b) Oki, M.; Shimizu, A.; Kihara, H.; Nakamura, N. *Chem. Lett.* **1980**, *9*, 607.
- 8 (a) Ojima, I.; Vu, A. T.; Boonafux, D. *Science of Synthesis vol. 1*; ed. Lautens, M.; Georg Thieme Verlag: Stuttgart, 2001; section 1.5. (b) Bleeke, J. R.; Donaldson A. J. *Organometallics* **1988**, *7*, 1588.
- 9 Perrin, D. D.; Armarego, W. L. F.; Perrin, D. R. *Purification of Laboratory Chemicals* 2nd ed.; Pergamon Press: New York, 1980.
- 10 Sheldrick, G. M., SADABS, 1996, University of Göttingen, Germany.
- 11 Sheldrick, G. M., SHELXL97, University of Göttingen, Germany.
- 12 For B3LYP functional: (a) Becke, A. D. *J. Chem. Phys.* **1993**, *98*, 5648. (b) Lee, C.; Yang, W.; Parr, R. G. *Phys. Rev. B* **1988**, *37*, 785. (c) Stephens, P. J.; Devlin, F. J.; Chabalowski, C. F.; Frisch, M. J. *J. Phys. Chem.* **1994**, *98*, 11623. For the LanL2DZ basis set: Hay, P. J.; Wadt, W. R. *J. Chem. Phys.* **1985**, *82*, 299.
- 13 Gaussian 09 rev A.02. Frisch, M. J.; Trucks, G. W.; Schlegel, H. B.; Scuseria, G. E.; Robb, M. A.; Cheeseman, J. R.; Scalmani, G.; Barone, V.; Mennucci, B.; Petersson, G. A.; Nakatsuji, H.; Caricato, M.; Li, X.; Hratchian, H. P.; Izmaylov, A. F.; Bloino, J.; Zheng, G.; Sonnenberg, J. L.; Hada, M.; Ehara, M.; Toyota, K.; Fukuda, R.; Hasegawa, J.; Ishida, M.; Nakajima, T.; Honda, Y.; Kitao, O.; Nakai, H.; Vreven, T.; Montgomery, Jr., J. A.; Peralta, J. E.; Ogliaro, F.; Bearpark, M.; Heyd, J. J.; Brothers, E.; Kudin, K. N.; Staroverov, V. N.; Kobayashi, R.; Normand, J.; Raghavachari, K.; Rendell, A.; Burant, J. C.; Iyengar, S. S.; Tomasi, J.; Cossi, M.; Rega, N.; Millam, N. J.; Klene, M.; Knox, J. E.; Cross, J. B.; Bakken, V.; Adamo, C.; Jaramillo, J.; Gomperts, R.; Stratmann, R. E.; Yazyev, O.; Austin, A. J.; Cammi, R.; Pomelli, C.; Ochterski, J. W.; Martin, R. L.; Morokuma, K.; Zakrzewski, V. G.; Voth, G. A.; Salvador, P.; Dannenberg, J. J.; Dapprich, S.; Daniels, A. D.; Farkas, Ö.; Foresman, J. B.; Ortiz, J. V.; Cioslowski, J.; Fox, D. J. Gaussian, Inc., Wallingford CT, 2009.
- 14 Ayala, P. Y.; Schlegel, H. B. *J. Chem. Phys.* **1998**, *108*, 2314.
- 15 Tormena, C. F.; Rittner, R.; Abraham, R. J.; Basso, E. A.; Fiorin, B. C. *J. Phys. Org. Chem.* **2004**, *17*, 42.
- 16 (a) Wong, M. W. *Chem. Phys. Lett.* **1996**, *256*, 391. (b) Wheeler, S. E.; McNeil, A. J.; Müller, P.; Swager, T. M.; Houk, K. N. *J. Am. Chem. Soc.* **2010**, *132*, 3304.
- 17 Gaillard, S.; Slawin, A. M. Z.; Nolan, S. P. *Chem. Comm.* **2010**, *46*, 2742-2744.
- 18 Casarini, D.; Lunazzi, L.; Mazzanti, A. *Eur. J. Org. Chem.* **2010**, 2035-2056.
- 19 Enders, D.; Gielen, H.; Runsink, J.; Breuer, K.; Brode, S.; Boehn, K. *Eur. J. Inorg. Chem.* **1998**, 913-919.
- 20 Corbera, R.; Sanau, M.; Peris, E. *Organometallics* **2006**, *25*, 4002-4008.
- 21 Scott, N. M.; Dorta, R.; Stevens, E. D.; Correa, A.; Cavallo, L.; Nolan, S. P. *J. Am. Chem. Soc.* **2005**, *127*, 3516-26.
- 22 Bringmann, G.; Price Mortimer, A. J.; Keller, P. A.; Gresser, M. J.; Garner, J.; Breuning, M. *Angew. Chem. Int. Ed.* **2005**, *44*, 5384-5427.
- 23 W., Gil; T. Lis, A., M. Trzeciak; J. J. Ziołkowski; *Inorg. Chim. Acta* **2006**, 2835-2841

9 Catalysis

9.1 Introduction

As previously showed in the introduction (paragraph 1-8), Rh(I)-NHC complexes are active in the hydrosilylation of terminal alkynes and in the addition of benzaldehydes to phenylboronic acid.

Complexes **4a-i** (Figure 9.1-1) have been tested as catalyst precursors in these kind of reactions in order to shed light on the influence of steric encumbrance and of the amide Boc functionalization on the NHC ligands on the catalytic activity and selectivity.

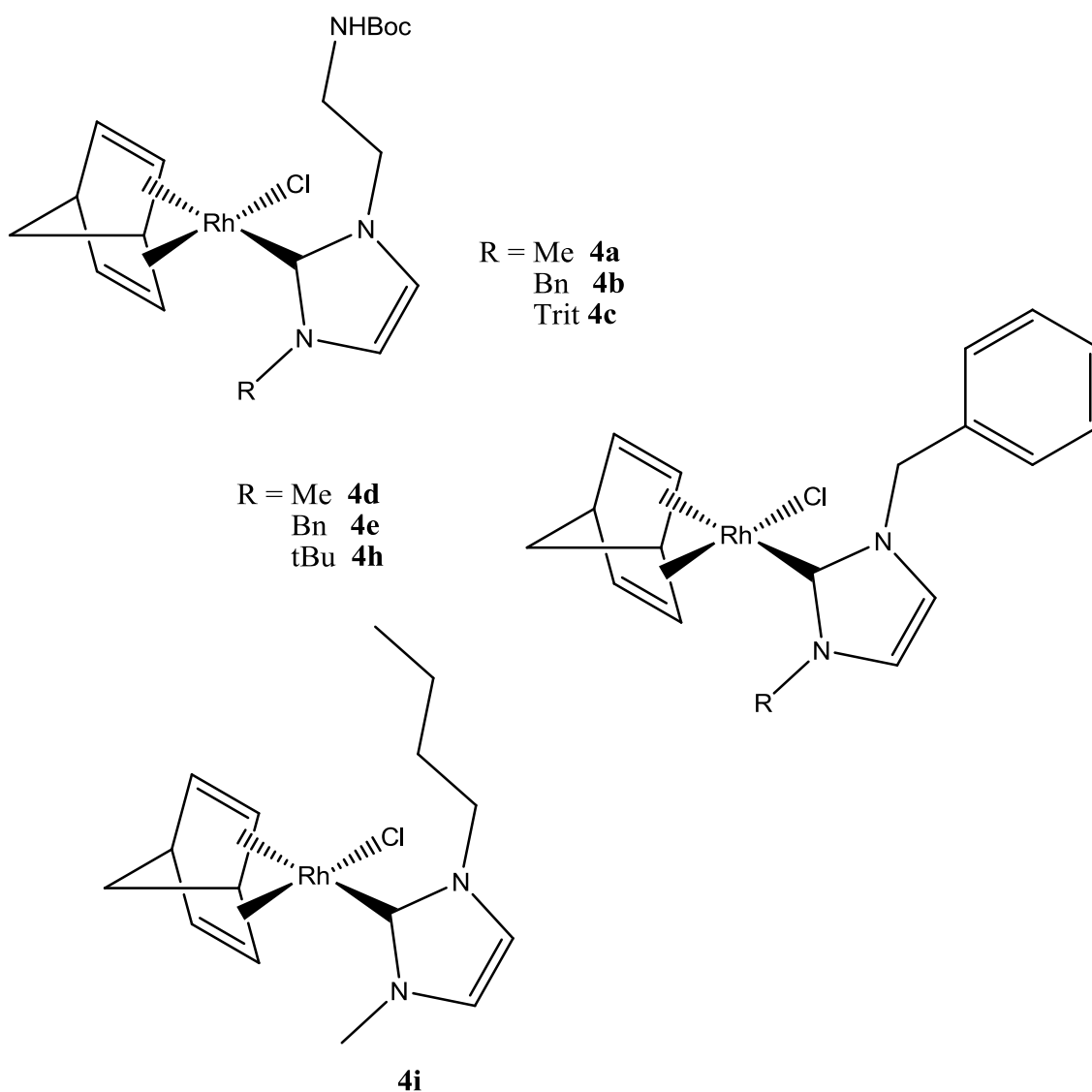


Figure 9.1-1

9.2 Results and discussion

Hydrosilylation of terminal alkynes. The potential of the Rh(I) complexes **4a-i** (Figure 9.1-1) as catalysts was examined in the hydrosilylation of 1-alkynes (Scheme 9.2-1). The catalytic reactions were carried out in CDCl₃ at +25 °C or 60°C with a catalyst loading of 1% or 0.1% using a slight excess of HSiMe₂Ph and were routinely monitored by ¹H-NMR spectroscopy. The influence of the 1-alkyne has been studied using phenylacetylene, 4-ethynyl-toluene, 1-hexyne, triethylsililacetylene and 1,1-diphenyl-2-propyn-1-ol as substrates.

9.2.1 Hydrosilylation at 25°C with a catalyst loading of 1%

9.2.1.1 Phenylacetylene

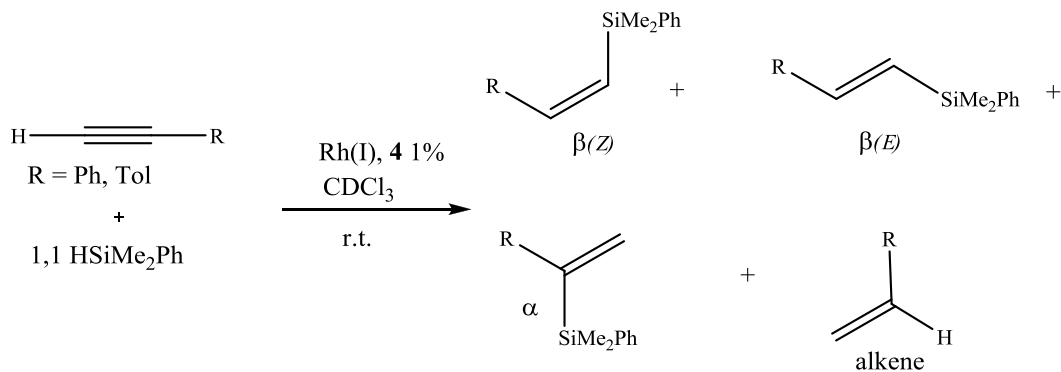
Hydrosilylation of phenylacetylene has been performed with catalyst **4a**, **4b**, **4c**, **4d**, **4h** and **4i**. Significant data are reported in Table 9.2-1. Further data and details are available in the Appendix 9.5.

Table 9.2-1 Hydrosilylation of phenylacetylene at 25°C with a catalyst loading of 1%.

Entry	Alkyne	cat	Time (h)	Conv. (%)	E (%)	Z (%)	alfa (%)	alkene (%)
1	PhC≡CH	4a	0,3	80	29	56	15	0
2	PhC≡CH	4a	6	>99	41	41	13	5
3	PhC≡CH	4a	192	>99	74	0	14	12
4	PhC≡CH	4b	0,3	66	23	51	11	15
5	PhC≡CH	4b	22	>99	51	24	15	10
6	PhC≡CH	4b	192	>99	75	0	15	10
7	PhC≡CH	4c	0,3	0	0	0	0	0
8	PhC≡CH	4c	144	>99	57	17	16	10
9	PhC≡CH	4c	192	>99	74	0	16	10
10	PhC≡CH	4d	2	34	33	50	12	5
11	PhC≡CH	4d	21	>99	25	63	9	3
12	PhC≡CH	4d	335	>99	74	13	9	4
13	PhC≡CH	4h	22	31	20	60	14	6
14	PhC≡CH	4h	142	>99	39	51	8	2
15	PhC≡CH	4h	244	>99	46	43	7	4
16	PhC≡CH	4i	0,5	8	26	62	12	0
17	PhC≡CH	4i	22	>99	26	60	10	4
18	PhC≡CH	4i	70	>99	46	39	10	5

As generally reported for transition metal catalyzed hydrosilylation of 1-alkynes,¹ and in particular for neutral and cationic Rh(I)-NHC hydrosilylation catalysts, the reaction is non selective and complexes **4a-i** converts the substrates in a mixture of the three possible isomeric vinylsilane

derivatives: $\beta(Z)$ or $\beta(E)$ 1-silyl-1-alkenes, products from the anti-Markovnikov addition, and α -2-silyl-1-alkene from the Markovnikov addition. Furthermore the formation of the corresponding alkene has been observed from these substrates (Scheme 9.2-1).



Scheme 9.2-1

Although **4a-i** completely converted all the substrates, **4a** with the amide Boc group, showed the best results in term of reaction rate (Figure 9.2-1 and Figure 9.2-2).

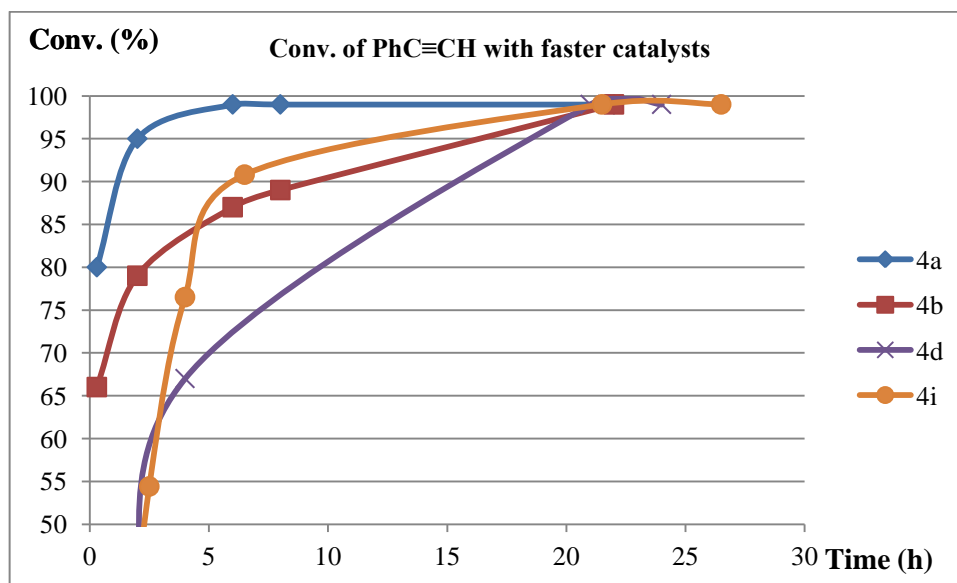


Figure 9.2-1 Reaction profile of conversion vs time for the hydrosilylation of PhC≡CH with complexes: **4a**, **4b**, **4d** and **4i**

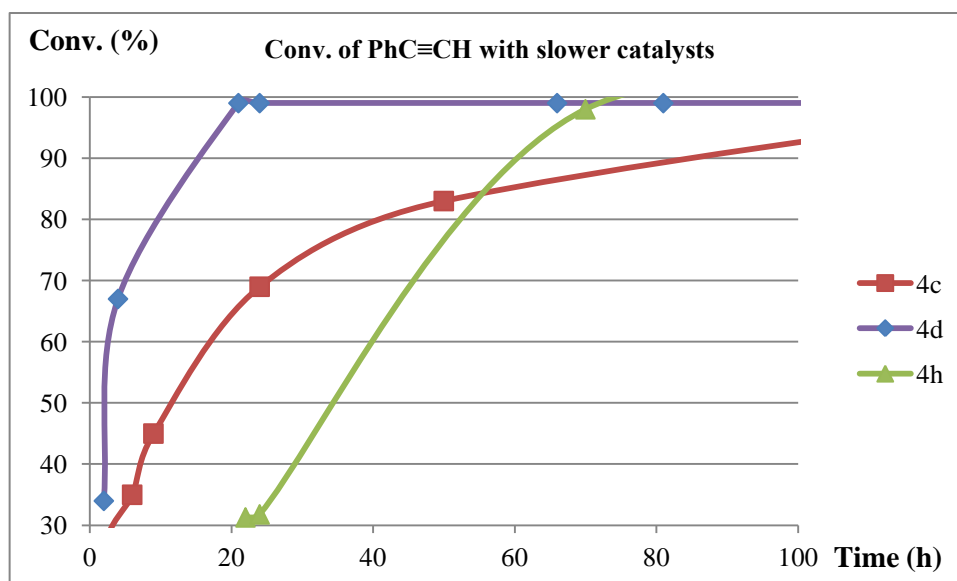


Figure 9.2-2 Reaction profile of conversion vs time for the hydrosilylation of PhC≡CH with complexes: **4c**, **4d** and **4h**

Due to the sensitive difference in the reaction rate of the complexes **4a,b,d,i** (Figure 9.2-1) and **4c,d,h** (Figure 9.2-2) the above reported graphics have been divided for the sake of clarity. The general behaviour of all the catalysts employed show that there is a detrimental effect on the reaction rate of the steric hindrance on the NHC ligand. As an example we can compare the results obtained with catalyst **4a-c** which have the same $-\text{CH}_2\text{CH}_2\text{NHBoc}$ side arm at one nitrogen atom of the imidazolium ring. In those cases total conversion of phenylacetylene has been reached within 6h in case of **4a** (R = Methyl, Table 9.2-1, entry 2), 22 h in case of **4b** (R = Benzyl, Table 9.2-1, entry 5), 144h in case of the most encumbered **4c** (R = Trytil, Table 9.2-1, entry 8). Furthermore the comparison between the reaction rate of complexes **4a** and **4i**, the latter being slower (Figure 9.2-1), allow us to demonstrate that the presence of $-\text{NHBoc}$ group influences in a positive way the reaction rate.

Interestingly performing the hydrosilylation of phenylacetylene in the presence of catalysts **4a-i** we did not observe formation of polyphenylacetylene isolated by Oro et al. employing similar complexes.¹ The β -(Z) vinylsilane is the major product until the substrate completely disappears. Once reached the complete conversion β -(Z) isomerizes to β -(E) vinylsilane which, at the end of the reaction, is always the major product. In Figure 9.2-3 an example of conversion and selectivities profiles vs. time is reported for the reaction of PhC≡CH and dimethylphenylsilane mediated by the best catalyst **4a**. The graph shows that β -(Z) and β -(E) vinylsilane profiles cross when the conversion is complete and the reaction goes further until β -(Z) completely converts to β -(E). The formation of α isomer (14%) and styrene (12%) (entry 3 in Table 9.2-1) affect the selectivity of the reaction.

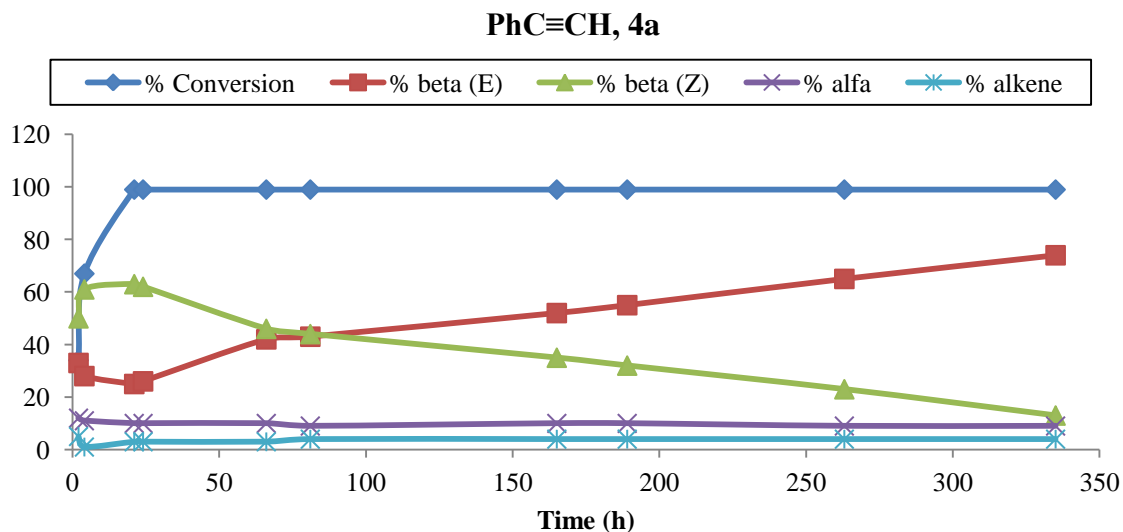


Figure 9.2-3 Reaction profile of conversion and selectivities vs. time for the hydrosilylation of PhC≡CH with **4a**

General data from all complexes **4a-i** (Table 9.2-1) show that α isomer is always identified in variable amount, 7-16%, while the alkene formation occurs in an amount of 4-10% (entry 6, 9, 12, 15, 18).

Selectivity behavior of catalysts **4a-i** is also summarized in the bar diagram of Figure 9.2-4, further detailed graphics are reported in Appendix 9.5.

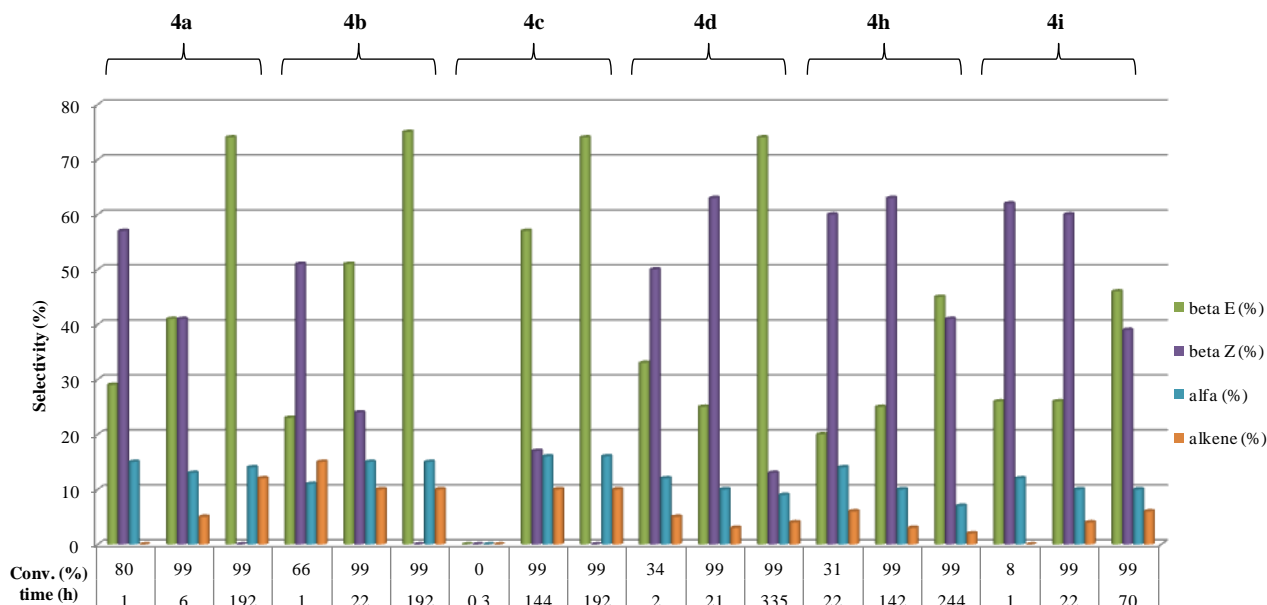


Figure 9.2-4 Hydrosilylation of phenylacetylene: conversions, selectivities and reaction times for precursors **4a-i**

9.2.1.2 Tolyacetylene

Hydrosilylation of tolyacetylene has been performed with catalyst **4a**, **4b**, **4c**, **4h** and **4i**. Significant data are reported in Table 9.2-2. Further data and details are available in the Appendix 9.5.

Table 9.2-2 Hydrosilylation of tolyacetylene at 25°C with a catalyst loading of 1%.

Entry	Alkyne	Cat	Time (h)	Conv. (%NMR)	% β (E)	% β (Z)	% α	% alkene
1	TolC \equiv CH	4a	0,3	87	32	52	16	0
2	TolC \equiv CH	4a	2	>99	54	33	13	0
3	TolC \equiv CH	4a	6	>99	85	0	15	0
4	TolC \equiv CH	4b	2	76	27	48	13	12
5	TolC \equiv CH	4b	22	>99	62	17	13	8
6	TolC \equiv CH	4b	192	>99	73	0	14	13
7	TolC \equiv CH	4c	0,3	0	0	0	0	0
8	TolC \equiv CH	4c	2	26	43	27	30	0
9	TolC \equiv CH	4c	144	>99	68	8	14	10
10	TolC \equiv CH	4c	192	>99	76	0	14	10
11	TolC \equiv CH	4h	22	74	11	82	7	0
12	TolC \equiv CH	4h	70	>99	25	70	5	0
13	TolC \equiv CH	4h	244	>99	75	17	5	3
14	TolC \equiv CH	4i	1	7	10	80	10	0
15	TolC \equiv CH	4i	22	>99	36	51	9	4
16	TolC \equiv CH	4i	70	>99	79	5	9	7

The conversions of tolyacetylene in function of time for catalysts **4a-i** depicted in the following Figure 9.2-5 confirm that the steric hindrance of the catalyst negatively affect the reaction rate.

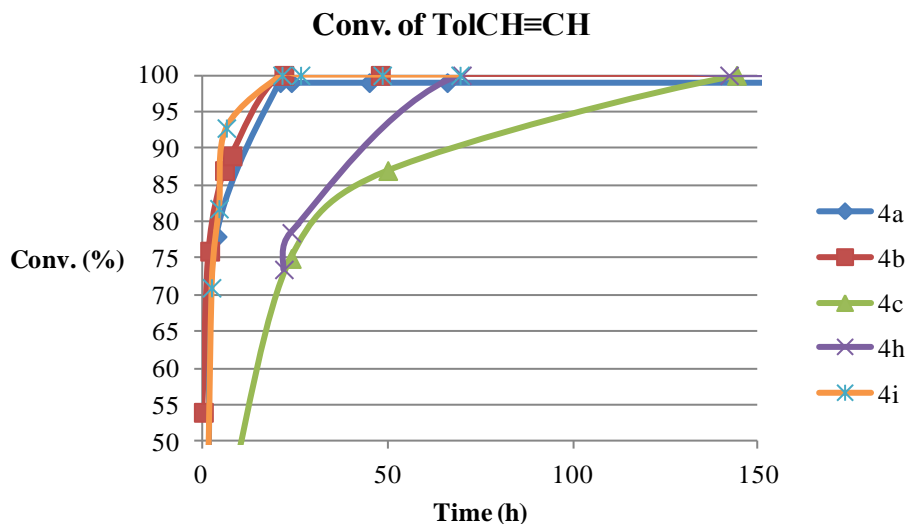


Figure 9.2-5 Reaction profile of conversion vs time for the hydrosilylation of TolC≡CH with complexes: **4a-i**

With regard to the selectivity we report as an example the results obtained with **4a** which appeared to be the best catalyst also with the latter substrate (Figure 9.2-6)

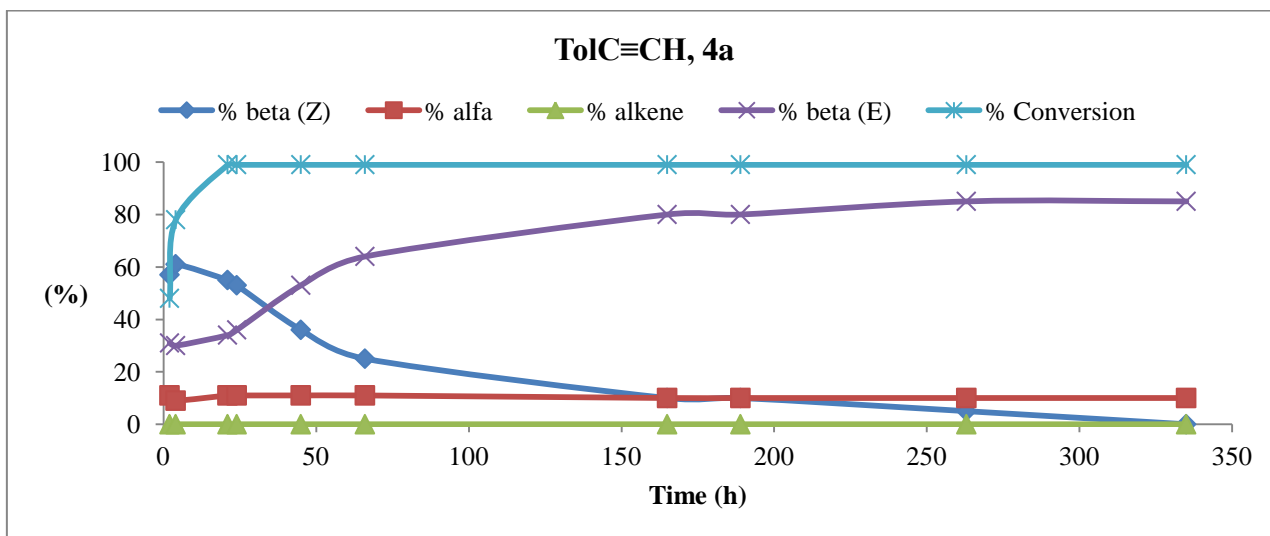


Figure 9.2-6 Reaction profile of conversion and selectivities vs. time for the hydrosilylation of TolC≡CH with **4a**

It is important to underline that, in term of selectivity, the best result has been obtained under the following conditions: tolylacetylene as the substrate, 25°C and 1% of catalyst loading employing **4a** as catalyst. This reaction leads to the formation of β-(E) 85% and α 15% isomers (entry 3) within 6 hours. No alkene formation has been observed in this case. Data for all the

complexes under study **4a-i** (Table 9.2-2) shows that the α isomer is always identified in variable amount, 4-13%, while the alkene formation is in an amount of 3-13% (entry 6, 10, 13, 16).

Selectivity behavior of catalysts **4a-i** is also summarized in the bar diagram of Figure 9.2-7, further detailed graphics are reported in Appendix 9.5.

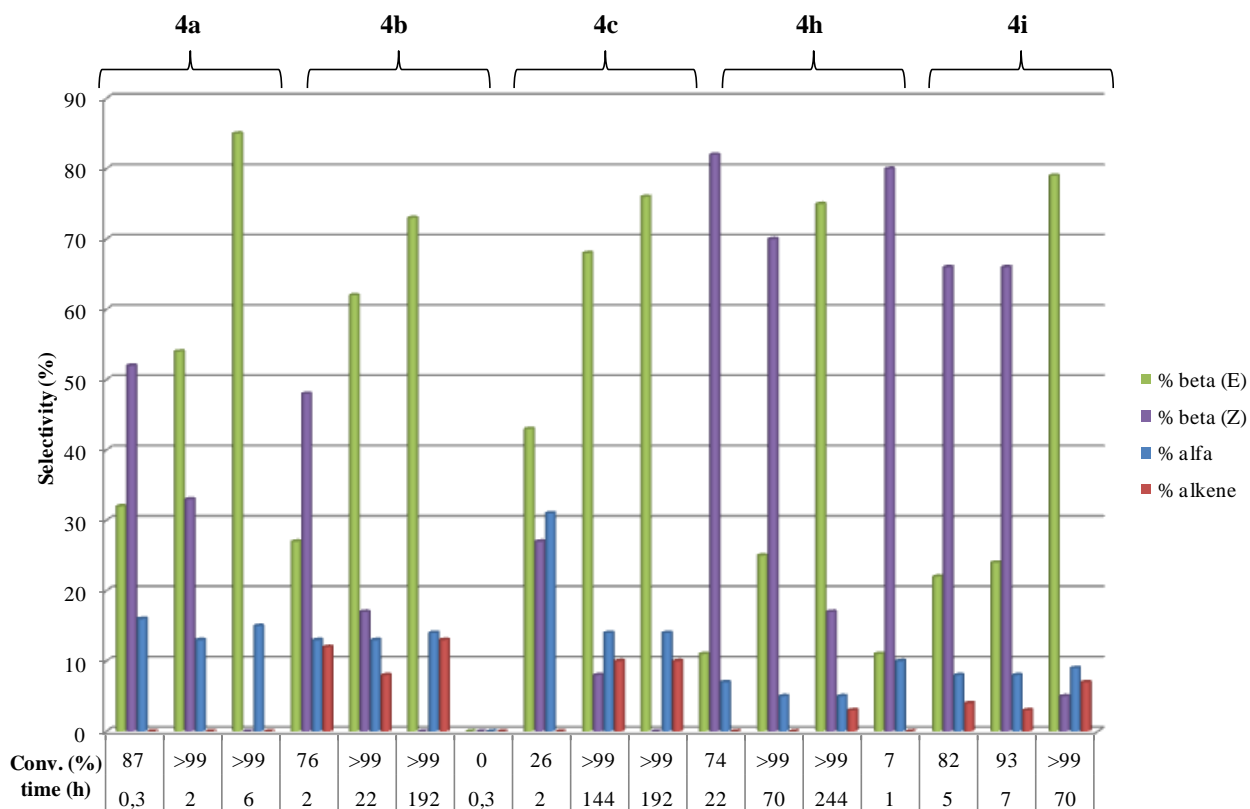


Figure 9.2-7 Hydrosilylation of tolylacetylene: conversions, selectivities and reaction times for precursors **4a-i**

9.2.1.3 Butylacetylene

Hydrosilylation of butylacetylene has been performed with catalyst **4a**, **4b**, and **4c**. Significant data are reported in Table 9.2-3. Further data and details are available in the Appendix 9.5.

Table 9.2-3 Hydrosilylation of *n*butylacetylene at 25°C with a catalyst loading of 1%.

Entry	Alkyne	Cat	time (h)	Conv. (%NMR)	% β (E)	% β (Z)	% α	% allyl
1	<i>n</i> BuC \equiv CH	4a	0,3	10	30	44	26	0
2	<i>n</i> BuC \equiv CH	4a	2	48	33	40	27	0
3	<i>n</i> BuC \equiv CH	4a	6	>99	43	18	23	16
4	<i>n</i> BuC \equiv CH	4a	22	>99	47	0	18	35
5	<i>n</i> BuC \equiv CH	4b	0,3	0	0	0	0	0
6	<i>n</i> BuC \equiv CH	4b	2	32	42	58	0	0
7	<i>n</i> BuC \equiv CH	4b	192	>99	44	0	16	40

8	<i>n</i> BuC≡CH	4c	9	0	0	0	0	0
9	<i>n</i> BuC≡CH	4c	24	26	37	42	21	0
10	<i>n</i> BuC≡CH	4c	192	>99	37	0	17	46

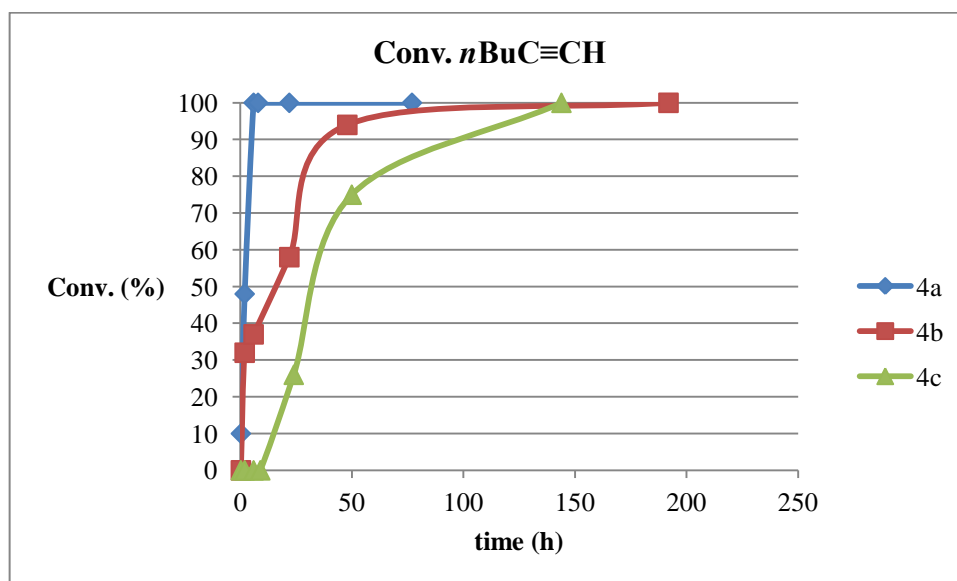
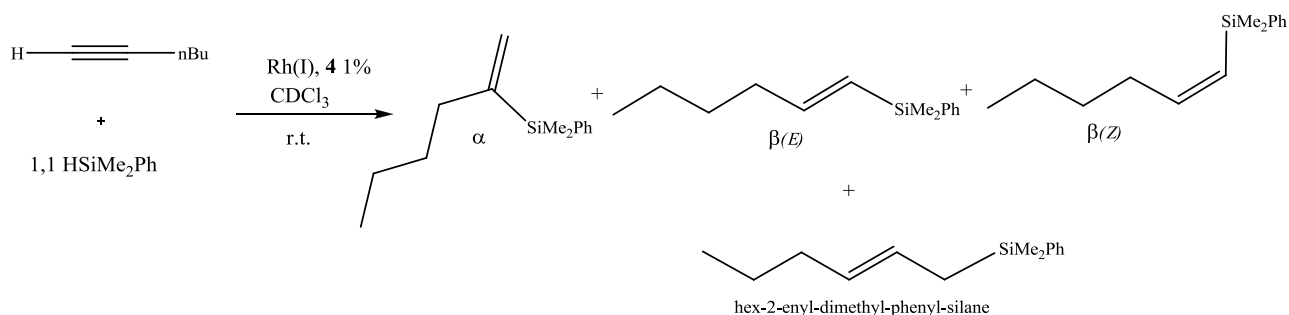


Figure 9.2-8 Reaction profile of conversion vs time for the hydrosilylation of *n*BuC≡CH with complexes: **4a-c**

When *n*BuC≡CH is employed as substrate (Table 9.2-3, Figure 9.2-8) the reaction rate is generally slower showing for example with **4a** a TOF of 24 h⁻¹ (*cf.* with phenylacetylene TOF = 48 h⁻¹ and tolylacetylene TOF = 50 h⁻¹). Furthermore once the conversion is complete the β -(*Z*) vinylsilane isomerizes into the hex-2-enyl-dimethyl-phenyl-silane (35-46%; entry 4, 7, 10,) instead of the β -(*E*) vinylsilane (Table 9.2-3, see for example Figure 9.2-9). This behavior is in line with what previously reported by Crabtree et al. in the hydrosilylation of 1-hexyne with HSiMePh₂ catalyzed by [Rh(PPh₃)₃Cl].²



Scheme 9.2-2

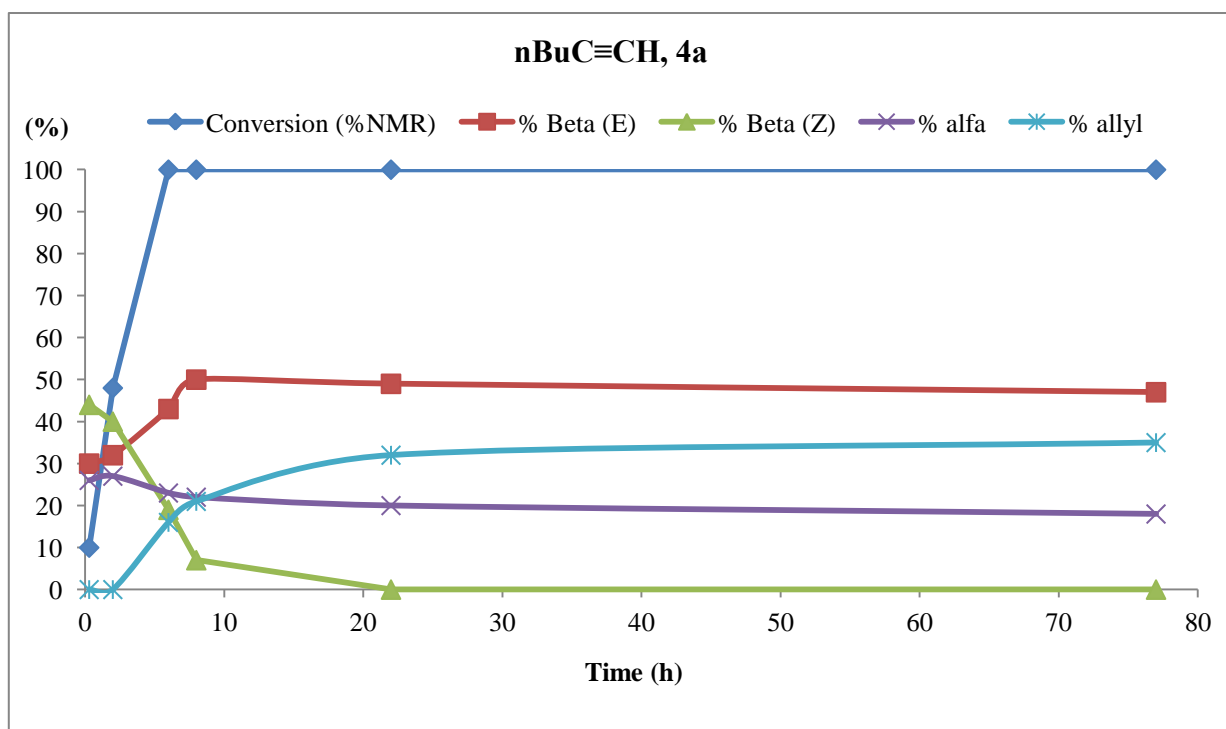


Figure 9.2-9 Reaction profile of conversion and selectivities vs. time for the hydrosilylation of $n\text{BuC}\equiv\text{CH}$ with **4a**

It is worth noting that, as above stated, the hydrosilylation of 1-hexyne requests a longer initiation time (Table 9.2-3).

In view of the fact that the alkynes steric encumbrance negatively affects the reaction rate (vide infra) and by comparison with literature data on the hydrosilylation of 1-hexyne,³ this behaviour has to be ascribed to an electronic effect. In particular a less activated metal-alkyne bond could inhibit the catalyst turnover slowing the insertion step.⁴

The conversion and selectivities of the best catalyst **4a** in which the peculiar, above described, isomerization of β -(Z) vinylsilane to the hex-2-enyl-dimethyl-phenyl-silane can be visualized in Figure 9.2-9 while the summary of the selectivity behavior is depicted in the following Figure 9.2-10.

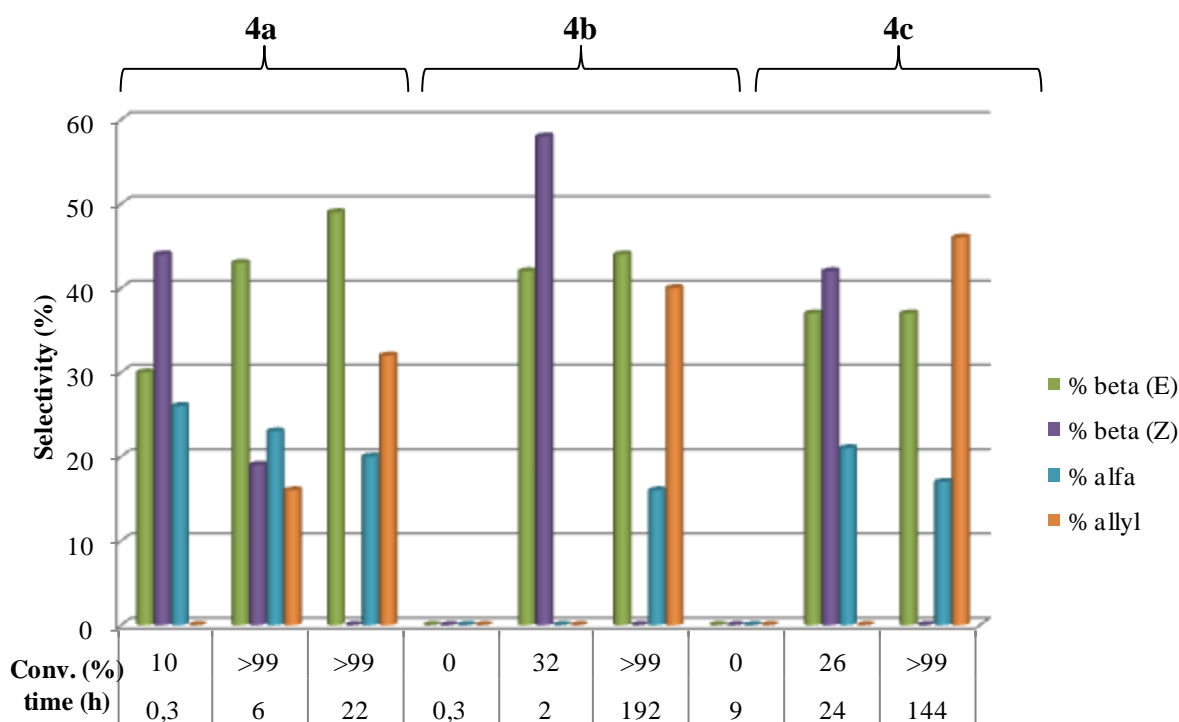


Figure 9.2-10 Hydrosilylation of $n\text{BuC}\equiv\text{CH}$: conversions, selectivities and reaction times for precursors **4a-c**

9.2.1.4 Triethylsilylacetylene and 1,1-diphenyl-2-propyn-1-ol

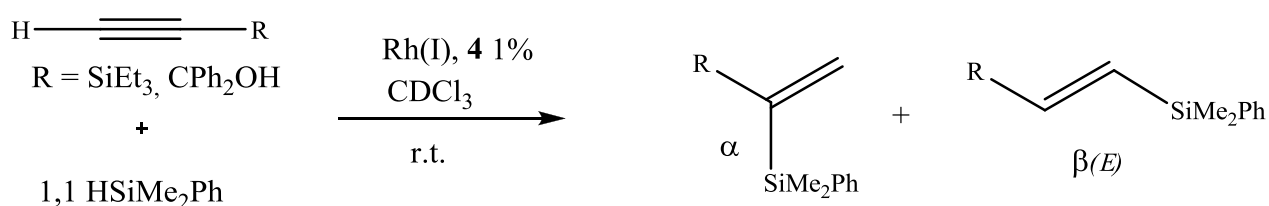
Hydrosilylation of triethylsilylacetylene and 1,1-diphenyl-2-propyn-1-ol has been performed in order to shed light on the effect of the steric encumbrance of the substrate on the catalytic activity and selectivity of the hydrosilylation reaction. Since the detrimental effect on the reaction rate of the steric hindrance on the NHC ligand was already demonstrated employing **4a-i** with $\text{PhC}\equiv\text{CH}$, $\text{ToIC}\equiv\text{CH}$ and $n\text{BuC}\equiv\text{CH}$; the effect of the steric encumbrance of the alkynes $\text{Et}_3\text{SiC}\equiv\text{CH}$ and $(\text{CPh}_2\text{OH})\text{C}\equiv\text{CH}$ has been tested with the best catalysts **4a**. Significant data are reported in

Table 9.2-4. Further data and details are available in the Appendix 9.5.

Table 9.2-4 Hydrosilylation of $\text{Et}_3\text{SiC}\equiv\text{CH}$ and $(\text{CPh}_2\text{OH})\text{C}\equiv\text{CH}$ at 25°C with a catalyst loading of 1%.

Entry	Alkyne	Cat	Time (h)	Conv. (%NMR)	% β (E)	% α
1	$\text{Et}_3\text{SiC}\equiv\text{CH}$	4a	0,3	31	61	39
2	$\text{Et}_3\text{SiC}\equiv\text{CH}$	4a	2-77	>99	51	49
3	$(\text{CPh}_2\text{OH})\text{C}\equiv\text{CH}$	4a	0,3	31	61	39
4	$(\text{CPh}_2\text{OH})\text{C}\equiv\text{CH}$	4a	2	47	67	33
5	$(\text{CPh}_2\text{OH})\text{C}\equiv\text{CH}$	4a	144	>99	69	31

Opposite to what observed with the previously discussed substrates (phenyl, tolyl and n-butylacetylene) and in agreement with what previously reported,¹ the reaction of dimethylphenylsilane with (triethylsilyl)acetylene $\text{Et}_3\text{SiC}\equiv\text{CH}$ in the presence of **4a** leads to the formation of only the two isomers $\beta(E)$ and α (Scheme 9.2-3 and Table 9.2-4). This behavior has been attributed to both the steric hindrance and the electronic characteristics of the precursor and can be confirmed catalyzing the reaction between 1,1-diphenyl-2-propyn-1-ol $(\text{CPh}_2\text{OH})\text{C}\equiv\text{CH}$ and dimethylphenylsilane with **4a**: also in this case only the formation of the $\beta(E)$ and α isomers occurred with a better selectivity in the former.



Scheme 9.2-3

Conversion vs time is reported for both the alkynes in Figure 9.2-11.

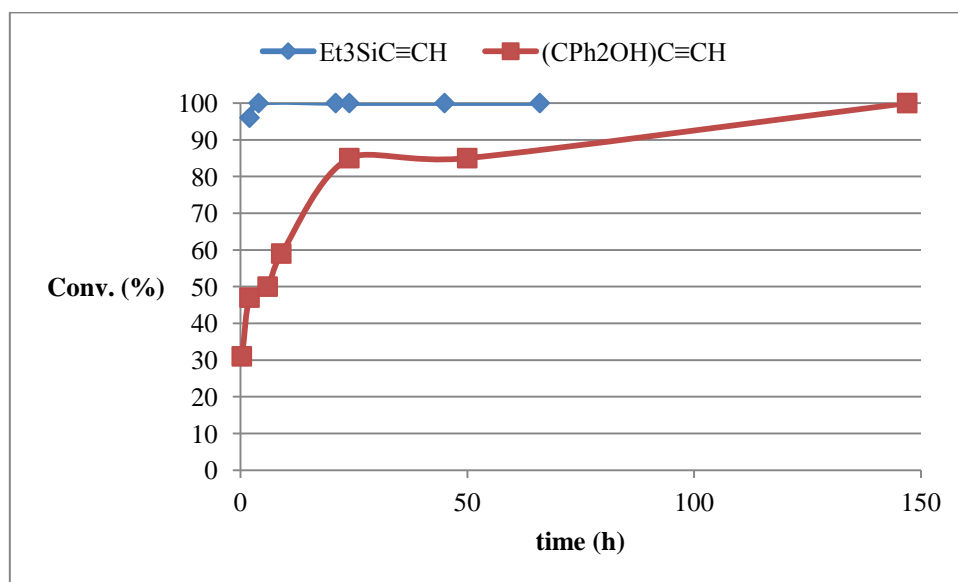


Figure 9.2-11 Reaction profile of conversion vs time for the hydro-silylation of $\text{Et}_3\text{SiCC}\equiv\text{CH}$ and $(\text{CPh}_2\text{OH})\text{C}\equiv\text{CH}$ with complex **4a**

General remarks for the alkynes behavior.

By comparing the alkynes conversions and selectivities when employing catalyst **4a**, as summarized in Figure 9.2-12, we can observe that the steric encumbrance of the alkyne also affects the reaction rate. While all the other substrates completely convert within 6 hours, the tertiary propargyl alcohol (CPh₂OH)C≡CH reaches the complete conversion only after 144 hours (Figure 9.2-12).

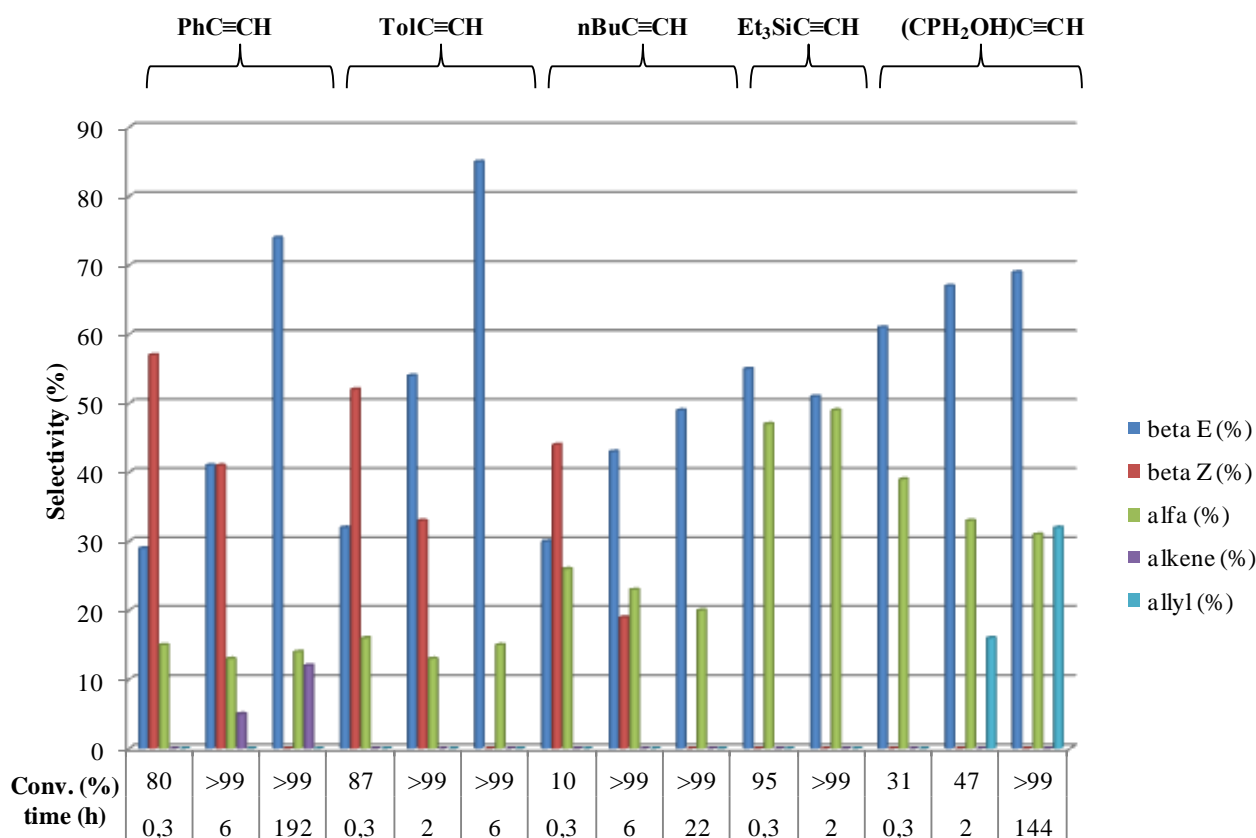


Figure 9.2-12 Conversions, selectivities and reaction times for **4a** with all substrates

Generally while the speed of the reaction is affected both by the steric encumbrance of the complexes **4a-i** and of the alkynes, the substituents on the N-heterocyclic ring of the catalysts **4a-i** do not seriously affect the selectivity, which is otherwise influenced by the steric hindrance and electronics of the alkyne (Figure 9.2-12). This behaviour is in accordance with the mechanism proposed for neutral and cationic amino rhodium NHC complexes.²

9.2.2 Hydrosilylation at 25°C with catalyst loading of 0,1%

Selected catalysts and substrates have been also employed in order to check the possibility of reducing the catalyst loading.

9.2.2.1 Phenylacetylene

Hydrosilylation of phenylacetylene has been performed with catalyst **4a**, **4d** and **4e**. Significant data are reported in Table 9.2-5. Further data and details are available in the Appendix 9.5.

Table 9.2-5 Hydrosilylation of phenylacetylene significant data at 25°C with a catalyst loading of 0,1%

Entry	Alkyne	cat	Time (h)	% Conversion	% β (E)	% β (Z)	% α	% alkene
1	PhC≡CH	4a	0,3	69	40	20	20	23
2	PhC≡CH	4a	12	83	54	6	20	20
3	PhC≡CH	4a	52	>99	60	0	20	20
4	PhC≡CH	4d	8	0	0	0	0	0
5	PhC≡CH	4d	74	30	22	65	8	5
6	PhC≡CH	4d	169	53	48	42	6	4
7	PhC≡CH	4d	121	44	35	51	8	6
8	PhC≡CH	4d	1080	87	90	1	4	5
9	PhC≡CH	4e	8	0	0	0	0	0
10	PhC≡CH	4e	74	23	32	55	14	1
11	PhC≡CH	4e	312	72	40	45	12	3
12	PhC≡CH	4e	504	77	54	32	10	4
13	PhC≡CH	4e	1080	91	76	9	10	5

The reduction of the catalyst loading down to 0.1 mol % with **4a**, **4d** and **4e** affected the catalytic performances in terms of reaction rate as expected (see Table 9.2-5). It provided anyway activity at room temperature, but in the latter case slower kinetics were found. Even in this case the best catalyst in term of reaction rate is represented by the less encumbered **4a** which reach the complete conversion within 52 h (entry 3). It shows a less selectivity if compared with **4a** at 1% loading (14% (α), 12% (alkene): Table 9.2-1, entry 3) vs **4a** at 0.1% loading (20% (α), 20% (alkene)) Table 9.2-5, entry 3). In the case of more encumbered catalysts **4d** and **4e** and in particular with **4d** the selectivity is in line with what observed with the higher loading.

With regard to reaction rate complexes **4d** and **4e** need a really long induction time, after 8 hours the conversion is 0 (entry 4, 9) and only after 74 hours 30% and 23% of conversion are observed (entry 5, 10). For phenylacetylene, the complete conversion has not been reached within the time put aside the experiment (1080 h) neither in case of **4d** nor **4e** catalyst; after that time, the conversion was 87 and 91% respectively (entry 8, 13). Unless what observed with **4a**, in the case of **4d** and **4e** that the lower catalyst loading, even if seriously affected the reaction rate, induced a better selectivity of the products when compared to the 1 mol % catalyst loading, e.g. for **4d** β-(E) = 74% (Table 9.2-1, entry 12) vs β-(E) = 90% (Table 9.2-5, entry 8) respectively. Additionally, as in

the experiment employing 1 mol % of the catalyst (Table 9.2-1, entry 3) the quantities of alkenes are constant almost with time.

9.2.2.2 Tolylacetylene

Hydrosilylation of tolylacetylene has been performed with catalyst **4a**, **4d** and **4e**. Significant data are reported in Table 9.2-6. Further data and details are available in the Appendix 9.5.

Table 9.2-6 Hydrosilylation of tolylacetylene significant data at 25°C with a catalyst loading of 0,1%

Entry	Alkyne	cat	Time (h)	Conv. (%NMR)	% β (E)	% β (Z)	% α	% alkene
1	TolC \equiv CH	4a	0,3	47	26	51	23	0
2	TolC \equiv CH	4a	2	68	30	48	18	4
3	TolC \equiv CH	4a	12	>99	66	13	15	6
4	TolC \equiv CH	4a	52	>99	79	0	14	7
5	TolC \equiv CH	4d	74	49	32	58	8	2
6	TolC \equiv CH	4d	121	71	57	34	6	3
7	TolC \equiv CH	4d	648	>99	90	1	3	6
8	TolC \equiv CH	4d	768	>99	91	1	3	5
9	TolC \equiv CH	4e	74	23	43	41	16	0
10	TolC \equiv CH	4e	169	85	49	28	13	3
11	TolC \equiv CH	4e	504	98	81	1	14	4
12	TolC \equiv CH	4e	648	98	80	1	15	4

When TolC \equiv CH was employed as a substrate under a catalyst loading of 0,1% and temperature of 25°C (Table 9.2-6), the reaction rate was slightly faster than for PhC \equiv CH but no significant difference can be observed in the behavior of this substrate if compared with phenylacetylene. The latter substrate leads to slightly better selectivity. In particular the best one has been obtained in β (E) with the catalyst **4d** (91%).

9.2.3 Hydrosilylation at 60°C with catalyst loading of 0,1%

In order to make the reaction faster with the low catalyts loading of 0.1%, encumbered catalysts **4d** and **4e** have been tested at 60°C. The results are summarized in Table 9.2-7 for phenylacetylene and Table 9.2-8 for tolylacetylene. For further detail see Appendix 9.5.

Table 9.2-7 Hydrosilylation of phenylacetylene significant data at 60°C with a catalyst loading of 0,1%

Entry	Alkyne	cat	Time (h)	% Conversion	% β (E)	% β (Z)	% α	% alkene
1	PhC≡CH	4d	1	12	56	13	26	5
2	PhC≡CH	4d	71	99	71	9	15	5
3	PhC≡CH	4d	245	>99	78	0	16	6
4	PhC≡CH	4e	1	8	43	27	15	15
5	PhC≡CH	4e	71	82	77	4	15	4
6	PhC≡CH	4e	149	>99	82	0	13	5

The increase of the temperature from 25 °C to 60 °C, affected the reaction rate and the selectivity (Table 9.2-7). For instance, in the phenylacetylene case, its complete conversion was reached after 71 h with the **4d** as the catalyst (entry 2), whereas the use of **4e** extended the reaction time until the complete conversion after 149 h (entry 6). The catalytic reactions under these conditions started immediately, the first NMR check after 1h., showed already 12 and 8% of conversion in the presence of **4d** and **4e** catalysts, respectively (entry 1, 4). In Figure 9.2-13 the reaction profiles of phenylacetylene with **4d** is reported as an example.

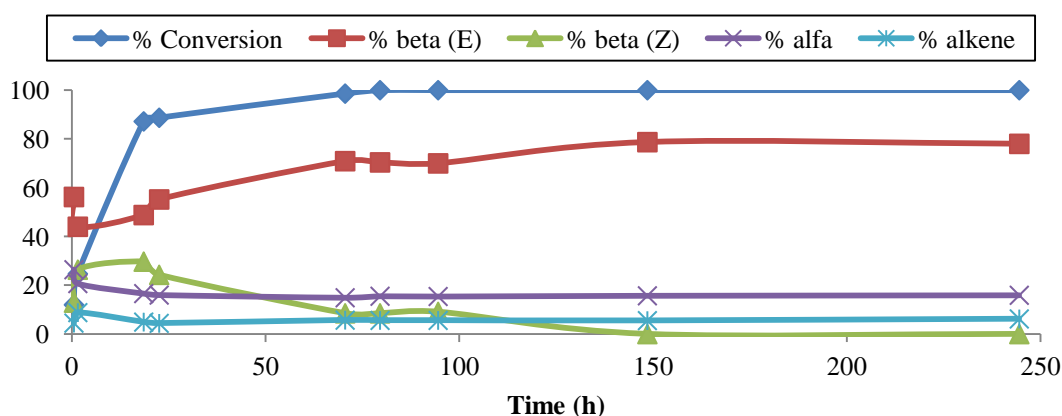


Figure 9.2-13 Reaction profile of conversion and selectivities vs time for the hydrosilylation of PhC≡CH with **4d**.

Table 9.2-8 Hydrosilylation of tolylacetylene at 60°C with a catalytic loading of 0,1.

Entry	Alkyne	cat	Time (h)	% Conversion	% β (E)	% β (Z)	% α	% alkene
1	TolC≡CH	4d	1	21	39	41	20	0
2	TolC≡CH	4d	23	98	71	11	18	0
3	TolC≡CH	4d	173	>99	85	0	15	0
4	TolC≡CH	4e	1	18	41	39	20	0
5	TolC≡CH	4e	71	>99	81	2	13	4
6	TolC≡CH	4e	149	>99	83	0	13	4

In case of tolylacetylene, this catalytic reaction is even faster, after first 1 h there was already 21 and 18% of conversion reached with **4d** and **4e** catalysts (entry 1, 4; Table 9.2-8), respectively. Moreover, at this temperature, the **4e** catalyst was found to provide better selectivity of the reactions with comparison to the catalyst **4d**, although, the **4e**, being more encumbered, shows a lower efficiency in terms of the reaction speed (Figure 9.2-14).

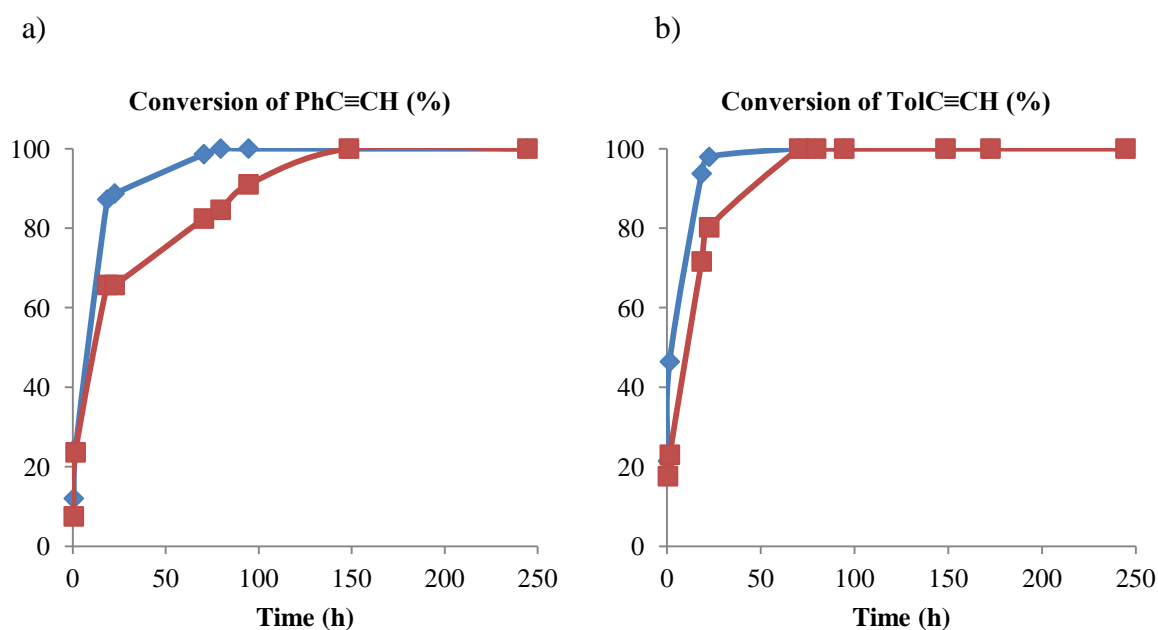
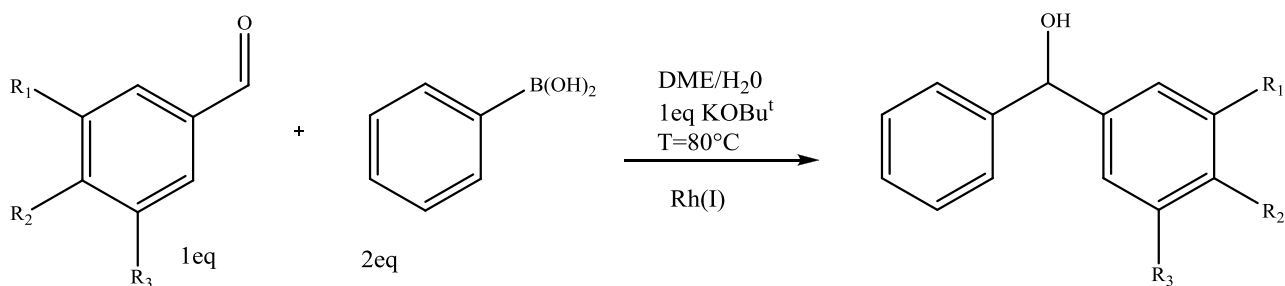


Figure 9.2-14 Reaction profile of conversion vs time for the hydrosilylation of PhC≡CH (a) and TolC≡CH (b) with complexes **4d** (blue) and **4e** (red).

Conversions as a function of time for hydrosilylation of phenylacetylene and tolylacetylene in the presence of **4d** and **4e** catalysts are summarized in Figure 9.2-14. Taking the phenylacetylene as an example after 149 h, the β -(Z) completely disappears, leaving 78% of β -(E) (entry 3) with **4d** and 82% with **4e** (entry 6). Selectivity behavior is in line with what observed at 25°C.

9.2.4 Addition of arylaldehydes to phenylboronic acid

Selected complexes **4a** and **4b** were also found to be active catalyst precursors for the addition of arylaldehydes to phenylboronic acid. The catalytic reactions were carried out in dimethoxyethane/water (3/1) in the presence of the aldehyde, an equimolar amount of KO^tBu and an excess of phenylboronic acid heating at +80 °C in the presence of rhodium carbene catalyst (1% mol) (Scheme 9.2-4).



Scheme 9.2-4 Addition of arylaldehydes to phenylboronic acid

Conversions and isolated yields were monitored by ¹H-NMR spectroscopy.⁵ The influence of the aldehyde has been studied using 4-chlorobenzaldehyde, 4-methoxybenzaldehyde, 3,4,5-trimethoxybenzaldehyde, 4-*tert*-butylbenzaldehyde, 4-cyanobenzaldehyde, 4-acetylbenzaldehyde. The results are summarized in Table 9.2-9.

Table 9.2-9 Addition of arylaldehydes with phenylboronic acid.

Entry	Aldehyde	Catalyst	time (h)	Conv. (%)	Yield (%)
1	4-Cl-PhCHO	4a	5	>99	78
2	4-Cl-PhCHO	4b	5	83	80
3	4-OMe-PhCHO	4a	8	42	38
4	4-OMe-PhCHO	4b	8	32	29
5	3,4,5-(tri-OMe)-PhCHO	4a	8	66	63
6	3,4,5-(tri-OMe)-PhCHO	4b	8	45	42
7	4- <i>t</i> Bu-PhCHO	4a	8	66	43
8	4- <i>t</i> Bu-PhCHO	4b	8	49	39
9	4-CN-PhCHO	4a	1	>99	87
10	4-CN-PhCHO	4b	1	96	75
11	4-C(O)Me-PhCHO	4a	2	>99	82
12	4-C(O)Me-PhCHO	4b	2	>99	80

Catalysts **4a,b** convert all the tested aldehydes in moderate to good yields. Better results have been obtained by employing the less encumbered **4a** catalyst, which showed to be faster in all the cases (e.g. TOFs for **4a** and **4b** with 4-Cl-PhCHO as substrate are 20 and 16 h⁻¹ respectively), and employing electron withdrawing -CN and -C(O)Me functionalized aldehydes (e.g. with 4-CN-PhCHO the TOF for **4a** is 99 h⁻¹) which quantitatively convert (NMR) within 2 h with high isolated yields (entries 9-12). Since the detrimental effect on the reaction rate of the steric hindrance on the NHC ligand was already demonstrated employing **4a,b** the addition of arylaldehydes with phenylboronic acid has not been tested with the other Rh(I)NHC derivatives **4c-h**. When lowering the electron deficiency of the aldehydes the conversions and reaction rates contextually decrease (entries 1-8). This behavior is in line with what reported by Miyaura for rhodium catalyzed addition

of arylboronic acid to aldehydes giving secondary alcohols, which is in general facilitated by the presence of an electron withdrawing group on the aldehydes,⁶ and with the results obtained by Imlinger and Buchmeiser for rhodium 1,3-R₂-tetrahydropyrimidin-2-ylidenes indicating the need for a highly nucleophilic metal center.⁴

9.3 Conclusions

In conclusion complexes **4a-i** were found active in the hydrosilylation of terminal alkynes and in the addition of arylaldehydes with phenylboronic acid. The best catalyst precursor is always the complex **4a**. The steric hindrance on the N-heterocyclic ligand and on the alkyne substrates proved to be detrimental for reaction rates. Steric encumbrance on the alkynes affects also selectivities: by employing hindered alkynes such as SiEt₃C≡CH or (CPh₂OH)C≡CH the hydrosilylation leads to the only formation of β-(E) and α isomers. Results obtained with catalyst **4i** demonstrated that the catalytic activity is somehow positively affected by the NHBoc substituent of the lateral chain. At the moment we are not able to justify this behavior, which could arise from the interaction between NHBoc group and the metal or the substrate during the catalytic cycle. Further studies such as DFT calculations will be explored in order to shed light on this question. Lowering the catalyst loading to 0.1 mol % of **4a**, **4d** and **4e** also provided activity at room temperature although slower kinetics were found. The same reaction performed at 60°C with **4d** and **4e** significantly decrease the reaction time, with comparable selectivities from catalyst loading of 0,1% at 25°C. The complexes **4a,b** have also been employed in the addition of arylaldehydes with phenylboronic acid and, like in the hydrosilylation case, the catalytic activity is negatively affected by the increasing steric hindrance; furthermore the best results were obtained using **4a** in the presence of aldehydes bearing electron withdrawing groups, such as 4-cyanobenzaldehyde and 4-acetylbenzaldehyde as substrates.

9.4 Experimental Part

Materials and Procedures. All reactions were carried out under Argon using standard J. Young tubes (hydrosilylation) or Schlenk techniques (addition of phenyl boronic acid to benzaldehyde). Solvents were dried and distilled under nitrogen prior to use; the deuterated solvents used, after being appropriately dried and degassed were stored in ampoules under argon on 4Å molecular sieves. The NMR spectra were recorded using Varian Inova 300 (¹H, 300.1; ¹³C, 75.5 MHz), Varian MercuryPlus VX 400 (¹H, 399.9; ¹³C, 100.6 MHz) instruments. The spectra were referenced internally to residual solvent resonances, full ¹H and ¹³C NMR assignments were done, when necessary. Phenylacetylene, 1-hexyne, 4-ethynyl-toluene, triethylsililacetylene, 1,1-Diphenyl-2-propyn-1-ol, dimethyphenylsilane, 4-chlorobenzaldehyde, 4-methoxybenzaldehyde, 3,4,5-

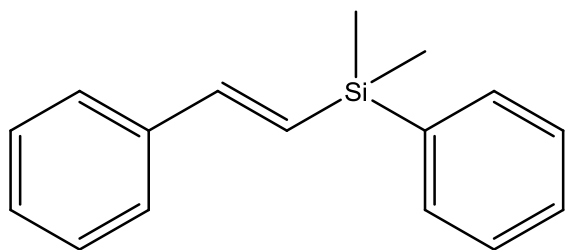
trimethoxybenzaldehyde, 4-*tert*-butylbenzaldehyde, 4-cyanobenzaldehyde, 4-acetylbenzaldehyde, phenylboronic acid were used as purchased from Sigma Aldrich.

9.4.1 General procedure for the Hydrosilylation of 1-Alkynes with HSiMe₂Ph

A J.Young valve NMR tube was charged under argon with the catalyst precursor (**4a-c**) (7.7×10^{-4} mmol or 7.7×10^{-5} mmol), CDCl₃ (0.6 mL), the corresponding alkyne (PhC≡CH, TolC≡CH, ⁿBuC≡CH, Et₃SiC≡CH or (CPh₂OH)C≡CH) (0.077 mmol), and a slight excess of HSiMe₂Ph (0.085 mmol). The solution was kept at T = 25°C or at 60°C and monitored by ¹H-NMR spectroscopy.

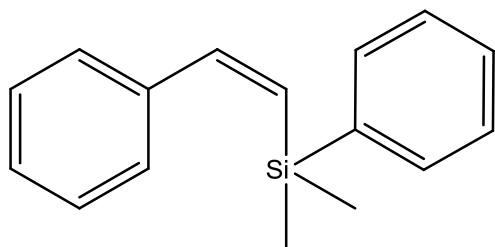
Further details on the NMR spectra and integrations are collected in Appendix 9.5.

9.4.2 Hydrosilylation products: ¹H-NMR characterizations.



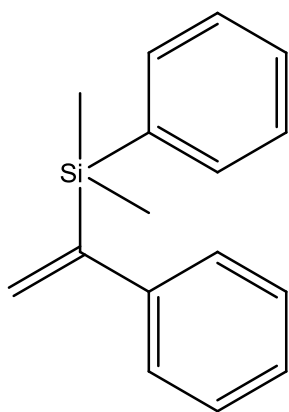
(E)-2- (dimethyl(phenyl)silyl)-1-phenyl-ethene (**1s**)⁷

¹H NMR (CDCl₃, 300 MHz): δ 7.6-7.2 (m, 5H), 7.0 (d, $J_{\text{H,H}} = 19$ Hz, 1H), 6.6 (d, $J_{\text{H,H}} = 19$ Hz, 1H), 0.36 (s, 6H) ppm.



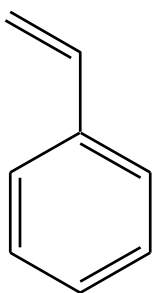
(Z)-2- (dimethyl(phenyl)silyl)-1-phenyl-ethene (**2s**)⁸

¹H NMR (CDCl₃, 300 MHz): δ 7.6-7.2 (m, 5H), 7.5 (d, $J_{\text{H,H}} = 15$ Hz, 1H), 6.0 (d, $J_{\text{H,H}} = 15$ Hz, 1H), 0.36 (s, 6H) ppm.



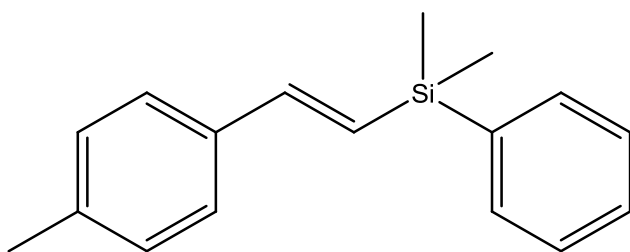
1-(dimethyl(phenyl)silyl)-1-phenyl-ethene (3s)⁷

¹H NMR (CDCl₃, 300 MHz): δ 7.6-7.3 (m, 5H), 5.98 (d, $J_{\text{H,H}} = 2.9$ Hz, 1H), 5.66 (d, $J_{\text{H,H}} = 2.9$ Hz, 1H), 0.41 (s, 6H) ppm.



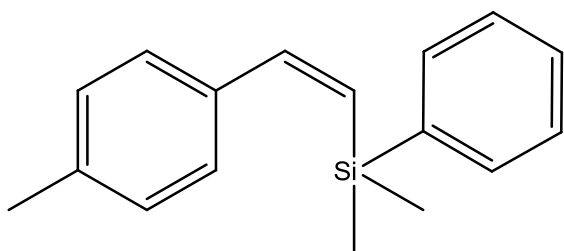
Styrene (4s)

¹H NMR (CDCl₃, 300 MHz): δ 7.50-7.10 (m, 5H), 6.69 (dd, $J_{\text{H,H}} = 18.0, 11.0$ Hz, 1H), 5.74 (d, $J_{\text{H,H}} = 18.0$, 1H), 5.22 (d, $J_{\text{H,H}} = 11.0$ Hz, 1H).



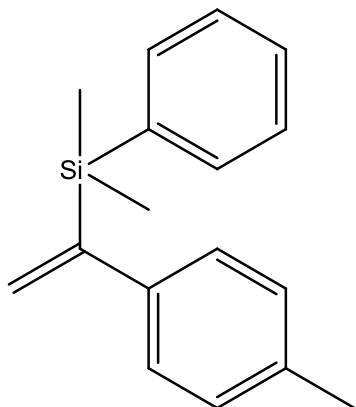
(E)-2-(dimethyl(phenyl)silyl)-1-Tolyl-ethene (5s)

¹H-NMR (CDCl₃): δ 7.60-7.16 (m, 9H), 6.96 (d, $J_{\text{H,H}} = 19.2$ Hz, 1H), 6.45 (d, $J_{\text{H,H}} = 19.2$ Hz, 1H), 2.36 (s, 3H), 0.49 (s, 6H) ppm.



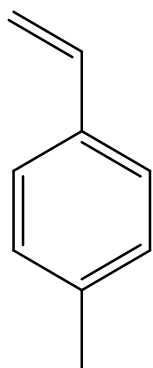
(Z)-2- (dimethyl(phenyl)silyl)-1-Tolyl-ethene (6s)⁹

¹H-NMR (CDCl₃): δ 7.60–7.52 (m, 2H), 7.43 (d, $J_{\text{H,H}} = 15.3$ Hz, 1H), 7.38–7.32 (m, 3H), 7.13 (d, $J_{\text{H,H}} = 8.1$ Hz, 2H), 7.06 (d, $J_{\text{H,H}} = 8.1$ Hz, 2H), 5.96 (d, $J_{\text{H,H}} = 15.0$ Hz, 1H), 2.30 (s, 3H), 0.28 (s, 6H) ppm.



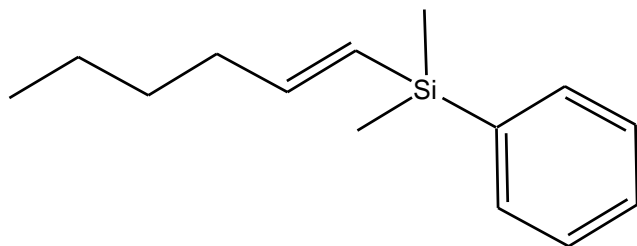
1-(dimethyl(phenyl)silyl)-1-Tolyl-ethene (7s)

¹H NMR (CDCl₃, 300 MHz): δ 7.6-7.3 (m, 4H), 5.93 (d, 1H, $J_{\text{H,H}} = 2.9$ Hz), 5.66 (d, 1H, $J_{\text{H,H}} = 2.9$ Hz), 2.35 (s, 3H), 0.30 (s, 6H) ppm.



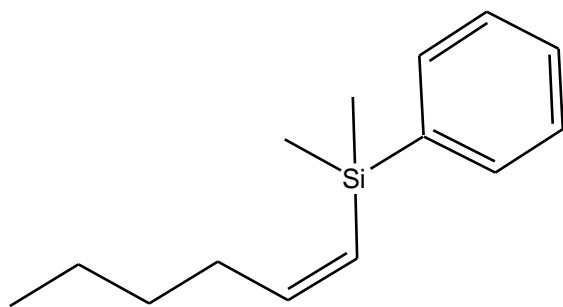
4-Methylstyrene (8s)

$^1\text{H NMR}$ (CDCl_3 , 300 MHz): δ 7.39 (d, $J_{\text{H,H}} = 8.0$ Hz, 2H), 7.20 (d, $J_{\text{H,H}} = 8.0$ Hz, 2H), 6.77 (dd, $J_{\text{H,H}} = 18.0, 11.0$ Hz, 1H), 5.78 (d, $J_{\text{H,H}} = 18.0$, 1H), 5.26 (d, $J_{\text{H,H}} = 11.0$ Hz, 1H), 2.41 (s, 3H).



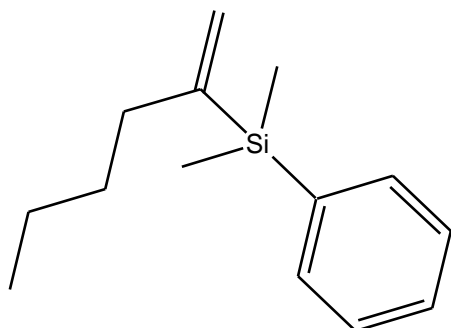
(E)-2- (dimethyl(phenyl)silyl)-1-hexene (9s)¹⁰

$^1\text{H NMR}$ (CDCl_3 , 300 MHz): δ 7.7-7.3 (m, 5H), 6.1 (dt, 1H, $J_{\text{H,H}} = 19$ Hz, 6.2 Hz, $\text{CH}_2\text{CH}=\text{}$), 5.7 (d, 1H, $J_{\text{H,H}} = 19$ Hz, $\text{SiCH}=\text{}$), 2.2-0.8 (m, 9H, ^nBu), 0.30 (s, 6H, SiMe_2) ppm.



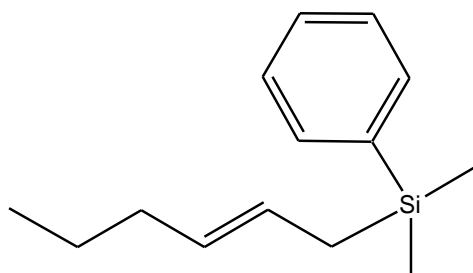
(Z)-2- (dimethyl(phenyl)silyl)-2-hexene (10s)¹⁰

$^1\text{H NMR}$ (CDCl_3 , 300 MHz): δ 7.7-7.3 (m, 5H, Ph), 6.4 (dt, 1H, $J_{\text{H,H}} = 14, 7.4$ Hz, $^n\text{BuCH}=\text{}$), 5.6 (d, 1H, $J_{\text{H,H}} = 14$ Hz), 2.2-0.8 (m, 9H, ^nBu), 0.38 (s, 6H, SiMe_2) ppm.



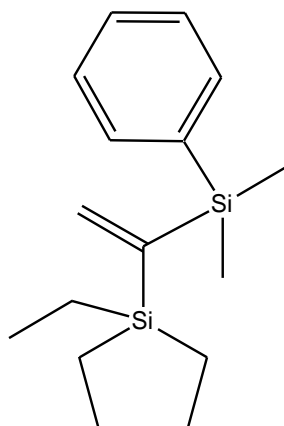
2-(dimethyl(phenyl)silyl)-1-hexene (11s)¹⁰

$^1\text{H NMR}$ (CDCl_3 , 300 MHz): δ 7.7-7.3 (m, 5H), 5.76 (d, 1H, $J_{\text{H,H}} = 2.9$ Hz), 5.38 (d, 1H, $J_{\text{H,H}} = 2.9$ Hz), 2.2-0.8 (m, 9H), 0.41 (s, 6H, SiMe_2) ppm.



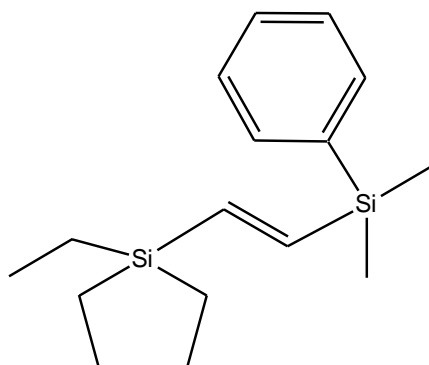
(E)-1-(Dimethylphenylsilyl)hex-2-ene (12s)¹¹

¹H NMR (CDCl₃, 300 MHz): δ 7.7-7.3 (m, 5H), 5.45-5.24 (m, 2H, =CHCH₂CH₂, =CHCH₂Si), 2.2-0.8 (m, 9H, CH₂CH₂CH₃, CH₂Si), 0.47 (s, 6H, SiMe₂) ppm.



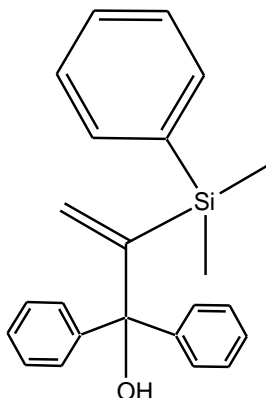
1-(Dimethylphenylsilyl)-1-(triethylsilyl)ethene (13s)¹²

¹H NMR (CDCl₃, 300 MHz): δ 7.35-7.19 (m, 5H, Ph), AB system (δ_A = 6.40, δ_B = 6.42, J_{A,B} = 5.2, 2H, CH), 0.64 (t, J_{H,H} = 7.8 Hz, 6H, CH₂), 0.32 (q, J_{H,H} = 7.8 Hz, 9H, CH₃), 0.19 (s, 6H, CH₃).



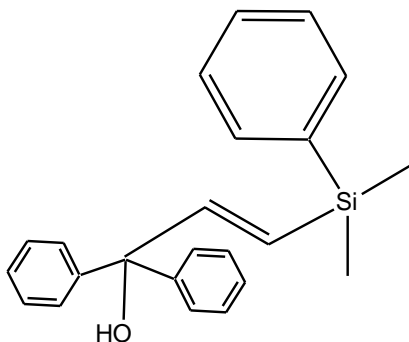
(E)-2-(Dimethylphenylsilyl)-1-(triethylsilyl)ethene (14s)¹²

$^1\text{H NMR}$ (CDCl_3 , 300 MHz): δ 7.32-7.15 (m, 5H, Ph), AB system ($\delta_{\text{A}} = 6.76$, $\delta_{\text{B}} = 6.65$, $J_{\text{A,B}} = 22.8$, 2H, CH), 0.76 (t, $J_{\text{H,H}} = 8.0$ Hz, 6H, CH_2), 0.41 (q, $J_{\text{H,H}} = 8.0$ Hz, 9H, CH_3), 0.15 (s, 6H, CH_3).



1-(Dimethylphenylsilyl)-1-(CPh₂OH) ethane (15s)¹³

$^1\text{H NMR}$ (CDCl_3 , 300 MHz): δ 7.77-7.24 (m, 15H, Ph), 5.72 (d, $J_{\text{H,H}} = 1.8$, 1H, CH_2), 5.28 (d, $J_{\text{H,H}} = 1.8$, 1H, CH_2), 0.39 (s, 6H, CH_3).



(E)-2-(Dimethylphenylsilyl)-1-(CPh₂OH) ethene (16s)

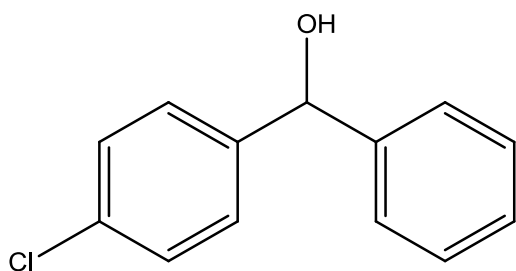
$^1\text{H NMR}$ (CDCl_3 , 300 MHz): δ 7.77-7.24 (m, 15H, Ph), 6.74 (d, $J_{\text{H,H}} = 18.8$, 1H, $=\text{CHCPh}_2\text{OH}$), 6.16 (d, $J_{\text{H,H}} = 18.8$, 1H, $=\text{CHSi}$), 0.35 (s, 6H, CH_3).

1.4.2 General procedure for the addition of arylaldehydes with phenylboronic acid.

Phenylboronic acid (0.600 g, 4.9 mmol), KO^tBu (2.45 mmol), the substituted aldehyde (4-chlorobenzaldehyde, 4-methoxybenzaldehyde, 3,4,5-trimethoxybenzaldehyde, 4-*tert*-butylbenzaldehyde, 4-cyanobenzaldehyde, 4-acetylbenzaldehyde) (2.45 mmol) the rhodium catalyst **4a** or **4b** (1% mol) and dimethoxyethane (7.5 mL) were introduced in a Schlenk tube and then

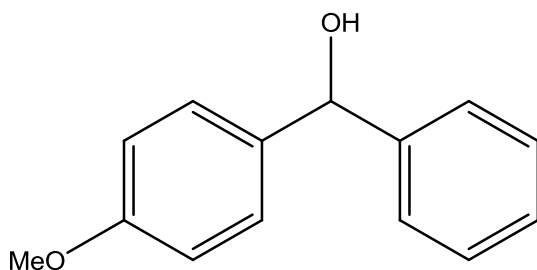
degassed H₂O (2.5 mL) was added. The resulting mixture was heated for 1-8 h at 80°C, cooled to ambient temperature, extracted with ethyl acetate (20 mL). After drying over Na₂SO₄ the organic phase was evaporated and the residue was purified by flash chromatography. The isolated yield has checked by ¹H-NMR spectroscopy. The reaction were identified by NMR comparison with literature reported data.¹⁰

Addition of arylaldehydes to phenylboronic acid products: ¹H-NMR characterizations.



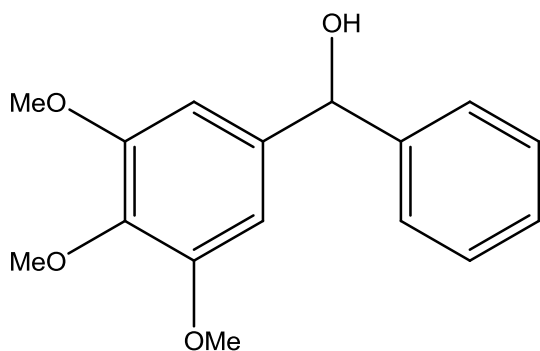
4-Chlorophenyl(phenyl)methanol⁵

¹H NMR (300 MHz, CDCl₃): δ 7.35-7.23 (m, 9H), 5.81 (br s, 1H), 2.22 (s, 1H) ppm. ¹³C NMR (75 MHz, CDCl₃): δ 143.3, 142.1, 133.1, 128.5, 128.4, 127.8, 127.7, 126.4, 75.3 ppm.



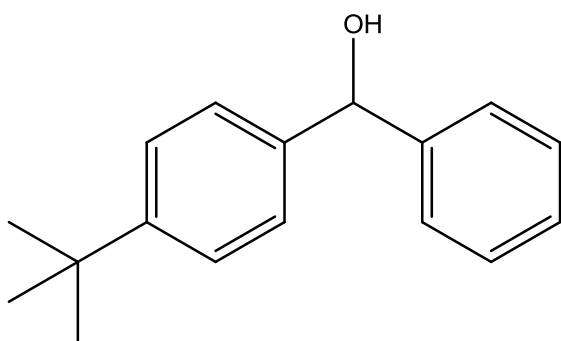
4-Methoxyphenyl(phenyl)methanol⁵

¹H NMR (300 MHz, CDCl₃): δ 7.39-7.26 (m, 7H), 6.89-6.85 (m, 2H), 5.82 (brs, 1H), 3.79 (s, 3H), 2.14 (brs, 1H) ppm. ¹³C NMR (75 MHz, CDCl₃): δ 159.0, 144.0, 136.2, 128.4, 127.9, 127.3, 126.4, 113.9, 75.8, 55.2 ppm.



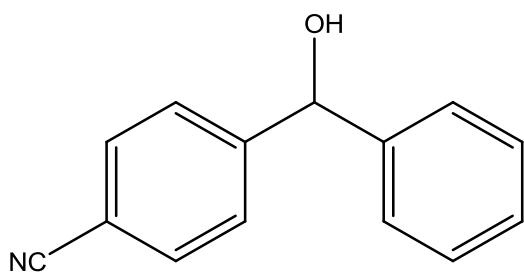
3,4,5 tri-methoxyphenyl(phenyl)methanol⁵

¹H-NMR (CDCl₃, 300 MHz) δ 7.39-7.19 (m, 3H), 6.61 (m, 2H), 5.78 (br s, 1H), 3.93 (s, 3H), 3.82 (s, 6H), 2.20 (s, 1H) ppm. ¹³C-NMR (CDCl₃, 75 MHz): δ 129.0, 127.9, 127.3, 105.0, 76.7, 60.8, 56.1 ppm.



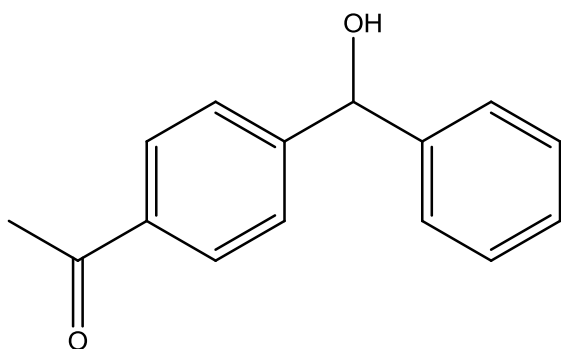
4-tert-Butylphenyl(phenyl)methanol⁵

¹H NMR (300 MHz, CDCl₃): δ 7.44–7.28 (m, 9H), 5.85 (br s, 1H), 2.06 (br s, 1H), 1.39 (s, 9H) ppm.



4-Cyanophenyl(phenyl)methanol⁵

¹H NMR (300 MHz, CDCl₃): δ 7.53 (m, 2H), 7.45 (m, 2H), 7.33-7.23 (m, 5H), 5.78 (s, 1H), 3.05 (br s, 1H) ppm. ¹³C NMR (75 MHz, CDCl₃): δ 148.9, 142.7, 132.1, 128.7, 128.0, 126.9, 126.5, 118.7, 110.7, 75.3 ppm.



4-Acetylphenyl(phenyl)methanol⁵

¹H NMR (300 MHz, CDCl₃): δ 7.93-7.91 (m, 2H), 7.51-7.49 (m, 2H), 7.37-7.26 (m, 5H), 5.89 (s, 1H), 2.57 (s, 3H), 2.40 (s, 1H), ppm. ¹³C NMR (75 MHz, CDCl₃): δ 198.2, 149.2, 143.2, 135.8, 128.5, 128.4, 127.6, 126.5, 126.4, 75.5, 26.4 ppm.

¹ Jimenez, M. V.; Perez-Torrente, J. J.; Bartolomè, M. I.; Gierz, V.; Lahoz, F. J.; Oro, L. A.; *Organometallics*, **2008**, *27*, 224

² Jun, C. H.; Crabtree, R. H. *J. Organomet. Chem.* **1993**, *447*, 177

³ (a) Poyatos, M.; Mas-Marzà, E.; Mata, J. A.; Sanau, M.; Peris, E. *Eur. J. Inorg. Chem.* **2003**, 1215. (b) Ojima, I.; Clos, N.; Donovan, R. J.; Ingallina, P. *Organometallics* **1990**, *9*, 3127.

⁴ de Bo, G.; Berthoz-Gelloz, G.; Tinant, B.; Markò, I. E. *Organometallics* **2006**, *25*, 1881.

⁵ The secondary alcohol derivatives were unambiguously characterized by comparison with literature NMR spectra. (a) Xing, C-H.; Hu, Q-S. *Tetrahedron Lett.* **2010**, *51*, 924. (b) Kuriyama, M.; Ishiyama, N.; Shimazawa, R.; Onomura O. *Tetrahedron*, **2010**, *66*, 6814. (c) Krasovskiy, A.; Straub, B. F.; Knochel, P. *Angew. Chem., Int. Ed.*, **2005**, *45*, 159. (d) Umeda, R.; Studer, A. *Org. Lett.* **2008**, *10*, 993..

⁶ (a) Yoshida, K.; Hayashi, T. In *Boronic Acids*; Hall, D. G., Ed.; Wiley-VCH: Weinheim, 2005; Chapter 4, pp 172. (b) Sakai, M.; Ueda, M.; Miyaura, N. *Angew. Chem., Int. Ed.* 1998, *37*, 3279

⁷ Nakamura, S.; Uchiyama, M.; Ohwada T. *J. Am. Chem. Soc.* **2004**, *126*, 11146.

⁸ Nishihara, Y.; Saito, D.; Tanemura, K.; Noyori, S.; Takagi K. *Org. Lett.* **2009**, *11*, 3546.

⁹ Katayama, H.; Taniguchi, K.; Kobayashi, M.; Sagawa T. *J. Organomet. Chem.* **2002**, *645*, 192.

¹⁰ Jun, C. H.; Crabtree R. H. *J. Organomet. Chem.* **1993**, *447*, 177.

¹¹ Schwieger, S.; Herzog, R.; Wagner, C.; Steinborn D. *J. Organomet. Chem.* **2009**, *694*, 3548.

¹² Jimenez, M. V.; Perez-Torrente, J. J.; Bartolome, M. I.; Gierz, V.; Lahoz, F. J.; Oro L. A. *Organometallics* **2008**, *27*, 224.

¹³ Takeuchi, R.; Nitta, S.; Watanabe D. *J. Org. Chem.* **1996**, *60*, 3045.

9.5 Appendix

9.5.1 Tables

Table 9.5-1 Hydrosilylation of phenylacetylene at 25°C with a catalyst loading of 1%.

Entry	Alkyne	cat	Time (h)	Conv. (%)	β E (%)	β Z (%)	α (%)	alkene (%)
1	PhC \equiv CH	4a	0	80	29	56	15	0
2	PhC \equiv CH	4a	2	95	21	63	16	0
3	PhC \equiv CH	4a	6	>99	41	41	13	5
4	PhC \equiv CH	4a	8	>99	44	32	14	10
5	PhC \equiv CH	4a	22	>99	45	30	15	10
6	PhC \equiv CH	4a	77	>99	47	28	14	11
7	PhC \equiv CH	4a	192	>99	74	0	14	12
8	PhC \equiv CH	4b	0	66	23	51	11	15
9	PhC \equiv CH	4b	2	79	24	50	15	11
10	PhC \equiv CH	4b	6	87	25	53	12	10
11	PhC \equiv CH	4b	8	89	26	51	13	10
12	PhC \equiv CH	4b	22	>99	51	24	15	10
13	PhC \equiv CH	4b	48	>99	62	15	14	9
14	PhC \equiv CH	4b	192	>99	75	0	15	10
15	PhC \equiv CH	4c	0	0	0	0	0	0
16	PhC \equiv CH	4c	2	26	32	19	21	28
17	PhC \equiv CH	4c	6	35	29	30	19	22
18	PhC \equiv CH	4c	9	45	28	39	15	18
19	PhC \equiv CH	4c	24	69	28	51	14	7
20	PhC \equiv CH	4c	50	83	34	41	15	10
21	PhC \equiv CH	4c	144	>99	57	17	16	10
22	PhC \equiv CH	4c	192	>99	74	0	16	10
23	PhC \equiv CH	4d	2	34	33	50	12	5
24	PhC \equiv CH	4d	4	67	28	60	11	1
25	PhC \equiv CH	4d	21	>99	25	63	10	2
26	PhC \equiv CH	4d	24	>99	26	62	10	2
27	PhC \equiv CH	4d	66	>99	41	45	10	4
28	PhC \equiv CH	4d	81	>99	43	44	9	4
29	PhC \equiv CH	4d	165	>99	52	35	9	4
30	PhC \equiv CH	4d	189	>99	55	32	9	4
31	PhC \equiv CH	4d	263	>99	65	22	9	4
32	PhC \equiv CH	4d	335	>99	74	13	9	4
33	PhC \equiv CH	4h	22	31	20	60	14	6
34	PhC \equiv CH	4h	24	32	19	55	11	5
35	PhC \equiv CH	4h	70	98	13	78	7	2
36	PhC \equiv CH	4h	142	>99	39	51	8	2

37	PhC≡CH	4h	166	>99	40	50	8	2
38	PhC≡CH	4h	214	>99	41	44	7	2
39	PhC≡CH	4h	244	>99	46	43	7	4
40	PhC≡CH	4i	1	8	26	62	12	0
41	PhC≡CH	4i	3	54	20	70	9	1
42	PhC≡CH	4i	4	77	22	63	10	5
43	PhC≡CH	4i	7	91	22	63	10	5
44	PhC≡CH	4i	22	>99	26	60	10	4
45	PhC≡CH	4i	27	>99	35	51	10	4
46	PhC≡CH	4i	49	>99	41	43	10	5
47	PhC≡CH	4i	70	>99	46	39	10	5

Table 9.5-2 Hydrosilylation of tolylacetylene at 25°C with a catalyst loading of 1%.

Entry	Alkyne	cat	Time (h)	Conv. (%NMR)	% β (E)	% β (Z)	% α	% alkene
1	TolC≡CH	4a	2	48	31	58	11	0
2	TolC≡CH	4a	4	78	30	61	9	0
3	TolC≡CH	4a	21	>99	34	55	11	0
4	TolC≡CH	4a	24	>99	36	53	11	0
5	TolC≡CH	4a	45	>99	53	36	11	0
6	TolC≡CH	4a	66	>99	63	24	13	0
7	TolC≡CH	4a	165	>99	78	8	14	0
8	TolC≡CH	4a	189	>99	80	7	13	0
9	TolC≡CH	4a	263	>99	85	5	14	0
10	TolC≡CH	4a	335	>99	85	0	15	0
11	TolC≡CH	4b	0	54	35	49	16	0
12	TolC≡CH	4b	2	76	27	48	13	12
13	TolC≡CH	4b	6	87	35	40	12	13
14	TolC≡CH	4b	8	89	40	36	14	10
15	TolC≡CH	4b	22	>99	62	17	13	8
16	TolC≡CH	4b	48	>99	71	8	12	9
17	TolC≡CH	4b	192	>99	73	0	14	13
18	TolC≡CH	4c	0	0	0	0	0	0
19	TolC≡CH	4c	2	26	43	27	30	0
20	TolC≡CH	4c	6	40	31	33	20	16
21	TolC≡CH	4c	9	46	31	39	16	14
22	TolC≡CH	4c	24	75	46	28	16	10
23	TolC≡CH	4c	50	87	66	11	14	9
24	TolC≡CH	4c	144	>99	68	8	14	10
25	TolC≡CH	4c	192	>99	76	0	14	10
26	TolC≡CH	4h	22	74	11	82	7	0
27	TolC≡CH	4h	24	79	11	82	7	0

28	TolC≡CH	4h	70	>99	25	70	5	0
29	TolC≡CH	4h	142	>99	54	38	5	3
30	TolC≡CH	4h	166	>99	61	31	5	3
31	TolC≡CH	4h	214	>99	70	22	5	3
32	TolC≡CH	4h	244	>99	75	17	5	3
33	TolC≡CH	4i	1	7	10	80	10	0
34	TolC≡CH	4i	3	71	25	68	7	0
35	TolC≡CH	4i	5	82	22	66	8	4
36	TolC≡CH	4i	7	93	24	65	8	3
37	TolC≡CH	4i	22	>99	36	51	9	4
38	TolC≡CH	4i	27	>99	46	41	9	4
39	TolC≡CH	4i	49	>99	67	17	9	7
40	TolC≡CH	4i	70	>99	79	5	9	7

Table 9.5-3 Hydrosilylation of Et₃SiC≡CH and (CPh₂OH)C≡CH at 25°C with a catalyst loading of 1%.

Entry	Alkyne	cat	Time (h)	Conv. (%NMR)	% β (E)	% α
1	Et ₃ SiC≡CH	4a	2	96	47	53
2	Et ₃ SiC≡CH	4a	4	>99	53	47
3	Et ₃ SiC≡CH	4a	21	>99	52	48
4	Et ₃ SiC≡CH	4a	24	>99	52	48
5	Et ₃ SiC≡CH	4a	45	>99	51	49
6	Et ₃ SiC≡CH	4a	66	>99	52	48
7	(CPh ₂ OH)C≡CH	4a	0	31	61	39
8	(CPh ₂ OH)C≡CH	4a	2	47	67	33
9	(CPh ₂ OH)C≡CH	4a	6	50	68	32
10	(CPh ₂ OH)C≡CH	4a	9	59	70	30
11	(CPh ₂ OH)C≡CH	4a	24	85	69	31
12	(CPh ₂ OH)C≡CH	4a	50	85	69	31
13	(CPh ₂ OH)C≡CH	4a	147	>99	69	31
14	Et ₃ SiC≡CH	4d	2	96	47	53
15	Et ₃ SiC≡CH	4d	4	99	53	47
16	Et ₃ SiC≡CH	4d	21	>99	52	48

Table 9.5-4 Hydrosilylation of *n*BuC≡CH: at 25°C with a catalyst loading of 1%.

Entry	Alkyne	Cat	time	Conv.	% β (E)	% β (Z)	% α	% allyl
--------------	---------------	------------	-------------	--------------	----------------	----------------	------------	----------------

			(h)	(%NMR)				
1	<i>n</i> BuC≡CH	4a	0,3	10	30	44	26	0
2	<i>n</i> BuC≡CH	4a	2	48	32	41	27	0
3	<i>n</i> BuC≡CH	4a	6	>99	43	19	22	16
4	<i>n</i> BuC≡CH	4a	8	>99	50	7	22	21
5	<i>n</i> BuC≡CH	4a	22	>99	49	0	20	31
6	<i>n</i> BuC≡CH	4a	77	>99	47	0	18	35
7	<i>n</i> BuC≡CH	4b	0,3	0	0	0	0	0
8	<i>n</i> BuC≡CH	4b	2	32	42	58	0	0
9	<i>n</i> BuC≡CH	4b	6	37	40	35	25	0
10	<i>n</i> BuC≡CH	4b	22	58	38	38	24	0
11	<i>n</i> BuC≡CH	4b	48	94	32	42	26	0
12	<i>n</i> BuC≡CH	4b	192	>99	44	0	16	40
13	<i>n</i> BuC≡CH	4c	0,3	0	0	0	0	0
14	<i>n</i> BuC≡CH	4c	2	0	0	0	0	0
15	<i>n</i> BuC≡CH	4c	6	0	0	0	0	0
16	<i>n</i> BuC≡CH	4c	9	0	0	0	0	0
17	<i>n</i> BuC≡CH	4c	24	26	37	42	21	0
18	<i>n</i> BuC≡CH	4c	50	75	33	31	36	0
19	<i>n</i> BuC≡CH	4c	144	>99	37	0	17	46

Table 9.5-5 Hydrosilylation of phenylacetylene at 25°C with a catalyst loading of 0,1%.

Entry	Alkyne	cat	Time (h)	% Conversion	% β (E)	% β (Z)	% α	% alkene
1	PhC≡CH	4a	0,3	69	40	20	20	20
2	PhC≡CH	4a	2	72	45	15	22	20
3	PhC≡CH	4a	6	78	50	10	20	20
4	PhC≡CH	4a	12	83	54	6	20	20
5	PhC≡CH	4a	52	>99	60	0	20	20
6	PhC≡CH	4d	1	0	0	0	0	0
7	PhC≡CH	4d	2	0	0	0	0	0
8	PhC≡CH	4d	4	0	0	0	0	0
9	PhC≡CH	4d	6	0	0	0	0	0
10	PhC≡CH	4d	8	0	0	0	0	0
11	PhC≡CH	4d	74	30	22	65	8	5
12	PhC≡CH	4d	121	44	35	51	8	6
13	PhC≡CH	4d	169	53	48	42	7	4
14	PhC≡CH	4d	241	60	65	25	7	3
15	PhC≡CH	4d	288	64	71	17	7	5
16	PhC≡CH	4d	312	64	76	12	6	6
17	PhC≡CH	4d	408	64	88	1	5	6
18	PhC≡CH	4d	504	64	88	1	5	6

19	PhC≡CH	4d	576	68	87	2	5	6
20	PhC≡CH	4d	648	68	88	4	4	4
21	PhC≡CH	4d	768	76	89	1	5	5
22	PhC≡CH	4d	912	82	89	2	4	5
23	PhC≡CH	4d	1080	87	90	1	4	5
24	PhC≡CH	4e	1	0	0	0	0	0
25	PhC≡CH	4e	2	0	0	0	0	0
26	PhC≡CH	4e	4	0	0	0	0	0
27	PhC≡CH	4e	6	0	0	0	0	0
28	PhC≡CH	4e	8	0	0	0	0	0
29	PhC≡CH	4e	74	23	31	55	13	1
30	PhC≡CH	4e	121	42	31	55	13	1
31	PhC≡CH	4e	169	58	30	55	12	3
32	PhC≡CH	4e	241	66	34	49	13	4
33	PhC≡CH	4e	265	66	39	48	11	2
34	PhC≡CH	4e	288	72	38	45	12	5
35	PhC≡CH	4e	312	72	40	43	12	3
36	PhC≡CH	4e	504	77	54	32	10	3
37	PhC≡CH	4e	576	78	59	26	11	4
38	PhC≡CH	4e	648	80	60	25	10	5
39	PhC≡CH	4e	768	83	68	18	10	4
40	PhC≡CH	4e	912	88	73	12	10	5
41	PhC≡CH	4e	1080	91	76	8	11	5

Table 9.5-6 Hydrosilylation of tolylacetylene at 25°C with a catalyst loading of 0,1%.

Entry	Alkyne	cat	Time (h)	Conv. (%NMR)	% β (E)	% β (Z)	% α	% alkene
1	TolC≡CH	4a	0,3	47	26	51	23	0
2	TolC≡CH	4a	2	68	30	48	18	4
3	TolC≡CH	4a	6	89	54	26	15	5
4	TolC≡CH	4a	12	>99	66	13	15	6
5	TolC≡CH	4a	52	>99	79	0	14	7
6	TolC≡CH	4d	1	0	0	0	0	0
7	TolC≡CH	4d	2	0	0	0	0	0
8	TolC≡CH	4d	4	0	0	0	0	0
9	TolC≡CH	4d	6	0	0	0	0	0
10	TolC≡CH	4d	8	0	0	0	0	0
11	TolC≡CH	4d	74	49	32	58	8	2
12	TolC≡CH	4d	121	71	57	34	6	3
13	TolC≡CH	4d	169	80	67	23	5	5
14	TolC≡CH	4d	241	87	84	7	4	5
15	TolC≡CH	4d	265	89	88	3	5	4

16	TolC≡CH	4d	288	91	87	4	4	5
17	TolC≡CH	4d	312	93	88	3	4	5
18	TolC≡CH	4d	408	95	89	2	4	5
19	TolC≡CH	4d	504	97	89	2	5	4
20	TolC≡CH	4d	576	97	89	2	4	5
21	TolC≡CH	4d	648	100	90	1	3	6
22	TolC≡CH	4d	768	100	91	1	3	6
23	TolC≡CH	4e	1	0	0	0	0	0
24	TolC≡CH	4e	2	0	0	0	0	0
25	TolC≡CH	4e	4	0	0	0	0	0
26	TolC≡CH	4e	6	0	0	0	0	0
27	TolC≡CH	4e	8	0	0	0	0	0
28	TolC≡CH	4e	74	23	43	41	16	0
29	TolC≡CH	4e	121	78	37	40	14	3
30	TolC≡CH	4e	169	85	49	28	13	3
31	TolC≡CH	4e	241	91	71	10	16	3
32	TolC≡CH	4e	265	93	78	4	15	3
33	TolC≡CH	4e	288	95	78	5	14	3
34	TolC≡CH	4e	312	96	80	1	15	4
35	TolC≡CH	4e	408	96	81	1	14	4
36	TolC≡CH	4e	504	98	81	1	14	4
37	TolC≡CH	4e	648	98	80	1	15	4

Table 9.5-7 Hydrosilylation of phenylacetylene at 60°C with a catalytic loading of 0,1%: significant data for complexes **4d** and **4e**

Entry	Alkyne	cat	Time (h)	% Conversion	% β (E)	% β (Z)	% α	% alkene
1	PhC≡CH	4d	1	12	56	13	26	5
2	PhC≡CH	4d	2	25	44	26	21	9
3	PhC≡CH	4d	19	87	49	30	16	5
4	PhC≡CH	4d	23	89	55	24	16	5
5	PhC≡CH	4d	71	99	71	9	15	5
6	PhC≡CH	4d	80	>99	71	9	16	4
7	PhC≡CH	4d	95	>99	71	9	15	5
8	PhC≡CH	4d	149	>99	79	0	16	5
9	PhC≡CH	4d	245	>99	78	0	16	6
10	PhC≡CH	4e	1	8	43	27	15	15
11	PhC≡CH	4e	2	24	35	25	30	10
12	PhC≡CH	4e	19	66	44	31	20	5
13	PhC≡CH	4e	23	66	47	31	19	3
14	PhC≡CH	4e	71	82	77	4	15	4
15	PhC≡CH	4e	80	85	78	4	15	3
16	PhC≡CH	4e	95	91	78	3	15	4

17	PhC≡CH	4e	149	>99	82	0	14	4
18	PhC≡CH	4e	245	>99	83	0	15	2

Table 9.5-8 Hydrosilylation of tolylacetylene at 60°C with a catalytic loading of 0,1%: significant data for complexes **4d** and **4e**

Entry	Alkyne	cat	Time (h)	% Conversion	% β (E)	% β (Z)	% α	% alkene
1	TolC≡CH	4d	1	21	39	41	21	0
2	TolC≡CH	4d	2	46	34	46	17	2
3	TolC≡CH	4d	19	94	75	4	17	5
4	TolC≡CH	4d	23	98	71	6	18	0
5	TolC≡CH	4d	71	>99	81	0	19	0
6	TolC≡CH	4d	80	>99	81	0	19	0
7	TolC≡CH	4d	95	>99	82	0	18	0
8	TolC≡CH	4d	149	>99	85	0	15	0
9	TolC≡CH	4d	173	>99	85	0	15	0
10	TolC≡CH	4e	1	18	41	38	21	0
11	TolC≡CH	4e	2	23	31	51	19	0
12	TolC≡CH	4e	19	72	71	12	14	4
13	TolC≡CH	4e	23	80	70	13	13	4
14	TolC≡CH	4e	71	>99	83	0	13	4
15	TolC≡CH	4e	80	>99	83	0	13	4
16	TolC≡CH	4e	95	>99	83	0	12	5
17	TolC≡CH	4e	149	>99	83	0	12	5
18	TolC≡CH	4e	173	>99	83	0	13	4
19	TolC≡CH	4e	245	>99	83	0	12	5

9.5.2 Graphics

Catalyst loading of 1% at 25°C

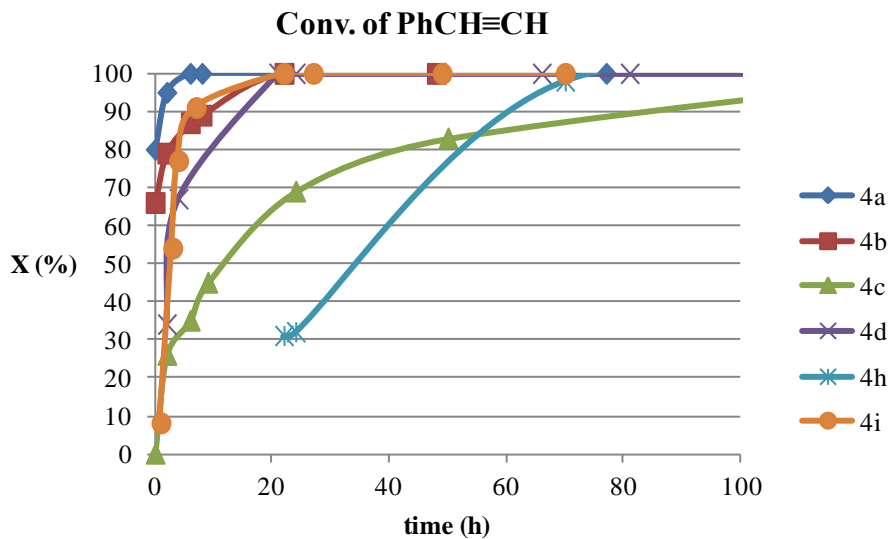


Figure 9.5-1 Conversion of PhCH≡CH catalyst loading 1% at 25°C

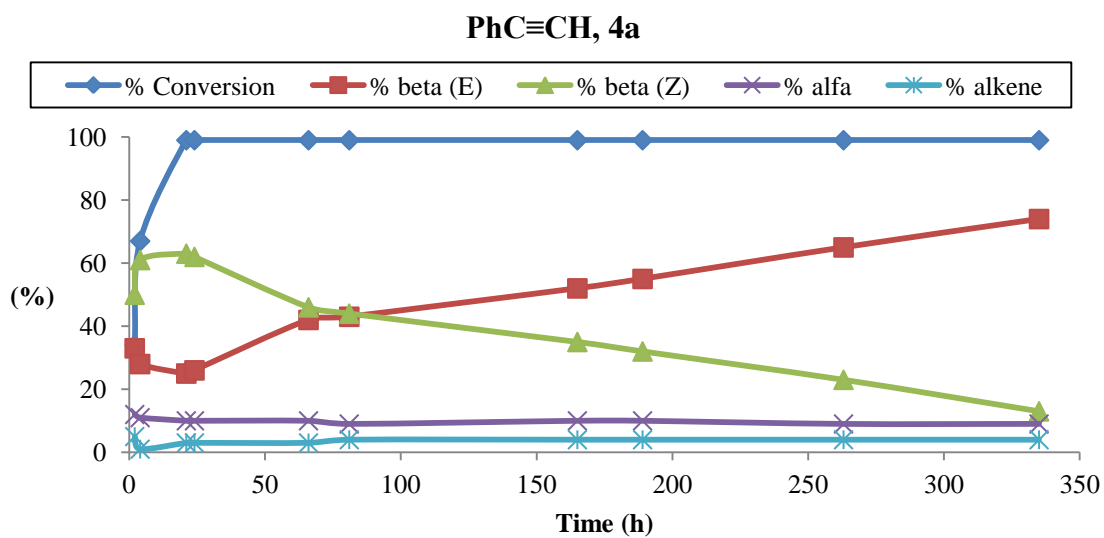


Figure 9.5-2 Conversion and selectivities for PhC≡CH with catalyst loading of 1% at 25°C

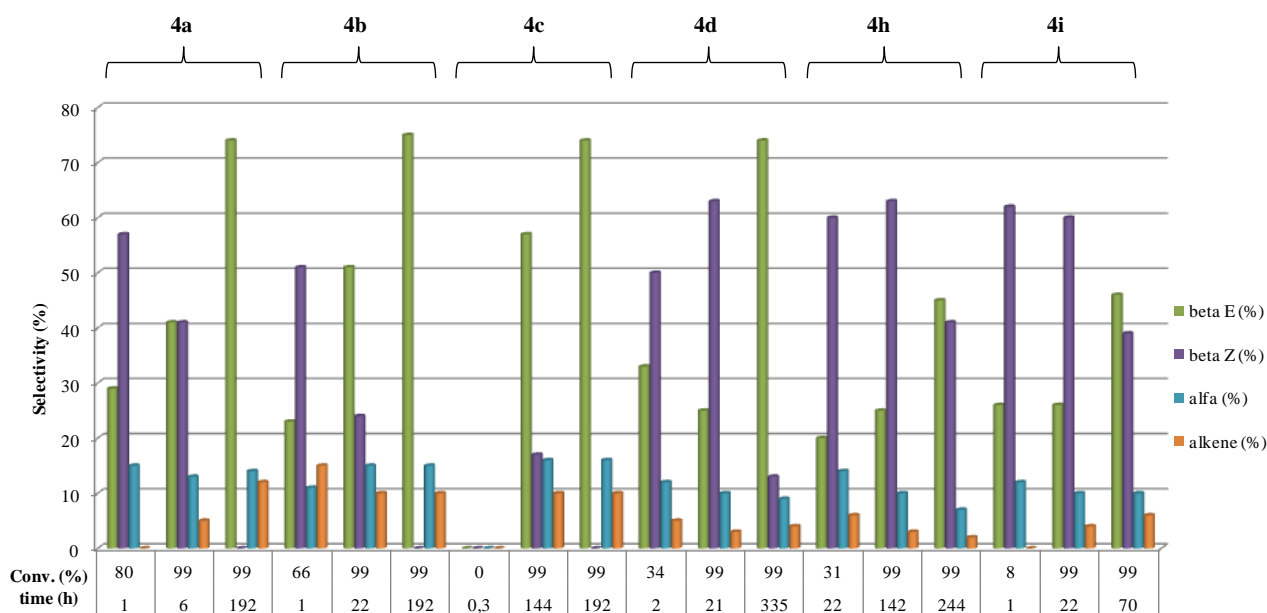


Figure 9.5-3 Selectivities, conversion and reaction time for PhC≡CH catalyst loading 1% at 25°C.

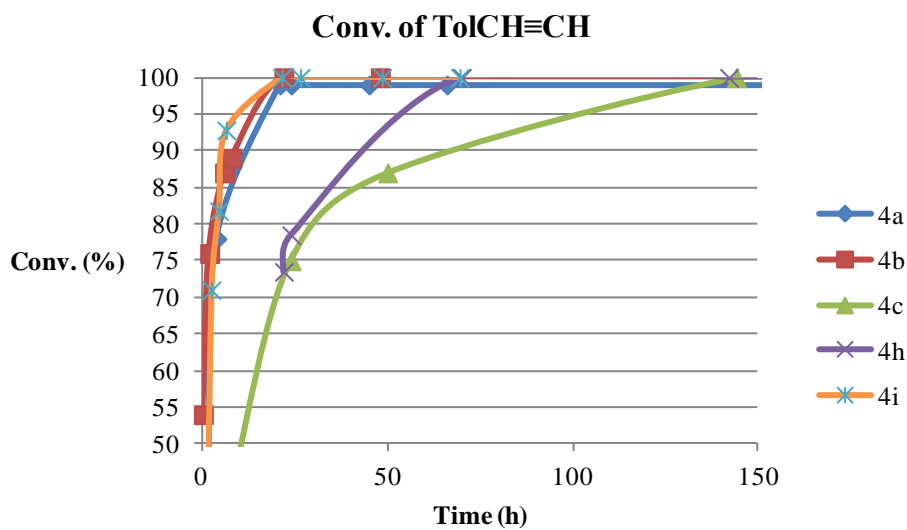


Figure 9.5-4 Conversion of TolCH≡CH catalyst loading 1% at 25°C.

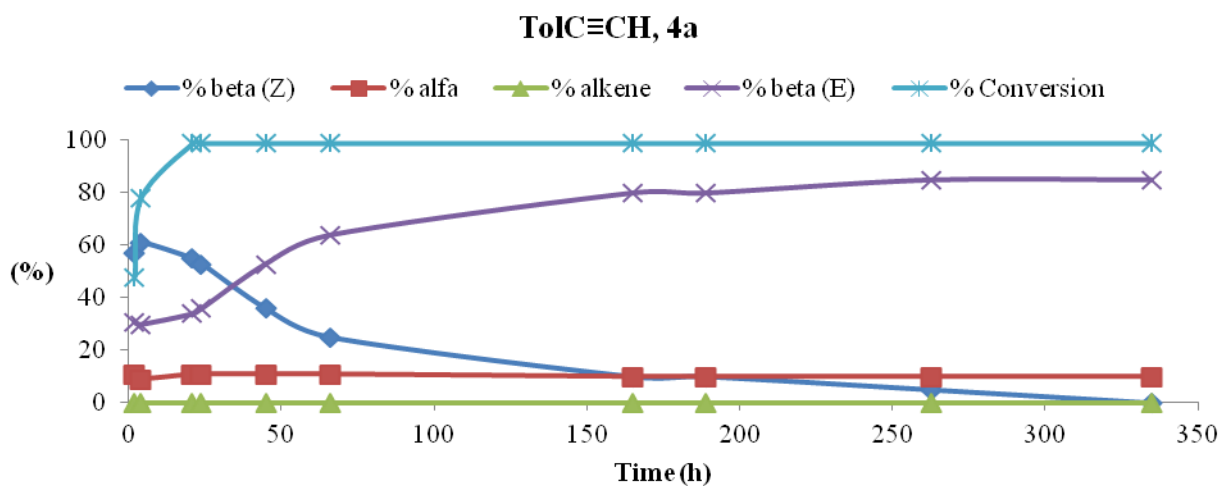


Figure 9.5-5 Conversion and selectivities for TolC≡CH with catalyst loading of 1% at 25°C.

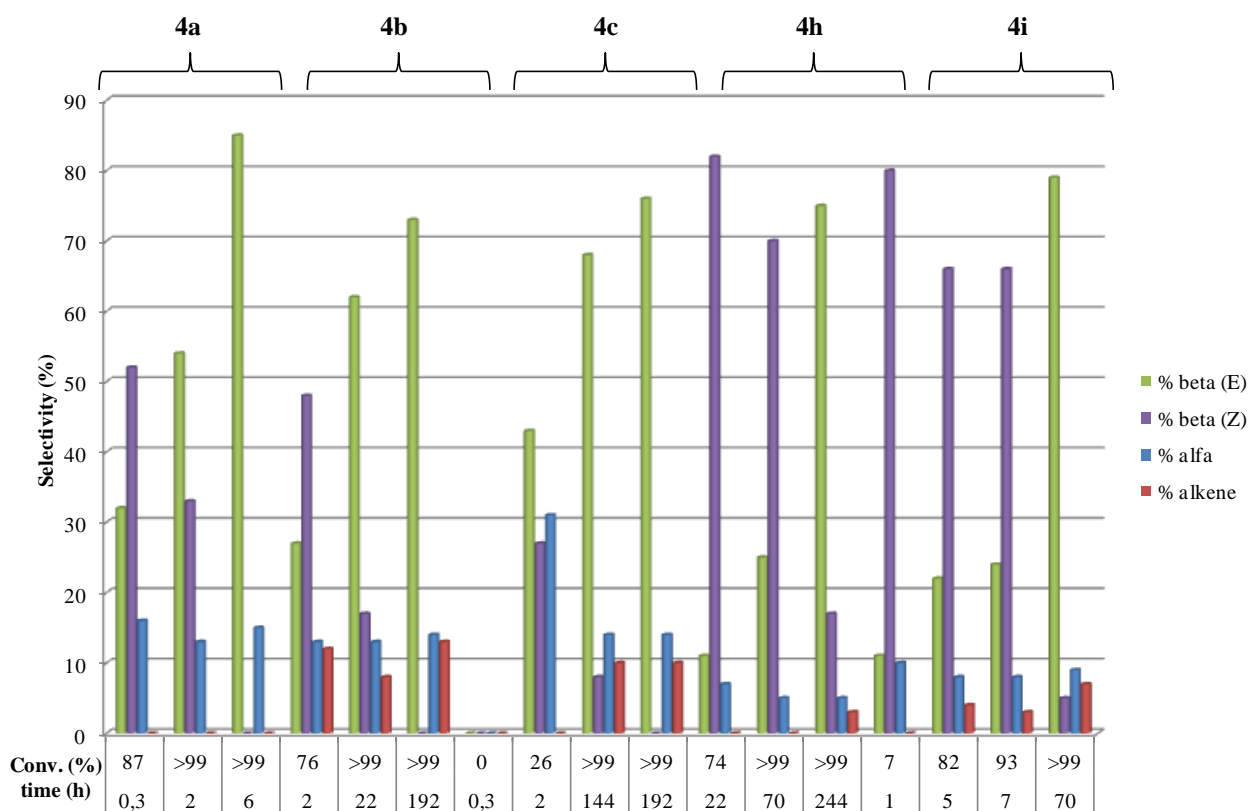


Figure 9.5-6 Selectivities, conversion and reaction time for TolC≡CH catalyst loading 1% at 25°C.

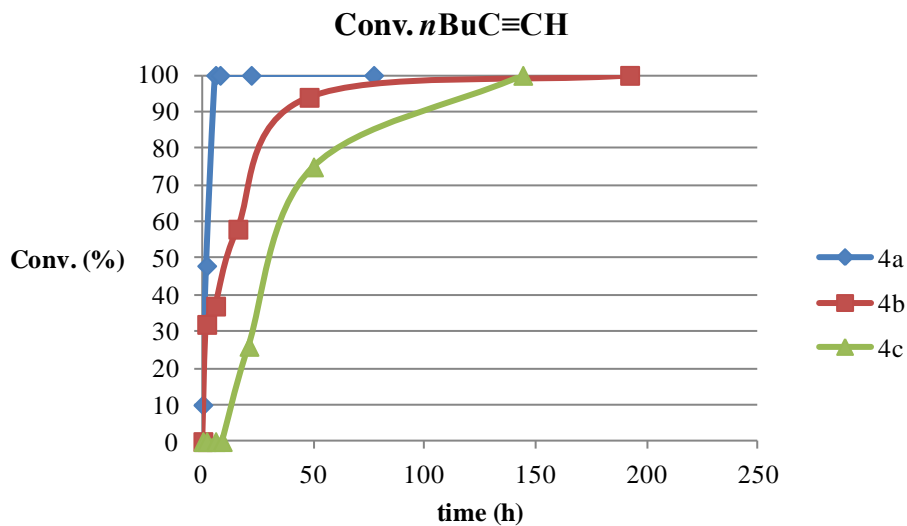


Figure 9.5-7 Conversion of $n\text{BuC}\equiv\text{CH}$, catalyst loading 1% at 25°C.

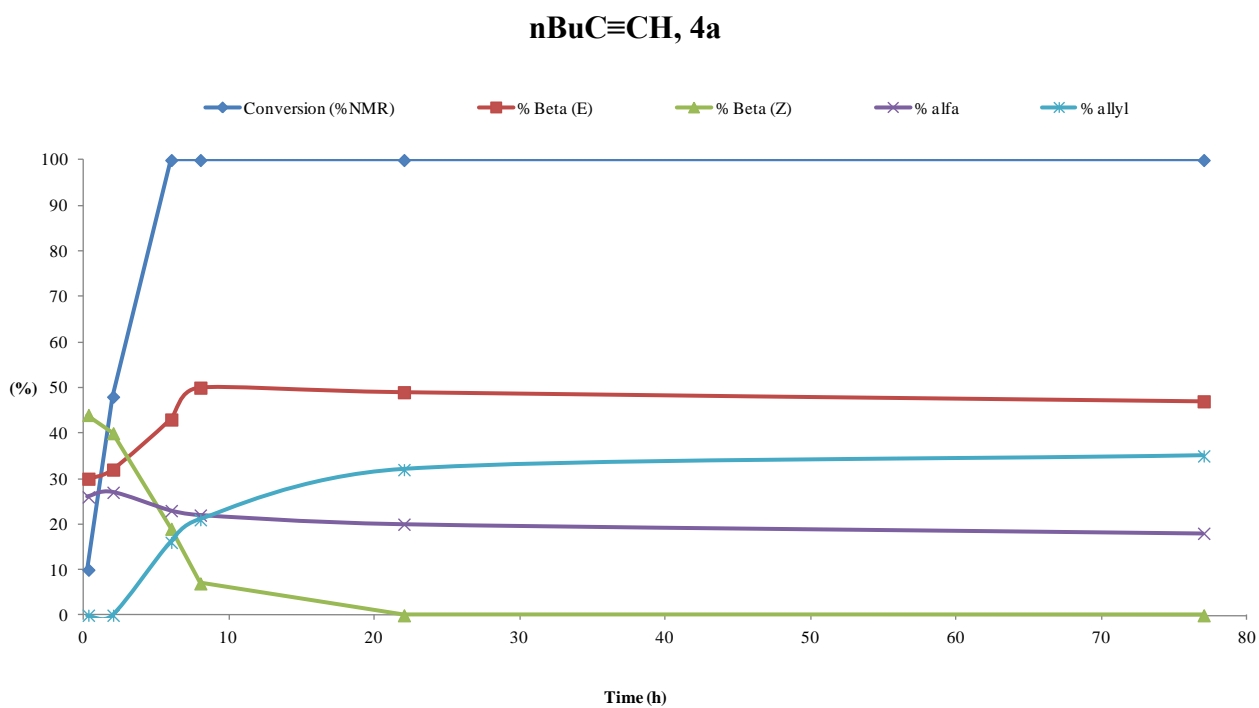


Figure 9.5-8 Conversion and selectivities of $n\text{BuC}\equiv\text{CH}$ catalyst loading 1% at 25°C.

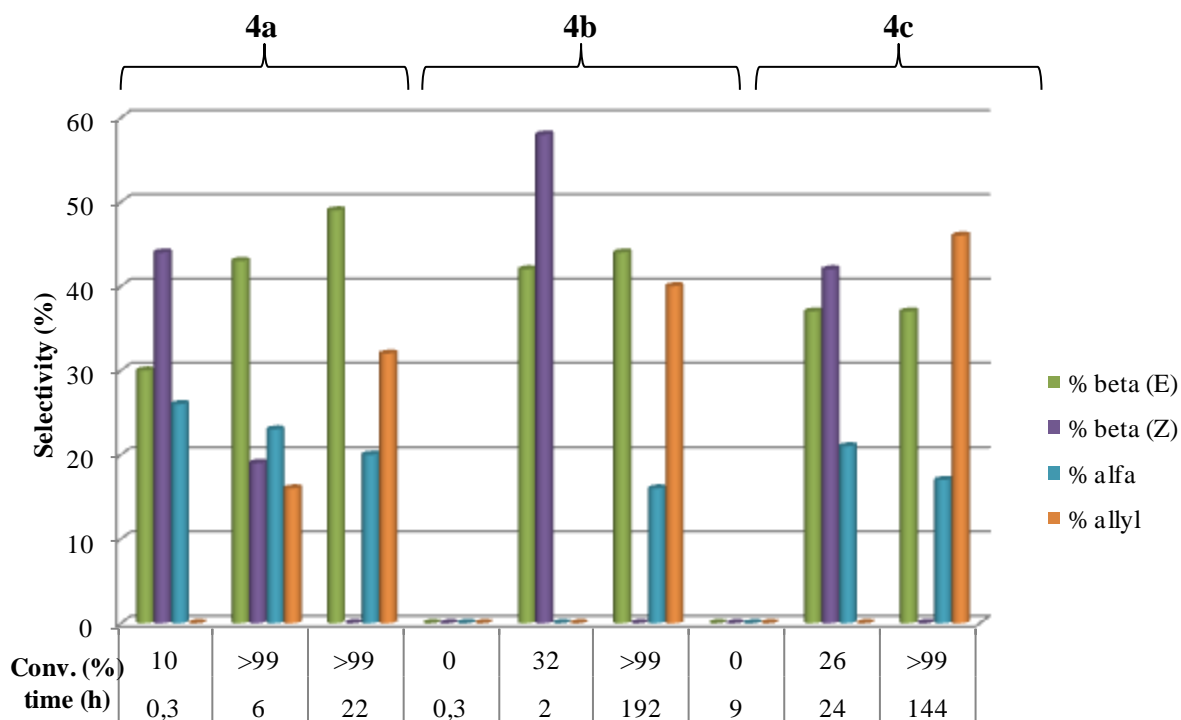


Figure 9.5-9 Selectivities, conversion and reaction time for $n\text{BuC}\equiv\text{CH}$ catalyst loading 1% at 25°C.

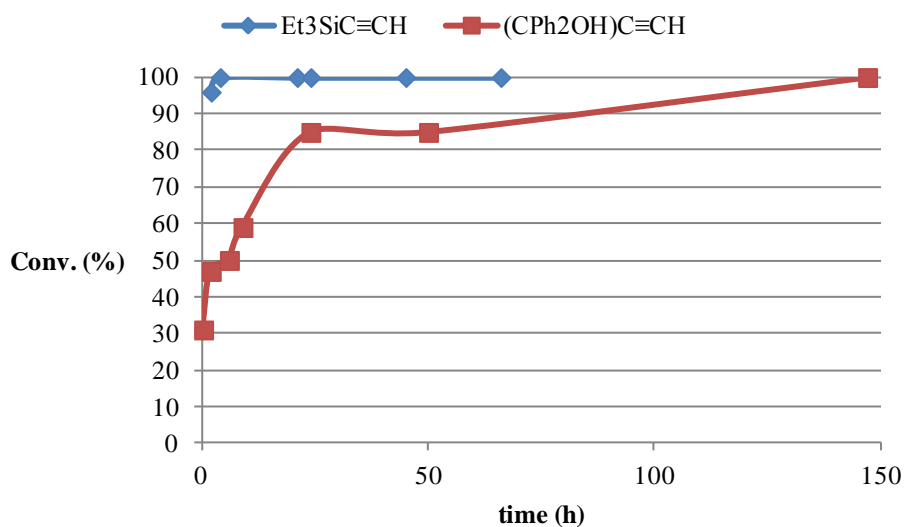


Figure 9.5-10 Conversion of $\text{Et}_3\text{SiC}\equiv\text{CH}$ and $(\text{CPh}_2\text{OH})\text{C}\equiv\text{CH}$ **4a** catalyst loading 1% at 25°C.

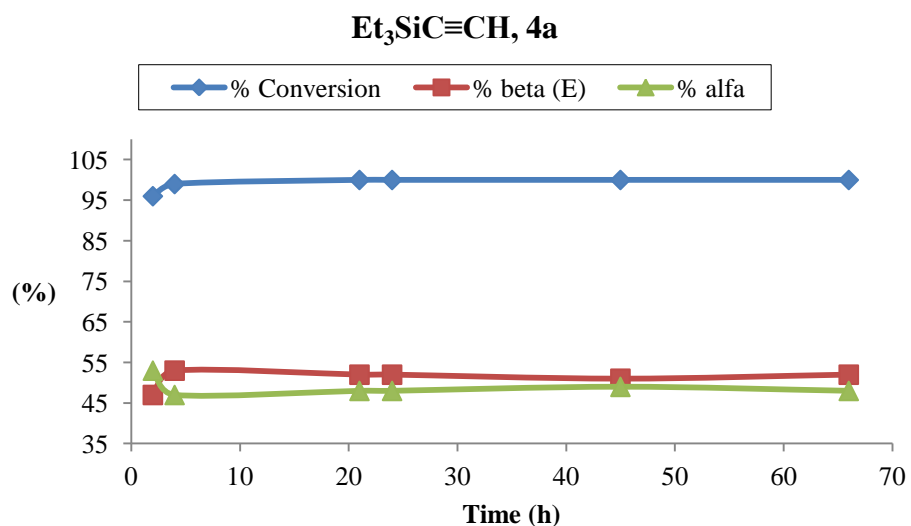


Figure 9.5-11 Conversion and selctivities of Et₃SiC≡CH catalyst loading 1% at 25°C.

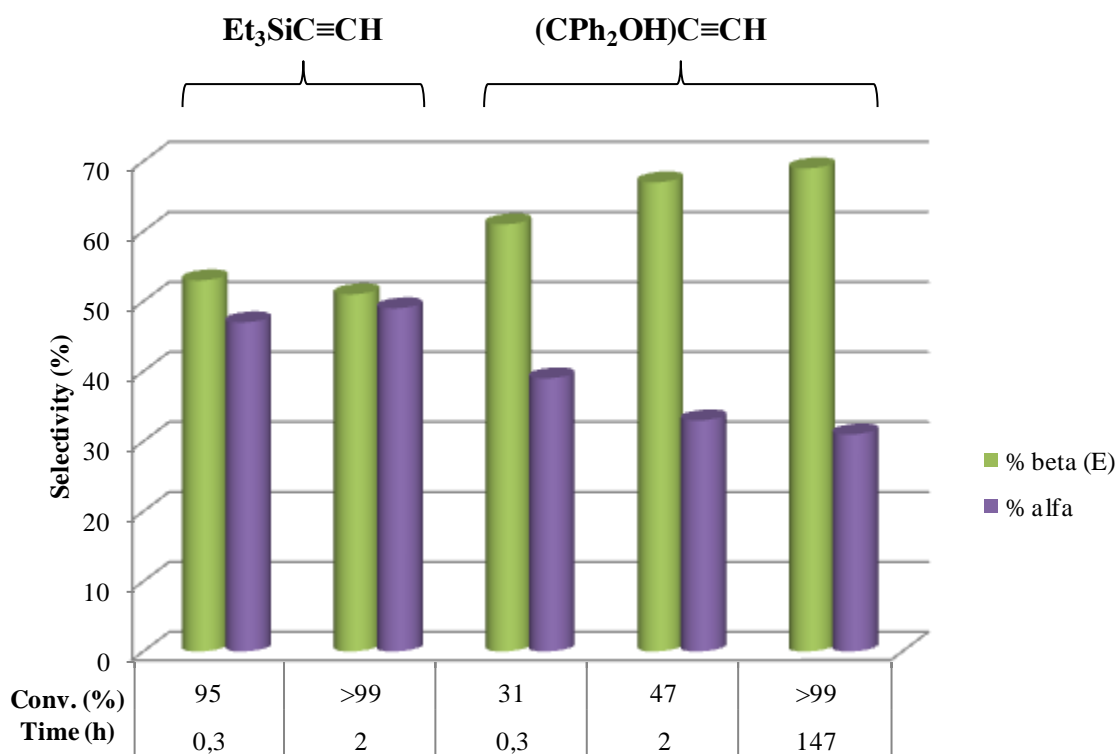


Figure 9.5-12 Selectivities, conversion and reaction time for Et₃C≡CH and (CPh₂OH)≡CH with **4a** catalyst loading 1% at 25°C.

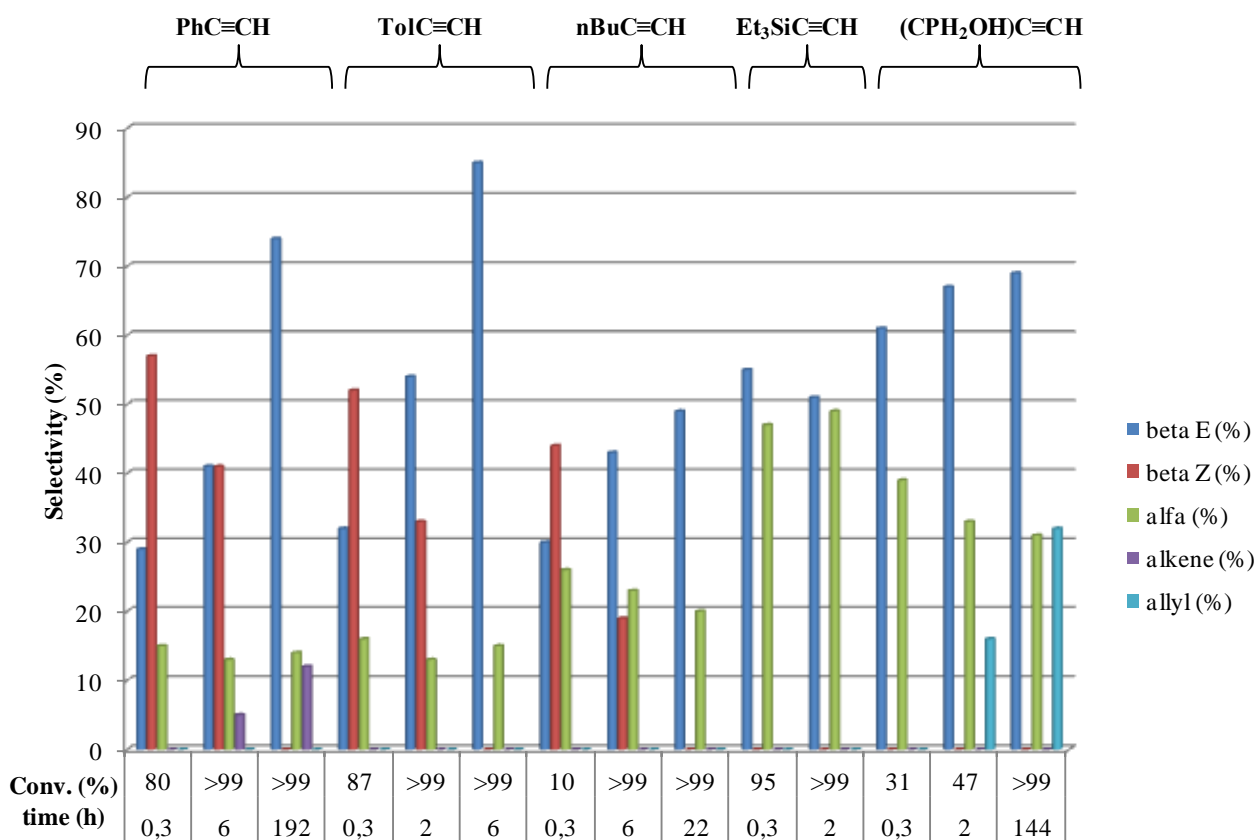


Figure 9.5-13 Selectivities, conversion and reaction time for all the substrates with **4a** catalyst loading 1% at 25°C.

Catalyst loading 0,1% at 25°C

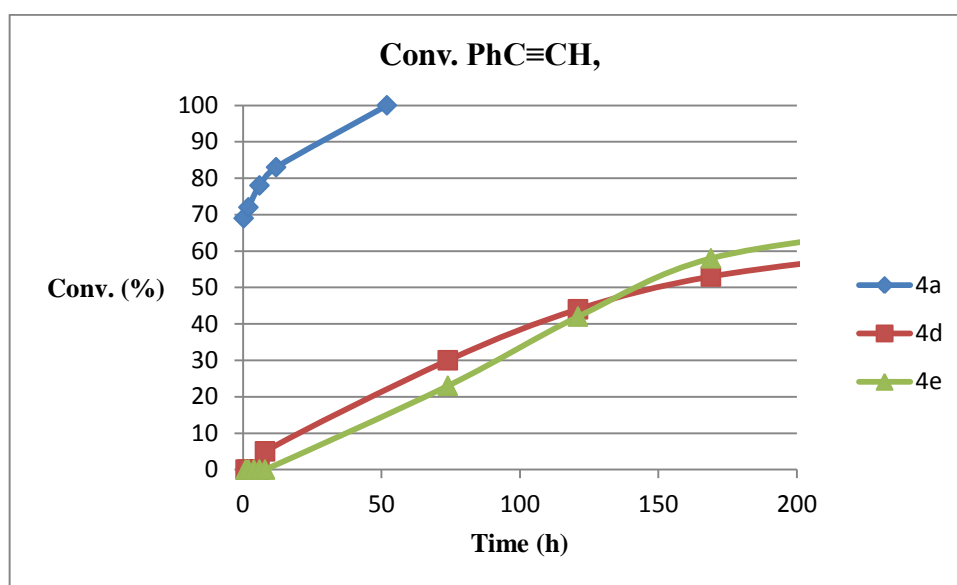


Figure 9.5-14 Conversion of PhC≡CH with a catalyst loading of 0,1% at 25°C.

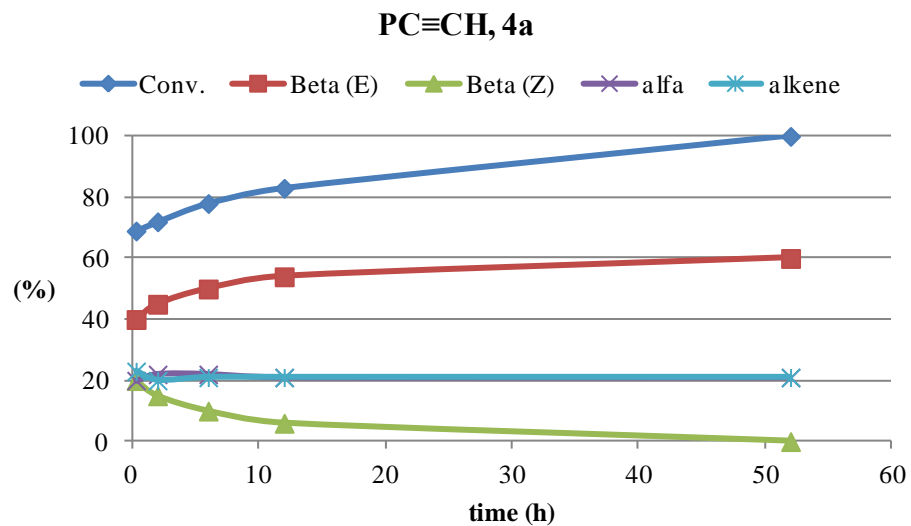


Figure 9.5-15 Conversion and selctivities of PhC≡CH with **4a**, catalyst loading 0,1% at 25°C.

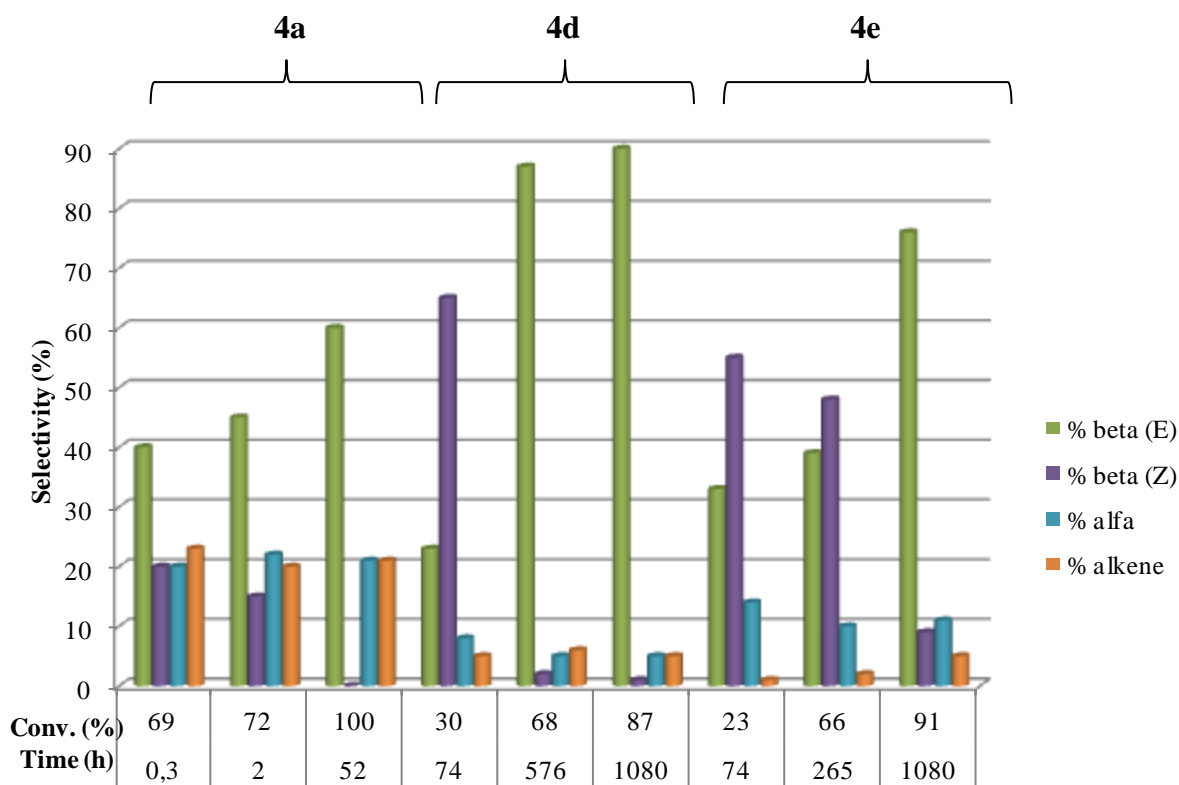


Figure 9.5-16 Selectivities, conversion and reaction time for PhC≡CH with **4a** catalyst loading 0,1% at 25°C.

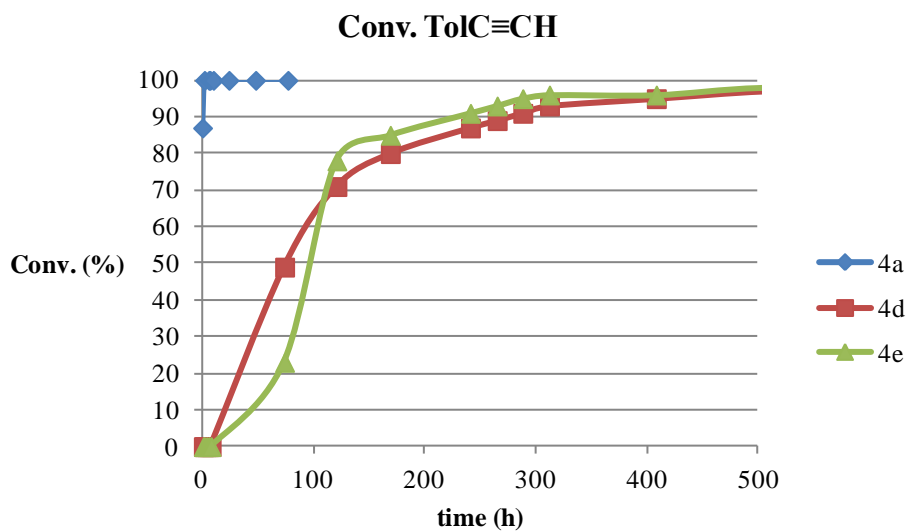


Figure 9.5-17 of PhC≡CH Conversion of TolC≡CH with a catalyst loading of 0,1% at 25°C.

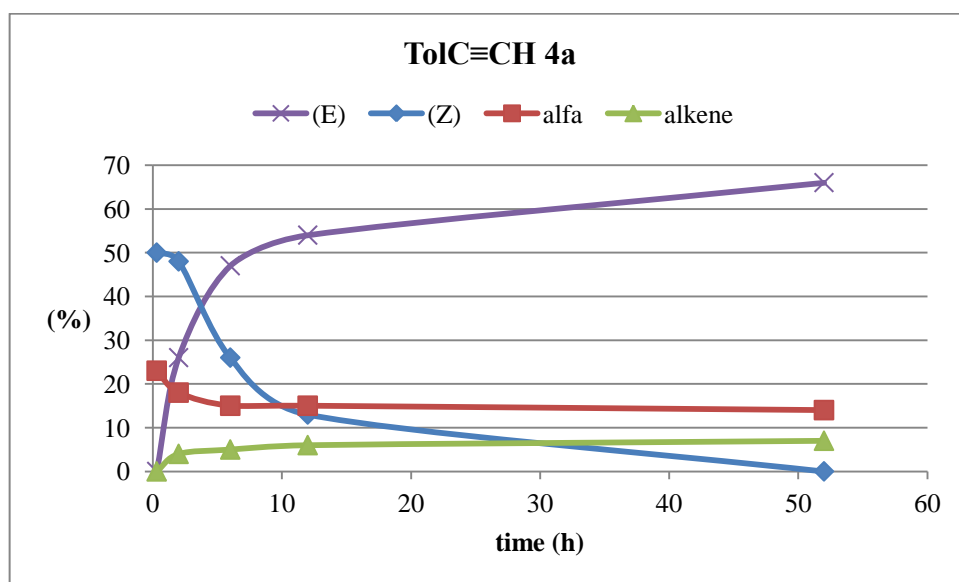


Figure 9.5-18 Conversion and selectivities of TolC≡CH with **4a**, cat. loading 0,1% at 25°C.

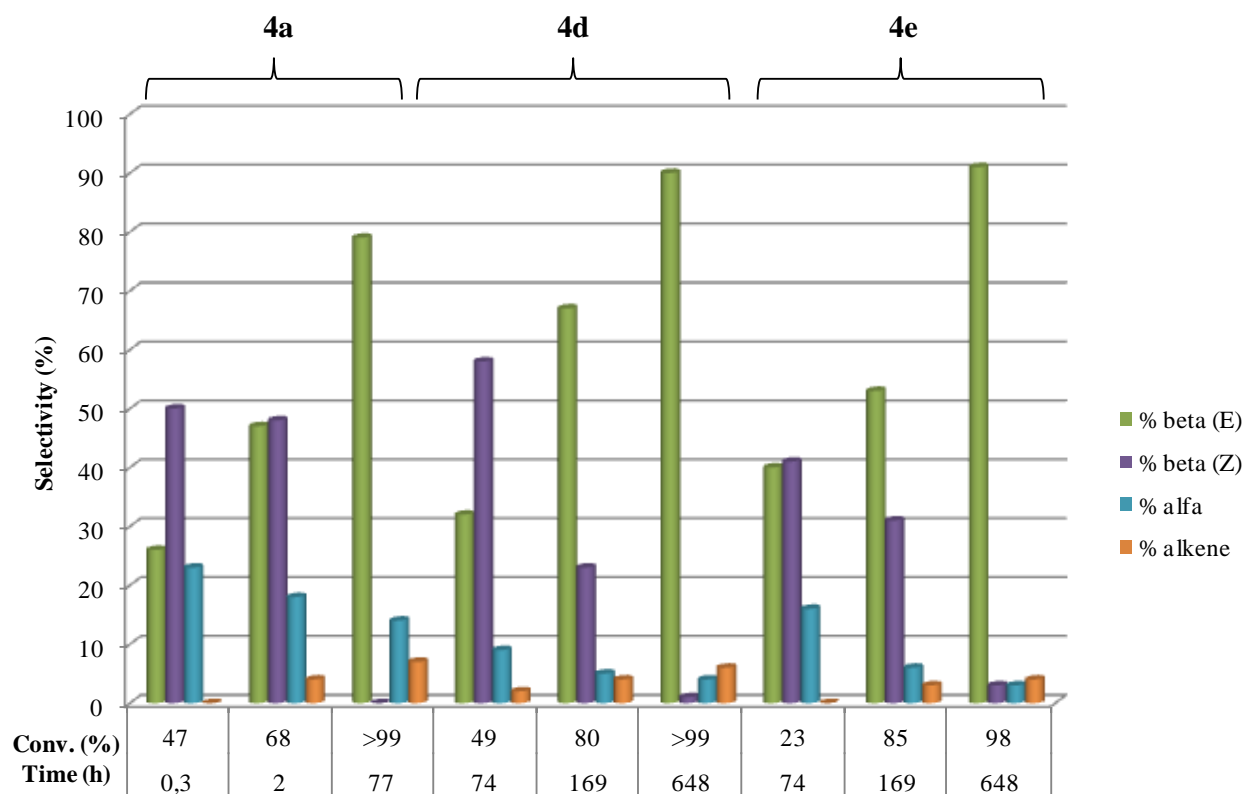


Figure 9.5-19 Selectivities, conversion and reaction time for TolC≡CH with **4a** catalyst loading 0,1% at 25°C.

Catalyst loading 0,1% at 60°C

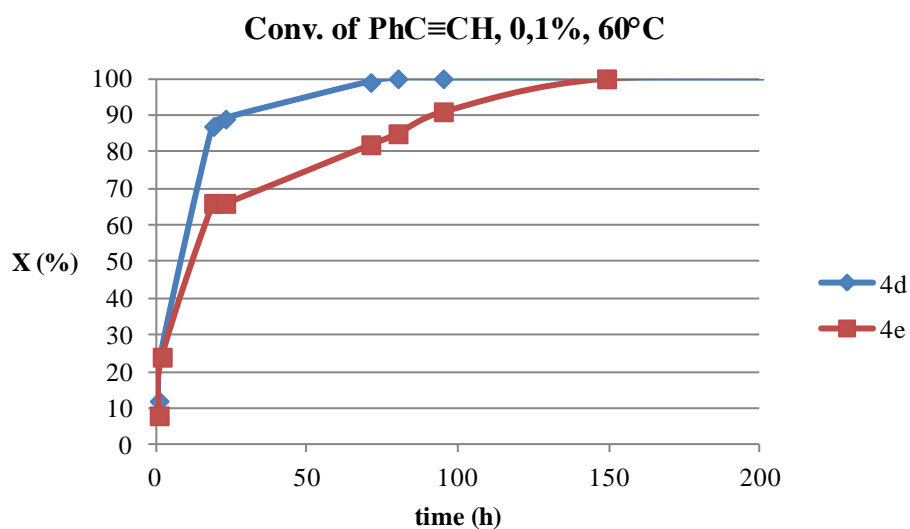


Figure 9.5-20 Conversion of PhC≡CH with catalyst loading of 0,1% at 60°C

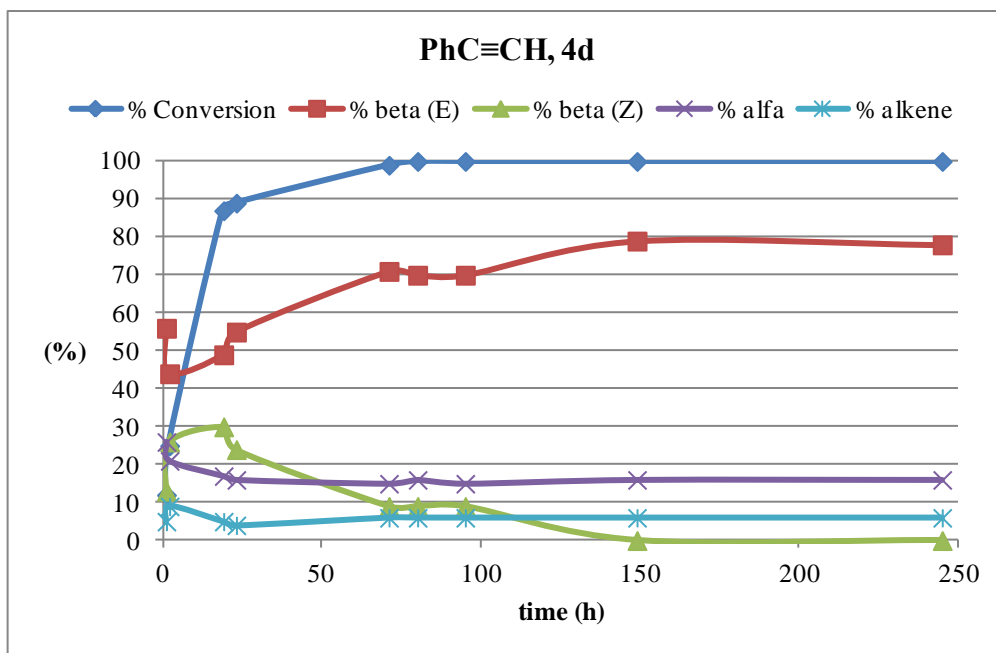


Figure 9.5-21 Conversion and selectivities of PhC≡CH with **4a**, catalyst loading 0,1% at 60°C

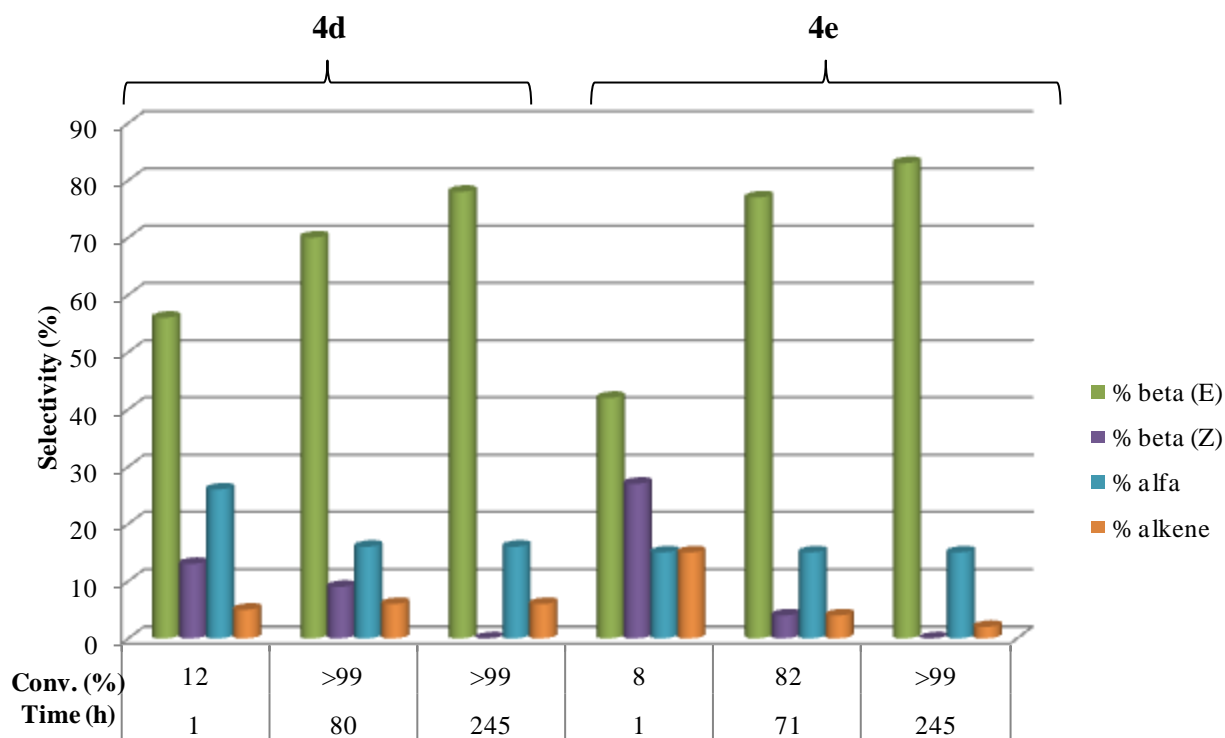


Figure 9.5-22 Selectivities, conversion and reaction time for PhC≡CH with **4a** catalyst loading 0,1% at 60°C

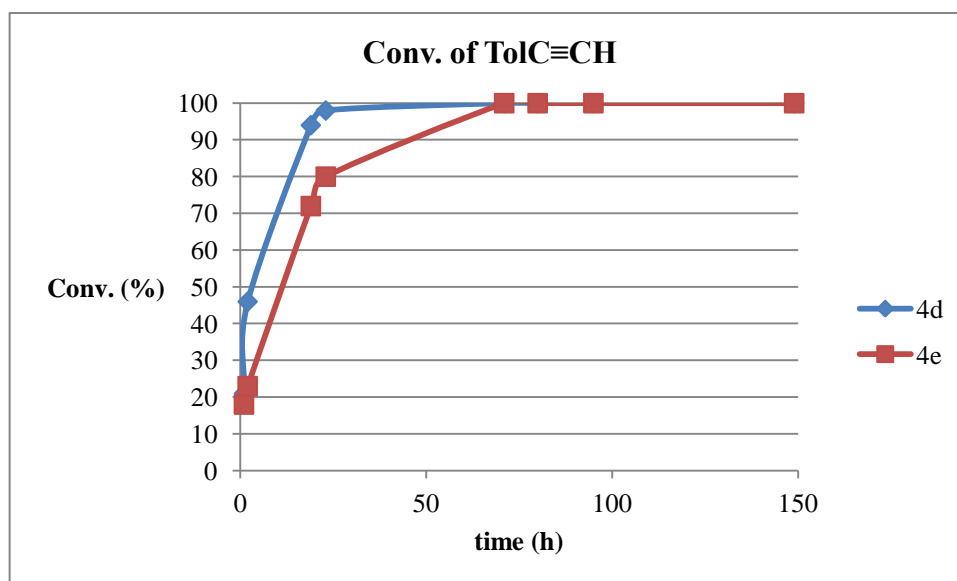


Figure 9.5-23 Conversion of TolC≡CH with catalyst loading of 0,1% and T = 60°C

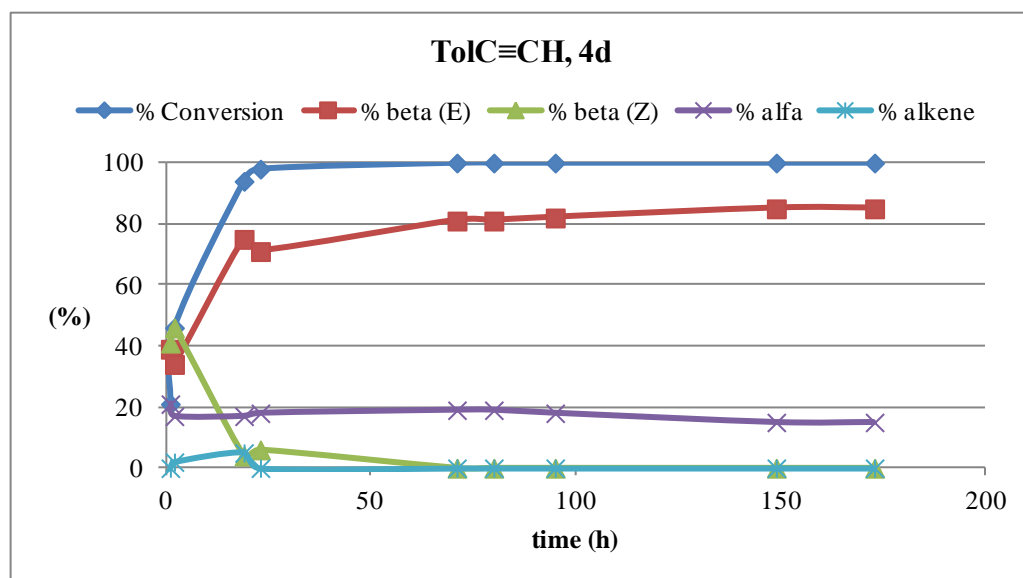


Figure 9.5-24 Conversion and selctivities of TolC≡CH with **4a**, catalyst loading 0,1% at 60°C

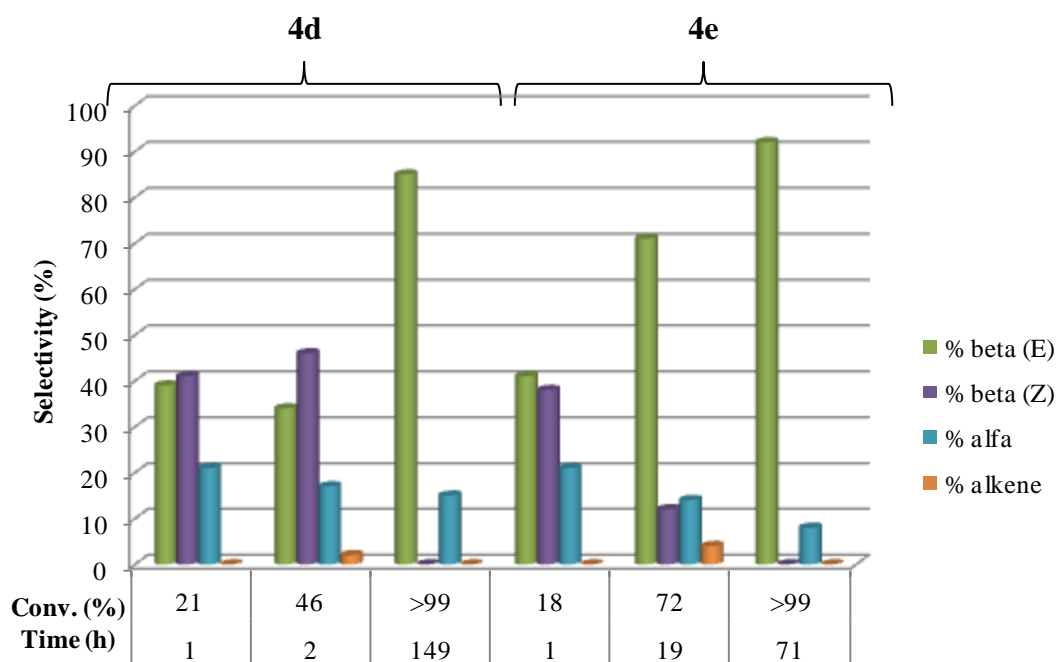


Figure 9.5-25 Selectivities, conversion and reaction time for TolC≡CH with **4a** cat. load. 0,1% at 60°C

9.6 NMR Spectra and integrations

NMR spectra and integrations are reported within an example of relative conversion and selectivity calculated percentages.

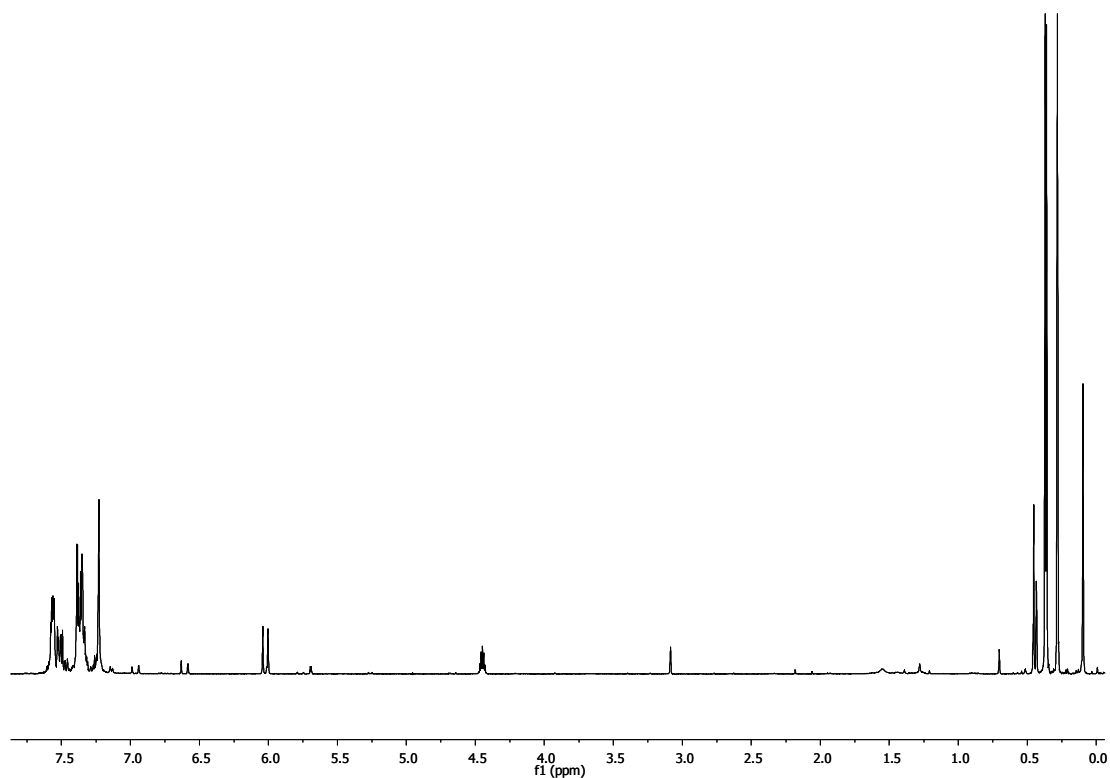


Figure 9.6-1 Hydro-silylation of $\text{PhC}\equiv\text{CH}$ with 1% **4b**; $t = 2$ h, conversion = 79 %, selectivities: **1s**- β (E) = 24%; **2s**- β (Z) = 50%; **3s**- α = 15%; **4s**-styrene = 11%.

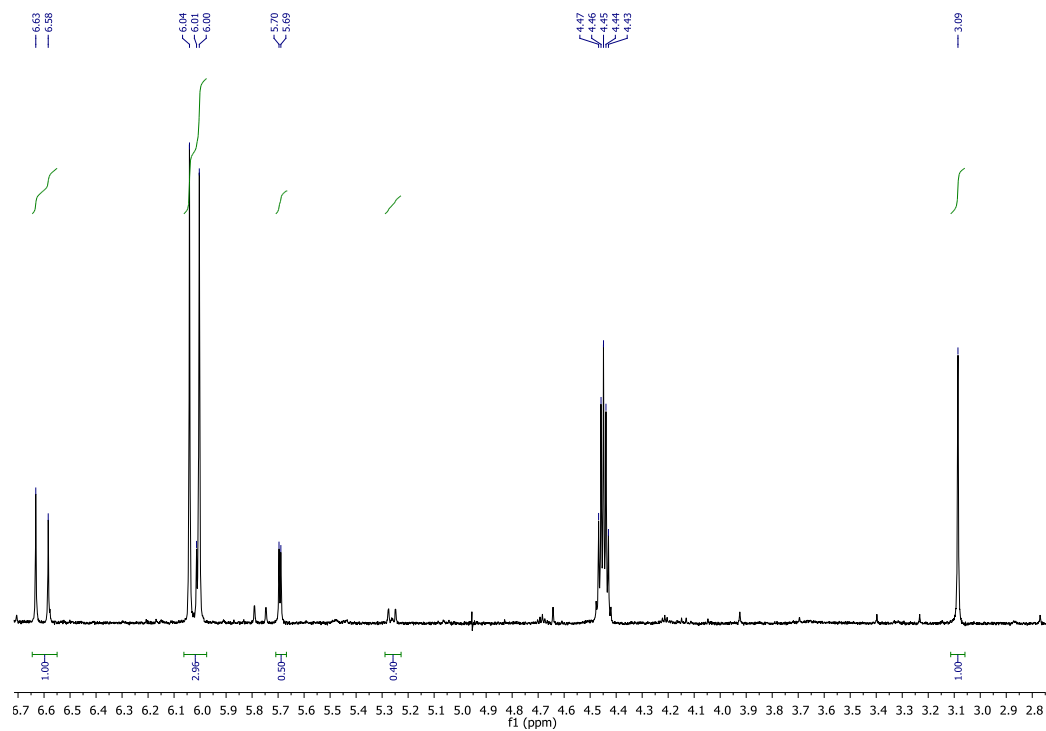


Figure 9.6-2 Hydro-silylation of $\text{PhC}\equiv\text{CH}$ with 1% **4b**; $t = 2$ h, conversion = 79 %, selectivities: **1s**- β (E) = 24%; **2s**- β (Z) = 50%; **3s**- α = 15%; **4s**-styrene = 11%. Enlargement.

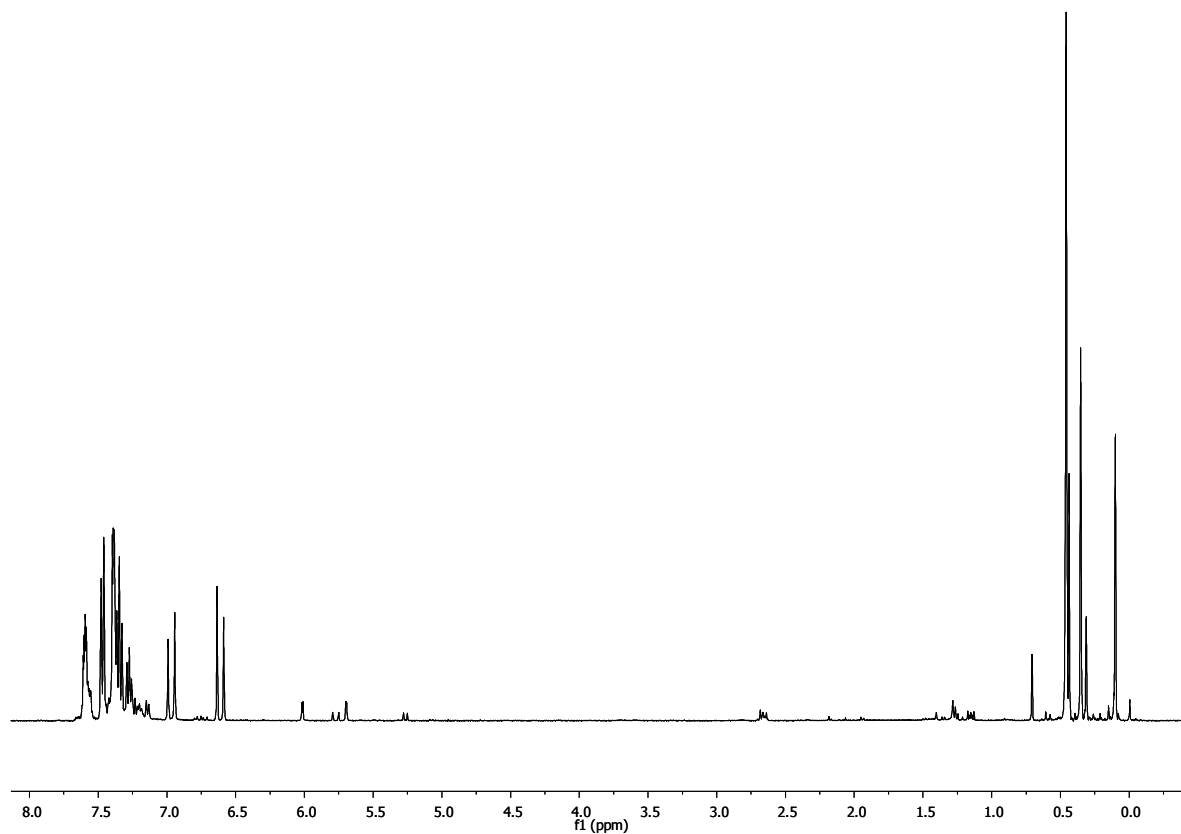


Figure 9.6-3 Hydrolylation of $\text{PhC}\equiv\text{CH}$ with 1% **4b**; $t = 8$ d, conversion $> 99\%$, selectivities: **1s- β (E)** = 75%; **3s- α** = 15%; **4s-styrene** = 10%.

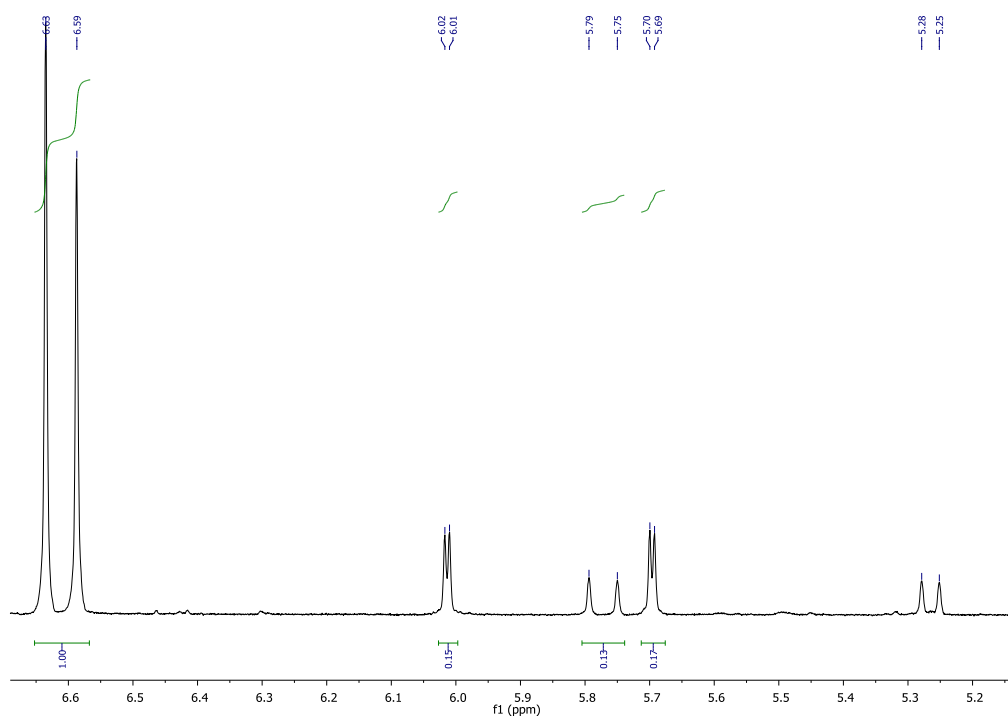


Figure 9.6-4 Hydro-silylation of $\text{PhC}\equiv\text{CH}$ with 1% **4b**; $t = 8$ d, conversion $> 99\%$, selectivities: **1s**- $\beta(\text{E}) = 75\%$; **3s**- $\alpha = 15\%$; **4s**-styrene = 10%. Enlargement.

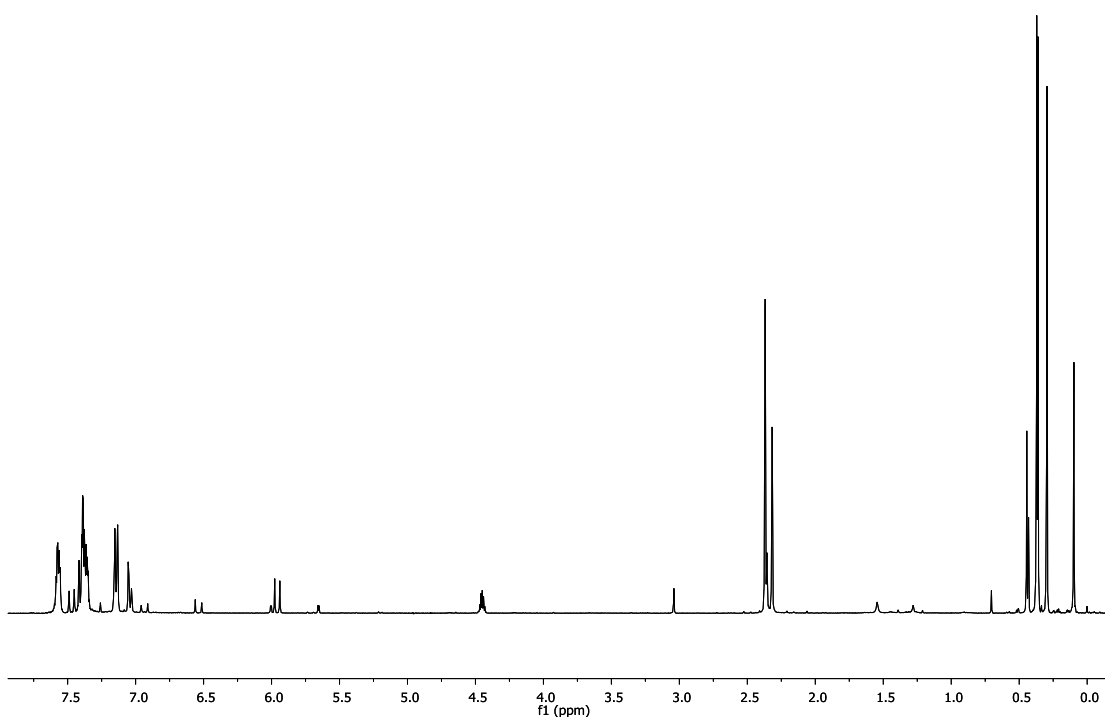


Figure 9.6-5 Hydro-silylation of $\text{TolC}\equiv\text{CH}$ with 1% **4b**; $t = 2$ h, conversion = 76%, selectivities: **5s**- $\beta(\text{E}) = 27\%$; **6s**- $\beta(\text{Z}) = 48\%$; **7s**- $\alpha = 13\%$; **8s**-methylstyrene = 12%.

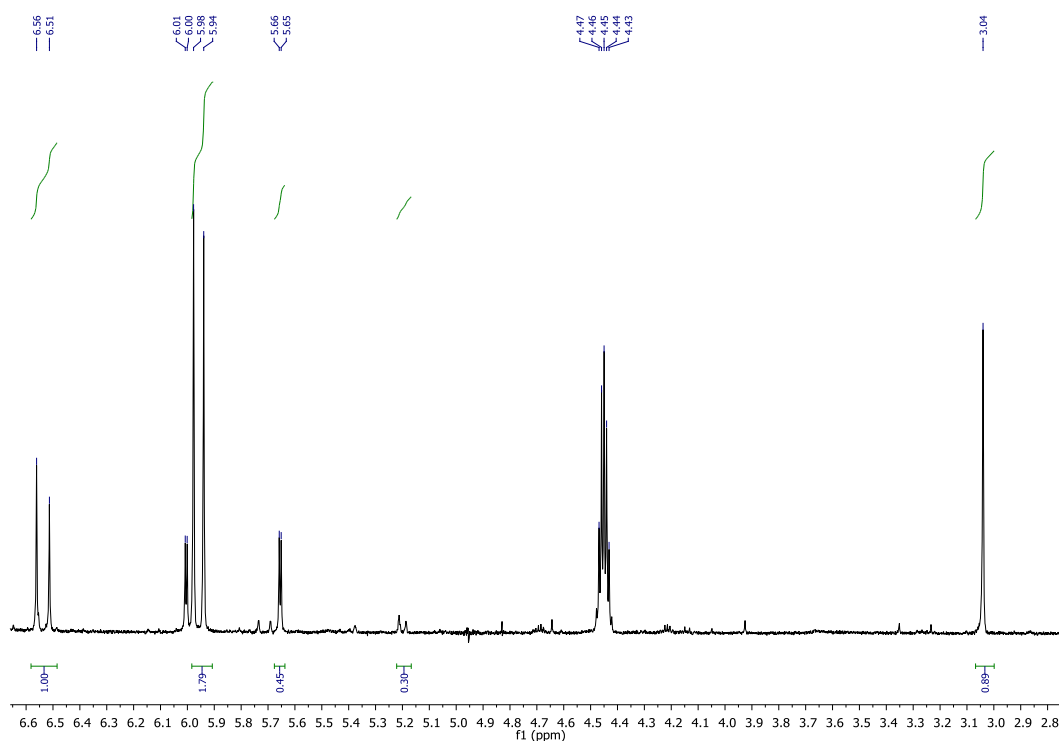


Figure 9.6-6 Hydrosilylation of TolC≡CH with 1% **4b**; $t = 2$ h, conversion = 76%, selectivities: **5s**- β (E) = 27%; **6s**- β (Z) = 48%; **7s**- α = 13%; **8s**-methylstyrene = 12%. Enlargement.

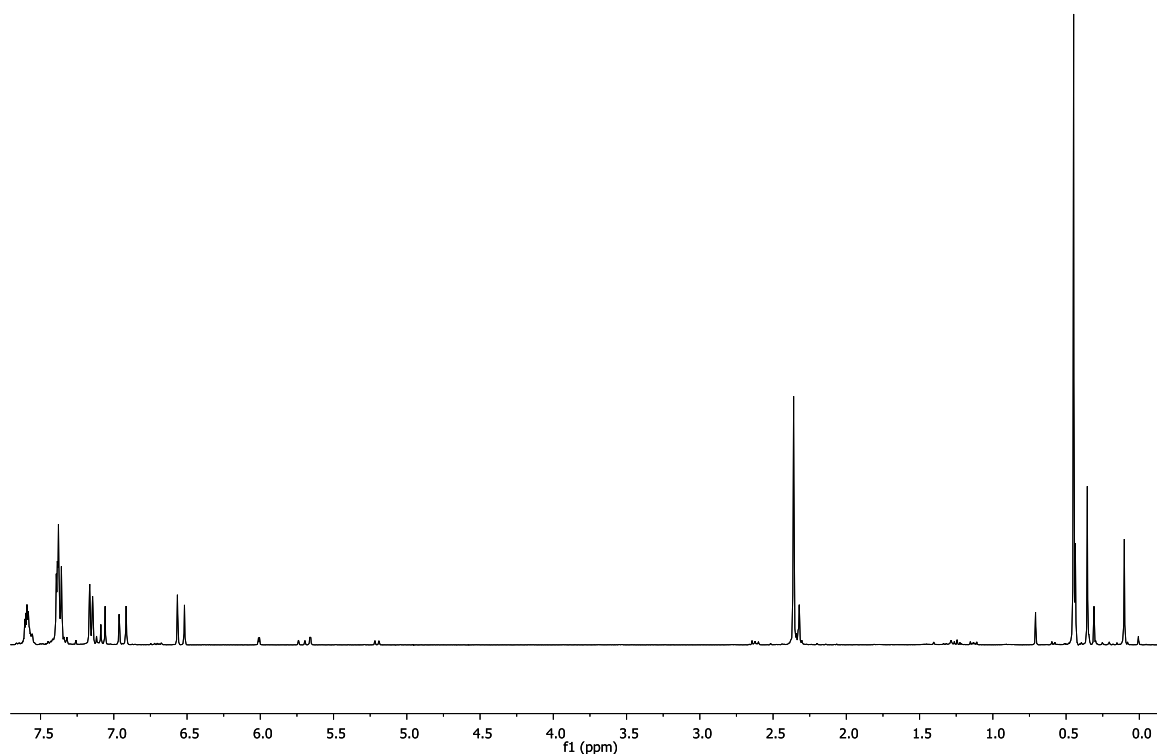


Figure 9.6-7 Hydrosilylation of TolC≡CH with 1% **4b**; $t = 8$ d, conversion > 99%, selectivities: **5s**- β (E) = 73%; **7s**- α = 14%; **8s**-methylstyrene = 13%.

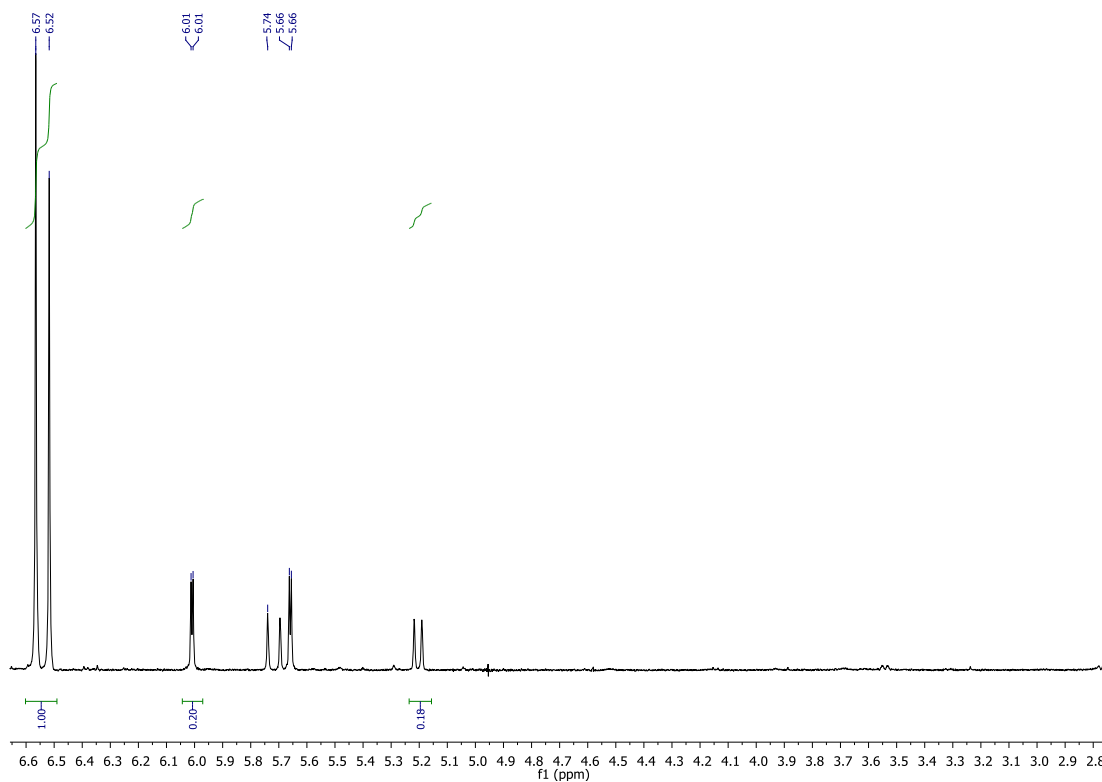


Figure 9.6-8 Hydrosilylation of TolC≡CH with 1% **4b**; $t = 8$ d, conversion > 99%, selectivities: **5s-β(E)** = 73%; **7s-α** = 14%; **8s**-methylstyrene = 13%. Enlargement.

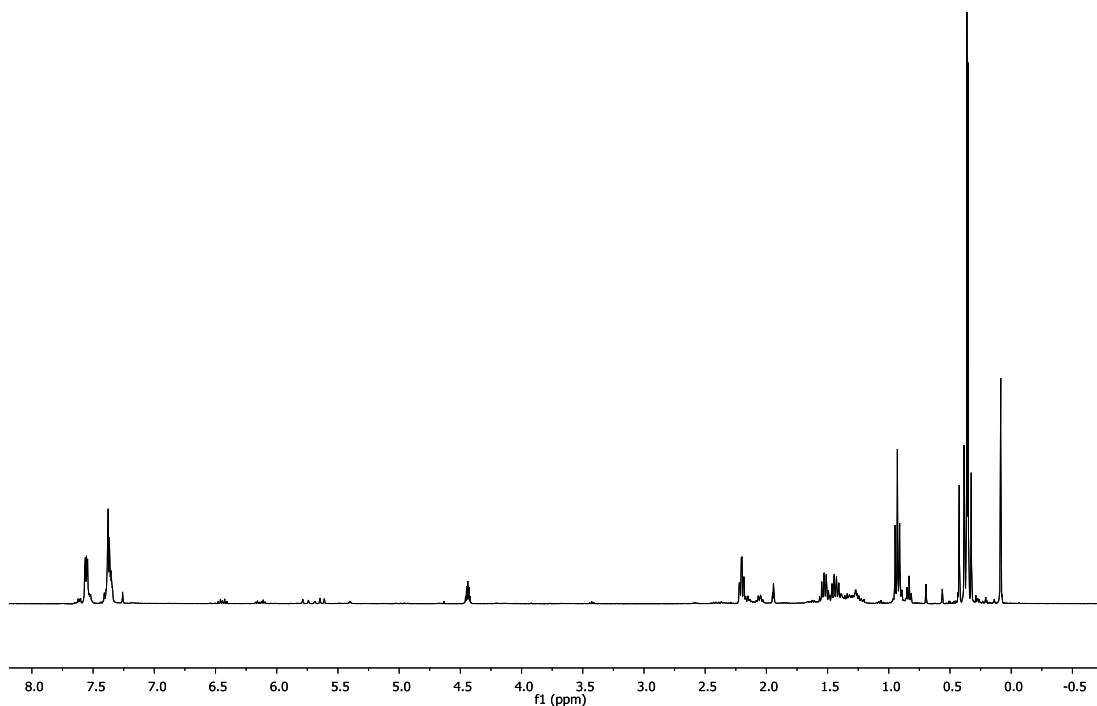


Figure 9.6-9 Hydrosilylation of $n\text{BuC}\equiv\text{CH}$ with 1% **4b**; $t = 22$ h, conversion = 58%, selectivities: **9s**- β (E) = 38%; **10s**- β (Z) = 38%; **11s**- α = 24%.

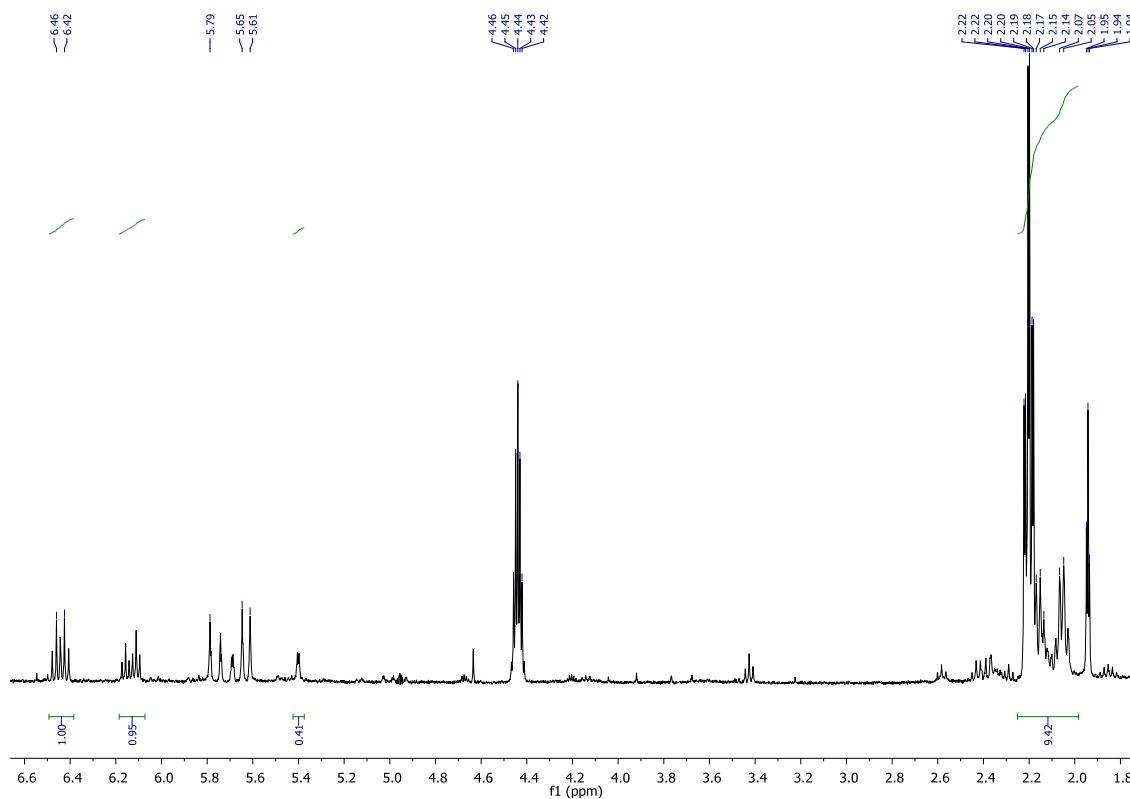


Figure 9.6-10 Hydrosilylation of $n\text{BuC}\equiv\text{CH}$ with 1% **4b**; $t = 22$ h, conversion = 58%, selectivities: **9s**- β (E) = 38%; **10s**- β (Z) = 38%; **11s**- α = 24%. Enlargement.

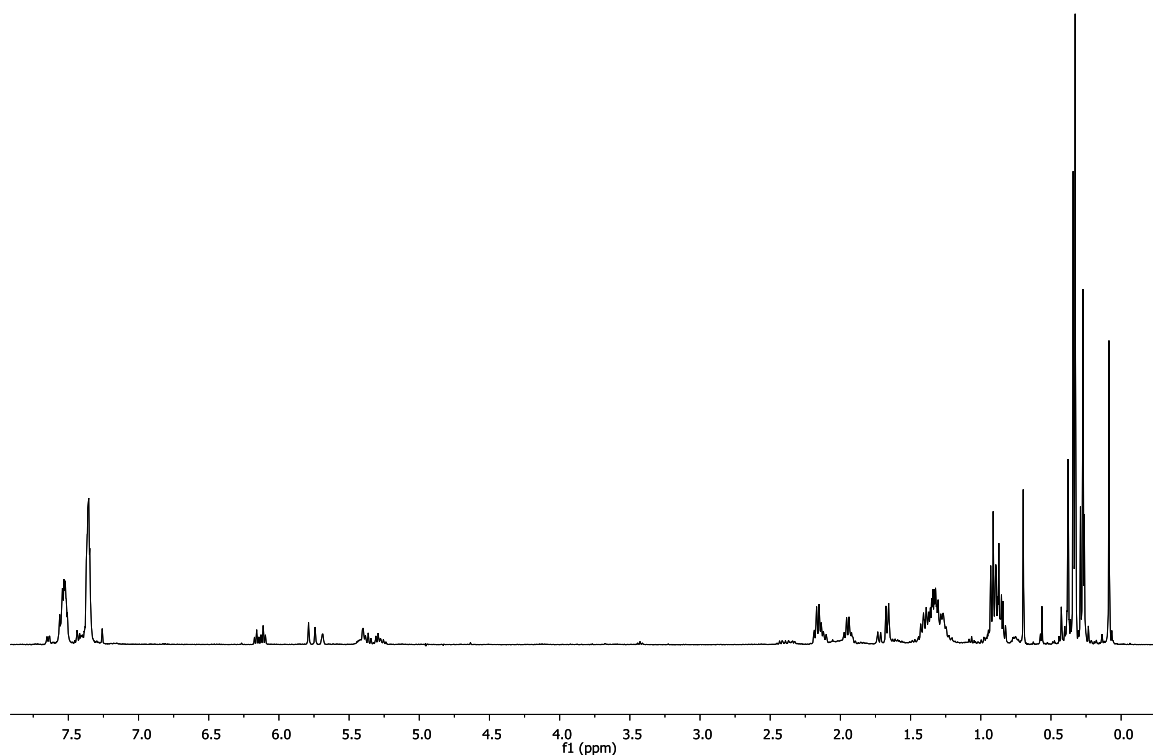


Figure 9.6-11 Hydrosilylation of $n\text{BuC}\equiv\text{CH}$ with 1% **4b**; $t = 8$ d, conversion > 99%, selectivities: **9s**- β (E) = 44%; **11s**- α = 16%; **12s**-allyl = 40%.

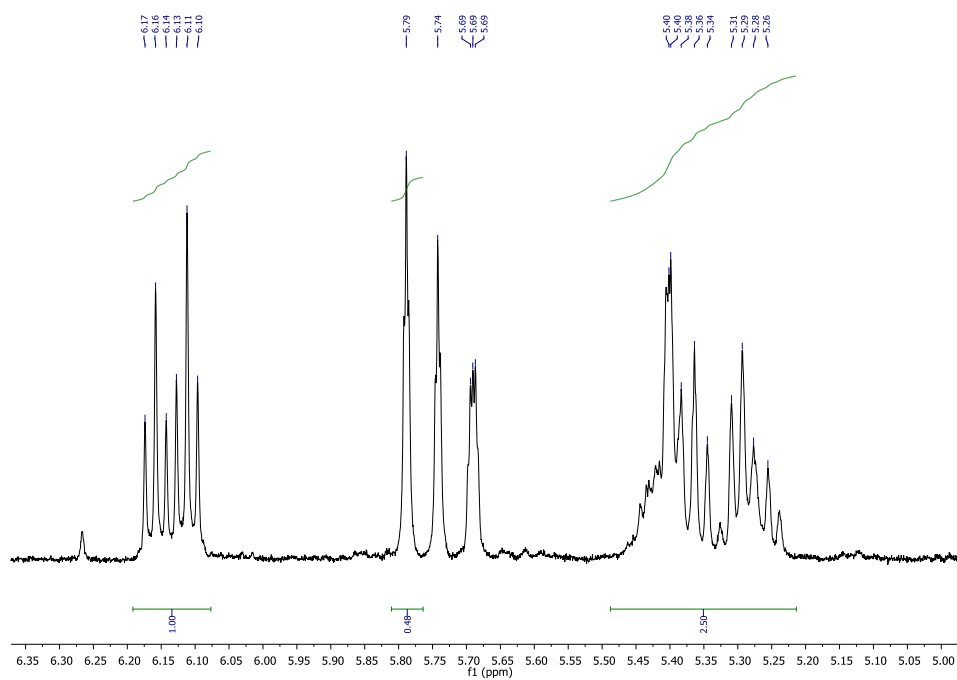


Figure 9.6-12 Hydrosilylation of $n\text{BuC}\equiv\text{CH}$ with 1% **4b**; $t = 8$ d, conversion $> 99\%$, selectivities: $9s\text{-}\beta(\text{E}) = 44\%$; $11s\text{-}\alpha = 16\%$; $12s\text{-allyl} = 40\%$. Enlargement.

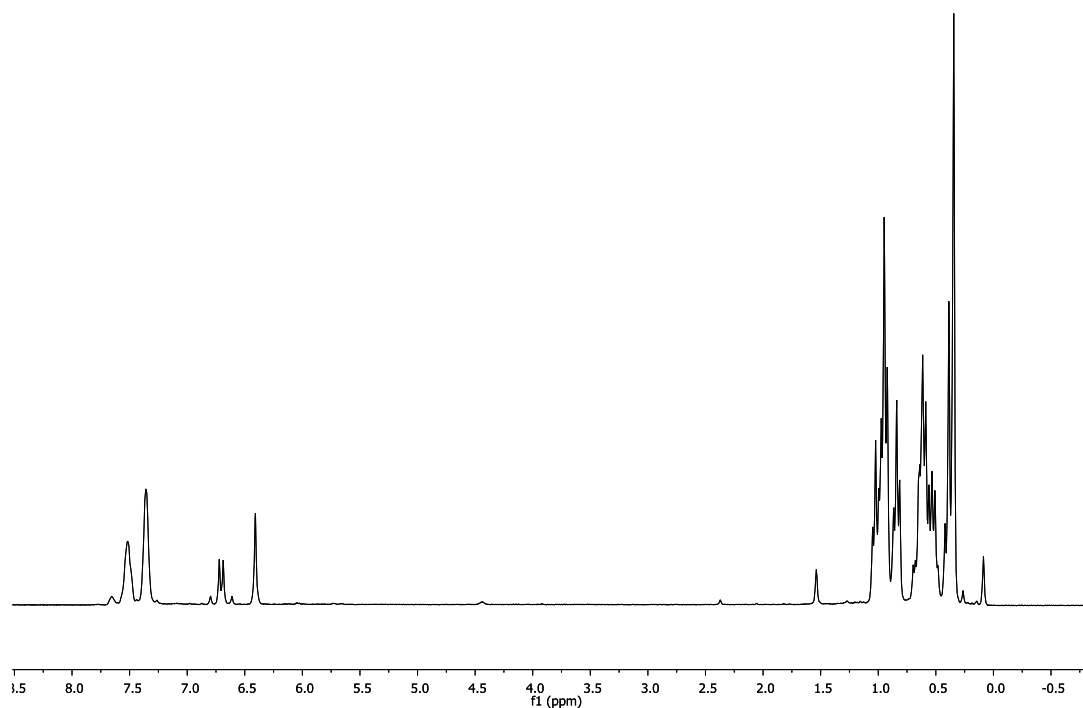


Figure 9.6-13 Hydrosilylation of $\text{Et}_3\text{SiC}\equiv\text{CH}$ with 1% **4a**; $t = 20$ min, conversion = 95 %, selectivities: $13s\text{-}\beta(\text{E}) = 53\%$; $14s\text{-}\alpha = 47\%$.

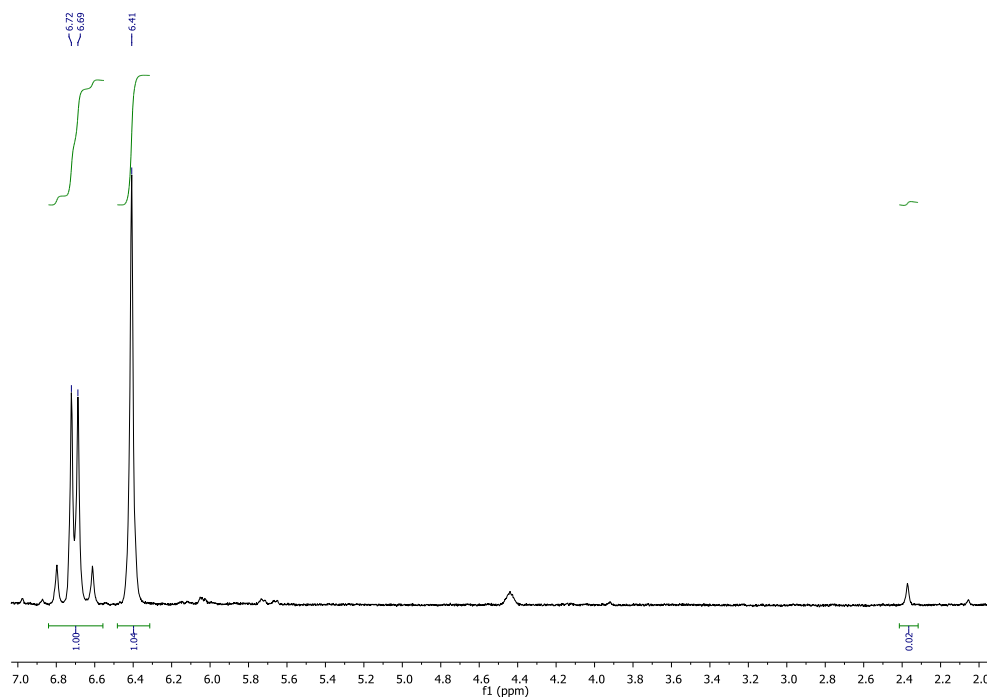


Figure 9.6-14 Hydrosilylation of $\text{Et}_3\text{SiC}\equiv\text{CH}$ with 1% **4a**; $t = 20$ min, conversion = 95 %, selectivities: **13s- β (E)** = 53%; **14s- α** = 47%. Enlargement.

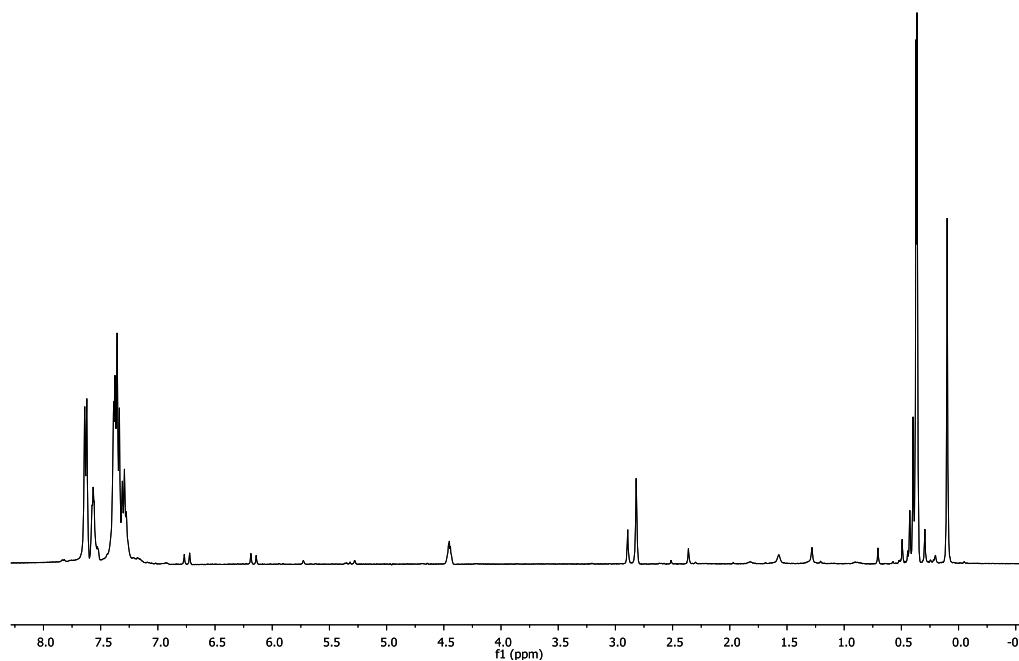


Figure 9.6-15 Hydrosilylation of $(\text{CPh}_2\text{OH})\text{C}\equiv\text{CH}$ with 1% **4a**; $t = 2$ h, conversion = 47 %, selectivities: **15s- β (E)** = 67%; **16s- α** = 33%.

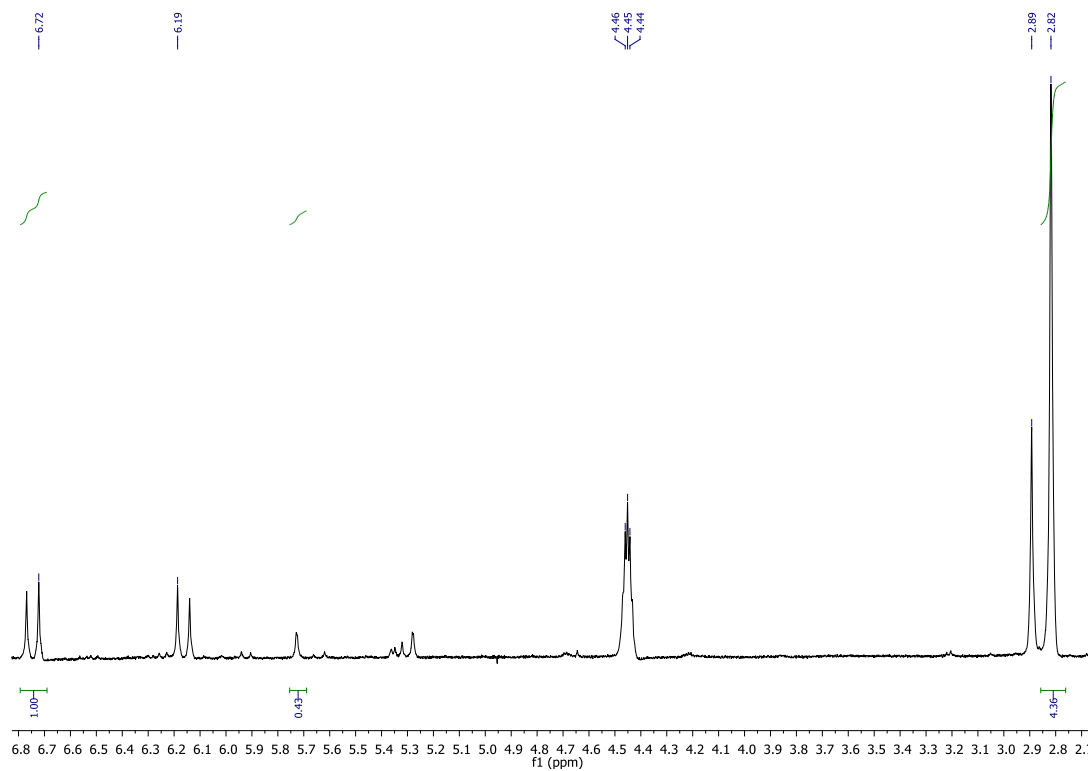


Figure 9.6-16 Hydrosilylation of $(\text{CPh}_2\text{OH})\text{C}\equiv\text{CH}$ with 1% **4a**; $t = 2$ h, conversion = 47 %, selectivities: **15s- β (E)** = 67%; **16s- α** = 33%. Enlargement.

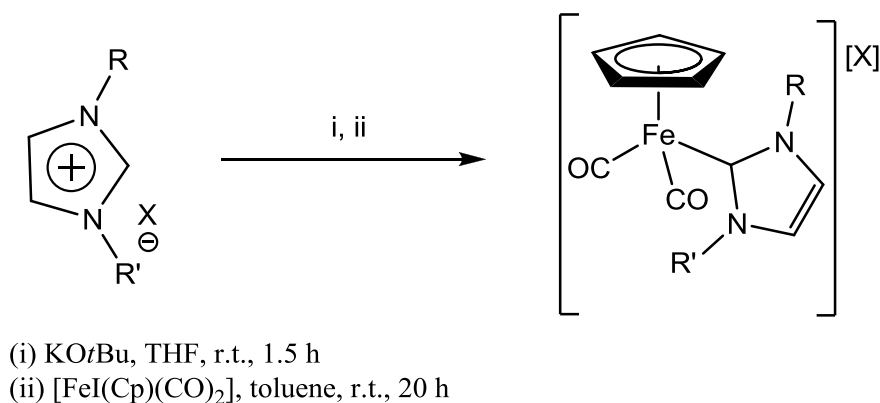
10 Iron-NHC Complexes

10.1 Introduction

Since iron complexes recently appeared to be valuable economic and non toxic alternative to the most employed noble metal in catalytic reaction as outlined in the general introduction, in the last part of my PhD thesis we focused our attention on the synthesis of Fe(NHC) complexes to be employed in the hydrosilylation of terminal alkynes instead of Rh(NHC) ones. Preliminary results obtained in this field are described in the following chapter.

10.2 Synthesis of Iron(II) Complexes

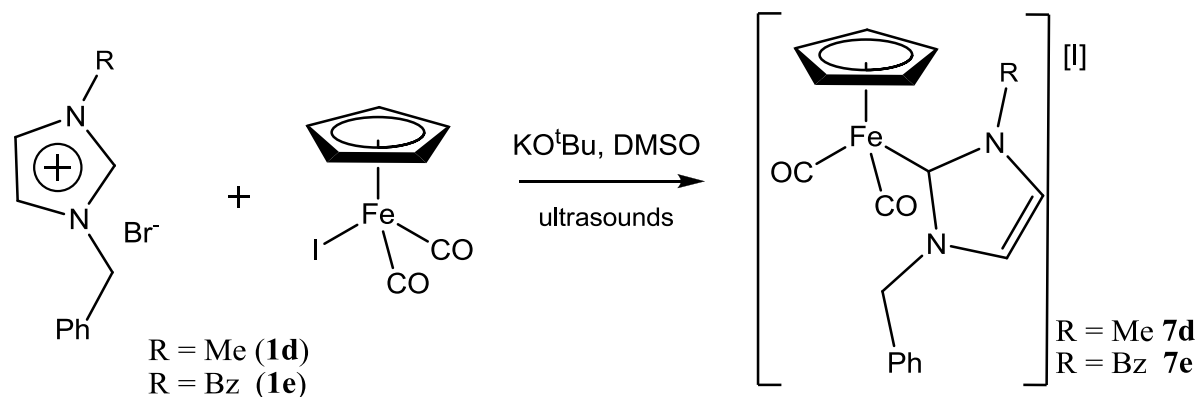
Inspired by the work of Albrecht et al.¹ in which a series of piano-stool iron(II) complexes bearing NHC and CO as ligands were synthesized via a free carbene route relying on a deprotonation of the imidazolium salt with a strong base (KO t Bu) and the subsequent metalation in situ with [FeI(Cp)(CO)₂] (Cp = η^5 -C₅H₅) as iron(II) precursor, imidazolium salts **1d** and **1e** have been used as precursors for the synthesis of new iron complexes. The conditions specified by Albrecht are reported in Scheme 10.2-1.



Scheme 10.2-1 Synthetic protocol leading to piano-stool iron(II) complexes.

However, despite several attempts under a variety of conditions, we found that this synthetic procedure leads to erratic results. One difficulty consisted in the poor solubility of the imidazolium salts in THF, which we tried to overcome making use of ultrasounds. Another problematic point of this protocol was the generation of free carbenes, which requires harsh conditions such as strong bases and the presence of impurities in the NHC proligand and/or in the iron carbonyl precursor can seriously compromise this synthesis; this problem has been highlighted recently by Royo,² who

proposed alternative route under mild conditions to iron-NHC complexes, mentioned in paragraph 1.7 of the Introduction chapter. Moreover, it was also reported by Youngs et al.³ that imidazolium salts bearing a methylene group on the side chain like **1d** (Scheme 10.2-2) lead decomposition. Considering these difficulties, the synthetic protocol of Albrecht has been modified, and the iron(II)-NHC complexes have been prepared by dissolving the imidazolium salts **1d** or **1e** with the iron precursor $[\text{FeI}(\text{Cp})(\text{CO})_2]$ in DMSO, followed by the sonication and the subsequent addition of 1.2 molar equivalent of the base KO^tBu (Scheme 10.2-2).



Scheme 10.2-2 Procedure for synthesis of iron(II)-NHC complexes optimized in our laboratory

The iron complexes in the cationic form have been isolated as brown solids in good yields ($Y \sim 60\%$); they are soluble in chlorinated solvents and toluene and completely insoluble in diethyl ether; they are air stable. Formation of the desired complexes was indicated by the presence of the two bands in IR spectrum at $\nu_s = 2049$ and $\nu_{as} = 2001 \text{ cm}^{-1}$, corresponding to the symmetric and antisymmetric stretchings of the CO molecule. It is noteworthy that the values are not so different from those in the precursor complex $[\text{FeI}(\text{Cp})(\text{CO})_2]$ (2041 and 1997 cm^{-1}), which indicates that the donor strength of the formally neutral carbene ligand to the $[\text{Fe}(\text{Cp})(\text{CO})_2]^+$ fragment is comparable to that of the anionic iodide.¹

As regards to the ^1H NMR spectra, their common feature is the expected imidazolium/Cp proton ratio: 2/5. The signal deriving from the Cp ligand appears at chemical shift δ 5.49 ppm which is typical for this group (Figure 10.2-1).

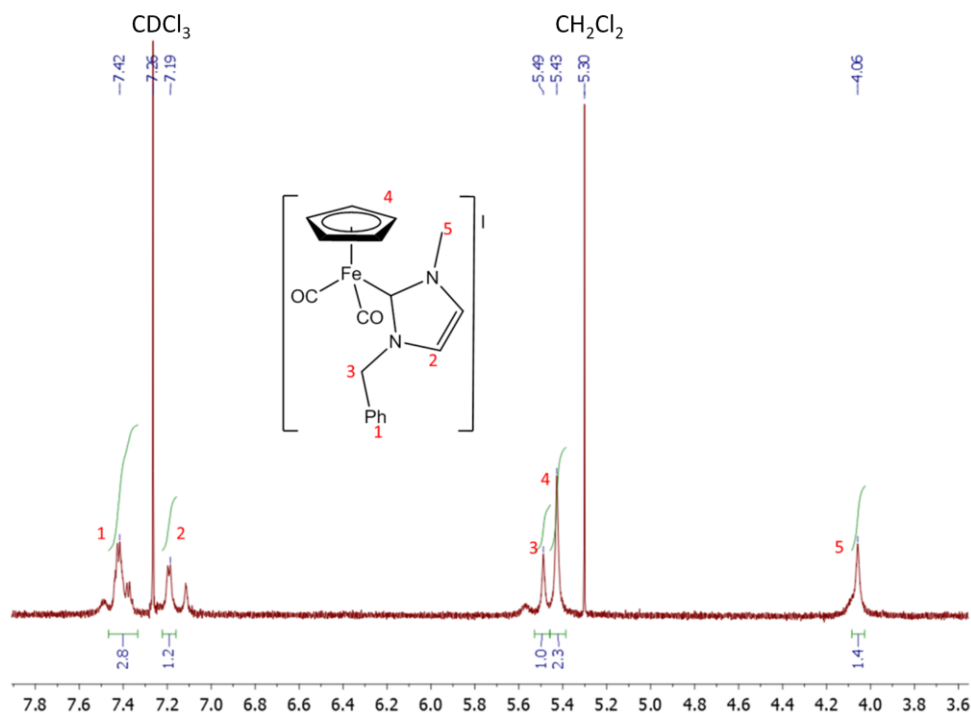
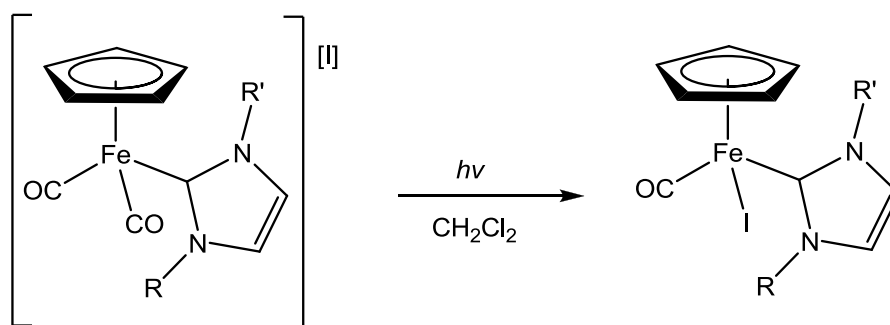


Figure 10.2-1 ^1H NMR spectrum of **7d**.

In the ^{13}C NMR spectra, the signal attributed to the CO ligands appears in a very low field, at 211.3 ppm, whereas the characteristic signal of carbenic carbon atom bonded to iron is found as a singlet at 164.4 ppm.

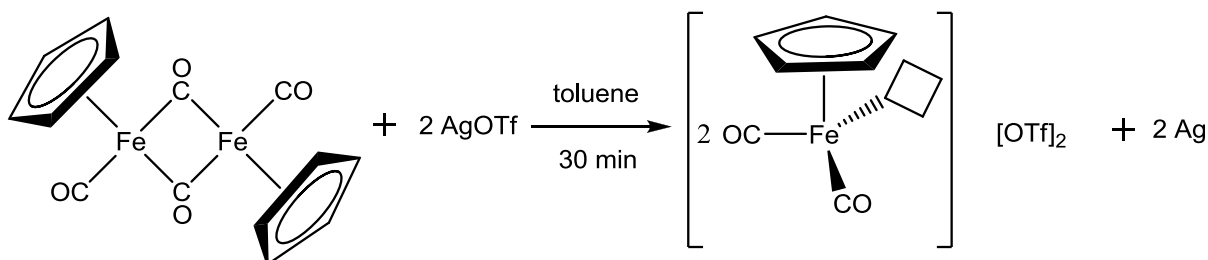
The future perspectives of the research in the field of the iron(II)-NHC complexes in our laboratory include a preparation of the corresponding neutral complexes by UV irradiation of the cationic forms, according to equation shown in Scheme 10.2-3; moreover, different synthetic routes leading to these complexes should be tried and optimized, favorably under mild conditions.



Scheme 10.2-3 Transformation of the cationic form of a piano-stool iron(II)-NHC complexes to the neutral form induced by $h\nu$ irradiation.

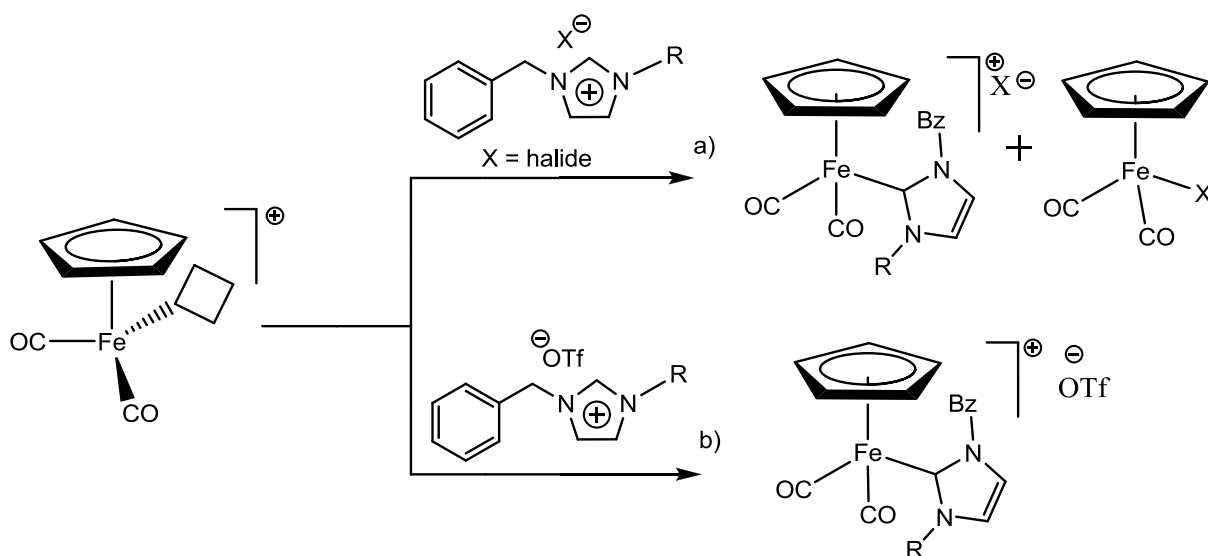
A work in this direction has already begun. This procedure consists in a redox reaction of the iron(I) dimer $[\text{Fe}_2(\text{Cp})_2(\text{CO})_4]$ with silver triflate (AgOTf) in toluene to afford two equivalents of the

iron(II) complex possessing one vacancy, since the triflate is a weakly coordinating anion (Scheme 10.2-4).



Scheme 10.2-4 Formation of the iron(II) complex bearing one vacancy in the redox reaction with silver triflate.

A subsequent addition of an imidazolium salt built likewise with a non-coordinating anion (X = OTf) should likely lead to the iron(II)-NHC complexes, whereas the same reaction carried out with the imidazolium halides could lead to the side formation of the undesired neutral complex with a halide in the coordination sphere of the iron (Scheme 10.2-5).



Scheme 10.2-5 Formation of the piano-stool iron(II)-NHC complexes with halide imidazolium salts (a) and with imidazolium salts built with a non-coordinating anions (b).

With this goal in mind, the ion exchange between bromide and the triflate in the imidazolium salt **1e** has been performed. The 1,3-dibenzyl-imidazolium triflate has been obtained in quantitative yield as a white solid and its formation has been confirmed by ¹H, ¹³C and ¹⁹F NMR spectroscopy. The significant high frequency shift of the characteristic signals deriving from CH₂ and NCHN in the NMR spectra has been observed, when compared to the bromide congener.

Further studies are currently in progress.

10.3 Experimental Section

Materials and Procedures. All reactions were carried out under argon using standard Schlenk techniques. Solvents were dried and distilled under nitrogen prior to use; the deuterated solvents, used after being appropriately dried and degassed, were stored in ampules under argon on 4Å molecular sieves. The prepared derivatives were characterized by elemental analysis and spectroscopic methods. The IR spectra were recorded with a FT-IR Perkin-Elmer Spectrum 2000 spectrometer. The NMR spectra were recorded using Varian Inova 300 (^1H , 300.1; ^{13}C , 75.5 MHz), Varian MercuryPlus VX 400 (^1H , 399.9; ^{13}C , 100.6 MHz), Varian Inova 600 (^1H , 599.7; ^{13}C , 150.8 MHz) instruments. The spectra were referenced internally to residual solvent resonances, and unless otherwise stated, they were recorded at 298 K for characterization purposes; full ^1H and ^{13}C NMR assignments were done; J.Young valve NMR tubes (Wilma) were used to carry out NMR experiments under inert conditions. ESI-MS analyses were performed by direct injection of methanol solutions of the metal complexes using a Waters ZQ 4000 mass spectrometer. Elemental analyses were performed on a Thermo-Quest Flash 1112 Series EA instrument. Sonication was performed on Elma S10H device with ultrasound frequency: 37 kHz and effective power (30W).

10.3.1 Synthesis of [FeCp(CO)₂{1-benzyl-3-methyl-imidazolin-2-ylidene}][I] (7d)

The iron complexes were synthesized using a literature method.^{1b}

To a suspension of imidazolium salt **1d** (0.107 g, 4.20 mmol) in dry THF (0.5 mL), KO^tBu (1.2 eq, 0.057 g, 5.08 mmol) was added and the mixture was sonicated at 35°C for 15 min; Then the solution was poured to a solution of [FeI(Cp)(CO)₂] (0.9 eq., 0.115 g, 3.78 mmol) in 1.3 mL of dry toluene. After 3h the formed precipitate was separated from the solvent by a filtration, washed once with dry toluene (1mL), and then extracted with dry DCM (2 x 2 mL). The solvent was evaporated in vacuum affording the crude product: **7d**.

IR (CH₂Cl₂ cm⁻¹): 2049 (νCO), 2002 (νCO). **^1H NMR** (300 MHz, CDCl₃): δ 7.43-7.19 (5H, Ph), 7.12 (2H, CH_{im}), 5.48 (2H, CH₂Ph), 5.39 (5H, Cp), 4.03 (3H, CH₃). **^{13}C NMR** (75 MHz, CDCl₃): δ 211.3 (2xCO), 164.4 (C-Fe), 134.6 (Cq), 129.6 (Ph), 129.4 (Ph), 128.8 (Ph), 127.9 (CH_{im})127.3 (CH_{im}), 87.6 (Cp), 55.8 (CH₂Ph), 41.3 (CH₃).

10.3.2 Synthesis of [FeCp(CO)₂{1,3-dibenzyl-imidazolin-2-ylidene}][I] (7e)

The imidazolium salt **1e** (0.100 g, 0.39 mmol) and the iron precursor FeI(CO)₂Cp (0.120 g, 0.39 mmol) were placed in a Schlenk and dissolved in DMSO-*d*₆ with the aid of ultrasounds. The complete dissolution of the two solid compounds was reached after 10 min and subsequently a

small excess (1.1 eq., 0.048 g, 0.43 mmol) of a base KO^tBu was added. After the addition, ultrasounds were applied for next 10 min to afford brown oil in a bottom of the Schlenk identified by IR as the desired product [Fe(CO)₂Cp{1,3-dibenzyl-imidazolin-2-ylidene}]I. The solvent above the oil was decanted and 10 ml of diethyl ether was added. After one week the solvent was removed in vacuum and the resulting solid was dissolved in deuterated chloroform for NMR analysis. **IR** (CH₂Cl₂ cm⁻¹): 2047 (νCO), 2000 (νCO). **¹H NMR** (300 MHz, CDCl₃): δ 7.46 (6H, Ph), 7.30-7.23 (4H, Ph), 7.04-7.00 (2H, CH_{im}), 5.48 (4H, CH₂Ph), 5.27 (5H, Cp). **¹³C NMR** (75 MHz, CDCl₃): δ 210.3 (2xCO), 163.5 (C-Fe), 133.8 (Cq), 129.6-127.1 (Ph) 127.4 (CH_{im}), 123.5 (CH_{im}), 86.8 (Cp), 55.6 (CH₂Ph).

¹ (a) Hashimoto, T.; Urban, S.; Hoshino, R.; Ohki, Y.; Tatsumi, K.; Glorius, F.; *Organometallics*, **2012**, *31*, 4474

(b) Mercks, L.; Labat, G.; Neels, A.; Ehlers, A.; Albrecht, M. *Organometallics* **2006**, *25*, 5648-5656

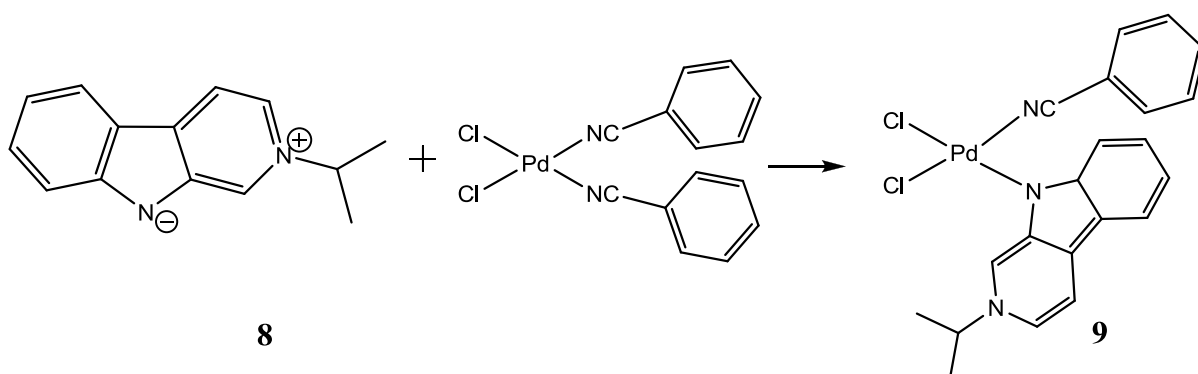
² Cardoso, J. M. S.; Royo, B. *Chem. Commun.* **2012**, *48*, 4944-4946.

³ Garrison, J. C.; Youngs, W. J. *Chem. Rev.* **2005**, *105*, 3978-4008

11 Study of Norharman and its potential in catalysis

Abstract

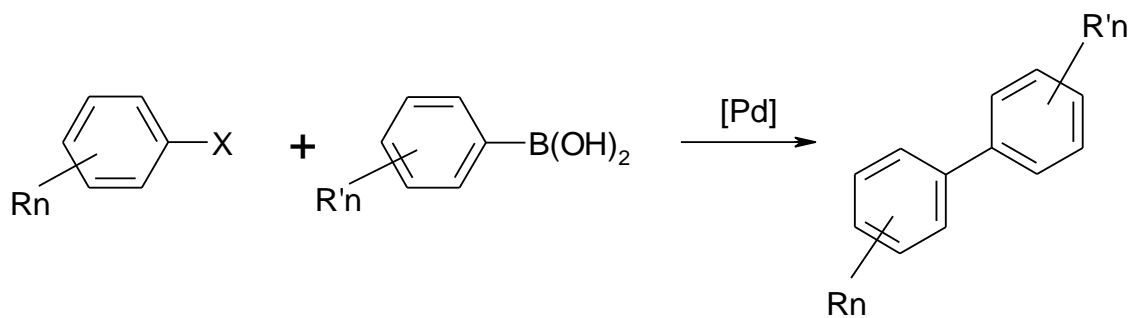
During a six months stay at the university of York (UK) under the supervision of Dr. R. E. Douthwaite a new *N*-donor ligand **8** derived from Norharman has been easily synthesized and successfully involved in palladium-catalyzed Suzuki cross-coupling of aryl bromides.



The use of 0.5 mol % of the in situ prepared palladium (II) complex **9** in the presence of 2 equivalents of Cs₂CO₃ as a base in DMF at 100°C afforded relatively high yields of biaryl products. The obtained yields depend on the degree of activation of the used aryl bromides.

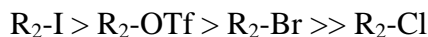
11.1 Introduction

The Suzuki-Miyaura (SM) cross-coupling reaction, which is generally referred in the literature as Suzuki reaction, is an organic reaction of an aryl- or vinyl-boronic acid with an aryl- or vinyl-halide catalyzed by palladium complexes. It provides a powerful and general methodology for the formation of carbon-carbon bonds (Scheme 11.1-1) and thus it is widely used to synthesize poly-olefins, styrenes, and substituted biphenyls.¹



Scheme 11.1-1 Suzuki Reaction

Instead of aryl- or vinyl- halides (R₂-X), the reaction can also be performed with pseudohalides, such as triflates (-OTf) and the relative reactivity of the reagents is given in a row as follows:



Boronic esters and organotrifluoroborate salts may be used instead of boronic acids.

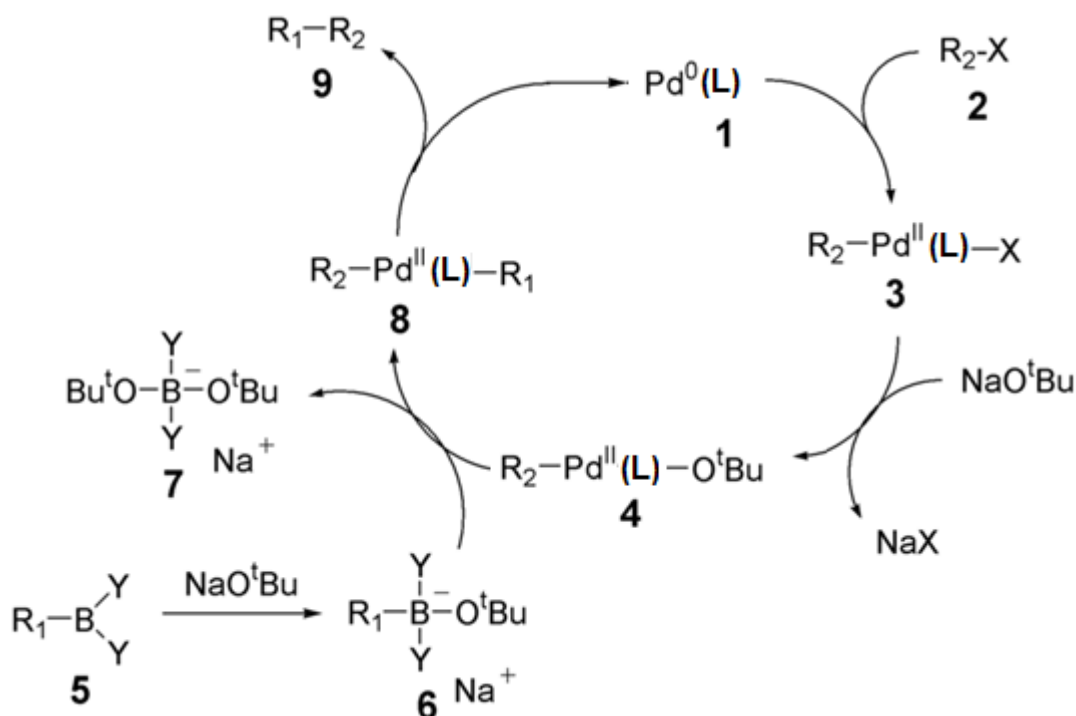
There is currently much interest in the development of catalysts that can activate aryl chlorides since these substrates are cheaper and more readily available than the corresponding bromides and iodides.²

One of the advantages of the Suzuki reaction is that the organoboron reagents used are fairly insensitive to water and oxygen, generally thermally stable and tolerant toward a variety groups. The boron-containing reagents and byproducts show low toxicity.³

The Suzuki-Miyaura reaction requires the use of a base, which is usually Na₂CO₃, but it has the drawback of being ineffective with sterically demanding substrates. Other bases often used are: K₂CO₃, Ba(OH)₂, K₃PO₄, TIOH, KF, NaOH, NaO^tBu and Cs₂CO₃.^{2,3} In case of base sensitive substrates, the possible alternatives are fluoride salts such as CsF or TBAF (Tetra-*n*-butylammonium fluoride).

The mechanism of SM¹ coupling (catalyzed particularly by palladium (0) complexes) is presented in Scheme 11.1-2 and consists of:

1. The first step is the oxidative addition of the halide **2** to palladium (0) catalyst **1** to form the organopalladium (II) species **3**.
2. Reaction with a base gives intermediate **4**, which via transmetalation with the boron-ate complex **6** forms the organopalladium (II) species **8**.
3. Reductive elimination restores the original palladium (0) catalyst **1** and the desired product **9**.



Scheme 11.1-2 The Suzuki-Miyaura reaction mechanism

The most active and routinely used catalysts for Suzuki reactions are composed of sterically demanding (bulky), electron-rich, basic phosphine-based systems. However, these compounds still have significant drawbacks such as the high sensitivity towards oxygen and/or the prices (availability) of the ligand.⁴

Compounds of class **8** (Figure 11.1-1) are known and exhibit important biological activity, however, the metal–ligand chemistry has never been examined. Alkali and transition metal complexes have been prepared to compare their properties to amido and common neutral ligands, such as phosphines and N-heterocyclic carbenes.⁵ Empirical data is supported by theoretical methods to better understand ligand bonding (particularly in the π system), ligand dynamics, and metal–ligand bonding. A catalyst prepared by combining a palladium precursor and the ligand derived from Norharman (Figure 11.1-1) was used in the palladium-catalysed Suzuki cross-coupling reactions of a series of aryl bromides with phenylboronic acid.

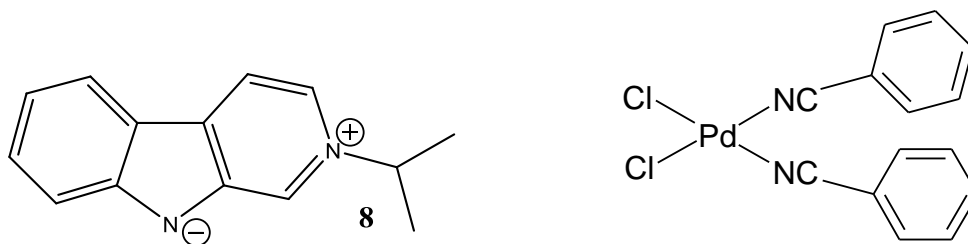


Figure 11.1-1 Ligand **8** and palladium precursor $\text{PdCl}_2(\text{PhCN})_2$

Norharman (Figure 11.1-2) is the prototypical β -carboline alkaloid that is the basic structural unit for a wide range of important naturally occurring compounds.⁶ Norharman is found in numerous plants and animals, including humans.⁶

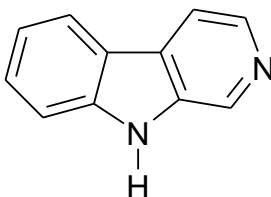
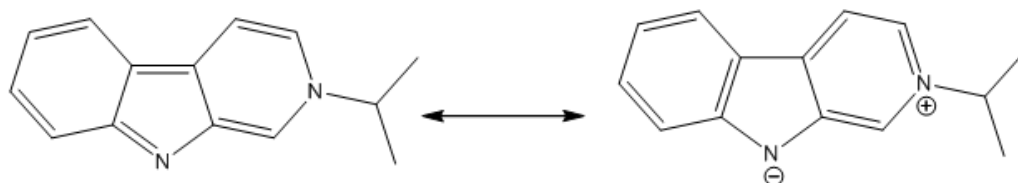


Figure 11.1-2 Structure of Norharman

It is also present in the environment, for example as one of the constituents of cigarette smoke and in food.⁶ The biological function of Norharman appears to be ambivalent, e.g. varies between toxicity and therapeutic use. It has already been investigated as a neurotoxin involved in Parkinson disease and as an agent in the mutagenesis of DNA, on the other hand it has been considered as a potential neuroprotector.

In last few years considerable attention has been given to explore the metal–ligand bonding and electron distribution in complexes involving the Norharman motif. The stability in water solution coupled with the nucleophilic character of the pyridine nitrogen atom (Scheme 11.1-3), make this system a promising new building block of organometallic catalysts.



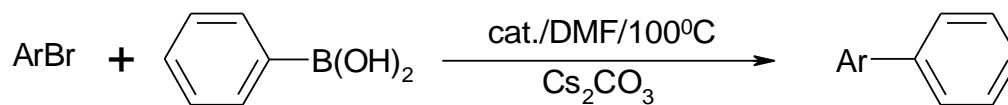
Scheme 11.1-3

11.2 Results and discussion

Synthesis of the ligand has been done following literature procedures.⁵ Preparation of the catalyst precursor **8** has been made in situ reaction and analyzed by IR spectroscopy (see Experimental Section). Prior to the catalysis study, calibration curves for products and substrates of Suzuki-Miyaura reaction were prepared for the gas chromatography procedure. Conversion degree was calculated from the following formula (Eq. 1):

$$\text{conversion} = \frac{\text{area of a product} \times \text{correction factor}}{\text{area of naphthalene}}$$

The scope of the Suzuki coupling was investigated by varying the aryl bromide under the optimized reaction conditions (Scheme 11.2-1).



Scheme 11.2-1

Table 11.2-1 Suzuki coupling of aryl bromides with phenyl boronic acid.

Entry	Aryl bromide	Catalyst (mol %)	Time (min)	Product	(%) Yield
1		0.5 No catalyst	260		93.5
					0
2		0.5	90		44.0
			170		52.2
			260		59.8
			overnight		84.1
3		0.5	130		58.7
			330		66.4
4		0.5	130		19.2
			420		37.4
5		0.5	70		30.7
			160		38.5
			260		41.9

			overnight		45.8
--	--	--	-----------	--	------

As expected, substrates containing electron-withdrawing groups such as cyano- and keto-groups were coupled with better yields than the electron rich, non activated substrates (bromobenzene, bromotoluene). In case of the highly activated 4-bromobenzonitrile, the excellent yield of 93.5% was reached after short time of 260 min (entry 1). Therefore, the reaction was tried without catalyst, but it did not work, which confirms the catalyst participation in the catalytic cycle as a necessary condition for the coupling.

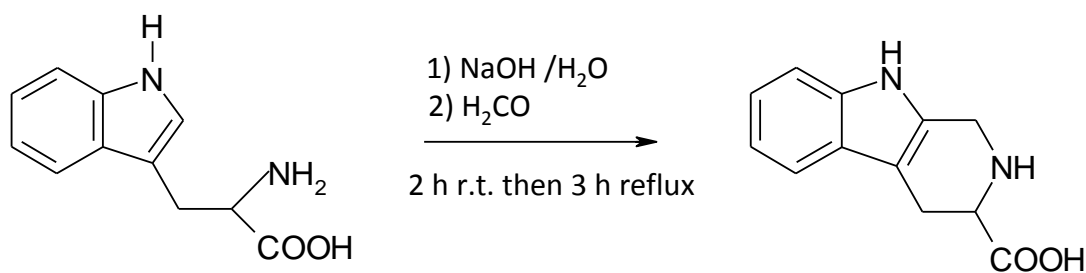
11.3 Conclusions

The structure of Norharman (β -carboline) can be easily modified in order to provide a good strong σ -donor ligand for palladium-mediated cross-coupling reaction of aryl bromides with phenylboronic acid. Further studies will be devoted to increase the yield for non-activated and deactivated aryl bromides by changing the reaction conditions and the catalyst loading.

11.4 Experimental Section

Materials and Procedures. All reactions were carried out under argon using standard Schlenk techniques. Solvents were dried and distilled under nitrogen prior to use; the deuterated solvents, used after being appropriately dried and degassed, were stored in ampules under argon on 4Å molecular sieves. The prepared derivatives were characterized by elemental analysis and spectroscopic methods. The IR spectra were recorded with a FT-IR Perkin-Elmer Spectrum 2000 spectrometer. The NMR spectra were recorded using Varian Inova 300 (^1H , 300.1; ^{13}C , 75.5 MHz), Varian MercuryPlus VX 400 (^1H , 399.9; ^{13}C , 100.6 MHz), Varian Inova 600 (^1H , 599.7; ^{13}C , 150.8 MHz) instruments. The spectra were referenced internally to residual solvent resonances, and unless otherwise stated, they were recorded at 298 K for characterization purposes; full ^1H and ^{13}C NMR assignments were done; J.Young valve NMR tubes (Wilmad) were used to carry out NMR experiments under inert conditions. ESI-MS analyses were performed by direct injection of methanol solutions of the metal complexes using a Waters ZQ 4000 mass spectrometer.

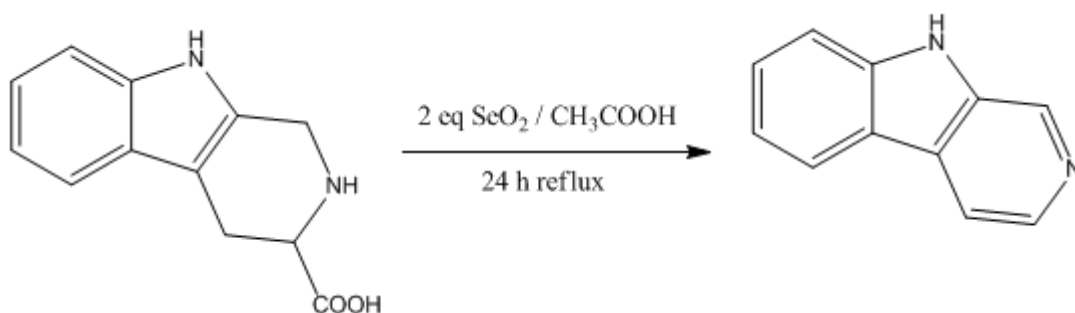
11.4.1 Synthesis of 1,2,3,4-Tetrahydro- β -carboline-3-carboxylic acid.⁵



Scheme 11.4-1

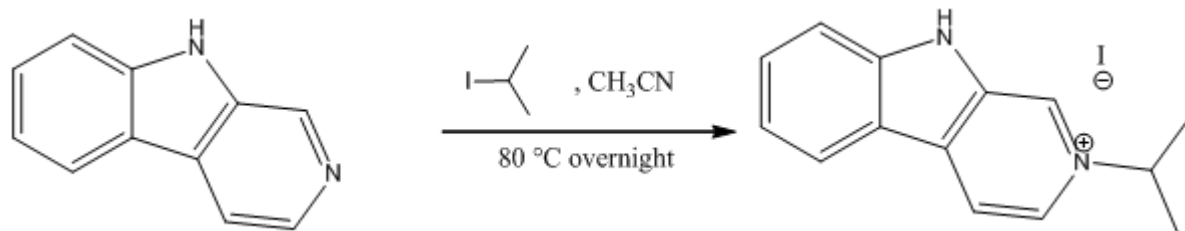
A mixture of (\pm)-tryptophan (20.0 g, 0.10 mol), NaOH (5.00 g, 0.13 mol) and H₂O (50 mL) was stirred until clear and then formalin (30%, 12.5 g) was added. The mixture was stirred at room temperature for 2 h, refluxed for 3 h and then its pH was adjusted to 5 with HCl and cooled. The precipitate was collected, washed well with H₂O, MeOH and CH₂Cl₂ and dried in vacuo leading to 9.49 g (47 %) of a white.

11.4.2 Synthesis of β -carboline⁵



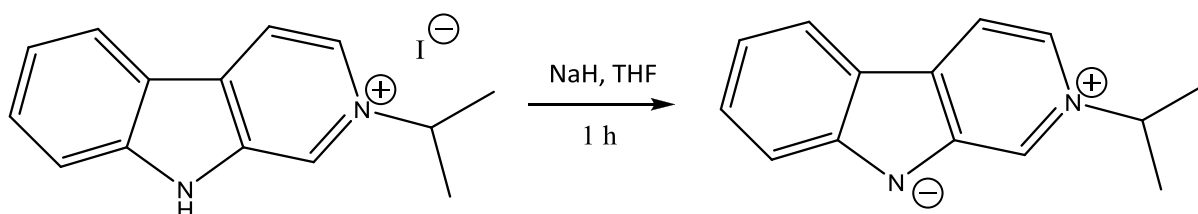
Selenium dioxide (10.0 g, 0.09 mol) was added to a suspension of 1,2,3,4-Tetrahydro- β -carboline-3-carboxylic acid (10.0 g, 0.05 mol) in glacial acetic acid (250 mL). The reaction mixture was brought to reflux, all solid material dissolved and the solution was held at reflux for 24 h. The mixture was vacuum filtered while hot, and the solvent was removed under reduced pressure to yield a red oil. Water (250 mL) was added to the oil and the pH adjusted to 10 (concentrated NH₄OH). The aqueous layer was extracted with EtOAc (3 x 200 mL). The EtOAc extracts were combined, extracted with 5% KCN (2 x 250 mL) and brine (1 x 250 mL), and dried (K₂CO₃). The solvent was removed under reduced pressure to yield a red solid, which was recrystallized from EtOAc to yield 4.84 g (60%) of product. ¹H NMR (300 MHz DMSO-*d*₆): δ 8.88 (s, 1H, NCH), 8.30 (d, 1H, J_{H,H} = 3 Hz, NCH), 8.21 (d, 1H, J_{H,H} = 6 Hz, Ph), 8.08 (d, 1H, J_{H,H} = 3 Hz, Ph), 7.57-7.51 (m, 3H, Ph), 7.22 (t, 1H, J_{H,H} = 7.5 Hz, Ph), 4.00 (s, 1H, NH).

11.4.3 Alkylation of β -carboline.⁵



To a solution of β -carboline (2.46 g, 0.02 mol) in 20 mL of acetonitrile in a Schlenk under argon atmosphere, 8 mL (0.07 mol) of isopropyl iodide were added. After stirring overnight, 10 mL of diethyl ether were added and after 12 h, a formation of yellow crystals was observed. The solvent was removed under vacuum and the solid was thoroughly washed with diethyl ether (3 x 10 mL) to yield 5.25 g (99%) of the product. $^1\text{H NMR}$ (400 MHz, CDCl_3): δ 1.8 (d, 6H, $J_{\text{H,H}} = 6.8$ Hz, $\text{CH}_{3(\text{A})}$), 5.13 (sept, 1H, $J_{\text{H,H}} = 6.6$ Hz $\text{CH}_{(\text{B})}$), 7.41 (ddd, 1H, $J_{\text{H,H}} = 8$ Hz, $J_{\text{H,H}} = 7$ Hz, $J_{\text{H,H}} = 1$ Hz, $\text{CH}_{\text{Ar}(\text{I})}$), 7.72 (ddd, 1H, $J_{\text{H,H}} = 8.2$ Hz, $J_{\text{H,H}} = 7$ Hz, $J_{\text{H,H}} = 1$ Hz, $\text{CH}_{\text{Ar}(\text{E})}$), 7.82 (dt, 1H, $J_{\text{H,H}} = 8.4$ Hz, $J_{\text{H,H}} = 1$ Hz, $\text{CH}_{\text{Ar}(\text{G})}$), 8.21 (dt, 1H, $J_{\text{H,H}} = 8.1$ Hz, $J_{\text{H,H}} = 1$ Hz, $\text{CH}_{\text{Ar}(\text{L})}$), 8.32 (dd, 1H, $J_{\text{H,H}} = 6.6$ Hz, $J_{\text{H,H}} = 1$ Hz $\text{CH}_{\text{Ar}(\text{F})}$), 8.44 (d, 1H, $J_{\text{H,H}} = 6.6$ Hz, $\text{CH}_{\text{Ar}(\text{K})}$), 9.99 (br s, 1H, $\text{CH}_{\text{Ar}(\text{C})}$), 12.16 (s, 1H, $\text{NH}_{(\text{D})}$). $^{13}\text{C NMR}$ (100 MHz, CDCl_3): δ 23.84 (C_1), 64.53 (C_2), 113.57 (C_8), 117.71 (C_{12}), 118.99 (C_{10}), 122.25 (C_9), 122.81 (C_7), 127.55 (C_3), 128.74 (C_{13}), 132.57 (C_6), 133.38 (C_{11}), 135.73 (C_4), 144.29 (C_5).

11.4.4 Deprotonation of the Norharman salt (**7**).⁵

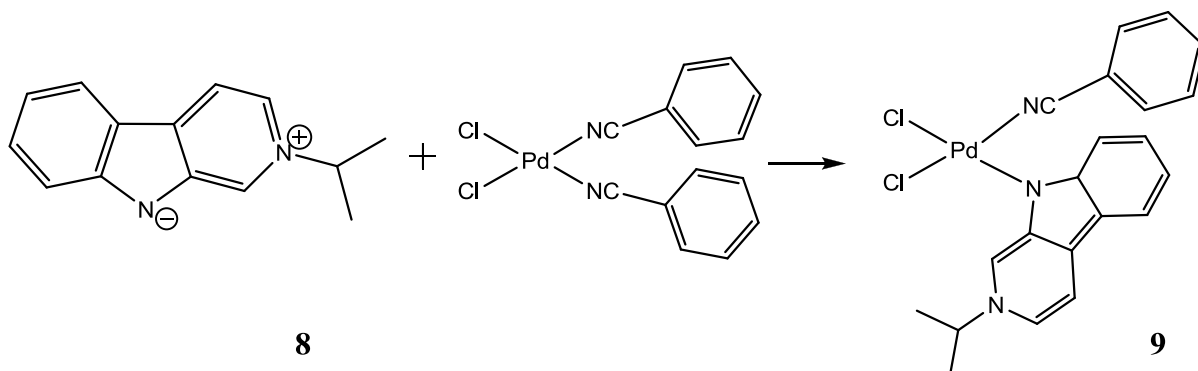


8

To a Schlenk filled with a slurry of **7** (1.00 g, 3.0 mmol) and 15 mL of THF, was added NaH (0.080 g, 3.3 mmol). The reaction mixture was stirred for 1 h. The resulting solution was filtered on celite in order to remove an excess of NaH. THF was removed in vacuum and the obtained solid was dissolved in 3 mL of dichloromethane. A precipitate of NaI was formed and removed by filtration on celite. The solvent was removed in vacuum affording 0.484 g (78%) of yellow solid identified as **7**. $^1\text{H NMR}$ (400 MHz, $\text{THF-}d_8$): δ 1.72-1.79 (m, 6H, $\text{CH}_{3(\text{A})}$), 4.85 (sept, 1H, $J_{\text{H,H}} = 7$ Hz, $\text{CH}_{(\text{B})}$), 6.98 (t, 1H, $J_{\text{H,H}} = 7$ Hz, CH_{Ar}), 7.36 (ddd, 1H, $J_{\text{H,H}} = 8$, $J_{\text{H,H}} = 7$, $J_{\text{H,H}} = 1$ Hz, CH_{Ar}), 7.72 (d, 1H, $J_{\text{H,H}} = 8$ Hz, $\text{CH}_{\text{Ar}(\text{E})}$), 7.87 (dd, 1H, $J_{\text{H,H}} = 6$ Hz, $J_{\text{H,H}} = 1$ Hz, CH_{Ar}), 8.12 (d, 1H, $J_{\text{H,H}} =$

8 Hz, CH_{Ar}), 8.18 (d, 1H, J_{H,H} = 8 Hz, CH_{Ar}), 10.17 (d, 1H, J_{H,H} = 1 Hz, CH_{Ar}). ¹³C NMR (125 MHz, THF-*d*₈): δ 23.8 (C₁), 63.3 (C₂), 115.7 (C₁₂), 117.7 (C_{Ar}), 119.6 (C_{Ar}), 121.9 (C₁₃), 122.3 (C_{Ar}), 122.8 (C_{Ar}), 128.6 (C_{Ar}), 131.9 (C_q), 133.5 (C₁₁), 147.6 (C₄), 159.6 (C_q).

11.4.5 Preparation of the catalyst.



To a Schlenk filled with 10 mL of acetonitrile were added: 0.051 g (0.24 mmol) of **8** and 0.093 g (0.24 mmol) of PdCl₂(PhCN)₂. The solution was left under stirring for 2 h. During that time a change of color from yellow to dark orange was observed and the solution was ready for catalysis purpose. The reaction was monitored by IR spectroscopy (Figure 11.4-1)

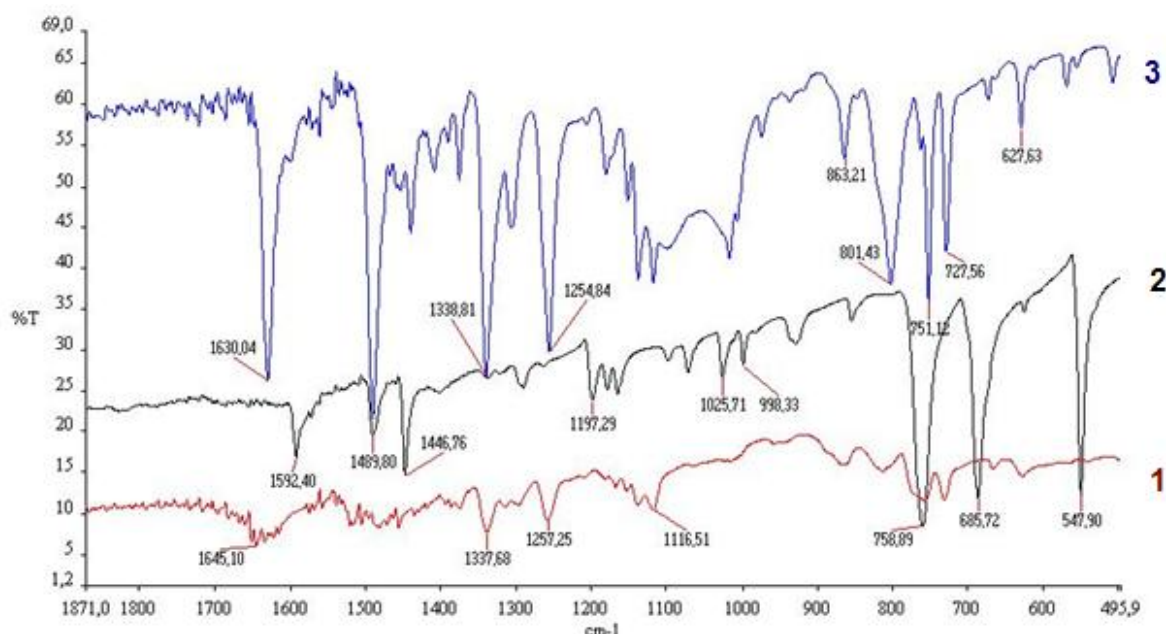


Figure 11.4-1 IR spectra of **8**, **7**, and PdCl₂(PhCN)₂

The differences between the IR spectrum of the product **9** and the spectra of the two substrates (**8** and PdCl₂(PhCN)₂) confirm the presence of the desired catalyst. The band at 1630 cm⁻¹ in the spectrum of the compound PdCl₂(PhCN)₂, attributed to the stretching frequency of the CN

group, is shifted with respect to the band in the spectrum of the compound **8** (1592 cm⁻¹) and disappears in the spectrum of the compound **9**. A significant changes are also observable in the fingerprint region of the spectra.

11.4.6 General procedure for the coupling reactions:

The prepared catalyst was introduced to a Schlenk tube under argon as an acetonitrile solution (0.17 mL, 0.5 mol %) via syringe. The solvent was removed in vacuo. The Schlenk was then charged with the appropriate aryl bromide (0.5 mmol), phenyl boronic acid (0.6 mmol), base Cs₂CO₃ (1.0 mmol) and naphthalene as a standard (0.5 mmol) under argon. DMF (6mL) was added as the solvent. The reaction mixture was then placed in an oil bath and heated at 100 °C for a time indicated in Table 2, cooled and quenched with ethyl acetate. The catalytic reactions were monitored by gas chromatography. During the reaction, 20 µL of the reaction mixture were taken by micropipette and dissolved in 10 mL of ethyl acetate to obtain 0.5 mM solution of naphthalene in every injection. The reaction sampling was optimized with respect to a systematic error made often in preparation of such low concentration solutions needed for gas chromatography.

References:

¹ http://en.wikipedia.org/wiki/Suzuki_reaction

² Gong, J.; Liu, G.; Du, C.; Zhu, Y.; Wu, Y.; *J. Organomet. Chem.* **2005**, *690*, 3963

³ Kingston, J.V.; Verkade, J.G.; *J.Org. Chem.* **2007**, *72*, 2816

⁴ Zapf, A.; Jackstell, R.; Rotaboul, R.; Riermeier, T.; Monsees, A.; Fuhrmann, C.; Shaikh, N.; Dingerdissen, U.; Beller, M.; *Chem. Commun.* **2004**, 38

⁵ Thatcher, R.J.; Johnson, D.G.; Slattery, J.M.; Douthwaite, R.E.; *Chem. Eur. J.* **2012**, *18*, 4329

⁶ Hagen, T.J.; Skolnick, P.; Cook, J.M.; *J. Med. Chem.* **1987**, *30*, 750-753.